LBL-37955
UC-401

Lawrence Berkeley Laboratory

UNIVERSITY OF CALIFORNIA

CHEMICAL SCIENCES DIVISION

Quantum Monte Carlo for Electronic Structure: Recent Developments and Applications

M.M.S. Rodríguez
(Ph.D. Thesis)

April 1994

REFERENCE COPY
Does Not
Circulate
Bldg. 50 Library.
LBL-37955
Copy 1

Prepared for the U.S. Department of Energy under Contract Number DE-AC03-76SF00098

DISCLAIMER

This document was prepared as an account of work sponsored by the United States Government. While this document is believed to contain correct information, neither the United States Government nor any agency thereof, nor the Regents of the University of California, nor any of their employees, makes any warranty, express or implied, or assumes any legal responsibility for the accuracy, completeness, or usefulness of any information, apparatus, product, or process disclosed, or represents that its use would not infringe privately owned rights. Reference herein to any specific commercial product, process, or service by its trade name, trademark, manufacturer, or otherwise, does not necessarily constitute or imply its endorsement, recommendation, or favoring by the United States Government or any agency thereof, or the Regents of the University of California. The views and opinions of authors expressed herein do not necessarily state or reflect those of the United States Government or any agency thereof or the Regents of the University of California.

LBL-37955

Quantum Monte Carlo for Electronic Structure: Recent Developments and Applications

María Milagros Soto Rodríguez
Ph.D. Thesis

Department of Chemistry
University of California, Berkeley

and

Chemical Sciences Division
Ernest Orlando Lawrence Berkeley National Laboratory
University of California
Berkeley, CA 94720

April 1994

This work was supported by the Director, Office of Energy Research, Office of Basic Energy Sciences, Chemical Sciences Division, of the U.S. Department of Energy under Contract No. DE-AC03-76SF00098.

Quantum Monte Carlo for Electronic Structure: Recent Developments and Applications

by

María Milagros Soto Rodríguez

B.S. (Haverford College) 1988

A dissertation submitted in partial satisfaction of the

requirements for the degree of

Doctor of Philosophy

in

Chemistry

in the

GRADUATE DIVISION

of the

UNIVERSITY OF CALIFORNIA at BERKELEY

Committee in charge:

Professor W.A. Lester, Jr., Chair

Professor B. Whaley

Professor H. Morrison

April 5, 1994

Quantum Monte Carlo for Electronic Structure: Recent Developments and Applications

Copyright © 1995

by

María Milagros Soto Rodríguez

The U.S. Department of Energy has the right to use this document
for any purpose whatsoever including the right to reproduce
all or any part thereof

Abstract

Quantum Monte Carlo for Electronic Structure:
Recent Developments and Applications

by

María Milagros Soto Rodríguez

Doctor of Philosophy in Chemistry
University of California at Berkeley
Professor William A. Lester, Jr. Chair

Monte Carlo (MC) methods are useful for evaluation of high dimensional integrals, simulation of random processes (such as diffusion), and to solve equations. In recent years, quantum Monte Carlo (QMC) methods have been found to give excellent results when applied to chemical systems. The main goal of the present work is to use QMC to perform electronic structure calculations. In QMC, we use a Monte Carlo simulation to solve the Schrödinger equation, taking advantage of its analogy to a classical diffusion process with branching. (The version of QMC which employs no branching is known as variational Monte Carlo (VMC).) Importance sampling reduces the variance in the computed averages by directing the walk, by means of a drift term, towards the most important regions in configuration space where the trial wave function (Ψ_T) is large. The density of walkers in the diffusion process cannot be negative; so, the probability density for importance sampling, given by the product of the QMC solution and the trial wave function, must be positive. This goal is achieved by imposing the boundary condition that the trial and the exact wave function have the same nodal surfaces, i.e., the random walk is performed separately in each nodal volume of the trial function by preventing any configuration from crossing a node; this is known as the fixed-node approximation. There are many variations of MC for electronic structure and we shall review a few. In the present work we focus on how to extend the usefulness of QMC to more meaningful molecular systems. Our study is aimed at questions concerning polyatomic and large atomic number (Z) systems.

The accuracy of the solution obtained is determined by the accuracy of the trial wave function's nodal structure. Efforts in our group have given great emphasis to finding optimized wave functions for the QMC calculations. Little work had been done by systematically looking at a family of systems to see how the best wave functions evolve with system size. In this work we present a study of trial wavefunctions for C, CH, C_2H and C_2H_2. The goal is to study how to build wavefunctions for larger systems by accumulating knowledge from the wave functions of its fragments as well as gaining some knowledge on the usefulness of multi-reference wave functions.

In a MC calculation of a heavy atom, for reasonable time steps (in VMC, this is a time step giving a $\approx 50\%$ acceptance ratio) most moves for core electrons are rejected. For this reason

true equilibration is rarely achieved. A method proposed by Batrouni and Reynolds[1] modifies the way the simulation is performed without altering the final steady-state solution. It introduces an acceleration matrix chosen so that all coordinates (i.e., of core and valence electrons) propagate at comparable speeds. A study of the results obtained using their proposed matrix (the inverse of the Hessian of the "potential" $U = -2\ln|\Psi_T|$ is chosen) suggests that it may not be the optimum choice. In our work we have found that the desired mixing of coordinates between core and valence electrons is not achieved when using this matrix.

[1]G.G. Batrouni and P.J. Reynolds. Accelerated Green's function Monte Carlo: Avoiding Critical Slowing Down in Simulations Containing Large-Z Atoms. *unpublished.*

Dedication

To Mañín, Basilisa, Chingolo and Remeneo

Contents

Dedication i

Table of Contents ii

List of Figures v

List of Tables vii

Acknowledgments ix

1 Introduction to Electronic Structure Methods 1

1.1 Hartree-Fock and the correlation problem 1

1.2 Post-Hartree-Fock methods 6

1.2.1 Configuration Interaction (CI) and Multi-Configuration Self-Consistent Field (MCSCF) 7

1.2.2 Complete Active Space Self-Consistent Field (CASSCF) 9

1.2.3 Many-Body Perturbation Theory 10

1.2.4 Gaussian-1 (G-1) and Gaussian-2 (G-2) 11

1.3 Quantum Monte Carlo for electronic structure 11

2 Quantum Monte Carlo 12

2.1 Theory 12

2.1.1 Monte Carlo methods 12

2.1.2 Introduction to quantum Monte Carlo 14

2.1.3 Importance sampling 16

2.1.4 Fixed-node diffusion quantum Monte Carlo 18

2.1.5 Variational Monte Carlo 25

2.1.6 Exact QMC methods 26

2.2 Applications 31

2.2.1 Previous Results 31

2.2.2 The H_3 system 31

2.3 Making QMC accessible - size problem 33

2.3.1 Large Z 33

2.3.2 Polyatomic systems 34

3 Acetylene system **38**
3.1 Introduction . . . 38
3.2 CH containing systems . . . 41
3.2.1 Carbon - C . . . 41
3.2.2 Methylidene - CH . . . 44
3.2.3 Ethynyl Radical - C_2H . . . 58
3.2.4 Acetylene - C_2H_2 . . . 65
3.3 Discussion . . . 74
3.4 Conclusion and future directions . . . 76

4 Accelerated Variational Monte Carlo **78**
4.1 Introduction . . . 78
4.1.1 Equilibration problem in variational Monte Carlo . . . 79
4.1.2 Acceleration methods . . . 84
4.1.3 Accelerated variational Monte Carlo . . . 85
4.2 Applications . . . 87
4.2.1 Effect on simulation features . . . 87
4.2.2 Effect on autocorrelation time . . . 95
4.3 Conclusion and future directions . . . 103

Epilogue **104**

A Definitions **105**
A.1 Atomic units . . . 105
A.2 Born-Oppenheimer Approximation . . . 106
A.3 Slater-type and Gaussian-type orbitals (STOs and GTOs) . . . 109
A.3.1 Nomenclature . . . 110
A.4 The variational principle . . . 112
A.5 Configuration State Functions . . . 112
A.6 Density matrices and natural orbitals . . . 112
A.7 Dissociation energies . . . 113
A.7.1 Zero Point Energy . . . 113
A.7.2 Isodesmic and isogyric reactions . . . 114
A.8 Local energy . . . 114
A.8.1 Cusp condition . . . 115
A.9 Growth estimator . . . 115
A.10 Green's functions . . . 116
A.10.1 Free Particle Green's function . . . 116
A.10.2 Integral equations . . . 118
A.11 The jackknife statistic . . . 119
A.12 Glossary . . . 121

B Other results **122**
B.1 Fluorine . . . 122

C Programs **126**
C.1 Monte Carlo Programs . . . 126
C.1.1 QMagiC . . . 126
C.1.2 Acceleration routines . . . 138
C.2 *Ab initio* programs . . . 139
C.2.1 ALCHEMY II, HONDO and GAMESS . . . 139

Bibliography **140**

List of Figures

1.1 Iterative algorithm followed by most SCF programs. 7
1.2 Effects of the theoretical model chosen on the quality of the energy results obtained. 9

2.1 Evolution of configurations during a random walk. Each box represents a fictitious walker, with the large circle as the nucleus, and 3 smaller circles as the electrons. The figure illustrates a diffusion step followed by branching. 22
2.2 Radial dependence of Jastrow functions. 35
2.3 Time step extrapolation of the QMC energy of the saddle point in the H_3 reaction coordinate (i.e. transition state). 36
2.4 Reaction coordinate for the H + H_2 exchange reaction calculated by QMC with DZ trial function, compared to the *ab initio* points computed by Liu. 37

3.1 (a) Energy vs. time step behavior for C using J_{ee} and J_{een} correlation functions. (b) Time step bias of the results in (a) compared with those obtained using basis B (Table 3.7) and no correlation function. 43
3.2 Energy vs. time step plot using basis C. 48
3.3 Time step extrapolations for CH using wave functions based on basis A and B, respectively. 54
3.4 Variational and QMC results for three different types of wavefunction at Cade and Huo's equilibrium geometry, $R_e = 2.124a_0$. (a) Selected QMC results, (b) QMC and variational results. 55
3.5 CH geometry optimization. (a) SCF comparison with basis B and C. (b) SCF vs different levels of CASSCF with basis B. (c) Effect of f-functions on the equilibrium geometry using basis C. 56
3.6 SCF energies obtained using STO vs. STO-6G basis sets. Energies from the GAMESS program have been shifted for convenience in plotting. R(C-C) is held constant at 2.276 a_0, ($r_{CH} = 1.991a_0$ and $r_{CC} = 2.276a_0$ was the minimum found by GAMESS). 63
3.7 SCF PES of ethynyl radical using basis B. 64
3.8 Time step extrapolation for C_2H with Basis B SCF. 64
3.9 Carter presented the first figure in Ref. [129]. They represent all possible dissociation channels for C_2H_2. The second figure compares the last column in the first figure to our QMC results. 66
3.10 Comparison of SCF energies obtained using STO and STO-6G basis sets for C_2H_2. 71
3.11 Two views of the SCF PES computed for acetylene using ALCHEMY II. 72
3.12 Time step extrapolation for C_2H_2 using basis B (SCF). 73
3.13 Histogram of energy data for C_2H_2 per time step. 73

4.1 VMC algorithm 82
4.2 Acceptance ratio behavior in different radial intervals, for given attempted $\langle \Delta R \rangle$. 83
4.3 Comparison of acceptance ratios and accepted $\langle \Delta R \rangle$'s for Ne at $\tau = .01$ when a unit matrix or M is used in the different radial regions. 92
4.4 Average radial moves for non-accelerated as well as accelerated walks. 93
4.5 $\langle \Delta R/R \rangle$ vs R for both accelerated and non accelerated walks. 94
4.6 Electron exchange of a Ne walker in 50-step walk. 94
4.7 Typical autocorrelation functions for non-accelerated and accelerated runs of carbon atom. 99
4.8 Block energies for non-accelerated and accelerated oxygen calculations. 100
4.9 Energy distribution of non-accelerated and accelerated runs for oxygen. 400 walkers, 50000 steps. 101
4.10 Energies along sample VMC walks. 102

B.1 Energy vs time step for F using single- and multi-determinant trial functions. . . 125

List of Tables

2.1 Total electronic energies(a.u.) of some small systems, calculated using FNQMC. 31

2.2 Total energies of H_3 ($R_1 = R_2 = 1.757a_0$), and energy barriers ($E_b = E(H_3) - E(H) - E(H_2)$) for hydrogen exchange reaction. 33

3.1 Popular choices for correlation functions used in QMC 41

3.2 Clementi's DZ basis set used for carbon atom (^{3}P) calculations 42

3.3 Energies of C(^3P) atom using Clementi's DZ basis set and various correlation functions, as well as the % correlation recovered. 42

3.4 Equilibrium distances (R_e) binding energies, (D_e), and total energies obtained for the CH($^2\Pi$) radical. 46

3.5 Cade and Huo basis set, without f-functions, for CH. 50

3.6 QMC energies and % correlation recovered for CH using Basis C for different correlation functions. Binding energies are computed using Clementi basis set with matching correlation function. 50

3.7 Basis Sets used for CH systems. 51

3.8 Configuration State Functions for CH($^2\Pi$) with 3 active electrons (5 actual CSFs and 6 determinants). The 4-electron inactive space has configuration $1\sigma^2 2\sigma^2$. . 51

3.9 Configuration State Functions for CH($^2\Pi$) with 5 active electrons (18 actual CSFs and 24 determinants). The 2-electron inactive space has configuration $1\sigma^2$. . . . 52

3.10 Comparison of QMC energies obtained for CH using basis A and basis B. SCF denotes the single reference wavefunction using the SCF MOs; MCSCF(3e) and MCSCF(5e) refer to the wavefunctions described by the multi-reference expansions with 3 and 5 active electrons. 52

3.11 Determinant coefficients for each basis set for CH($^2\Pi$) with 3 active electrons (5 actual CSFs and 6 determinants) 53

3.12 Determinant coefficients for each basis set for CH($^2\Pi$) with 5 active electrons (18 actual CSFs and 24 determinants) 53

3.13 CH($^2\Pi$) binding energies using basis B. 57

3.14 Equilibrium distances r_{CH} and r_{CC}, and total energies obtained for ethynyl radical, C_2H ($\tilde{X}^2\Sigma^+$). 61

3.15 Equilibrium distances r_{CH} and r_{CC}, total and dissociation energies for acetylene, C_2H_2 ($\tilde{X}^1\Sigma_g^+$). 70

3.16 Jackknife method applied to σ of each time step in QMC data to remove bias. . 75

3.17 Extrapolated energies using QMC data and jackknife estimation of data. 76

4.1 Electron movement data of Ne using a guided Metropolis algorithm at $\tau = 0.03$ and 3000 MC steps. $[a, b)$ is defined as $a \leq R < b$. All quantities are in a.u. $\langle \Delta R \rangle = 0.23241 a_0$. Average acceptance ratio = 0.83. 83
4.2 Effects of acceleration on electron movement (ΔR) and acceptance ratios (AR) at beginning of a sample VMC simulation. Observations were done on the first 10 steps of the Monte Carlo walk from the minimum configuration for which M was computed. 90
4.3 Average movement data for individual electrons in several atoms taking 50000 steps at given values of τ. 91
4.4 Autocorrelation times (T_{corr}), energies (E_{HF}, E_{local}) and acceptance ratios (AR) for C,N,O and Ne atoms, for different ensemble sizes (N_k) and walk parameters (time step, τ, number of blocks, N_b, and number of steps per block, N_s). 96

A.1 Atomic Units[a] 107
A.2 Conversion factors for energy units used throughout this work. 108
A.3 Slater Type Orbitals in Cartesian coordinates and in spherical polar coordinates, according to the type of molecular bond to which they contribute. 111

B.1 QMC energies at different time steps for F using single- and multi-determinant trial functions 123
B.2 Basis set used for F ($1s^2 2s^2 2p^5$) single-determinant calculation 123
B.3 Gaussian basis set used for F multi-determinant calculation 124
B.4 Trial function used for F^- ($1s^2\ 2s^2\ 2p^6$) calculation 124

C.1 Versions of QMagiC currently available (and stored in CFS) 128
C.2 *Ab initio* programs used in this work, and contact person (e-mail address) to obtain code and documentation. 139

Acknowledgments

Disclaimer: *After doing much research on the subject, I have come to the conclusion that people never properly acknowledge those who help in the completion of their Ph.D. Hence, I apologize beforehand for all the omissions I am about to make, but please consider the limited time I have to recall all the help received on the last 6 years. (Has it been that long!)*

First I want to thank my parents for their loving support throughout the years, and specially in the last few years when this work seemed to never end. Their lives have always been an example of hard work and perseverance and I don't think I would have ever been able to get this far without their undying faith in me.

Second I want to thank Oliver for making the writing of this dissertation "fun" and fast.

I also want to thank my friends and former college roommates, Caroline, Janet and Terry for listening to my endless complaints about graduate school during the last few years. Also, special thanks to Mari Maldonado for helping me put things into perspective. I hope that she is correct and that someday we will both look back on these days and laugh; I certainly don't feel much like laughing today! Thanks to Joy Andrews for being there with her lovely children, Mortimer and Prunella. Her musical talents were greatly appreciated, but most of all, thanks just for being herself.

Thanks to Joe for his friendship during the hardest years in school as well as for multiple readings of this document, and many helpful comments and criticism. Thanks to Sarah Stoll for teaching me how to drive a tank and for being a good friend. I wish her luck in her new academic life. Thanks to Dario and Paola for good food and music, and thanks to professor Ade Odutola for watching me eat and for his friendship.

On a more "professional" category, I wish to acknowledge certain individuals and institutions who made this work possible. I am mostly indebted to Dr. A.D. McLean of the Almaden Research Center for all his guidance in using the ALCHEMY II programs as well as many in-

sightful discussions on post-Hartree Fock methods. I want to also thank Dr. M. Yoshimine for helping in the installation of the ALCHEMY II programs to our RISC workstation.

Thanks to professors Slavica Matacic and Colin MacKay for being an inspiration to all their students. Thanks to Dr. Brian Hammond for introducing me to the wide world of QMC. Thanks to Dr. Kent (a.k.a. R.K.) Owen for his suggestion to use LaTeX for writing this document as well as lots of nagging when preparing for my pre-lim. (After having lunch with him for a month, the actual pre-lim was a breeze!) Thanks to Dr. Peter J. Reynolds for many helpful discussions on the acceleration subject and for reading and commenting on parts of this work. Thanks to professor Zhiwei Sun for helping me out of the acceleration slump. If it weren't for him, I might still be helplessly staring at my results! Thanks to Dr. R.K. Owen, Dr. B.L. Hammond, Dr. D. Bressanini and Dr. R.N. Barnett for careful reading and helpful comments on this document.

Thanks to other former and current members of the Lester group for helping my graduate school tenure become bearable: Joy for the "troncomóvil," Ade for teaching me to play Monopoly, Zhiwei for his wok and the acupressure, Dario and Laurent for their lessons on Europe, Maudie for always giving a friendly and helpful hand, especially with the Berkeley and LBL bureaucracies, Eric for the occasional "ACK!", Will for the pickled garlic, and Mark for bringing non-scientific literature into the office.

Last but not least, thanks to my research adviser, professor William A Lester, Jr. for his academic, financial and computational support. His guidance concerning the academic and scientific world is greatly appreciated.

The first 3 years of my graduate career were funded in part by the NSF Graduate Minority Fellowship program. This research was supported in part by the Director, Office if Basic Energy Research Sciences, Chemical Sciences Division of the U.S. Department of Energy under Contract No. DE-AC03-76SF00098.

Chapter 1

Introduction to Electronic Structure Methods

The determinant is a passionate function.

D. Husemoller

One hopes that in the future many experiments (e.g., finding stable and non-pernicious drugs, identifying transient species in chemical reactions) will be complemented by theoretical methods since physical conditions could be simulated by computations on the given system. Electronic structure theory, based on solving the Schrödinger equation to get the energy and wave function which describe the chemical system, has been greatly enhanced by the development of computer technology (i.e., vector and parallel machines) and astute algorithms to overcome the difficulties inherent in these problems. The search for novel approaches that take full advantage of these machines' capabilities continues. The purpose of this chapter is to introduce the reader to terms in electronic structure theory which will be used throughout the rest of this work. In addition, a glossary containing and referencing abbreviations and acronyms used is given in Appendix A.12. More detailed (and better illustrated) treatises on the subject can be obtained from the literature[1, 2].

1.1 Hartree-Fock and the correlation problem

We shall present now a short introduction to the solution of the electronic structure problem using the Hartree-Fock (HF) approach. Good sources for an overview of the HF method can be found in [3, 4].

To describe a molecule, start with a time-independent Hamiltonian in atomic units (see

Appendix A.1) which we assume to be non-relativistic,

$$\hat{\mathcal{H}}_{molecular} = -\sum_{i=1}^{N}\frac{1}{2}\nabla_i^2 - \sum_{A=1}^{M}\frac{1}{2M_A}\nabla_A^2 - \sum_{i=1}^{N}\sum_{A=1}^{M}\frac{Z_A}{r_{iA}} + \sum_{i=1}^{N}\sum_{j>i}^{N}\frac{1}{r_{ij}} + \sum_{A=1}^{M}\sum_{B>A}^{M}\frac{Z_A Z_B}{R_{AB}}\ , \quad (1.1)$$

where r_{ij}, r_{iA}, and R_{AB} are electron-electron, electron-nucleus and internuclear distances, respectively; M is the number of nuclei; N is the number of electrons; and M_A, and Z_A, Z_B are the mass and atomic number of each nucleus A, B, respectively. The first two terms are the kinetic energies of the electrons and the nuclei, respectively. The third term is the electron-nucleus attraction, and the fourth and fifth are the electron-electron and nuclear-nuclear repulsion terms, respectively.

A second approximation may be introduced at this point. The Born-Oppenheimer approximation (for a more detailed description see Appendix A.2) assumes that the nuclei remain fixed in space with respect to the electrons. Therefore, the second term in the Hamiltonian (i.e. kinetic energy of the nuclei) can be neglected, and the fifth term (which we will refer to as V_{AB}) will be constant since the internuclear distance, R_{AB}, is considered fixed for the time scale in question. We will work with a simpler Hamiltonian:

$$\hat{\mathcal{H}}_{molecular} = \hat{\mathcal{H}}_{el} + V_{AB} \quad (1.2)$$

where

$$\hat{\mathcal{H}}_{el} \equiv -\sum_{i=1}^{N}\frac{1}{2}\nabla_i^2 - \sum_{i=1}^{N}\sum_{A=1}^{M}\frac{Z_A}{r_{iA}} + \sum_{i=1}^{N}\sum_{j>i}^{N}\frac{1}{r_{ij}} \quad (1.3)$$

is the electronic Hamiltonian, and

$$V_{AB} \equiv \sum_{A=1}^{M}\sum_{B>A}^{M}\frac{Z_A Z_B}{R_{AB}}\ . \quad (1.4)$$

Using this Hamiltonian in the Schrödinger equation, $\hat{\mathcal{H}}\Psi = E\Psi$, allows us to write

$$\begin{aligned}(\hat{\mathcal{H}}_{el} + V_{AB})\Psi &= E_{tot}\Psi \\ \hat{\mathcal{H}}_{el} &= (E_{tot} - V_{AB})\Psi \\ \hat{\mathcal{H}}_{el}\Psi &= \varepsilon_{el}\Psi \end{aligned} \quad (1.5)$$

where $\varepsilon_{el} = E_{tot} - V_{AB}$. Equation 1.5 is the electronic Schrödinger equation which can be solved treating the nuclear coordinates as parameters. The nuclear Hamiltonian, $\hat{\mathcal{H}}_{nuc}$, is found from Eq. 1.1 to be

$$\begin{aligned}\hat{\mathcal{H}}_{nuc} &= -\sum_{A=1}^{M}\frac{1}{2M_A}\nabla_A^2 + \langle\hat{\mathcal{H}}_{el}\rangle + V_{AB} \\ &= -\sum_{A=1}^{M}\frac{1}{2M_A}\nabla_A^2 + E_{tot}(\{R_A\})\ , \end{aligned} \quad (1.6)$$

where $\langle\hat{\mathcal{H}}_{el}\rangle$ represents an average over the electronic Hamiltonian, and E_{tot} is the potential for nuclear motion which depends parametrically on R_A. The term E_{tot} constitutes a nuclear potential energy surface (PES) which describes the energy as a function of nuclear position in the Born Oppenheimer approximation. This PES is obtained by solving the electronic Schrödinger equation, and this work is concerned mainly with methods to solve the electronic structure problem.

Going back to the electronic Hamiltonian, $\hat{\mathcal{H}}_{el}$, we readily see that it can be rewritten and divided into one- and two- electron parts:

$$\hat{\mathcal{H}}_{el} = \sum_{i=1}^{N} \hat{h}(i) + \sum_{i=1}^{N}\sum_{j>i}^{N} \frac{1}{r_{ij}} \tag{1.7}$$

where $\hat{h}(i)$ is a one-electron Hamiltonian which involves both kinetic and potential energies in the field created by the nuclei in the system. Or in more abstract terms, the Hamiltonian[1] is a sum of a one-electron operator and a two-electron operator, i.e., $\hat{\mathcal{H}} = \hat{\mathcal{O}}_1 + \hat{\mathcal{O}}_2$.

The one-electron operator, $\hat{\mathcal{O}}_1 = \sum_{i=1}^{N} \hat{h}(i)$ corresponds to the Hamiltonian of a system of non-interacting electrons. Since the $\hat{h}(i)$'s have a set of eigenfunctions $\{\chi_j\}$, known as *spin orbitals*, such that $\hat{h}(i)\chi_j = \varepsilon_j\chi_j$, the eigenfunctions corresponding to $\hat{\mathcal{O}}_1$ are products of these spin orbitals $\{\chi_j\}$ for each electron,

$$\Psi = \chi_1(\vec{x}_1)\chi_2(\vec{x}_2)\cdots\chi_N(\vec{x}_N) \,. \tag{1.8}$$

This type of wave function is known as a *Hartree product*, and its eigenvalue is the sum of the spin orbital energies, ε_j, mentioned above. However, Hartree products do not account for instantaneous correlation among electrons, nor satisfy the anti-symmetry required for fermions. Since electrons are indistinguishable, the anti-symmetry requirement says that the wave function must change sign with the interchange of two electrons. That anti-symmetry is a reason why normalized "linear combinations" of Hartree products known as *Slater determinants* are used instead, i.e.,

$$\Psi = \frac{1}{\sqrt{N!}} \begin{vmatrix} \chi_1(\vec{x}_1) & \chi_2(\vec{x}_1) & \cdots & \chi_N(\vec{x}_1) \\ \chi_1(\vec{x}_2) & \chi_2(\vec{x}_2) & \cdots & \chi_N(\vec{x}_2) \\ \vdots & \vdots & \ddots & \vdots \\ \chi_1(\vec{x}_N) & \chi_2(\vec{x}_N) & \cdots & \chi_N(\vec{x}_N) \end{vmatrix} , \tag{1.9}$$

or

$$\Psi = \frac{1}{\sqrt{N!}} \sum_{i=1}^{N!} (-1)^{p_i} \hat{P}_i \{\chi_1(\vec{x}_1)\chi_2(\vec{x}_2)\cdots\chi_N(\vec{x}_N)\} \,, \tag{1.10}$$

[1] From now on we will refer to $\hat{\mathcal{H}}_{el}$ as "the Hamiltonian", or simply $\hat{\mathcal{H}}$, and ε_{el} as E.

where p_i is the permutation number, $\hat{P}_i$ is the permutation operator, and χ_i's are spin orbitals.[2] One can also write this Slater determinant as $|\Psi\rangle = |\chi_1(\bar{x}_1)\chi_2(\bar{x}_2)\cdots\chi_N(\bar{x}_N)\rangle = |\chi_1(1)\chi_2(2)\cdots\chi_N(N)\rangle$, using Dirac notation.[3] Contrary to Hartree products, the Slater determinant does not specifically assign electrons to spin orbitals. The spin orbitals contain the variational parameters we will eventually choose to adjust. The spin orbitals have spatial and spin factors specified as follows. Usually a set of molecular orbitals (MOs) $\{\psi_i\}$ is chosen and electrons of α and β spin are then assigned to these MOs according to the state of the system.[4] This arrangement will constitute the reference electron configuration. The individual MOs are expressed as linear combinations of n basis functions $\{\phi_\mu\}$, i.e.,

$$\psi_i = \sum_{\mu=1}^{n} c_{\mu i}\phi_\mu \ . \tag{1.11}$$

These basis functions usually correspond to each of the atoms in the system.[5] This is known as a linear combination of atomic orbitals, or LCAO approximation. A description of options for these basis functions is given in Appendix A.3. The coefficients $c_{\mu i}$ are known as the MO coefficients, and they are our variational parameters.

By projecting Eq. 1.5 (where $\hat{\mathcal{H}}_{el}$ is given by Eq. 1.7) with $\langle\Psi|$, and using the variational principle,[6] i.e.,

$$E = \frac{\langle\Psi|\hat{\mathcal{H}}|\Psi\rangle}{\langle\Psi|\Psi\rangle} \geq E_0 \ , \tag{1.12}$$

one can find an upper bound to the ground electronic state energy. More explicitly, $\langle\Psi|\hat{O}_1 + \hat{O}_2|\Psi\rangle = \langle\Psi|E|\Psi\rangle$ which for a normalized $|\Psi\rangle$ implies that

$$E = \langle\Psi|\hat{O}_1|\Psi\rangle + \langle\Psi|\hat{O}_2|\Psi\rangle \ . \tag{1.13}$$

The first term in Eq. 1.13 for a Slater determinant $|\Psi\rangle$ such as given by Eq. 1.9 is given by

$$\langle\Psi|\hat{h}(k)|\Psi\rangle \ = \ \sum_{j=1}^{N}\langle\chi_j(k)|\hat{h}(k)|\chi_j(k)\rangle \ \equiv \ \sum_{j=1}^{N}\langle j|\hat{h}|j\rangle \ = \ \sum_j h_{jj} \ , \tag{1.14}$$

where N is the number of spin orbitals (which also corresponds to the number of electrons) in the Slater determinant (Eq. 1.9), k refers to the coordinates of the k-th electron, and $\{\chi_j\}$ are

[2] Notice that Slater determinants satisfy anti-symmetry, but do not account for correlation of electrons with opposite spins. Instantaneous electron correlation is necessary to account for the fact that electrons repel each other. This feature is not described explicitly when all electrons are treated on average.

[3] On occasion one will stop using the symbol for the spin orbital as well, and refer to it just by its index, i.e., $|\Psi\rangle = |12\cdots N\rangle$, where the order of the indexes will indicate which electron. Since electrons are indistinguishable, the assignment of electrons to specific spin orbitals will not play a vital role in notation.

[4] That is, each electron j may be characterized by $\chi_i(j) = \psi_i(j)\alpha(j)$, or $\chi_i(j) = \psi_i(j)\beta(j)$ depending on its spin.

[5] As a convention, roman letters will be used to index the spin and molecular orbitals, while greek letters will be used to index the basis functions.

[6] The variational principle is briefly described in Appendix A.4.

orthogonal. These integrals are called one-electron integrals, since they depend only upon the coordinates of one electron. The $\hat{O}_2$ operator leads to more complicated two-electron integrals,

$$\begin{aligned}\langle\Psi|\frac{1}{r_{12}}|\Psi\rangle &= \frac{1}{2}\sum_i^N\sum_j^N\left\{\langle\chi_i(1)\chi_j(2)|\frac{1}{r_{12}}|\chi_i(1)\chi_j(2)\rangle - \langle\chi_i(1)\chi_j(2)|\frac{1}{r_{12}}|\chi_j(1)\chi_i(2)\rangle\right\} \\ &\equiv \frac{1}{2}\sum_i^N\sum_j^N\{\langle ij|ij\rangle - \langle ij|ji\rangle\} \ , \end{aligned} \tag{1.15}$$

where the $\langle ij|ij\rangle \equiv J_{ij}$ are known as the Coulomb integrals and the $\langle ij|ji\rangle \equiv K_{ij}$ are the exchange integrals. The complete general expression for an upper bound of the ground state energy in a closed-shell system is

$$E_0 = \sum_{j=1}^N\langle j|\hat{h}|j\rangle + \frac{1}{2}\sum_i^N\sum_j^N\{\langle ij|ij\rangle - \langle ij|ji\rangle\} \ . \tag{1.16}$$

We want to find a procedure to minimize this energy with respect to the MO coefficients $\{c_{\mu i}\}$ introduced above. It will be an iterative procedure since one must first guess a wave function with an initial set of parameters to be varied in order to minimize the energy. The new parameters are used as initial guess for the second iteration, and so on.

At this point, it is convenient to define two operators,

$$\hat{J}_j\chi_i = \left[\int d\vec{x}_2\chi_j^*(2)\frac{1}{r_{12}}\chi_j(2)\right]\chi_i(1) \ , \tag{1.17}$$

and

$$\hat{K}_j\chi_i = \left[\int d\vec{x}_2\chi_j^*(2)\frac{1}{r_{12}}\chi_i(2)\right]\chi_j(1) \ , \tag{1.18}$$

where $\hat{J}_j$ is a local operator known as the Coulomb operator which describes Coulomb repulsion between electrons in orbital χ_i and electrons in orbital χ_j, and $\hat{K}_j$ is a non-local operator known as the exchange operator which switches electrons between orbitals. These definitions are necessary because we wish to write the Hamiltonian as a sum of one-electron operators, i.e. $\hat{\mathcal{H}} = \sum\hat{\mathcal{H}}_{1e}$, since it simplifies and separates as $\hat{\mathcal{H}}_{1e} = \hat{h} + V_{HF}$ where $\hat{h}$ includes the one-electron part, the kinetic energy $(-\frac{1}{2}\nabla_i^2)$ and nuclear-electron attraction $(-\sum_{A=1}^M\frac{Z_A}{r_{iA}})$, and $V_{HF} = \sum_j(\hat{J}_j - \hat{K}_j)$ is the average potential experienced by an electron in the field of the $N-1$ other electrons. These one-electron operators constitute the Fock operator, $\hat{\mathcal{F}}(i) = \hat{h}(i) + \sum_j(\hat{J}_j(i) - \hat{K}_j(i))$, and lead to the Fock equations, $\hat{\mathcal{F}}(i)|\chi\rangle = \sum_j^N\varepsilon_{ij}|j\rangle$, where ε_{ij}'s are the orbital energies. As mentioned above, these equations are solved iteratively until convergence, to give us the energy of a single electron in the field of the other electrons, and, therefore, the procedure is known as the *self-consistent field* (SCF) method. The SCF method ignores instantaneous correlation between electrons since each electron *feels* the influence of the other electrons only on average. The term Hartree-Fock limit usually conveys SCF results in the limit of a complete basis set.

At this point we wish to recall the LCAO approximation we introduced in Eq. 1.11, and use the linear expansion in the Fock equations,

$$\begin{aligned} \hat{\mathcal{F}}\chi_i &= \varepsilon_i \chi_i \\ \hat{\mathcal{F}}\left(\sum_{\mu=1}^{N} c_{\mu i}|\mu\rangle\right) &= \varepsilon_i \left(\sum_{\mu=1}^{N} c_{\mu i}|\mu\rangle\right) . \end{aligned} \tag{1.19}$$

Multiplying by $\langle\nu|$ yields,

$$\begin{aligned} \langle\nu|\hat{\mathcal{F}}\sum_{\mu=1}^{N} c_{\mu i}|\mu\rangle &= \langle\nu|\varepsilon_i \sum_{\mu=1}^{N} c_{\mu i}|\mu\rangle \\ \sum_{\mu=1}^{N} c_{\mu i}\langle\nu|\hat{\mathcal{F}}|\mu\rangle &= \varepsilon_i \sum_{\mu=1}^{N} c_{\mu i}\langle\nu|\mu\rangle \\ \sum_{\mu=1}^{N} c_{\mu i}F_{\nu\mu} &= \varepsilon \sum_{\mu=1}^{N} S_{\nu\mu}c_{\mu i} \\ \mathbf{FC} &= \mathbf{SC}\varepsilon , \end{aligned} \tag{1.20}$$

where $F_{\nu\mu} \equiv \langle\nu|\hat{\mathcal{F}}|\mu\rangle$, and $S_{\nu\mu} \equiv \langle\nu|\mu\rangle$ are defined as the Fock and overlap matrices, respectively, ε is a diagonal matrix containing the orbital energies, and C contains the expansion coefficients $\{c_{\mu i}\}$ from Eq. 1.11. Equations 1.20 are known as the Roothan-Hall equations[5].

Now we have the desired iterative procedure to compute the ground-state energy. A flowchart with the basic algorithm is shown in Fig. 1.1. By repeating the procedure at different nuclear positions, one can construct the PES of the nuclear motion. In that fashion, equilibrium geometries which minimize the total ground state energy can be found as well. Computationally speaking the calculation of the one- and two- electron integrals is the most time consuming step, as well as very demanding on machine capabilities for fast storage and retrieval.

1.2 Post-Hartree-Fock methods

Even though the HF approximation yields good energies for small systems and is qualitatively accurate for others, it fails in describing many important properties, such as dissociation energies, dipole moments, and other quantities sensitive to electron correlation. These properties require instantaneous correlation among electrons to be treated explicitly. The correlation energy is defined as the difference between the exact non-relativistic energy of the system, E_{exact}, and Hartree-Fock energy, i.e.,

$$E_{corr} = E_{exact} - E_{HF} . \tag{1.21}$$

Sections 1.2.1-1.2.4 will give a brief survey of some of the most popular and successful methods available to treat the correlation problem. The methods presented are not chosen just because

Figure 1.1: Iterative algorithm followed by most SCF programs.

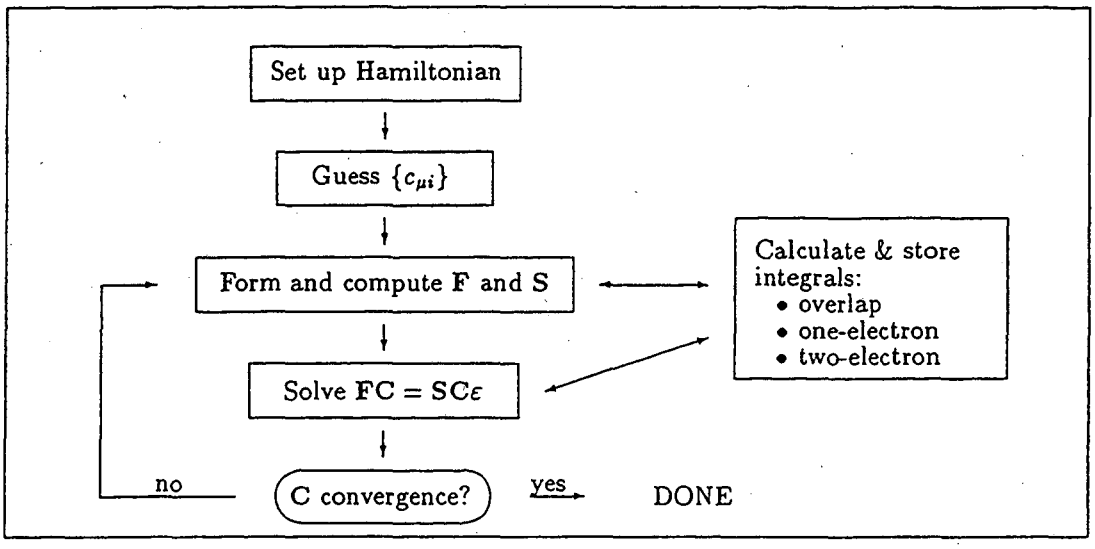

of their popularity, but also because results using such methods will be presented in Chapter 3 for comparison. More detailed discussions can be found in the literature, and references will be provided in each section when appropriate.

1.2.1 Configuration Interaction (CI) and Multi-Configuration Self-Consistent Field (MCSCF)

The configuration interaction (CI) method is the first of the approaches using multi-determinant wave functions to be introduced in this section. First let us describe how a single-reference CI calculation is performed. On a HF calculation of an n-electron system described by an N-function basis set, the result is $2N$ spin orbitals, N for each α and β spin to obtain a single-determinant wave function, $\Psi_0 = |\chi_1\chi_2\cdots\chi_n\rangle$. The rest of the spin orbitals which remain unoccupied ($2N - n$ of them) are known as virtual orbitals. New determinants can be created by occupying one or more of the virtual orbitals to replace occupied orbitals (while enforcing the correct spin state of the system). The CI procedure determines the coefficients, c_i, in the determinant expansion,

$$|\Psi\rangle = c_0|\Psi\rangle + \sum_{ia} c_i^a|\Psi_i^a\rangle + \sum_{i<j}\sum_{a<b} c_{ij}^{ab}|\Psi_{ij}^{ab}\rangle + \cdots \quad . \tag{1.22}$$

CI approaches are classified according to how far these substitutions are carried out: e.g. single substitutions or Ψ_i^a, double substitutions or Ψ_{ij}^{ab}, etc.[7] In this manner, one has single and doubles CI (SDCI or CISD) in which both single and double substitutions are used;[8] and likewise go all the way to Full CI (FCI). In principle, FCI recovers complete correlation if the one-electron basis is complete. However FCI is limited in practice by the size of the basis chosen. (See Fig. 1.2.)

SDCI calculations are known to overlook the effect of simultaneous pair correlation and are not size consistent. Size consistency means that "the energy of a many-particle system, even in the presence of interactions becomes proportional to the number of particles (N) in the limit $N \longrightarrow \infty$."[1] For instance, a SDCI calculation on a dimer would not allow for double excitations in each of the monomers since that would imply quadruple excitations. However, if one wants to compare the dimer with its dissociated products, both dimer and monomers should have been treated at the same level of theory. Langhoff and Davidson[7] pointed out that quadruple excitations are not negligible for many electron systems. In a CI study on the N_2 molecule[7], exhaustive calculations were done to determine an empirical formula to account for quadruple excitations in DCI,

$$\Delta E_{\text{quad}} = (1 - c_0^2)\Delta E_{\text{DE}} \ , \tag{1.23}$$

where c_0 is the coefficient of the SCF determinant in the resulting normalized DCI wavefunction, ΔE_{quad} is the contribution of quadruple excitations and ΔE_{DE} is the contribution from the doubles. This formula, known as the Davidson correction, proved to correct the correlation energy, such that the resulting energy from the DCI calculation is size consistent, and it holds for expansions dominated by the reference configuration. For large systems, however, the Davidson correction breaks down, as $c_1, \ldots, c_N \approx c_0$.

One does not always need to start a CI calculation from a HF wave function; with the necessary computer support, multi-reference CI (MRCI or MCCI) calculations are commonly used. However diagonalization of the CI matrix is not a trivial task and although the accuracy increases with the addition of configurations, the larger the expansion the slower the convergence shall be as well. With the availability of large computers and powerful diagonalization procedures CI calculations have become routine.

Another useful post-Hartree Fock method is that of the multiconfiguration self-consistent field (MCSCF). MCSCF can be also thought of as a "truncated CI expansion" in which orbital parameters as well as determinant coefficients are optimized. To do an MCSCF calculation one needs to establish a small number of configurations, usually chosen to describe the system's main features. For instance, if one wished to study the dissociation of a molecule, it would be in order

[7] $\chi_{i,j,k,\ldots}$ is used for occupied spin orbitals, and $\chi_{a,b,c,\ldots}$ is used for virtual spin orbitals. Therefore, Ψ_i^a signifies replacing occupied χ_i by virtual χ_a.

[8] The term quadratic configuration interaction (QCI) is used by Pople *et al.* [6] for a modified CI procedure which yields size consistent results while all terms are still second order.

Figure 1.2: Effects of the theoretical model chosen on the quality of the energy results obtained.

Hartree-Fock	Improving Correlation Treatment →	Full CI
Improving Basis Set Expansion ↓		
Complete Basis Set HF limit		Exact solution of S.E.

to include configurations which will give proper dissociation to each corresponding species. It is common practice to use the wave function resulting from an MCSCF calculation as the reference wave function for a more extensive CI calculation (i.e., MRCI) to follow.

Figure 1.2 shows a popular representation which compares the effectiveness of single and multi-reference approaches in solving the electronic Schrödinger equation. An excellent presentation of the CI method is given in [1], and of the MCSCF method in [8].

1.2.2 Complete Active Space Self-Consistent Field (CASSCF)

CASSCF is an MCSCF in which the MC used constitutes the complete space of all active configurations.[9] As mentioned above, HF theory breaks down whenever the electrons require significant rearrangement, for instance when describing formation or breaking of chemical bonds. A more complicated description of a wave function that can handle these processes within the MO model, can be found in MCSCF theory, mentioned in Sec. 1.2.1 above. Roos *et al.* [9] suggested the following approach to combine the best of the CI and MCSCF approaches while keeping in mind which orbitals are important in estimating the quantity of interest.

Their multi-configuration wave function consists of two sets of occupied orbitals: *inactive* and *active*. The inactive orbitals are doubly occupied in all determinants in the expansion and do not become involved in the chemical process of interest.[10] The active orbitals define a subspace in which a full CI is performed. These orbitals should include (but not be limited to) the orbitals undergoing change during the chemical reaction. For example, they may constitute

[9] The following overview on the CASSCF method comes from [9].

[10] In practice these orbitals are expected to have occupation number two.

a full valence CI including all valence orbitals, all excited states, etc. This constitutes the complete active space (CAS) wave function, and natural orbitals (NOs)[11] are chosen in order to get faster convergence of the CI. Roos *et al.* state that "NOs are particularly suited to obtaining 'chemical insight' into the results of the [CASSCF] calculation[9]." By using a FCI in the active space, there will be no bias in the choosing of configurations since the FCI contains all possible distributions of active electrons among the active orbitals satisfying all possible spin couplings corresponding to the total spin quantum numbers. Once the CAS wave function has been established, an MCSCF calculation is performed in which all parameters (i.e., both determinant and MO coefficients) are variationally optimized.

1.2.3 Many-Body Perturbation Theory

Even though CI systematically improves upon the HF approximation, it is not size-consistent except at the FCI level. Perturbation theory (PT), however, provides an alternative which is size-consistent at each level, since instead of truncating the Hamiltonian matrix, as is done in limited CI calculations, it is treated as the sum of two parts, one of which is small enough to be considered a perturbation.

To carry out such a calculation, the total Hamiltonian is divided into a zeroth-order part, $\hat{\mathcal{H}}_0$, which has known eigenfunctions and eigenvalues, and a perturbation $\hat{\mathcal{V}}$, i.e., $\hat{\mathcal{H}} = \hat{\mathcal{H}}_0 + \hat{\mathcal{V}}$. The Møller-Plesset[10] (MP) approach takes $\hat{\mathcal{H}}$ to be the exact electronic Hamiltonian operator, and $\hat{\mathcal{H}}_0$ as the HF operator, i.e., a sum of one-electron Fock operators, $\hat{\mathcal{H}}_0 = \sum_i \hat{\mathcal{F}}(i)$. Therefore, the perturbation $\lambda\hat{\mathcal{V}}$ is defined as $\lambda\hat{\mathcal{V}} = \lambda(\hat{\mathcal{H}} - \hat{\mathcal{H}}_0)$, and the eigenvalue to zeroth-order is the HF energy, E_0^{HF}, corresponding to a particular Slater determinant, the eigenfunction to zeroth-order, Ψ_0^{HF}. One can follow Rayleigh-Schrödinger perturbation theory (RSPT),[12]

$$\begin{aligned} \Psi_{exact} &= \Psi_0^{\mathrm{HF}} + \lambda\Psi_1 + \lambda^2\Psi_2 + \ldots \\ E_{exact} &= E_0^{\mathrm{HF}} + \lambda E_1 + \lambda^2 E_2 + \ldots \end{aligned} \tag{1.24}$$

to find each MP correction to different orders, corresponding to the order of λ in Eq. 1.24.

The terms MP2 and MP4 refer to the cases where MP theory is carried out to second and fourth order, respectively. MP2 recovers a large percentage of the correlation energy and yields a better optimized geometry than HF. A comparison of CI and MPPT methods is given in [13], which shows the trends in size consistency for MP and the lack of size consistency in CI.

[11] See Appendix A.6.

[12] RSPT can be found in most introductory quantum mechanics books[11, 12].

1.2.4 Gaussian-1 (G-1) and Gaussian-2 (G-2)

The Gaussian-1 (G-1)[14] and Gaussian-2 (G-2)[15] methods of Pople, *et al.* are recent empirical methods to produce high accuracy results. Their main objective is to obtain equilibrium geometries, total electronic energies, and harmonic frequencies associated with local minima on the PES to be used in calculating zero point energy (ZPE) corrections, ΔE(ZPE). G-1 employs previous theoretical experience (e.g., geometry optimization techniques and higher polarization functions) and empirical data (e.g., corrections to obtain exact H and H_2 results) to correct upon MP4 energies. G-2 improves on G-1 theory by estimating the error in some of the G-1 corrections.

1.3 Quantum Monte Carlo for electronic structure

The rest of this work deals with the implementation of Monte Carlo (MC) methods to determine atomic and molecular electronic structure. Quantum Monte Carlo (QMC) uses a random walk to perform electronic structure calculations without directly depending on the quality (or complexity) of a wave function, but greatly improving on post-Hartree Fock results. This is accomplished, usually recovering over 90% of the correlation energy, without need of large basis set expansions nor extensive determinant expansions. The method is easily vectorized and its structure is easily parallelized as well. The computation and storage of integrals, which becomes the rate determining step in an SCF calculation, are not necessary for QMC since the random walk only requires the calculation of first and second order derivatives of a given trial function, which provides great flexibility in choosing such a function. The QMC method is presented in detail in Chapter 2.

Chapter 2

Quantum Monte Carlo

The imaginary numbers are a wonderful flight of God's spirit; they are almost an amphibian between being and not being.
Gotterfied Wilheim von Leibnitz, 1702

For something imaginary, they cause an awful lot of trouble.
Joseph B. Rucker, 1989

2.1 Theory

2.1.1 Monte Carlo methods

The main tactic in Monte Carlo (MC) methods is to solve a problem by simulation at a large number of randomly chosen points. This randomness has earned MC its name in relation to games of chance. MC methods can be used for solving multi-dimensional problems such as the simulation of physical processes (e.g., diffusion), the solution of differential equations (e.g., the Schrödinger equation) and the evaluation of high dimensional integrals. It is our intention to give a brief overview of one of these applications to get better acquainted with the power of MC before attempting to implement it in our electronic structure application.

A common use of Monte Carlo methods is in the evaluation of high dimensional integrals [16, 17], which cannot be evaluated using standard quadratures or grid methods. We shall briefly give an overview of how Monte Carlo is used to evaluate the integrand at a large number of random points which can be sampled from a known distribution to obtain the integral. Suppose we wish to evaluate the integral

$$I = \int f \, d\tau \tag{2.1}$$

for a known function f in a known volume τ. This integral can be found by evaluating the function f at N randomly chosen points, which are uniformly distributed in the volume τ. For

instance in the one-dimensional case, [1]

$$I = \int_a^b f(x)dx \approx \frac{(b-a)}{N}\sum_{i=1}^{N} f(x_i) . \tag{2.2}$$

where $\{x_i\}$ are randomly chosen with equal probability in the interval $[a, b]$. An estimate of the error for the value obtained from such a procedure is given by the laws of statistics to be

$$\sigma_I^2 \approx \frac{1}{N}\sigma_f^2 = \frac{1}{N}\left[\frac{1}{N}\sum_{i=1}^{N}(f(x_i))^2 - \left(\frac{1}{N}\sum_{i=1}^{N} f(x_i)\right)^2\right] , \tag{2.3}$$

and it is determined by the deviation of f from its average value within the volume of integration.

Although this method will give us eventually the quantity we desire to obtain, it can be inefficient if we spend too much time sampling where f is small. We wish at this point to introduce the concept of importance sampling. The uncertainty in the Monte Carlo quadrature will be proportional to the variance of the integrand in Eq. 2.2. If we multiply and divide the integrand by a positive normalized weight function $w(x)$ such that

$$\int_a^b dx\ w(x) = 1 , \tag{2.4}$$

then the integral in Eq. 2.2 can be expressed as

$$I = \int_a^b dx\ w(x)\ \frac{f(x)}{w(x)} \approx \frac{(b-a)}{N}\sum_{i=1}^{N}\frac{f(x_i)}{w(x_i)} , \tag{2.5}$$

where x is distributed according to $w(x)$. One way to generate points from the distribution $w(x)$ is to change variables from x to y such that

$$y(x) = \int_a^x dx' w(x') , \tag{2.6}$$

such that

$$\frac{dy}{dx} = w(x); \quad y(x=a) = 0; \quad y(x=b) = 1 , \tag{2.7}$$

and the integral becomes

$$I = \int_0^1 dy\ \frac{f(x(y))}{w(x(y))} . \tag{2.8}$$

To evaluate the integral in Eq. 2.8 by Monte Carlo one evaluates f/w at a random sampling of points distributed according to y over the interval $[0, 1]$:

$$I \approx \frac{1}{N}\sum_{i=1}^{N}\frac{f(x(y_i))}{w(x(y_i))} . \tag{2.9}$$

[1] Integral evaluation by Monte Carlo is generally less efficient than most other methods for integrals of low dimensions.

If we choose a w which approximates f, f/w is a very smooth integrand, and the variance will be small. Also in Eq. 2.7 we can readily see that the distribution of points x is $dy/dx = w(x)$. The points sampled will be concentrated around the most "important" points $\{x\}$ where w (and consequently f) is large. The choice of w is determined by our ability to sample from it, either using Eqs. 2.6 and 2.9.

The one dimensional problem can be generalized to the N-dimensional case, $I = \int d\vec{x} f(\vec{x})$ for $\vec{x} = (x_1, x_2, \ldots, x_N)$, using

$$I \approx \frac{1}{M}\sum_{i=1}^{M} f(\vec{x}_i) \ , \tag{2.10}$$

where the components of $\vec{x}_i$ are chosen randomly and independently according to a known distribution. A normalized weight function $w(\vec{x})$ can be introduced as for the one-dimensional case presented above.

2.1.2 Introduction to quantum Monte Carlo

Quantum Monte Carlo (QMC) uses a Monte Carlo simulation to solve the Schrödinger equation, taking advantage of its analogy with classical diffusion processes[18, 19, 20]. The evolution in (real) time of concentration C can be described by

$$\frac{\partial C}{\partial \mathrm{t}} = D\nabla^2 C - kC \tag{2.11}$$

which is a diffusion equation with first order kinetics. The system described by the concentration function C can be simulated using this equation. A formal analogy can be made between Eq. 2.11 and the familiar time-dependent electronic Schrödinger equation in atomic units (c.f. Appendix A.1.):

$$-i\frac{\partial \Phi(\vec{R},\mathrm{t})}{\partial \mathrm{t}} = -\frac{1}{2}\nabla^2\Phi(\vec{R},\mathrm{t}) + V\Phi(\vec{R},\mathrm{t}) \ . \tag{2.12}$$

The only difficulty with this analogy is found in the complex nature of $\Phi(\vec{R},\mathrm{t})$. We know that $\Phi(\vec{R},\mathrm{t}) = e^{-iE\mathrm{t}}\phi(\vec{R})$, while C is obviously a real non-negative quantity. In order to interpret the wavefunction $\Phi(\vec{R},\mathrm{t})$ as a concentration, it has to be a real quantity as well. Therefore, we consider the Schrödinger equation in imaginary time ($t = i\mathrm{t}$):

$$-\frac{\partial \Phi(\vec{R},t)}{\partial t} = -D\nabla^2\Phi(\vec{R},t) + V(\vec{R})\Phi(\vec{R},t) \tag{2.13}$$

where $\vec{R}$ refers to a 3-N dimensional vector specifying the coordinates of the N electrons in the molecule, $\Phi(\vec{R},t)$ is the time-dependent many-body wave function of the system, $D \equiv \frac{1}{2}$, and $V(\vec{R})$ is the potential energy of the molecule given by

$$V(\vec{R}) = \sum_{i>j}\frac{1}{r_{ij}} - \sum_{i,\alpha}\frac{Z_\alpha}{r_{i\alpha}} + \sum_{\alpha>\beta}\frac{Z_\alpha Z_\beta}{r_{\alpha\beta}} \ , \tag{2.14}$$

where $r_{i\alpha}$ are distances from electron i to nucleus α, and r_{ij} and $r_{\alpha\beta}$ are interelectronic and internuclear distances, respectively. Now Eq. 2.12 becomes an ordinary differential equation with real variables, and therefore Φ can be interpreted as a concentration of imaginary particles called walkers or "psips." Anderson introduced the term Ψ particles or "psips" in [18, 21] to differentiate the imaginary particles in the QMC process from the particles in the physical system.

Equation 2.13 has the same form as Eq. 2.11. If we have the first term of Eq. 2.13 alone, the result is Fick's second law of diffusion:

$$\frac{\partial \Phi(\vec{R},t)}{\partial t} = D\nabla^2\Phi(\vec{R},t) , \tag{2.15}$$

which relates a first order derivative in time to a second order derivative in space of the time dependent wavefunction $\Phi(\vec{R},t)$, with diffusion constant D. On the other hand, if we only consider the second term in Eq. 2.13, i.e.,

$$\frac{\partial \Phi(\vec{R},t)}{\partial t} = -V(\vec{R})\,\Phi(\vec{R},t) , \tag{2.16}$$

we are left with a first order rate process in which the wavefunction grows or dies off depending on the sign of the rate constant $V(\vec{R})$. Since we are considering the wave function Φ in this context as a density of (imaginary) particles, this rate constant affects the population by determining how many of these particles are created or destroyed. That is, walkers can be allowed to propagate by diffusion (Eq. 2.15) and "branching" (Eq. 2.16) in a random walk in order to simulate Eq. 2.13.

The formal solution to Eq. 2.13 can be found by expanding the time-dependent wavefunction $\Phi(\vec{R},t)$ in a complete set of eigenfunctions of the Hamiltonian:

$$\Phi(\vec{R},t) = \sum_{i=0}^{\infty} c_i\phi_i(\vec{R})e^{-E_i t} \tag{2.17}$$

In the long time limit, $t \rightarrow \infty$, high energy states decay and the only surviving term is the ground state wavefunction, ϕ_0, with corresponding energy E_0,

$$\lim_{t\rightarrow\infty} \Phi(\vec{R},t) = c_0\phi_0(\vec{R})e^{-E_0 t} . \tag{2.18}$$

It is convenient to introduce an arbitrary reference energy, E_T, into the imaginary time dependence in Eqs. 2.17 and 2.18 which can be adjusted such that it reduces oscillations in the exponential term:

$$\begin{aligned} \Phi(\vec{R},t) &= \sum_{i=0}^{\infty} c_i\phi_i(\vec{R})e^{-(E_i-E_T)t} \\ \lim_{t\rightarrow\infty} \Phi(\vec{R},t) &= c_0\phi_0(\vec{R})e^{-(E_0-E_T)t} . \end{aligned} \tag{2.19}$$

Notice that if E_T (to be called the trial energy henceforth) is set to the ground state energy, the solution loses its time dependence and we are left with an equilibrium solution, i.e., $\frac{\partial\Phi(\vec{R},t)}{\partial t} = 0$.

The evolution of the wavefunction $\Phi(\vec{R},t)$ can be simulated using the Monte Carlo procedure. One must first choose an ensemble of imaginary particles (elsewhere called walkers, psips, or configurations) to represent the wave function at time zero. Each walker is a 3-N dimensional vector ($\vec{R}$) representing the positions of all N electrons in the system. These configurations evolve in a random walk with branching by allowing the electrons to diffuse while the nuclei remain fixed,[2] as follows. After taking a time step τ,[3] each walker takes a random step $\Delta\vec{R}$. The step is accepted with probability $\mathcal{Q}$ [4] ($0 < \mathcal{Q} < 1$) and branching of the new configuration is decided according to a multiplicity $\mathcal{M} \propto e^{-V\tau}$, given by first-order kinetics.[5] If the new configuration is accepted with probability $\mathcal{Q}$, $\mathcal{M}$ copies of the new configuration will appear in the updated ensemble. The energy can be computed at each step from the averaged potential as shown by Anderson in [18, 21]. Once equilibration is achieved, these energies can be averaged to obtain the energy of the system. At long times, the distribution of configurations will represent the ground state wavefunction, $\phi_0(\vec{R})$. Once more it is important to emphasize that because Eq. 2.13 is in imaginary time, this process does not correspond to any real dynamics.

2.1.3 Importance sampling

Thus far in our discussion, branching depends directly on the potential $V(\vec{R})$. However, since $V(\vec{R})$ diverges as two particles approach each other, there will be large fluctuations in the ensemble size causing large variances in the averages. Therefore we introduce importance sampling in order to use a distribution different from $\Phi(\vec{R},t)$ and still obtain the same averages, but reduce the fluctuations by sampling only most probable regions in space.

One can multiply the time dependent Schrödinger equation in imaginary time (Eq. 2.13) by a known trial function $\Psi_T(\vec{R})$,

$$-\Psi_T(\vec{R})\frac{\partial\Phi(\vec{R},t)}{\partial t} = \Psi_T(\vec{R})\left\{-D\nabla^2\Phi(\vec{R},t) + V\Phi(\vec{R},t) - E_T\Phi(\vec{R},t)\right\} . \tag{2.20}$$

Add and substract the terms $2D\Phi(\vec{R},t)\nabla^2\Psi_T(\vec{R})$ and $2D\nabla\Phi(\vec{R},t)\nabla\Psi_T(\vec{R})$ from Eq. 2.20,

$$\begin{aligned}-\frac{\partial\Phi(\vec{R},t)\Psi_T(\vec{R})}{\partial t} &= -D\Psi_T\nabla^2\Phi + (V-E_T)\Phi\Psi_T + 2D\Phi\nabla^2\Psi_T - 2D\Phi\nabla^2\Psi_T \\ &\quad +2D\nabla\Phi\nabla\Psi_T - 2D\nabla\Phi\nabla\Psi_T . \end{aligned} \tag{2.21}$$

[2] In principle this method is not constrained by the Born Oppenheimer approximation mentioned in Chapter 1. However, the QMC approach presented in this work deals only with the solution of the electronic Schrödinger equation. For instance, Traynor *et al.*[22] have done QMC calculations without the Born Oppenheimer constraint.

[3] Notation used in this chapter: t is used for real time, t for imaginary time and τ for time steps.

[4] Anderson's simple algorithm[18] did not have a probability for acceptance/rejection. The configurations simply were killed if $\mathcal{M} = 0$.

[5] As done with the reference or trial energy in Eq. 2.19, an offset or reference potential, V_{ref}, can be used for this probability[18, 21].

And finally, rearrange terms and rewrite Eq. 2.21 in terms of a new distribution, $f(\vec{R},t) = \Phi(\vec{R},t)\Psi_T(\vec{R})$:

$$
\begin{aligned}
-\frac{\partial f(\vec{R},t)}{\partial t} &= [-D\Psi_T\nabla^2\Phi - D\Phi\nabla^2\Psi_T - 2D\nabla\Psi_T\nabla\Phi] + [(-D\nabla^2\Psi_T + V\Psi_T)\Phi - E_T\Psi_T\Phi] \\
&\quad +2D\nabla\Phi\nabla\Psi_T + 2D\Phi\nabla^2\Psi_T \\
&= -D\nabla^2(\Phi\Psi_T) + \left[\frac{-D\nabla^2\Psi_T + V\Psi_T}{\Psi_T} - E_T\right](\Phi\Psi_T) + D\nabla\cdot(2\Phi\nabla\Psi_T)\,, \qquad (2.22)
\end{aligned}
$$

to obtain a new equation with diffusion $\{-D\nabla^2 f\}$, branching $\{(E_L(\vec{R}) - E_T)f\}$, and drift $\{D\nabla\cdot(f\vec{F}_Q)\}$ terms,

$$
\begin{aligned}
&= -D\nabla^2 f + \left[\frac{\hat{\mathcal{H}}\Psi_T}{\Psi_T} - E_T\right] f + D\nabla\cdot\left(f\frac{2\nabla\Psi_T}{\Psi_T}\right) \\
-\frac{\partial f}{\partial t} &= -D\nabla^2 f + (E_L(\vec{R}) - E_T)f + D\nabla\cdot(f\vec{F}_Q)\,. \qquad (2.23)
\end{aligned}
$$

In Eq. 2.23 we have introduced two new quantities: (1) the *local energy*, E_L (cf. Appendix A.8.),

$$
E_L(\vec{R}) \equiv \frac{\hat{\mathcal{H}}\Psi_T(\vec{R})}{\Psi_T(\vec{R})} = \frac{(\hat{T}\Psi_T(\vec{R}) + \hat{V}\Psi_T(\vec{R}))}{\Psi_T(\vec{R})}\,; \qquad (2.24)
$$

and (2) the *quantum force*, $\vec{F}_Q$, which is a gradient to a potential field, $\ln|\Psi_T|^2$,

$$
\vec{F}_Q(\vec{R}) \equiv \frac{2\nabla\Psi_T(\vec{R})}{\Psi_T(\vec{R})} = \nabla\ln|\Psi_T(\vec{R})|^2\,. \qquad (2.25)
$$

There are several advantages to importance sampling. First, the new drift term, $D\nabla\cdot(f\vec{F}_Q)$, imposes a drift velocity so that configurations will move towards the most probable regions in space where Ψ_T, chosen to approximate ϕ_0, is large. Second, the new (first order) rate term, $(E_L - E_T)f$, now depends on the local energy, $E_L(\vec{R})$. The local energy $E_L(\vec{R})$ is a smoother function than the potential $V(\vec{R})$, since the kinetic energy term, $\hat{T}\Psi_T/\Psi_T$, can cancel the singularities in $V(\vec{R})$.[6] (The requirement on Ψ_T that the local kinetic and potential energies cancel out singularities is known as the cusp condition[20].) Now the energies averaged are "local energies." Hence for a good choice of Ψ_T, E_L can be made nearly constant, therefore keeping the size of the ensemble approximately constant as well, greatly reducing the statistical fluctuations[23], and thus increasing the sampling efficiency. Also, the ensemble average of E_L over the asymptotic distribution yields the ground state energy thanks to the hermiticity of the Hamiltonian:

$$
\langle E_L\rangle = \frac{\int d\vec{R}\, f(\vec{R})E_L}{\int d\vec{R}\, f(\vec{R})} = \frac{\int d\vec{R}\,\phi_0\Psi_T\left[\frac{\hat{\mathcal{H}}\Psi_T}{\Psi_T}\right]}{\int d\vec{R}\,\phi_0\Psi_T} = \frac{\int d\vec{R}\,[\phi_0\hat{\mathcal{H}}]\Psi_T}{\int d\vec{R}\,\phi_0\Psi_T} = E_0\,. \qquad (2.26)
$$

[6] For example, Anderson's first approach did not use guiding functions, and obtained the energies by sampling from the potential [18, 21]. In [23] he showed improvement by a factor of ten with the inclusion of a trial function.

It becomes obvious from Eq. 2.26 that the choice of trial function affects only the variance of the average, not the average value itself. This constitutes one of the main strengths of QMC, since the results of the calculations will be insensitive to the choice of Ψ_T, while still recovering the correlation energy. This means that, in principle, choices of atomic basis set, functional form, etc. will not directly influence the averages. For molecular systems, one usually chooses Ψ_T as a product of a linear combination of Slater determinants of molecular spin orbitals (See Sec. 1.1.), and a correlation function which depends on the interparticle distances. A single determinant has been found to give excellent results in most cases. (For examples, see Sec. 2.2.1.) Some Ψ_T choices will be discussed in more detail in Sec. 2.1.4.4.

2.1.4 Fixed-node diffusion quantum Monte Carlo

The variant of QMC which imposes the short time and fixed-node approximations is known as fixed-node diffusion quantum Monte Carlo (FNDQMC or FNDMC)[20]. The term diffusion Monte Carlo (DMC) is used when at least the short-time approximation is made. In the following two sections these approximations are described. A presentation of the computational algorithm and a discussion on trial functions follow.

2.1.4.1 Short-time approximation

We may write the Schrödinger equation in integral form by slightly manipulating Eq. 2.17. Expanding $\Phi(\vec{R},0)$ in eigenfunctions ϕ_n of the Hamiltonian, then $\Phi(\vec{R},0) = \sum_n c_n \phi_n(\vec{R})$, where the c_n coefficients are given by

$$c_n = \int d\vec{R} \;\; \phi_n^*(\vec{R})\Phi(\vec{R},0) \; . \tag{2.27}$$

Using this last expression for the eigenstate expansion coefficients in Eq. 2.17,

$$\Phi(\vec{R}',t) = \sum_n \left[\int d\vec{R} \; \phi_n^*(\vec{R})\Phi(\vec{R},0) \right] e^{-tE_n} \phi_n(\vec{R}') \; , \tag{2.28}$$

which is equivalent to (by interchanging the order of integration and summation)

$$\Phi(\vec{R}',t) = \int d\vec{R} \left[\sum_n \phi_n^*(\vec{R})\phi_n(\vec{R}')e^{-tE_n} \right] \Phi(\vec{R},0) \; . \tag{2.29}$$

This equation formally relates the wavefunction $\Phi(\vec{R}',t)$ to the initial wavefunction, $\Phi(\vec{R},0)$. Since we recognize Eq. 2.29 as the Schrödinger equation in integral form, we can define

$$G(\vec{R} \rightarrow \vec{R}';t) \equiv \sum_n \phi_n^*(\vec{R})\phi_n(\vec{R}')e^{-tE_n} \tag{2.30}$$

as the Green's function. (See Appendix A.10.) Although this formal definition is useless for practical computations since we do not know E_n and $\phi_n(\vec{R})$, we can still apply the formalism in

a more practical form. The evolution of $\phi(\vec{R}',t)$ is represented by means of the Green's function to be

$$\Phi(\vec{R}',t+\tau) \;=\; \int d\vec{R}\; G(\vec{R}\rightarrow\vec{R}';\tau)\Phi(\vec{R},t)\;, \tag{2.31}$$

where $G(\vec{R}\rightarrow\vec{R}';\tau)$ is the transition probability of moving from configuration $\vec{R}$ to $\vec{R}'$ in time τ. Since (after introduction of importance sampling) we think of the distribution $f(\vec{R},t)$ as a concentration or density of imaginary particles, we can approximate it with an ensemble of walkers which will propagate using $G(\vec{R}\rightarrow\vec{R}';\tau)$. For this reason, $G(\vec{R}\rightarrow\vec{R}';\tau)=\langle\vec{R}'|e^{-\tau\hat{\mathcal{H}}}|\vec{R}\rangle$ is known as the "propagator," since a given distribution $f(\vec{R},t)$ can be propagated for a finite time interval τ using the Green's function. The probability of moving a walker with coordinates $\vec{R}$ to position $\vec{R}'$ is given by

$$\frac{|\Psi_T(\vec{R})|}{|\Psi_T(\vec{R}')|}\times G(\vec{R}\rightarrow\vec{R}';\tau)\;, \tag{2.32}$$

and detailed balance is obtained by using the ratio of the probability of going from $\vec{R}$ to $\vec{R}'$ and the probability of going back from $\vec{R}'$ to $\vec{R}$ (See Eq. 2.38.) as the weight to accept the move. Also, G is a solution to Eq. 2.13 with boundary condition $G(\vec{R}\rightarrow\vec{R}';0)=\delta(\vec{R}'-\vec{R})$. Unfortunately we still don't know how to evaluate $G(\vec{R}\rightarrow\vec{R}';\tau)$.

In general,

$$G(\vec{R}\rightarrow\vec{R}';t) \;=\; \langle\vec{R}'|e^{-t\hat{H}}|\vec{R}\rangle \;=\; \langle\vec{R}'|e^{-t(\hat{T}+\hat{V})}|\vec{R}\rangle\;, \tag{2.33}$$

but since $\hat{T}$ and $\hat{V}$ do not commute, Eq. 2.33 is still analytically unsolvable! However, for small time steps τ we may approximate the Taylor expansion of the exponential as follows:

$$\begin{aligned} e^{\tau(\hat{T}+\hat{V})} &= \tau(\hat{T}+\hat{V}) + \frac{\tau^2}{2!}(\hat{T}+\hat{V})^2 + \frac{\tau^3}{3!}(\hat{T}+\hat{V})^3 + \cdots \\ &= \tau\hat{T} + \frac{\tau^2}{2!}\hat{T}^2 + \frac{\tau^3}{3!}\hat{T}^3 + \cdots + \tau\hat{V} + \frac{\tau^2}{2!}\hat{V}^2 + \frac{\tau^3}{3!}\hat{V}^3 + \cdots \\ &\qquad + \frac{\tau^2}{2!}(\hat{T}\hat{V}+\hat{V}\hat{T}) + \cdots \\ &\approx e^{-\tau\hat{T}}e^{-\tau\hat{V}} + \mathcal{O}(\tau^2) \end{aligned} \tag{2.34}$$

Using this approximation one can solve Eq. 2.33 and get the Green's function for the short-time approximation (STA),

$$G_{\mathrm{STA}}(\vec{R}\rightarrow\vec{R}';\tau) \;=\; (4\pi D\tau)^{-3N/2}e^{-(\vec{R}'-\vec{R})^2/4D\tau}e^{-(V(\vec{R})-E_T)D\tau}\;, \tag{2.35}$$

which is a product of the free particle diffusion Green's function (See Appendix A.10.1.) and a branching term which determines the multiplicity or (growth/death) of the ensemble. After the inclusion of importance sampling, our propagator becomes

$$G^f_{\mathrm{STA}}(\vec{R}\rightarrow\vec{R}';\tau) \;=\; (4\pi D\tau)^{-3N/2}e^{-(\vec{R}'-\vec{R}-D\tau\vec{F}_Q(\vec{R}))^2/4D\tau}e^{-[(E_L(\vec{R})+E_L(\vec{R}'))/2-E_T]D\tau}\;. \tag{2.36}$$

This $G^{f}_{\mathrm{STA}}(\vec{R} \rightarrow \vec{R}';\tau)$ is the short-time approximation which solves Eq. 2.23 for the mixed distribution $f = \Psi_T \phi$.

This approximation leaves us with a first-order error in the energy.[7] In practice, this approximation means that several calculations at small time steps are required in order to compute a DMC energy. These results are extrapolated by linear regression to $E(\tau \rightarrow 0)$. Examples of these time-step extrapolations will be presented in the present work whenever a QMC energy is determined (e.g., see Fig. 2.3). This dependence of the DMC energy on time step (i.e., non-zero slope of E vs. τ curve) is known as "time-step bias." A discussion on the time-step bias of the energy and its linearity is presented at length in Ref. [29]. Determining how small the time step should be in order to get linear dependence of the energy is not always obvious. In practice, one computes and collects the local energy at each step of the random walk, averaging over the walkers. The averages along the walk are divided into *blocks* to eliminate serial correlation, i.e., the smaller the time step taken, the larger the block needs to be. When such small time steps are taken, it becomes very difficult to obtain uncorrelated averages since the correlation among blocks increases as τ gets smaller, and we are forced to consider a new problem. Autocorrelation will be discussed in more detail in Chapter 4.

2.1.4.2 Fixed node approximation

One final consideration comes from the anti-symmetric nature of the wave functions we must use in describing fermions, i.e., such wave functions must change sign with interchange of two electrons.[8] We also know that we must have a positive density of walkers in Eq. 2.23. Since this density is given by $f(\vec{R},t)$, which is a product of a known trial function, $\Psi_T(\vec{R})$, and the unknown exact ground state wavefunction, $\Phi_0(\vec{R},t)$, this could pose a problem where Ψ_T and Φ_0 differ in sign.

In the "fixed-node" approach presented here, the nodes of Ψ_T are imposed on Φ_0. This is implemented by rejecting any walker that crosses the nodes of Ψ_T. In this manner the simulation is performed in each nodal volume (i.e., volumes defined by the nodes of Ψ_T), and the DMC energy will be limited by how well the nodes of the chosen Ψ_T approximate those of the exact ground-state function $\Phi_0(\vec{R},t)$. If Ψ_T has the exact nodes of the system, then $f_\infty = \phi_0 \Psi_T$, and the DMC energy will converge to the exact ground-state energy. Otherwise, a fixed-node state, $f_\infty = \tilde{\phi}_0 \Psi_T$, where $\tilde{\phi}_0$ is the fixed-node solution will be obtained. This is known as the fixed-node (FN) approximation[20]. The fixed-node method was introduced to electronic structure problems by Anderson in [21].

[7] Moskowitz and Schmidt[24] claimed that the Green's function given in Eq. 2.36 was not a correct short-time approximation (i.e., in the limit of $\tau \rightarrow 0$). Three papers[25, 26, 27] quickly followed to correct the error, and the contradiction was settled[28].

[8] This requirement leads to the "sign problem" in QMC.

An important repercussion of the fixed-node approximation is that the computed energy now depends on the nodes of Ψ_T. For special cases in which the nodes are known from either spin[30] or spatial[21] symmetry, the fixed-node solution is exact. Unfortunately, little is known about the complicated geometry of the nodal hypersurfaces for many-body systems.[9] Reynolds *et al.* showed in [20] that given a set of nodes, the FN energy is a variational upper bound to the ground-state energy. The fixed-node approximation also leads to an additional time-step bias. This bias arises when a walker crosses two nodes or the same node twice without being detected in a single time step. The "cross-recross"[21] error incorrectly increases the population near the nodes. Table 2.1 shows examples of the quality of results obtained in the past using the FN approximation.

2.1.4.3 Algorithm

In Sec. 2.1.4.1 we mentioned how the QMC walk is performed at different time steps by taking many very small steps which are then collected into blocks large enough to eliminate serial correlation. Our implementation of the DMC algorithm for one block is as follows:

(0) Choose Ψ_T

(1) Choose N_k configurations to form the initial ensemble distributed according to $f(\vec{R}, 0) = |\Psi_T|^2$

(2) For each step,

(a) For each configuration k,

(1) For each electron i,

(a) Calculate local energy, $E_L(\vec{R}_i)$, and quantum force, $\vec{F}_Q(\vec{R}_i)$.

(b) Move electron coordinate according to

$$\vec{R}_i' = \vec{R}_i + D\tau\vec{F}_Q(\vec{R}_i) + \vec{\chi}\,, \tag{2.37}$$

where $\vec{\chi}$ is a normalized random Gaussian number ($\langle\chi^2\rangle = 2D\tau$).

(c) Calculate new local energy, $E_L(\vec{R}_i')$, and quantum force, $\vec{F}_Q(\vec{R}_i')$.

(d) Reject move if node is crossed.

(e) Accept move ($\vec{R}_i'$ becomes $\vec{R}_i$) according to Metropolis-like[19] weight:

$$W(\vec{R}_i', \vec{R}_i) = \frac{|\Psi_T(\vec{R}_i')|^2\, G(\vec{R}_i' \to \vec{R}_i, \tau)}{|\Psi_T(\vec{R}_i)|^2\, G(\vec{R}_i \to \vec{R}_i', \tau)} \tag{2.38}$$

and update.

(2) Calculate $E_L(\vec{R}')$, branching ($M \equiv e^{D\tau[(E_L(\vec{R})+E_L(\vec{R}'))/2-E_T]}$) and other quantities of interest.

(3) Add ME_L and M to running totals.

[9] See [31] and references therein.

Figure 2.1: Evolution of configurations during a random walk. Each box represents a fictitious walker, with the large circle as the nucleus, and 3 smaller circles as the electrons. The figure illustrates a diffusion step followed by branching.

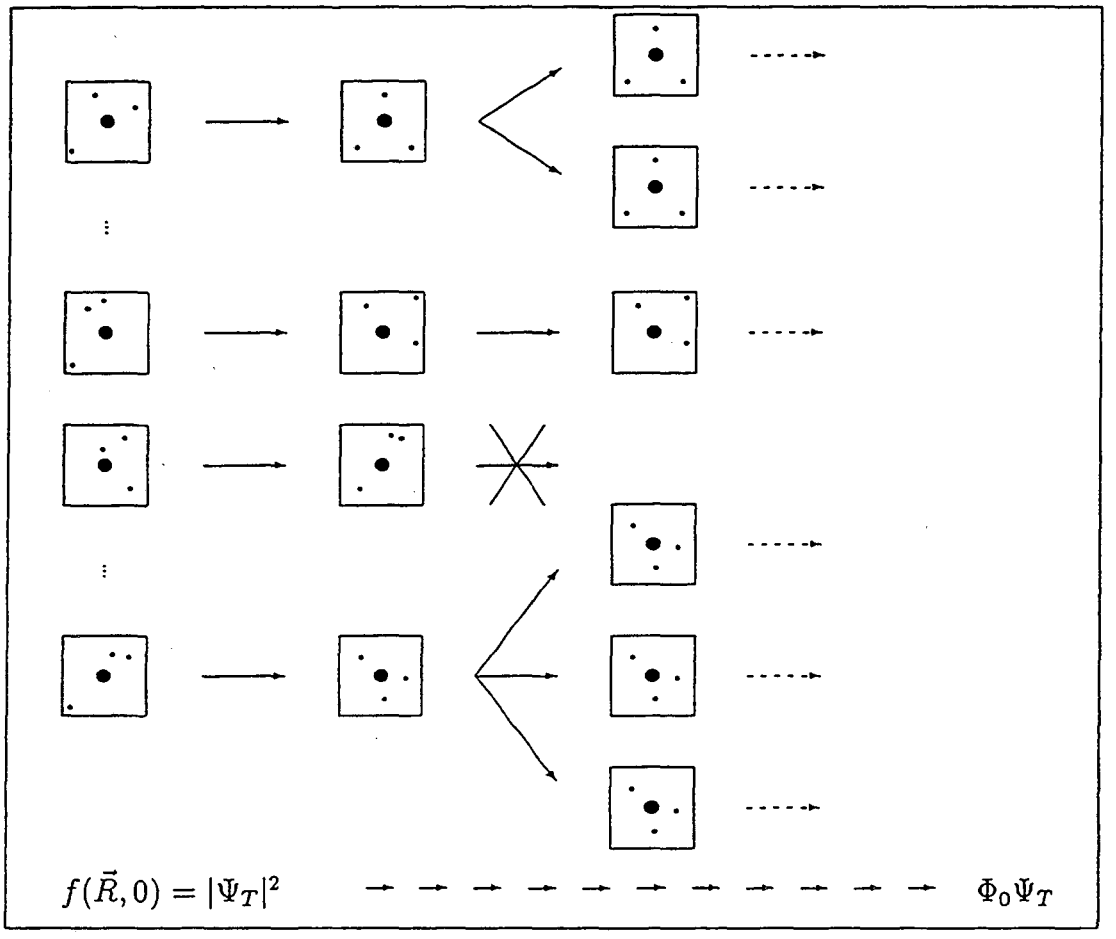

(4) Make M copies of the configuration.

(b) Average local energies, i.e., $\langle E_L\rangle_k \approx \langle ME_L\rangle_k/\langle M\rangle_k$.

(c) Update trial energy.

(d) Print block averages.

Figure 2.1 illustrates a few walkers, and what happens to them during diffusion followed by branching. In the diffusion step, the electron moves to a new position, and depending on its probability, the configuration will move on, or die off. The first walker branches to create two new configurations, while the last one creates three, and one of the walkers dies off. The program used in this work to implement the above algorithm is called QMagiC and is documented in Appendix C.

2.1.4.4 Trial functions

The trial function Ψ_T plays an important role in the implementation of the FNDMC algorithm. It is used as the guiding function for the evolution of the ensemble in the FNDMC process. The branching term in Eq. 2.23 depends on the "excess local energy"[32] $(E_L(\vec{R}) - E_T)$, which for $\Psi_T \approx \Phi(\vec{R}, t)$ will imply a smooth $E_L(\vec{R})$, and result in a multiplicity $M \sim 1$.

The second, and perhaps most important role of the trial function in FNDMC, is in fixing the nodes of the system to approximate the nodes of the exact ground state wave function. Unfortunately, very little is known about the nodal hypersurfaces involved in this type of computation. Although some work on studying the nodes of trial functions has been done within the QMC framework[31, 33], there is still a long way to go along these lines.

Ideally one wants a trial function that is as simple and compact as possible since one needs to compute Ψ_T, its first $(\partial\Psi_T/\partial x_i)$, and second $(\partial^2\Psi_T/\partial x_i^2)$ derivatives at each step of the walk.(See Sec. 2.1.4.3.) The trial function should also be as accurate as possible, give the smallest possible statistical variance, and have a small time step bias. We know that if the trial function is the exact wave function, the variance and the time step bias would disappear. Barnett presented some work related to determining trial functions whose time step biases were negligible in [34]. In that work, several small systems (such as H_3, Li, LiH) were studied using different wave functions which satisfied both the electron-electron and (on average) electron-nuclear cusp conditions. It was found that the extrapolated energy coincided with the smallest time steps tried, so the time step bias was considered insignificant. Unfortunately, lack of time-step bias cannot be generally assumed, even for highly accurate wave functions, especially lacking general knowledge of what the "smallest" time step ought to be. In Chapter 3 we shall study more closely how the wave function choice for a family of systems affects the recovery of the correlation energy, variance and time step bias of QMC calculations.

A popular choice for Ψ_T has been to use a variational (HF or post-HF) wave function multiplied by a correlation factor, i.e., $\Psi_T = A \cdot C$, where A is a Slater determinant or linear combination of Slater determinants, and C is a correlation factor (typically chosen to be an exponential such that no nodes are introduced) which explicitly includes factors of interparticle distances. In this type of wave function, the location of the nodes of Ψ_T, which determine the FN energy, depend on the Slater determinant(s) of molecular spin orbitals (See Sec. 1.1.) obtained from a previous variational calculation using standard quantum chemistry computer programs. If A is composed of a single determinant, a spin factorization into α and β electrons is possible, i.e., $A = D^\alpha D^\beta$, to speed up the computation and to incorporate spin into the walk.

At this point it is useful to recall that even though the fixed-node energy is an upper bound, QMC is not a variational method,[10] and it directly simulates electron correlation. For

[10] QMC is not variational since it does not apply the variational principle to optimize parameters.

instance, in *ab initio* methods one needs large expansions of basis functions and determinants, i.e., these methods do not account for instantaneous correlation unless large expansions are employed to better approximate correlation effects on the results. An example can be found in the case of a QMC study of Li_2[35] wave functions, where a compact (four-determinant) wave function is sufficient to properly treat dissociation and achieve chemical accuracy. However, it has been shown[36] that polarization functions can play an important role in properly describing the system in QMC. For example, state-of-the-art *ab initio* calculations could include up to *g*-functions for an atom such as C[37], while *d*- functions might suffice for accuracy in QMC.

Since a large basis set slows down the calculation (especially in QMC), our group uses a cubic spline routine[38], an approach introduced by Garmer and Anderson in [39] to fit the MOs of the wave function. This procedure is done only once at the beginning of each calculation, therefore reducing the CPU time it takes to compute a large AO expansion at every step in the walk. This type of capability also enables one to study and correct the cusp behavior of large contracted GTO basis sets[11] by QMC. In a study on the F atom, it was found that the lack of cusp of the GTO basis in the region near $R = 0$ caused serious problems in the calculation of the QMC energy[38]. In Gaussian orbitals, the wave function's first derivative is 0 at the origin, while for Slater orbitals it is discontinuous. This means that during the random walk as electrons get close to the nucleus, the quantum force will push them away when using Slaters, while if using Gaussians the electrons might get undesirably close. (This results in non-physically low energies, which can branch out of control.[12]) A solution to this problem was attempted by extrapolating the correct cusp behavior for each MO, but the procedure proved to be too cumbersome.[13] The good news is that in QMC we can always use STO functions which inherently do not have this problem, the bad news is that since STO functions are so hard to integrate in *ab initio* approaches, there has been little done on obtaining STO-based (single- or multi-determinant) wave functions for non-linear molecules.

Let us now turn our attention to the correlation factor, C, mentioned above. Since C is chosen to have the form e^U, it is always positive and therefore introduces no nodes.[14] As a consequence, the DMC energy will not be affected by the choice of U and its parameters; on the other hand, U can be chosen to minimize the variance and time step bias of the walk. U can include both electron-electron and electron-nuclear distances. In the past, U has been chosen

[11] Contracted GTO basis sets defined in Appendix A.3.

[12] Since the branching term $\exp[-(E_L - E_T)]$ blows up.

[13] The additional approximation involved finding the point at which the Gaussian's first derivative changed sign and then substituting the knots in the spline by those from a Slater until it reached $r = 0$ to ensure that the first derivative had proper cusp behavior at the origin.

[14] The use of linear combinations of Slater determinants with correlation factors on each term of the expansion has not been fully explored yet. In this type of trial function, the correlation factor would obviously affect the position of the nodes.

to satisfy the cusp conditions[15] of the Schrödinger equation[20]. One popular form of U is the linear Padé-Jastrow form,

$$U_{ij} = \frac{ar_{ij}}{1+br_{ij}}, \tag{2.39}$$

where the coefficient a is fixed to satisfy the cusp condition (see Appendix A.8.1), and the second parameter b can be optimized in a MC walk. Figure 2.2 shows electron-electron and electron-nuclear Jastrow functions; their effects on the trial function can be inferred from the Coulomb interaction between the charged particles. That is, the electron-electron repulsion will make the wave function small for $r_{ij} \rightarrow 0$, while the electron-nuclear attraction will make the wave function large when $r_{i\alpha} \rightarrow 0$.

Other functional forms can be used as well, but we will not go into detail here. Two other forms will be introduced in Chapter 3. Several papers have been written on parameter optimization for QMC based on minimization of either the variational energy[40] or its variance [41, 42]. Efforts to optimize correlation function parameters, Slater determinant and MO coefficients simulatenously[35] have had limited success in improving the nodes of the trial function. Such an optimization runs the risk of introducing undesirable new nodes into the trial function. On the other hand, Umrigar[43] succeeded in a similar all parameter optimization on a more flexible (more optimized parameters) wave function to lower the QMC energy of some small systems. As systems get larger, such approaches get prohibitive.

In Chapter 3, we perform some numerical experiments on how to choose a trial function for a polyatomic system. We base our study on experience gained from QMC studies on its fragments. This should give some insight on how to tackle more complex systems.

2.1.5 Variational Monte Carlo

Variational Monte Carlo (VMC) evaluates the expectation values of an operator of a trial wave function Ψ_T by Monte Carlo (MC) integration. For instance, the expectation value of the Hamiltonian is

$$\langle\hat{\mathcal{H}}\rangle = \frac{\langle\Psi_T|\hat{\mathcal{H}}|\Psi_T\rangle}{\langle\Psi_T|\Psi_T\rangle} = \frac{\int d\vec{R} f(\vec{R}) E_L}{\int d\vec{R} f(\vec{R})} = \frac{\int d\vec{R}|\Psi_T|^2 \left[\frac{\hat{\mathcal{H}}\Psi_T}{\Psi_T}\right]}{\int d\vec{R}|\Psi_T|^2} = \langle E_L\rangle . \tag{2.40}$$

Since no analytical integration is required, VMC provides an inexpensive and competitive way of computing properties of wave functions which are computationally too difficult for *ab initio* methods[44, 45]. One example of this is obtaining energies of wave functions that include electron correlation explicitly due to the difficulty in computing the integrals. For instance, the type of trial functions discussed in Sec. 2.1.4.4 would make integration an insurmountable task. Coldwell and Lowther presented a VMC calculation using Hylleraas-type functions in [46]. Also, VMC

[15] See Appendix A.8.1.

can yield properties such as derivatives[47] and polarizabilities[45] as "pure expectation values," which in DMC become "mixed expectation values"[34]. Mixed expectation values are difficult to obtain at the same level of accuracy of pure expectation values.

Another common use of VMC is for the variational optimization of parameters in the wave functions. Since VMC samples the local energy, E_L, of a known trial wave function,[16] we know that for wave functions other than the exact, the variance will be non-zero. (See Appendix A.8.) By minimizing the variance of trial functions, VMC can be used to approximate the exact solution.

VMC has no time step bias which makes its convergence much faster than for DMC since larger time steps can be used. This results in shorter, less correlated (i.e., more efficient) walks, and no time-step extrapolations. Like in DMC, importance sampling can be included in VMC to bias the walk. That is, the walk can be guided by a drift vector, $\vec{F}_Q$, just as shown in Sec. 2.1.3. Operationally, the implementation of VMC is identical to the DMC algorithm presented in Sec. 2.1.4, except for the lack of branching. In VMC there will be no creation or death of walkers, so the number of walkers is constant. Another difference with the FNDMC procedure is in the treatment of the nodes, since no attention is being paid to the location of the nodes in the wave function, or to walkers that cross those nodes. The guided VMC algorithm will be discussed at greater length in Chapter 4.

2.1.6 Exact QMC methods

As their name suggests, "exact" QMC methods attempt to perform the simulation described in Sec. 2.1.4, lifting the short-time and fixed-node approximations. Eliminating the STA requires sampling from the exact Green's function without necessarily knowing its analytical form. Several efforts have proved succesful in this direction; for instance, early work by Kalos[48], and more recently by Ceperley[49] and Anderson[50, 51]. However, removing the FN approximation, which was originally introduced as a solution to the fermion "sign-problem," constitutes a greater challenge. Recently, there has been a surge of different new approaches to this end[50, 52].

2.1.6.1 Sampling the exact Green's function

Ceperley and Alder[49, 53] succeeded in sampling the exact propagator for small systems with their Green's function Monte Carlo (GFMC)[17] method. This approach strives to sample the exact GF, without knowing it analytically by means of intermediate walks. The first step in

[16] This can be contrasted with DMC which samples the exact ground state wave function and uses the trial function as a guiding function.

[17] Some authors use the term GFMC as a general name for all QMC methods which use a Green's function in their random walks. In this work we shall use GFMC for exact GF methods only.

this endeavor is to relate the exact GF to an approximate trial Green's function, G_D,[18] given by

$$G_D(\vec{R},\vec{R}';\tau) \;=\; (4\pi D\tau)^{-3N/2} e^{-(\vec{R}'-\vec{R}-D\tau\vec{F}_Q(\vec{R}))^2/4D\tau} \;. \tag{2.41}$$

An expansion of the exact Green's function, G, is generated in terms of an approximate G_T, as

$$G(\vec{R},\vec{R}';\tau) \;=\; G_T(\vec{R},\vec{R}';\tau) \;+\; \int_0^\tau dt \int d\vec{R}''\, G(\vec{R},\vec{R}'';\tau-t) K(\vec{R}'',\vec{R}';t) \;, \tag{2.42}$$

which is a Fredholm integral equation of the second kind,[19] where $G_T(\vec{R},\vec{R}';0) = \delta(\vec{R}-\vec{R}')$ for small times τ, and the kernel K, given by

$$K(\vec{R}'',\vec{R}';t) \;=\; -\left[\hat{\mathcal{H}}(\vec{R}'') + \frac{\partial}{\partial t}\right] G_T(\vec{R}'',\vec{R}';0) \;, \tag{2.43}$$

provides a transition probability to an intermediate $\vec{R}''$ between $\vec{R}$ and $\vec{R}'$. Equation 2.42 is averaged over time with probability distribution function (p.d.f.) $\frac{1}{\Delta}e^{-\tau/\Delta}$ such that one gets a time-independent GF,

$$\tilde{G}(\vec{R},\vec{R}') \;=\; \int_0^\infty \frac{d\tau}{\Delta}\, e^{\tau(E_T-1/\Delta)} \frac{\Psi_T(\vec{R})G(\vec{R},\vec{R}';\tau)}{\Psi_T(\vec{R})} \;, \tag{2.44}$$

where $\tilde{G}$ is the Laplace transform of G in time. Equation 2.42 becomes

$$\tilde{G}(\vec{R},\vec{R}') \;=\; \tilde{G}_T(\vec{R},\vec{R}') \;+\; \Delta \int d\vec{R}''\, \tilde{G}(\vec{R},\vec{R}'')\tilde{K}(\vec{R}'',\vec{R}') \;, \tag{2.45}$$

where $\tilde{G}_T$ and $\tilde{K}$ are defined as $\tilde{G}$ was defined in Eq. 2.44 (i.e., averaged over time); and the evolution of the probability distribution is

$$f_{n+1}(\vec{R}) = \int d\vec{R}'\tilde{G}(\vec{R},\vec{R}')f_n(\vec{R}') \tag{2.46}$$

where f_n is called the n-th generation.

The general scheme of the algorithm is as follows:

(1) Starting at $\vec{R}$, sample a time step from p.d.f. $\frac{1}{\Delta}e^{-\tau/\Delta}$.

(2) Diffuse and drift with G_D (as in DMC), getting to new $\vec{R}'$ in space.

(3) Branch with direct multiplicity,

$$m_D(\vec{R},\vec{R}';\tau) = e^{E_T\tau} \frac{\Psi_T(\vec{R})G_T(\vec{R},\vec{R}';\tau)}{\Psi_T(\vec{R}')G_D(\vec{R},\vec{R}';\tau)} \;, \tag{2.47}$$

obtained from the first term in the integral equation (see Ref. [49]). These will be called direct configurations.

[18] We can readily recognize this as the diffusion Green's function derived in Appendix A.10.1, after importance sampling has been added.

[19] See Appendix A.10.2 for definition and solution by successive substitution scheme.

(4) Generate intermediate configurations by branching with multiplicity

$$m_I(\vec{R},\vec{R}';\tau) \;=\; \frac{K(\vec{R},\vec{R}';\tau)m_D(\vec{R},\vec{R}';\tau)\Delta}{G_T(\vec{R},\vec{R}';\tau)} \;. \tag{2.48}$$

This is the first iteration in Eq. 2.45 since $\tilde{G}_T$ has been substituted in the integral as a first approximation to $\tilde{G}$. These intermediate configurations are not included in the averages, but originate new random walks.

(5) The intermediates continue steps (2)-(4)[20] to correctly sample $\tilde{G}(\vec{R},\vec{R}')$.

(6) When all intermediates generated have been processed, the f_1 generation has been sampled and it is time to move on to the second generation. Since a variable time step is used, the time-step bias is removed and use of larger time steps allows for more efficient sampling. However, this increase in efficiency is undermined by the creation of intermediate walkers which do not contribute to averages.

We next present the GFMC method for nodeless systems by Kalos[54] as recently described by Anderson *et al.* in [50]. Start by expressing the time-independent Schrödinger equation

$$-\,D\nabla^2\Psi(\vec{R}) + V(\vec{R})\Psi(\vec{R}) = E\Psi(\vec{R}) \tag{2.49}$$

as

$$-\,\nabla\Psi(\vec{R}) + k^2\frac{V(\vec{R})}{E}\Psi(\vec{R}) \tag{2.50}$$

where $k^2 \equiv -E/D$. The Green's function for Eq. 2.50 is

$$G_0(\vec{R},\vec{R}') = \left(\frac{1}{2\pi}\right)^{3N/2}(k|\vec{R}-\vec{R}'|)^{1-3N/2} \times K_{3N/2-1}(k|\vec{R}-\vec{R}'|)\;, \tag{2.51}$$

where K_υ is the modified Bessel function of the second kind. Thus, writing Eq. 2.50 in integral form,

$$\Psi(\vec{R}) = \int G_0(\vec{R},\vec{R}')\frac{V(\vec{R})}{E}\Psi(\vec{R}')\;d\vec{R}'\;, \tag{2.52}$$

determines the sampling procedure when solved iteratively.

Importance sampling is included[55] with a positive guiding function Ψ_G.[21] Multiply Eq. 2.52 by Ψ_G and rewrite it in terms of a new function $\phi(\vec{R}) = \Psi(\vec{R})\Psi_G(\vec{R})$ to obtain

$$\phi(\vec{R}) = \int \frac{\Psi_G(\vec{R})}{\Psi_G(\vec{R}')}G_0(\vec{R},\vec{R}')\frac{V(\vec{R})}{E}\phi(\vec{R}')\;d\vec{R}'\;. \tag{2.53}$$

The energy is determined from distribution $\phi(\vec{R})$ samples, and the sampling algorithm is as follows:

(1) Weight of configuration at $\vec{R}$ in distribution $\phi(\vec{R})$ is multiplied by $V(\vec{R})/E$.

[20] $\langle m_I\rangle < 1$ to ensure termination of process.

[21] It is not necessary that $\Psi_G = \Psi_T$.

(2) Each configuration having weight W is divided into $m = int(W+u)$ configurations of $W = 1$, where u is a random number in $[0,1]$. If $m = 0$, the configuration is deleted.
(3) The configuration is moved to $\vec{R}'$, sampled from distribution $G_0(\vec{R}, \vec{R}')$.
(4) Weight is multiplied by $\Psi_G(\vec{R})/\Psi_G(\vec{R}')$ to produce a new weight in distribution $\phi(\vec{R})$. Repeat from (1) to continue the sampling.

2.1.6.2 Overcoming the sign problem

Early efforts by Ceperley and Alder introduced a "released-node" approach in [49]. In the nodal-relaxation method[49], walkers are allowed to live for a few generations after crossing the nodes of Ψ_T before being killed. These walkers are followed and a negative sign is assigned to those that have crossed a node an odd number of times, while a positive sign is assigned to those with even number of crossings. These signs affect their contribution to the averages, and as a result the Fermi energy can be obtained from the difference between even and odd walkers. However, this process is not numerically stable since the expectation values will be lost in the noise as the number of positive and negative walkers increases with each generation (although the difference between the two may remain constant). For this reason, the released-node energy is known as a "transient estimate."

In a different effort, Kalos and Zhang[48, 52] take advantage of the concept of interacting pairs of positive and negative walkers that Arnow *et al.* introduced in [56]. This method uses different guiding functions for the positive and negative populations, and each walker carries a sign which identifies them. In their algorithm each walker interacts with the rest of the ensemble, and equal numbers of positive and negative walkers are kept in order to represent a wave function, $\psi = \psi^+ + \psi^-$ that is anti-symmetric under interchange of like spins. The importance function of each population is required to bias walkers toward regions in space with corresponding sign. The algorithm is stabilized by randomly smoothing the population by permutation, i.e., positive walkers become negative walkers after an odd permutation of like spins and vice versa. The results have been favorable in all test cases, even when poor trial functions were used. Results for He, Li and Be using this method are presented in [48].

Another recent approach by Anderson and coworkers is presented in [50]. This method attempts to learn from previous experience and incorporates the best features of both Ceperley and Alder's nodal release[49] and Kalos *et al.* exact cancellation[52, 56] methods, described above. The method is applied in [22] for an exact treatment of the hydrogen molecule, in [57] for the PES of the H + H_2 exchange reaction, and in [51] for the He-He interatomic potential. Our description here comes from [50].

Start by assigning weights W ($W \geq 0$) and signs s ($s = \pm 1$) to each configuration, and defining the quantities, $G_1 = G_0(\vec{R}, \vec{R}_1)$ and $G_2 = G_0(\vec{R}, \vec{R}_2)$. The combined distribution of

moves for two configurations with $s_1 = +1$ and $s_2 = -1$, weights W_1 and W_2, and positions $\vec{R}_1$ and $\vec{R}_2$, is given by combined weight W and sign s, such that

$$sW = W_1G_1 - W_2G_2 \tag{2.54}$$

$\vec{R}_1'$ is chosen as usual (Sec. 2.1.6.1) from $G_0(\vec{R}, \vec{R}_1')$, and the new weight is given by

$$W_1(\text{new}) = \max\{[W_1G_1 - W_2G_2], 0\}/G_1 \ . \tag{2.55}$$

$\vec{R}_2'$ is chosen independently from G_2 with new weight,

$$W_2(\text{new}) = \max\{[W_2G_2 - W_1G_1], 0\}/G_2 \ . \tag{2.56}$$

Since

$$W_1(\text{new})G_1 = W_1G_1 - W_2G_2 = W \ , \tag{2.57}$$

this procedure gives the distribution W in the positive region, and

$$W_2(\text{new})G_2 = W_2G_2 - W_1G_1 = W \ , \tag{2.58}$$

in the negative region. Overlaping configurations with opposite sign cancel each other while distant ones will retain their weights. Multiple cancellations are also easily incorporated in the algorithm as follows:

(1) A set of configurations is selected for multiple cancellation and their $\vec{R}$, W, s, and $\vec{R}'$ are computed as usual by sampling $G_0(\vec{R}, \vec{R}')$.

(2) For each configuration calculate G_iW_i for its new position $\vec{R}'$ and G_jW_j for all other configurations considered at same $\vec{R}'$ position.

(3) If any $G_jW_j > G_iW_i$, the W_i for the new configuration is set to zero. If $G_iW_i > G_jW_j$ for all j, the new weight and sign are

$$(sW)_i = \frac{s_iW_i + \sum_{all\ j\ in\ i} s_jW_j}{s_iW_i} \tag{2.59}$$

(4) Repeat for all configurations in multiple cancellation groups.

In practice, configuration space is divided into cells, and cancellation groups are selected within each cell.

The product $\Psi\Psi_G$ we mentioned in the previous section, from where the QMC energy is computed, is now given by the net density of configurations (positive - negative), and the energy is given by

$$E = \frac{\sum_i s_iW_i \left(\frac{\Psi_T}{\Psi_G}\right)_i \left(\frac{\hat{\mathcal{H}}\Psi_0}{\Psi_0}\right)_i}{\sum_i s_iW_i \frac{\Psi_T}{\Psi_G}_i} \ . \tag{2.60}$$

2.2 Applications

2.2.1 Previous Results

Table 2.1 shows some results for small systems calculated by FNQMC. It is clear from these numbers that FNQMC does quite well in recovering the correlation energy in most cases, between 98-100%. Even more accurate results have been obtained with the exact GFMC methods mentioned in Sec. 2.1.6, but since our work here is in the context of fixed-node diffusion MC, we wish to show the quality of such calculations. In systems such as H_2 and H_3^+, which have no nodes, QMC will automatically sample the exact energy for any nodeless Ψ_T employed. Calculations on other systems such as Li, Li_2, LiH and Be can easily be carried out with compact Ψ_T's to yield excellent results.

Table 2.1: Total electronic energies(a.u.) of some small systems, calculated using FNQMC.

System	QMC	% corr.	Ref.
H_2	-1.17451(10)	100(1)	[41]
H_3^+	-1.3433(5)	100	[40]
	-1.34387(5)	100	[58]
Li	-7.47809(24)	100.0(5)	[34]
LiH	-8.06908(43)	98.7(5)	[34]
Li_2	-14.9945(4)	100	[35]
Be	-14.6657(7)	98.0(8)	[59]
CH_4	-40.5063(22)	97.3(7)	[60]
N	-54.5765(12)	93.1(6)	[61]
N_2	-109.517(79)[a]	96(14)	[62]
F	-99.727(34)[a]	100(11)	[62]
F^-	-99.8273(34)	92.0	[63]

[a]Energies computed using fixed-node domain GFMC[62].

2.2.2 The H_3 system

The hydrogen exchange reaction, $H + H_2 \rightleftharpoons H_2 + H$, is the simplest chemical reaction, and therefore, one of the systems most studied ever. In 1988, theoretical studies [64] gave calculated integral cross sections which were in disagreement with experimental results of Nieh and Valentini[65]. The experimentalist group claimed to have observed resonances in their cross sections while theoreticians claimed they were a smooth function of the energy. The potential energy surface used for these calculations was based on the analytical fit function by Truhlar and Horowitz[66] for the extensive CI calculations done by Siegbahn and Liu[67, 68] in 1978 (LSTH). Even though there was no evidence suggesting the problem in the cross sections was due to

the surface, the fact that all scattering calculations based on it gave identical results renewed interest in reexamining it by other methods. Our initial purpose was to compute the transition state region for the potential energy surface with QMC to provide additional information in regions not emphasized by Liu in his calculations or by the fit function. The controversy was eventually resolved in favor of the theoreticians, and our work concentrated on working along the reaction path. However this project was a great pedagogical tool to get me started into the nuts and bolts of the electronic structure QMC game. Therefore, it will be presented in that context, especially since all the necessary ingredients of a QMC calculation are present: (1) determination of equilibrium geometry for the calculation (in this case, the transition state, linear H_3); (2) determination of best possible trial function to be used, either from an *ab initio* calculation or from the literature; (3) choice of correlation functions and their parameters; and finally (4) QMC calculation at a set of time steps τ followed by a time-step extrapolation to determine the fixed-node energy with (5) estimation of the variance.

2.2.2.1 Transition state and reaction coordinate by QMC

As mentioned before, Liu[67, 69] performed an extensive CI study on the PES for the hydrogen exchange reaction in the linear[67] and 3-d[68] cases. Truhlar and Horowitz[66] provided an analytical fit for their results in [66]. In 1984, Barnett *et al.*[70, 33] performed a QMC study comparing different types of trial functions using the energy barrier of the H_3 system as a benchmark.[22] Ceperley and Alder also tackled the system with the GFMC with release-node method in [49]. In 1992, another QMC study on the H_3 system was presented by Anderson in [57], using the latest in exact QMC methods (See Sec. 2.1.6) on 320 IBM RS/6000 workstations working in parallel. The results obtained by those few studies (without doubt, there have been countless more) are presented chronologically in Table 2.2.

This work consisted first of a determination of the geometry and energy of the transition state by DMC as described in Sec. 2.1.4. Two single-determinant trial functions were used, with DZ and DZP basis sets, taken from [33]. The geometry, i.e., $R_1 = R_2 = 1.757a_0$ determined by Liu[67], was verified variationally for the DZ basis set. QMC energies were computed for these two wave functions at the determined geometry, and are shown in Table 2.2, where they are compared with other results mentioned before. The energy barrier, $E_b = E(H_3) - E(H) - E(H_2)$, is computed using the exact energies for H (E = -0.5a.u.) and H_2 (E = -1.1744746a.u.[71]). Since H and H_2 have no nodes, FNDMC provides the exact energy for both systems. As Barnett found in [33], the DZ wave function does considerably better than its larger counterpart. The time-step extrapolation of the DZ results, shown in Fig. 2.3, suggests that the time-step bias of this trial function is very small. Also notice that only an electron-electron correlation function

[22] We will concern ourselves with the effects of the types of trial functions used to obtain the QMC energy in Chapter 3, and turn our attention here to the system in question, i.e., H_3.

Table 2.2: Total energies of H_3 ($R_1 = R_2 = 1.757a_0$), and energy barriers ($E_b = E(H_3) - E(H) - E(H_2)$) for hydrogen exchange reaction.

Method	Energy (a.u.)	E_b (kcal/mole)[a]	Ref.	Year
CI	-1.6581	$\leq$ 10.28	[67]	1973
CI	-1.65876	$\leq$ 9.86	[69]	1984
exact estimate	-1.65919	9.59(6)	[69]	1984
QMC (Ψ_T^{UHF})	-1.65822(41)	$\leq$ 10.20(26)	[70]	1984
QMC (Ψ_T^{RHF})	-1.65903(40)	$\leq$ 9.69(25)	[70]	1984
GFMC + RN	-1.6591(1)	$\leq$ 9.65(8)	[49]	1984
QMC (Ψ_T(SD,DZ))		$\leq$ 9.70(13)	[33]	1985
this work, Ψ_T(DZ)	-1.658840(535)	$\leq$ 9.81	-	1989
this work, Ψ_T(DZP)	-1.658688(778)	$\leq$ 9.91	-	1989
exact GFMC	-1.659154(14)	9.61(1)	[57]	1992

[a] E_b is shown as an upper bound obtained by using the exact energies of H and H_2 [71].

with parameters $a = 0.5$, $b = 1.0$ was used, and that no electron-nuclear correlation factor was used.

After establishing the geometry of the transition state, we calculated the energies at several other points along the reaction coordinate published by Liu in [67], and compared them with the QMC results. Figure 2.4 shows such a comparison between the results of the CI calculations and QMC. The two curves overlap within the error bars of the QMC results, although the CI results remain slightly below the average QMC energies. Since our QMC energies coincided with the previous best results,[23] and we lacked derivative capability,[24] we decided not to go beyond the calculation of the reaction coordinate.

2.3 Making QMC accessible - size problem

2.3.1 Large Z

Perhaps the most essential variable to slow down a QMC calculation is the nuclear charge, Z[73]. To deal with the heavy-atom problem in QMC, we need to reduce the estimated computation time, T_{est}, which scales as $T_{est} \propto Z^{6.5}$[74]. One notices that though core electrons require the smallest step, the valence electrons largely determine chemical properties such as bond strengths, polarizabilities, electron affinities, and ionization potentials, as well as molecular geometries. If one treats only the valence electrons, the computation time no longer

[23] That is, those considered as best results at the time [67, 69]. The calculations by Anderson shown in Table 2.2 using massively parallel machines were not yet available.

[24] Past efforts to obtain derivatives in FNDMC have met with very limited success[72]. This was not an impediment to complete the calculation of a PES, just a small disadvantage when comparing with the current state of some other methods.

depends on Z but on the screened nuclear or effective charge. Under this direction many approaches have been suggested, such as valence-only methods, (effective core potentials[72, 74], model potentials[75, 76], pseudo-Hamiltonians[77]), and approximate all-electron methods (including all-electron damped-core QMC[78] and effective two-electron potentials[79]). All these approaches treat core and valence electrons more or less separately which implies that core and valence electrons have hardly exchanged. However, our studies have shown that core and valence electrons exchange quite often[80] throughout the random walk. Acceleration algorithms have been "recently" proposed to speed up convergence of all electrons. We will discuss, and closely examine one of these methods in Chapter 4.

2.3.2 Polyatomic systems

In this chapter we have presented the basics of the quantum Monte Carlo method, as well as some results on a benchmark system. As mentioned in Sec. 2.3.1, we are slowed down by Z and the number of electrons in our systems. Also, efforts have concentrated in optimizing the approach to do atomic, or small diatomic systems. The obvious questions to formulate at this point are: (1) Is it possible to do other systems of chemical interest? (2) How competitive is the QMC accuracy compared with standard *ab initio* methods? For QMC to survive in this game, it is time to expand the usefulness of QMC to larger polyatomic systems, such as those routinely found in laboratories! Some of the work done in the past along these lines includes work done on the N_2 molecule[61], Li clusters[29], and on bulk hydrogen at 0°K[81]. Given the extraordinary amount of computation required to acquire convergence of methods which promise chemical accuracy, such as CASSCF and CI, and given the type of empirical data needed for the likes of the G-1 and G-2 methods, it does not seem so unreasonable to spend similar computation effort and obtain an energy which is exact within its variance, and little (or none) *a priori* knowledge included to bias the results.

Figure 2.2: Radial dependence of Jastrow functions.

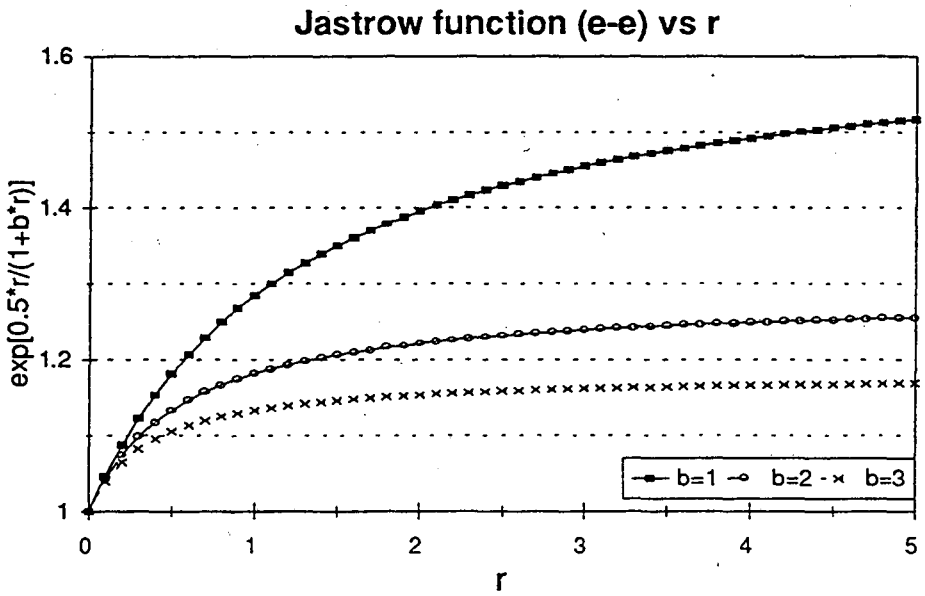

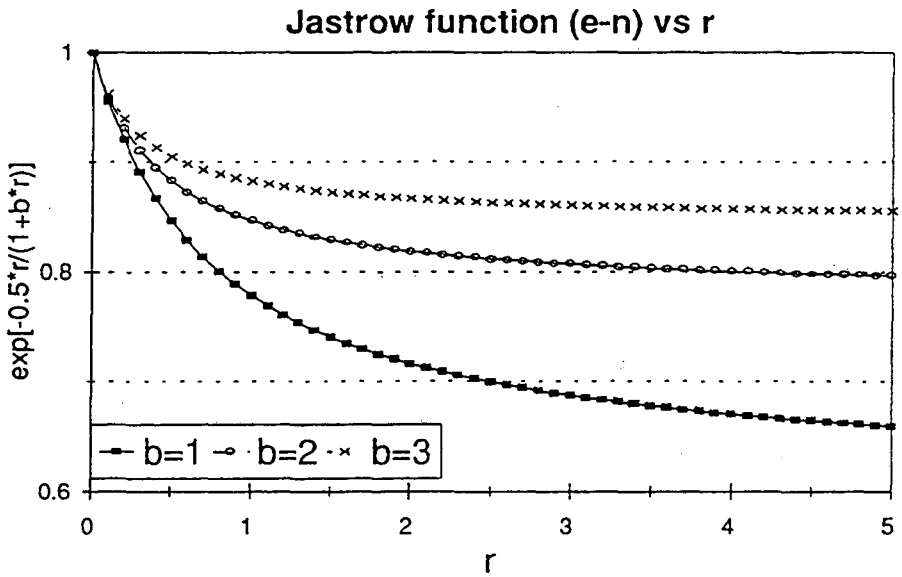

Figure 2.3: Time step extrapolation of the QMC energy of the saddle point in the H_3 reaction coordinate (i.e. transition state).

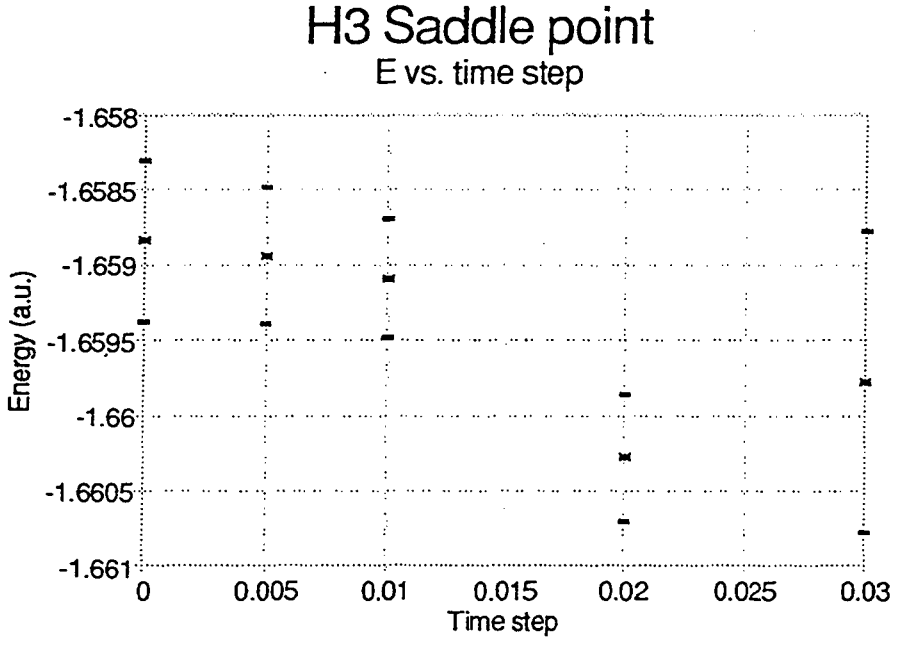

Figure 2.4: Reaction coordinate for the H + H_2 exchange reaction calculated by QMC with DZ trial function, compared to the *ab initio* points computed by Liu.

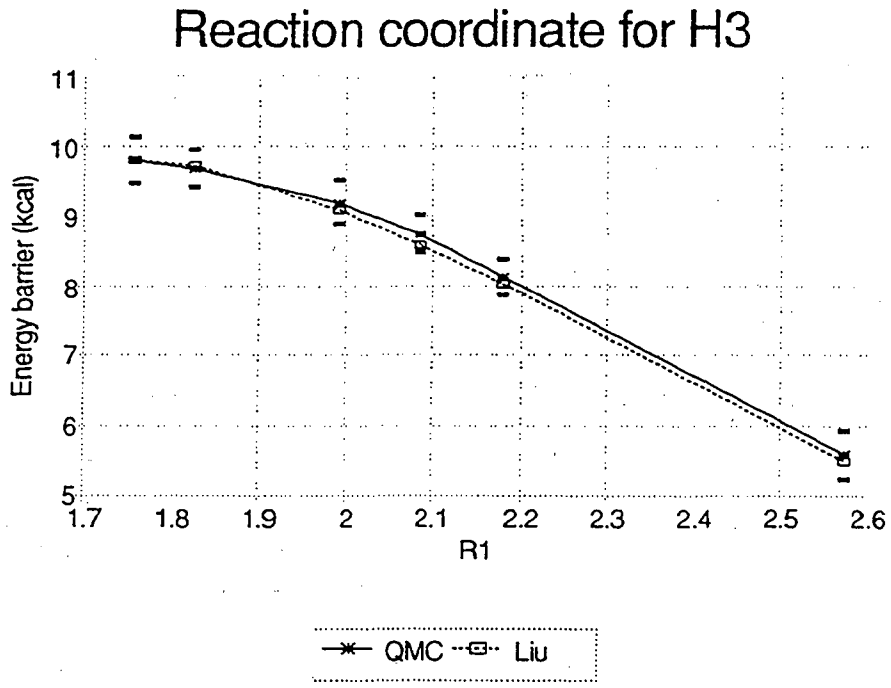

Chapter 3

Acetylene system

... if you are really smart you will be able to solve it with your fingers; if you are less smart you will need a slide rule; if you are kind of dumb, you can use a calculator; but if you are really stupid, you will need a CRAY supercomputer.

Prof. I. Oppenheim

3.1 Introduction

In quantum mechanics, if one were to know the wave function for a system, one would be able to determine the observables of that system. Indeed, one of the most important goals of a quantum chemistry calculation is the determination of the wave function. However, obtaining an analytical form for the wave function of a multi-body system is not a trivial task, and the only exact solution known is for the H-atom.

Our FNDMC calculations pose a different type of requirement on the wave function chosen. We saw in Sec. 2.1.4.4 that a popular choice of the QMC trial function, Ψ_T, is the form $\Psi_T = A \cdot C$ where A is constructed from one-electron functions, $A \equiv \sum(Slater\ determinants)$, which can be obtained from a previous SCF and/or post-Hartree Fock calculation (see Secs. 1.1 and 1.2) and $C = C_{ee} \cdot C_{en}$ of the form $C = e^U$, is a correlation function which explicitly includes factors of the interparticle distances. Some choices for U are shown in Table 3.1. Extensive work has been done on optimizing the parameters for all these functional forms by variationally minimizing either the energy[40] or the variance[42], with methods such as fixed-sample[41], or correlated sampling[47].

In QMC since we do not evaluate integrals, we are not concerned about the difficulties such correlation functions would pose to *ab initio* calculations. Our only concern is in the location of the nodes of the trial function in relation to the nodes of the true wavefunction, since in the approach used here (i.e., FNDMC) we choose to impose the fixed-node approximation. Given

there is little known about the nodal hypersurfaces of most trial functions used, one can use wave functions obtained from standard quantum chemistry programs and investigate their utility.

In practice, QMC trial wave functions can be wisely chosen to give excellent results. As mentioned in Sec. 2.2.2, Barnett *et al.*[33, 70] presented a wave function study using the H_3 system as a benchmark. Even in such a small system, it was proven that a poor choice of Ψ_T can yield a poor energy. The study in [70] concentrated on deciding which type of SCF trial function (spin-restricted or spin-unrestricted) has the lower QMC energy. It was found that the spin-restricted SCF Ψ_T gave the better nodal description of the ground state wave function. In [33], a similar study was performed on H_3, this time testing the effects of choice of basis functions. Among the basis sets used were combinations of SZ and DZ on the central and outer hydrogens; a basis including bond-functions; and a basis including up to d-functions on the three hydrogens! It was found that a DZ basis on all the hydrogens gave the best QMC energy and that the basis closest to the HF limit was the worst in accuracy as well as efficiency. In this case it was shown[33] that the higher energy was due to an additional node appearing in the larger wave function. Wavefunctions need to be examined for the possibility of spurious nodes.

Work by Garmer and Anderson[39, 82] on obtaining the PES for the $F + H_2 \rightarrow HF + H$ reaction showed that for F atom larger basis sets are required. In [39], MCSCF-type wave functions were tried and found not to contribute much to improving the correlation recovered., while undermining the efficiency of the walk. The random walk grew "prohibitively expensive" as it approached one of Schaefer's wave function expansions with 214 configurations. Extended basis sets were compared to minimal STO and DZ basis sets. The MOs were expressed using cubic splines for efficiency and it was found that the expanded basis set gave better results than the DZ, which in turn performed better than the minimal STO-NG basis set.

Harrison and Handy[59] did an all-electron calculation on the Be system and found slightly different results as far as the single-determinant (SD) vs. multi-determinant (MD) issue is concerned. In their work a modest two-configuration wave function including a $2s^2 \rightarrow 2p^2$ excitation gave better results than the use of a single-configuration trial function ($1s^2 2s^2$), as expected. Likewise, Christiansen[83] found that a two-configuration wave function did much better for Be using relativistic effective potentials. Similar results were shown in [84] for the ionization potential of Mg. Their work found that the MD wave function not only gave better energy and variance, but it took much less time than the SD wave function. They argued that although MD wave functions can adversely affect the energy by addition of anomalous nodes into the wave function, the only nodes relevant to their study would occur when the electrons approach each other far away from the nucleus. The situation would clearly be more complicated as more electrons become involved, or when the core electrons are included.

More explicitly, Sun *et al.* showed in [35] how great care must be taken in choosing and optimizing the one-electron part of a trial function when the determinant expansion is small.

They did calculations with single-determinant and four-determinant wave functions, and then proceeded to optimize the correlation factors, as well as the MO parameters. They found that a variationally "optimized" trial function does not necessarily improve on the QMC energy, even if multi-determinant functions are used.[1]

In spite of all this and other work, it seems that finding an appropriate trial function for FNDMC is a rather serendipitous task. We propose in this work to examine closely a well known family of systems, working with basis sets used in the past for individual fragments, and see how the wave functions need to evolve as the systems grow.

The acetylene system and its dissociation fragments (C_2H, CH and C) were chosen for this study for several reasons. First, there was an interest in reevaluating the dissociation energy of the C-H bond in acetylene after experiments by Green *et al.*[85] found an upper bound ($\leq$ 126.647(2) kcal/mole) lying below most previous experimental and theoretical work. A wave of work followed to verify this result, and our work might have shed some light on the controversy. Also, since all fragments in this system have been examined so thoroughly, it offered an excellent opportunity to use known data (such as equilibrium geometries, basis sets, and correlation functions) to test our work. A systematic study of wave functions in systems on which an atom is added one at a time (i.e., from C to CH to C_2H to C_2H_2) might suggest a systematic process for choosing wave functions in the future. Lastly, it would be a useful study of QMC on polyatomic systems since most exciting work so far has been done on atomic and diatomics.

[1] In variational calculations, the inclusion of more determinants always lowers the energy.

Table 3.1: Popular choices for correlation functions used in QMC

Function	Description		e-e	e-n
Padé-Jastrow	$U = \sum_{i<j} \frac{ar_{ij}}{1+br_{ij}}$	J_{ee}	x	
	$U = \sum_{i,A} \frac{ar_{iA}}{1+br_{iA}}$	J_{en}		x
Sun	$U = -a_0 e^{(-a_1 r_{ij} + a_2 r_{ij}^2 \cdots)}$	S_{ee}	x	
Boys-Handy	$U = \sum_{I,i<j} \sum_k^{N(I)} \Delta(m_{k,I}, n_{k,I}) c_{kI} \left[\bar{r}_{iI}^{m_{kI}} \bar{r}_{jI}^{n_{kI}} + \bar{r}_{jI}^{m_{kI}} \bar{r}_{iI}^{n_{kI}} \right] \bar{r}_{ij}^{o_{kI}}$; $\bar{r}_{iI} \equiv \frac{b_I r_{iI}}{1+b_I r_{iI}}$; $\bar{r}_{jI} \equiv \frac{b_I r_{jI}}{1+b_I r_{jI}}$; $\bar{r}_{ij} \equiv \frac{d_I r_{ij}}{1+d_I r_{ij}}$	J_{een}	x	x

3.2 CH containing systems

As done in the H_3 study (Sec. 2.2.2), we started by computing the energies with the simplest possible wavefunction; that is, a single determinant, which is then multiplied by a correlation function which explicitly depends on interparticle distances. We then studied the effect of the type of correlation function on the QMC results. The types of correlation functions used, J_{ee}, J_{en}, S_{ee}, and J_{een}[86, 87], are shown in Table 3.1. Separate studies were done in order to examine the effects of the one-particle part of the wave function on the QMC results. In this context, single and multi-determinant wave functions will be discussed in separate sections for each CH containing fragment, when appropriate.

3.2.1 Carbon - C

The results for C atom were obtained using a cubic spline routine since large basis sets were used (See Sec. 2.1.4.4) to approximate the radial part of the MOs used in the formation of the Slater determinant. Table 3.2 shows the first one-particle basis set used for C atom, and Table 3.3 shows the energies obtained using this basis set with correlation functions of the J_{ee} and J_{een} forms. Parameters for J_{een} were taken from Ref. [86], and for J_{ee} were optimized to give the lowest variance.. The purpose of this calculation was to determine if the variance and time step bias improvement (see Fig. 3.1a) attained by computing the larger correlation function compensates for the amount of CPU time it takes to compute. The amount of correlation

recovered is irrelevant since the one-particle basis, and therefore the nodes of the trial function, remained unchanged.

The time step extrapolation for both types of correlation function used are shown in Fig. 3.1a. It is clear that the time step bias of the J_{een} correlation function is better than the J_{ee} alone, and that the variance of the extrapolated result is better as well. We found that the variance improved by 25% while the computer time increased by 15%, indicating that the improvement justifies the extra computational effort.

The third result in Table 3.3 corresponds to a different basis set (Basis B in Table 3.7) to be introduced in Sec. 3.2.2.2. Figure 3.1b shows a comparison of the results in Fig. 3.1a with the results from Basis B. Since no correlation function was used to obtain these results, the time step bias is much worse for the new basis. Even though the time step bias suffered, it recovered about 5% more of the correlation energy.

Table 3.2: Clementi's DZ basis set used for carbon atom (^{3}P) calculations

1σ	2σ	1π	Type	ζ
0.91214	-0.16317	0.0	1s	5.3767
0.09163	-0.03424	0.0	1s	8.9820
-0.00135	0.49825	0.0	2s	1.3089
0.00430	0.58156	0.0	2s	2.0131
0.00329	-0.08564	0.0	2s	5.6319
0.0	0.0	0.24762	2p	0.9554
0.0	0.0	0.57770	2p	1.4209
0.0	0.0	0.23561	2p	2.5873
0.0	0.0	0.01090	2p	6.3438

Table 3.3: Energies of C(^3P) atom using Clementi's DZ basis set and various correlation functions, as well as the % correlation recovered.

Basis Set	Correlation Function	E_{QMC} (a.u.)	% E_{corr} recovered
Clementi	J_{ee}	-37.830018(663)	90.36%
	J_{een}	-37.829454(483)	90.00%
McLean	- [a]	-37.83529(335)	94.8%

[a] No correlation function

Figure 3.1: (a) Energy vs. time step behavior for C using J_{ee} and J_{een} correlation functions. (b) Time step bias of the results in (a) compared with those obtained using basis B (Table 3.7) and no correlation function.

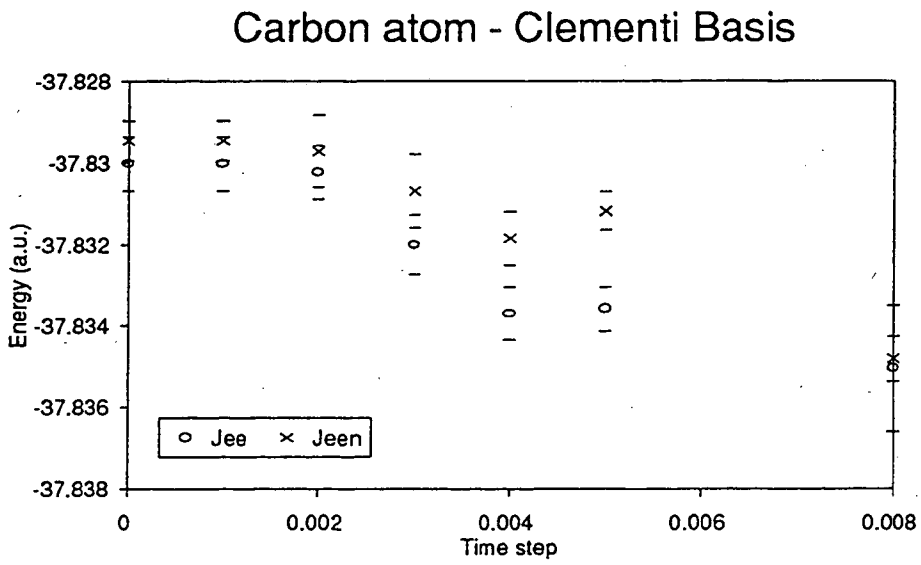

(a)

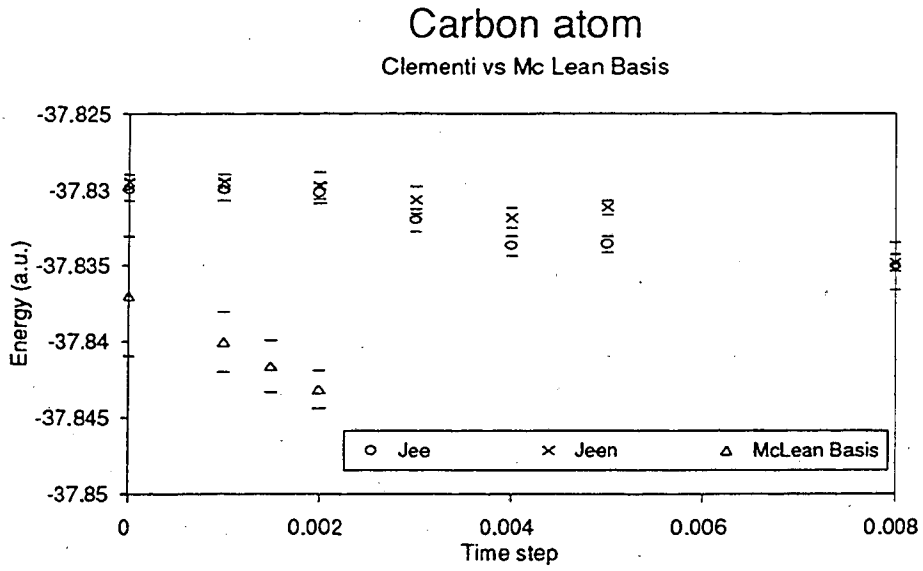

(b)

3.2.2 Methylidene - CH

3.2.2.1 Introduction

Earlier work is summarized in Cade and Huo's extensive study of the first and second row hydrides in 1967[88]. They established a basis set near the Hartree-Fock limit, on which most later studies are based on. Their equilibrium radius for the CH radical was $R_e = 2.124a_0$, which agreed with the previous work (both theoretical and experimental) they cited in their paper[88].

Liu and Verhaegen[89] carried out SCF calculations to provide an estimate for energies of the states of CH. Their "semi-empirical" calculations do not represent variational calculations (as CI/MCSCF calculations would), since they used previously published orbitals to establish correspondence between the AO's and the MO's: $1\sigma \sim 1s_C$, $2\sigma \sim 2s_C$, $3\sigma \sim 3p_c$, $1\pi \sim 2p_C$ and $4\sigma \sim 1s_H$. These orbitals were then used to form reference configurations which were "empirically corrected" for correlation. They used this method to find potential curves for lowest lying electronic states of CH: $^2\Pi$, $^4\Sigma^-$, $^2\Delta$, $^2\Sigma^-$, $^4\Sigma$ and $^2\Sigma^+$.

A few years later, Lie and Clementi estimated the exact energy of CH (along with the rest of the diatomic hydrides) using a semi-empirical functional of the HF-type density[90]. This result, -38.4863a.u., was compared with the "exact non-relativistic" energy for CH, -38.4761a.u., also estimated by Clementi.

Lie *et al.*[91] studied the potential curves of the first five states of CH with CI calculations. They are:

$$
\begin{array}{ll}
X^2\Pi & 1\sigma^2 2\sigma^2 3\sigma^2 1\pi \\
a^4\Sigma^- & 1\sigma^2 2\sigma^2 3\sigma(1\pi^2, {}^3\Sigma^-) \\
A^2\Delta & 1\sigma^2 2\sigma^2 3\sigma(1\pi^2, {}^1\Delta) \\
B^2\Sigma^- & 1\sigma^2 2\sigma^2 3\sigma(1\pi^2, {}^3\Sigma^-) \\
C^2\Sigma^+ & 1\sigma^2 2\sigma^2 3\sigma(1\pi^2, {}^1\Sigma^+)\ .
\end{array}
$$

For the ground state (i.e., $X^2\Pi$) they determined $R_e = 2.113a_0$ and $D_e = 3.51$eV. At this point, it may be convenient to briefly present the configuration state functions (CSFs)[2] they used for this state, since they will be useful in our own study. First, since HF theory does not lead to correct dissociation, one should start with the expected HF CSFs in the limit $R = \infty$. In this case, these CSFs would be the hydrogen and carbon atoms in their respective ground[3] and

[2] See Appendix A.5.

[3] The association of MOs to AOs done by Liu and Verhaegen is still valid here, so one needs four $\sigma-$ and one $\pi-$ type orbitals: ($1s_\sigma$, H), ($1s_\sigma$, C), ($2s_\sigma$, C), ($2p_\sigma$, C) and ($2p_\pi$, C).

excited states, as well as (C^+, H^-) and (C^-, H^+) ion pairs:

$$
\begin{array}{lll}
X^2\Pi: & 1\sigma^2 2\sigma^2 3\sigma^2 1\pi & 1\sigma^2 3\sigma^2 1\pi^3 \\
 & 1\sigma^2 2\sigma^2 4\sigma^2 1\pi & 1\sigma^2 4\sigma^2 1\pi^3 \\
 & 1\sigma^2 2\sigma^2 (3\sigma 4\sigma,\ ^1\sigma^+) 1\pi & 1\sigma^2 (3\sigma 4\sigma,\ ^1\sigma^+) 1\pi^3 \\
 & 1\sigma^2 2\sigma^2 (3\sigma 4\sigma,\ ^3\sigma^+) 1\pi & 1\sigma^2 (3\sigma 4\sigma,\ ^3\sigma^+) 1\pi^3
\end{array}
\tag{3.1}
$$

The CSFs on the left are needed to dissociate to the $1s^2 2s^2 2p^2$ configuration of carbon and the ground state of hydrogen. The CSFs on the right allow a two reference description of C in the infinite separation limit: $C_1 1s^2 2s^2 2p^2 + C_2 1s^2 2p^4$. More CSFs were created after defining valence and external orbitals, and generating all possibilities with the 5 active electrons (in this case all electrons outside the 1σ orbital) distributed in different combinations among the valence and external sets. This approach was described in detail in Ref. [92] and in Sec. 1.2.

Siegbahn[93] presented a MC-CI (multireference-CI using a CASSCF wavefunction as the reference) study of the dissociation of acetylene into two CH($^2\Pi$) radicals. In the CASSCF, 32 configurations were chosen for acetylene to allow for the proper dissociation of the C-C bond, without altering the C-H bond. The 32 configurations were later used as references for SD MC-CI calculation for a total of 178,000 configurations and solved approximately using a contracted CI scheme. The calculations used a contracted basis set[4] from Dunning-Huzinaga[94, 95]. For carbon, (10s,6p) was contracted to (5s,4p) plus $d(\zeta = 1.0)$ polarization, and for hydrogen (4s) was contracted to (3s) plus $p(\zeta = 0.65)$ polarization. He found R_e values of $2.096a_0$ and $2.111a_0$ at the CASSCF and MC-CI levels, respectively.

More recent work includes, CASSCF/MRSD CI calculations with extensive(!) basis sets by Bauschlicher and Langhoff[96], G-1 of Pople *et al.*[14], as well as GFMC work by Subramaniam *et al.*[62]. Pople *et al.*[14] presented their results for CH as part of the test cases introducing the "new" G-1 method (see Sec. 1.2.4). Subramaniam *et al.*[62] used the fixed-node domain GFMC method to compute binding energies of several hydrides. They obtained an energy of -37.828(12)a.u. for C atom and -38.465(15)a.u. for CH, which leads to a binding energy (D_e) of 3.74(52)eV, and compared their results to many other studies to date.

Even though this summary does not fully assess all work done on this radical, it gives a good idea of the established values for the equilibrium geometry as well as the binding energy of CH. Table 3.4 presents a summary containing the values discussed in this section in comparison with our QMC results to be presented in the next two sections.

3.2.2.2 QMC with single determinant trial functions

Single-reference QMC calculations were done using three basis sets. Table 3.5 shows the Cade and Huo basis set (Basis C) as given in Ref. [88] and Table 3.7 shows the two other

[4] See Appendix A.3.1.

Table 3.4: Equilibrium distances (R_e) binding energies, (D_e), and total energies obtained for the CH($^2\Pi$) radical.

Name	Year	R_e (a_0)	D_e (eV)	Total Energy (a.u.)	Method	Ref.
Cade and Huo	1967	2.124	2.47	-38.2794	SCF - HF limit	[88]
Liu and Verhaegen	1970	2.090	3.46[a]	-38.4786	LCAO-MO-SCF	[89]
Lie *et al.*	1973	2.113	3.51	-38.41044	CI	[91]
Lie and Clementi	1974	2.110	3.60		Functional of	[90]
		2.124		-38.4863	HF density	
Siegbahn	1981	2.096			MCSCF	[93]
		2.111			MC-CI	
Bauschlicher	1987	2.120	3.46	-38.407880	Full CI	[96]
and Langhoff		2.123	3.61	-38.421872	MRSD CI + Q	
Pople *et al.*	1989		3.64	-38.4743	G-1 ($+\Delta E_{corr}$)	[14]
Subramaniam *et al.*	1992	2.11	3.74(52)	-38.465(15)	GFMC	[62]
this work (QMC)	1993	2.124	3.48(4)	-38.45797(118)	Basis C - J_{ee}	
			-	-38.46103(231)	Basis C - $S_{ee} + J_{en}$	
			3.61(4)	-38.46213(141)	Basis C - J_{een}	
			3.45(10)	-38.46199(193)	Basis B	
		2.116	3.36(17)	-38.45892(520)	Basis B	
Clementi	1974	2.124		-38.4761	Exact Non-rel.	[90]
Herzberg	1969	2.116	3.65	-	Expt.	cf. [62]

one-particle basis sets used. Basis A was obtained from Ref. [97] and Basis B from a private communication.[5] Because QMagiC[6] is limited to d-functions, we eliminated f-functions from basis sets obtained from the literature, and reoptimized the MO coefficients by SCF.

First, we did a calculation with the truncated Cade and Huo basis[88] from Table 3.5 using correlation functions of the forms shown in Table 3.1 at $R_e = 2.124a_0$[88]. The correlation functions used for each calculation were (1) electron-electron Jastrow, J_{ee}, only; (2) electron-electron double exponential function (S_{ee}) and electron-nuclear Jastrow (J_{en}) to be denoted as $S_{ee} + J_{en}$; and (3) electron-electron-nuclear function of Boys and Handy form[86], J_{een}. As with C atom, the parameters in the correlation functions were optimized variationally[98] with respect to variance. Results for this series of calculations are given in Table 3.6. We can see that, in all cases, between 90-95% of the correlation energy was recovered. The variance in the energy was (also) not improved greatly by more sophisticated forms of the correlation function, while the amount of CPU time the larger calculation (i.e., for J_{een}) consumed was increased by over a factor of 2. Figure 3.2 shows the time step extrapolations for the calculations using a wave function with each type of correlation function. It is clear that the time step bias improved for the J_{een} correlation function, but not dramatically so, since the uncertainties for both extrapolations for the J_{een} and the $S_{ee} + J_{en}$ overlap. The $S_{ee} + J_{ee}$ function did just as well in removing the time step bias, and took only a fraction of the CPU time J_{een} consumed. One conclusion to draw is that we cannot improve upon the ~90% correlation energy recovery with this particular one-particle (basis C), single reference wave function.

One possible reason for the poor recovery of the correlation energy by the Cade and Huo basis set was in eliminating the f-functions, although the MO coefficients of the functions ignored were very small in the original basis. From SCF calculations done using the other bases[7] (Basis sets shown on Table 3.7) we observe no significant difference in the result with f-functions and without f-functions. For instance, for Basis B we get E_{HF} = -38.27923501a.u. when f-functions are used while E_{HF} = -38.27887818a.u. without them; the difference in energy is less than 0.25 kcal/mole. To be more specific, Fig. 3.5c shows a similar comparison, this time finding the minimum SCF geometry using Cade and Huo's original basis set, and then that basis set omitting f-functions. Note some important points: (1) the energy of the truncated basis set (i.e., without f-functions) is not much higher than that of the non-truncated basis; and (2) the R_e obtained from each one of them are close to each other($R_e \approx 2.078a_0$), and (3) neither one is close to the one reported by Cade and Huo ($R_e = 2.124a_0$)! According to their paper, this minimum had been found and confirmed previously, both theoretical and experimentally.[8]

[5] Basis B was obtained from Dr. A.D. McLean at IBM, Almaden Research Center.

[6] See Appendix C.

[7] Also truncated to d-functions.

[8] Table XX, p. 642 in Ref. [88].

Figure 3.5a compares the SCF curves of both Basis sets B and C.[9] A similar comparison was done with the Basis B wave functions at 3 levels of theory used for the QMC calculations to be presented in the next section. These results are shown in Fig. 3.5b. As mentioned before, Fig. 3.5c shows the effect of f-functions on the equilibrium geometry using the Cade and Huo basis set. Once again, there is no obvious choice for the equilibrium geometry.

To examine this aspect (i.e., finding the optimum geometry), we did a calculation using Basis B at the experimental geometry[10] and obtained a QMC energy of -38.45892(520)a.u. Obviously, this energy overlaps with the $R_e = 2.124a_0$ energy found previously.

Figure 3.2: Energy vs. time step plot using basis C.

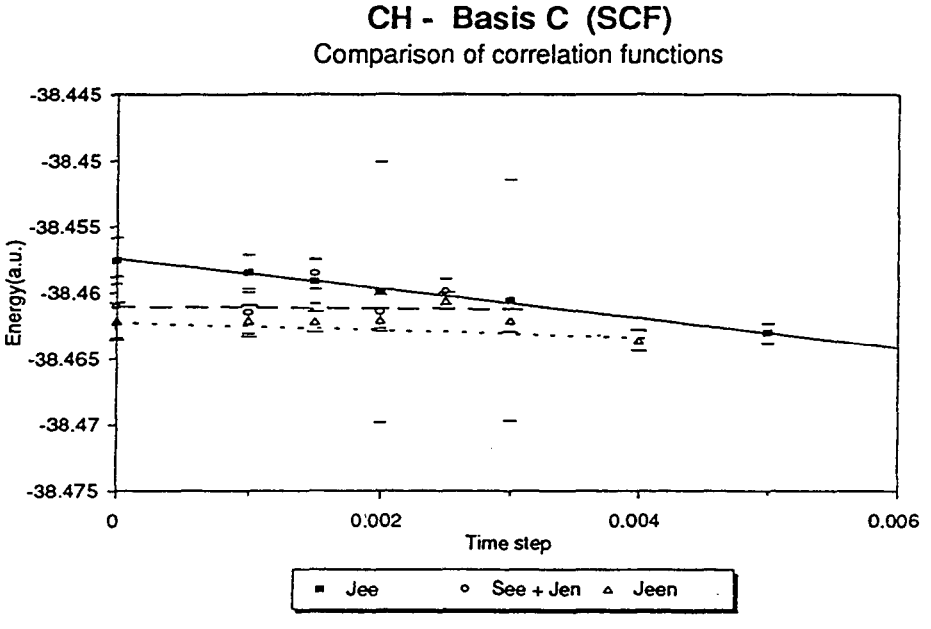

3.2.2.3 QMC with multi-determinant trial functions

For CH, we did CASSCF calculations with either 3 or 5 valence electrons and a very limited active space. To do this we generated all possible configurations using the ALCHEMY II programs[99]. The prototype configurations as well as their respective configuration state functions (CSFs) are listed on Tables 3.8 and 3.9. From these tables we can see that they contain

[9] Note that the plots show some of the curves shifted by a few atomic units for convenience in plotting on the same scale. This should not be confused as curve crossing, and the legend should be carefully read in order to figure out which curve is lower.

[10] Even though this did not correspond to a variational minimum in either of the 3 wavefunctions shown in Fig. 3.5

most of the configurations considered important in order to get proper dissociation in the CI study by Lie *et al.*[91] in Sec. 3.2.2.1 and listed in Eq. 3.1. The procedure they described in Ref. [91] to generate their CSFs is not very different from our own.

From an *ab initio* standpoint our modest expansion may seem trivial, but since our goal is to obtain trial functions for QMC which aside to being optimized for the system in question should be manageable, it is very reasonable to use such limited active spaces. A large configuration expansion in QMC would increase the computational effort beyond our capabilities. The variational and QMC energies obtained for these wavefunctions are shown on Table 3.10, and compared graphically in Fig. 3.4. It is clear from these numbers that when used for QMC the single reference wavefunctions do much better in recovering the correlation energy, since the single reference recovers $\sim$92% of the correlation energy while the multi-reference recovers $\sim$ 69%. This should not entirely come as a surprise, since our results depend on the ability of the trial function in reproducing the nodal structure of the true wavefunctions, not on the variational improvement of a wavefunction by adding new configuration states to its expansion, MCSCF or CI, as it may be the case. However, more works remain to be done to better understand the large gap in the resulting energies and to correct any source of error. Tables 3.11 and 3.12 show the determinant coefficients in each multi-determinant wave function. From these tables, one sees that the greatest contribution always comes from the reference configuration, which suggests that even a small addition of lesser configurations (the first coefficient is always $\geq$ 0.98 while the second largest coefficient is $\sim$ 0.15) will drastically change the nodes. We show time step extrapolations for these wave functions in Fig. 3.3.

Some problems were encountered due to bad configurations.[11] These bad configurations were discarded by doing short fixed-node equilibration runs at a large time step (75% acceptance) followed by a VMC run (85% acceptance seemed preferable to 50%[80]) A quantum force cutoff of 100 was used as well for these problem configurations[80]. (Suggestions on how to prepare an ensemble and perform QMC runs are summarized in Appendix C.)

[11] A configuration is considered "bad" if it always stays (or gets "trapped") in unfavorable regions of space. For a better description of what constitutes a bad configuration please see [80].

Table 3.5: Cade and Huo basis set, without f-functions, for CH.

Basis C							
1σ	2σ	3σ	1π	C	H	Type	ζ
0.12775	-0.00362	0.00147	0.0	x		1s	9.04883
0.92476	-0.21700	0.11652	0.0	x		1s	5.00904
-0.05659	-0.02541	0.00817	0.0	x		3s	6.05668
0.00256	0.47261	-0.26272	0.0	x		2s	2.06820
-0.00201	0.39416	-0.34519	0.0	x		2s	1.29799
0.00063	0.00331	0.00715	0.0	x		$2p_z$	6.54292
0.00286	0.02351	0.12504	0.0	x		$2p_z$	2.74247
-0.00223	0.13094	0.25644	0.0	x		$2p_z$	1.72601
-0.00049	0.07442	0.37236	0.0	x		$2p_z$	1.03933
0.0	0.0	0.0	0.00853	x		$2p_y$	6.71077
0.0	0.0	0.0	0.16838	x		$2p_y$	2.78970
0.0	0.0	0.0	0.45717	x		$2p_y$	1.61117
0.0	0.0	0.0	0.42280	x		$2p_y$	1.02112
0.00036	0.01691	0.01636	0.0	x		$3d_{3z^2-r^2}$	2.34850
-0.00060	0.03584	0.06354	0.0	x		$3d_{3z^2-r^2}$	1.23876
0.0	0.0	0.0	0.03306	x		$3d_{yz}$	1.58298
-0.00131	0.08818	-0.01952	0.0		x	1s	2.89843
0.00508	0.02167	0.35731	0.0		x	1s	1.34188
-0.00197	0.17537	-0.02359	0.0		x	2s	2.11216
0.00040	0.01893	0.00863	0.0		x	$2p_z$	2.22645
0.0	0.0	0.0	0.03171		x	$2p_y$	1.44660
0.0	0.0	0.0	0.00340		x	$3d_{yz}$	2.72637

Table 3.6: QMC energies and % correlation recovered for CH using Basis C for different correlation functions. Binding energies are computed using Clementi basis set with matching correlation function.

Correlation Function	E_{QMC} (a.u.)	% E_{corr} recovered	D_e (eV)
J_{ee}	-38.45797(118)	90.36%	3.48(4)
$S_{ee} + J_{en}$	-38.46103(231)	92.34%	
J_{een}	-38.46213(141)	92.90%	3.61(4)

Table 3.7: Basis Sets used for CH systems.

Basis Set A[a]						Basis Set B[b]						
σ	π	C	H	Type	ζ	σ	π	δ	C	H	Type	ζ
x		x		1s	9.055	x			x		1s	9.055
x		x		1s	5.025	x			x		1s	5.025
x		x		3s	6.081	x			x		3s	6.081
x		x		2s	2.141	x			x		2s	2.141
x		x		2s	1.354	x			x		2s	1.354
x	x	x		2p	6.827	x	x		x		2p	6.51
x	x	x		2p	2.779	x	x		x		2p	2.6005
x	x	x		2p	1.625	x	x		x		2p	1.4436
x	x	x		2p	1.054	x	x		x		2p	0.9023
x		x		3d	1.99175	x	x	x	x		3d	3.6407
	x	x		3d	2.13462	x	x	x	x		3d	2.0211
						x	x	x	x		3d	1.373
x			x	1s	1.2029	x				x	1s	1.6
x			x	1s	0.97493	x				x	1s	1.0
x			x	2p	1.72338	x				x	1s	0.625
x			x	3d	1.65	x	x			x	2p	2.0
	x		x	2p	0.7901	x	x			x	2p	1.4
	x		x	3d	2.31071	x	x	x		x	3d	2.33

[a] Basis A from Ref. [97].

[b] Basis B from Dr. A.D. McLean, IBM Almaden Research Center; private communication.

Table 3.8: Configuration State Functions for CH($^2\Pi$) with 3 active electrons (5 actual CSFs and 6 determinants). The 4-electron inactive space has configuration $1\sigma^2 2\sigma^2$.

Prototype Configuration	Prototype CSF	Determinant	#	Actual CSFs
$A\sigma^2 1\pi$	$3\sigma^2 1\pi$	$3\sigma^\alpha_\beta 1\pi^\alpha$	(1)	(1)
	$4\sigma^2 1\pi$	$4\sigma^\alpha_\beta 1\pi^\alpha$	(2)	(2)
$A\sigma B\sigma 1\pi$	$3\sigma 4\sigma 1\pi$	$3\sigma^\alpha 4\sigma_\beta 1\pi^\alpha$	(3)	$\frac{1}{\sqrt{2}}\cdot(3) - \frac{1}{\sqrt{2}}\cdot(4)$
		$3\sigma_\beta 4\sigma^\alpha 1\pi^\alpha$	(4)	
		$3\sigma^\alpha 4\sigma^\alpha 1\pi_\beta$	(5)	$-\frac{1}{\sqrt{6}}\cdot(3) - \frac{1}{\sqrt{6}}\cdot(4) + \sqrt{\frac{2}{3}}\cdot(5)$
$1\pi^3$	$1\pi^3$	$1\pi^{\alpha\alpha}_\beta$	(6)	(6)

Table 3.9: Configuration State Functions for CH($^2\Pi$) with 5 active electrons (18 actual CSFs and 24 determinants). The 2-electron inactive space has configuration $1\sigma^2$.

Prototype Configuration	Prototype CSF	Determinant	#	Actual CSFs
$A\sigma^2 B\sigma^2 1\pi$	$2\sigma^2 3\sigma^2 1\pi$	$2\sigma^\alpha_\beta 3\sigma^\alpha_\beta 1\pi^\alpha$	(1)	(1)
	$2\sigma^2 4\sigma^2 1\pi$	$2\sigma^\alpha_\beta 4\sigma^\alpha_\beta 1\pi^\alpha$	(2)	(2)
	$3\sigma^2 4\sigma^2 1\pi$	$3\sigma^\alpha_\beta 4\sigma^\alpha_\beta 1\pi^\alpha$	(3)	(3)
$A\sigma^2 B\sigma C\sigma 1\pi$	$2\sigma^2 3\sigma 4\sigma 1\pi$	$2\sigma^\alpha_\beta 3\sigma_\beta 4\sigma^\alpha 1\pi^\alpha$	(4)	$\frac{1}{\sqrt{2}}\cdot(4)-\frac{1}{\sqrt{2}}\cdot(5)$
		$2\sigma^\alpha_\beta 3\sigma^\alpha 4\sigma_\beta 1\pi^\alpha$	(5)	
		$2\sigma^\alpha_\beta 3\sigma^\alpha 4\sigma^\alpha 1\pi_\beta$	(6)	$-\frac{1}{\sqrt{6}}\cdot(4)-\frac{1}{\sqrt{6}}\cdot(5)+\sqrt{\frac{2}{3}}\cdot(6)$
	$3\sigma^2 2\sigma 4\sigma 1\pi$	$3\sigma^\alpha_\beta 2\sigma_\beta 4\sigma^\alpha 1\pi^\alpha$	(7)	$\frac{1}{\sqrt{2}}\cdot(7)-\frac{1}{\sqrt{2}}\cdot(8)$
		$3\sigma^\alpha_\beta 2\sigma^\alpha 4\sigma_\beta 1\pi^\alpha$	(8)	
		$3\sigma^\alpha_\beta 2\sigma^\alpha 4\sigma^\alpha 1\pi_\beta$	(9)	$-\frac{1}{\sqrt{6}}\cdot(7)-\frac{1}{\sqrt{6}}\cdot(8)+\sqrt{\frac{2}{3}}\cdot(9)$
	$4\sigma^2 2\sigma 3\sigma 1\pi$	$4\sigma^\alpha_\beta 2\sigma_\beta 3\sigma^\alpha 1\pi^\alpha$	(10)	$\frac{1}{\sqrt{2}}\cdot(7)-\frac{1}{\sqrt{2}}\cdot(8)$
		$4\sigma^\alpha_\beta 2\sigma^\alpha 3\sigma_\beta 1\pi^\alpha$	(11)	
		$4\sigma^\alpha_\beta 2\sigma^\alpha 3\sigma^\alpha 1\pi_\beta$	(12)	$-\frac{1}{\sqrt{6}}\cdot(7)-\frac{1}{\sqrt{6}}\cdot(8)+\sqrt{\frac{2}{3}}\cdot(9)$
$A\sigma^2 1\pi^3$	$2\sigma^2 1\pi^3$	$2\sigma^\alpha_\beta 1\pi^{\alpha\alpha}_\beta$	(13)	(13)
	$3\sigma^2 1\pi^3$	$3\sigma^\alpha_\beta 1\pi^{\alpha\alpha}_\beta$	(14)	(14)
	$4\sigma^2 1\pi^3$	$4\sigma^\alpha_\beta 1\pi^{\alpha\alpha}_\beta$	(15)	(15)
$A\sigma B\sigma 1\pi^3$	$2\sigma 3\sigma 1\pi^3$	$2\sigma^\alpha 3\sigma_\beta 1\pi^{\alpha\alpha}_\beta$	(16)	$\frac{1}{\sqrt{2}}\cdot(16)-\frac{1}{\sqrt{2}}\cdot(17)$
		$2\sigma_\beta 3\sigma^\alpha 1\pi^{\alpha\alpha}_\beta$	(17)	
		$2\sigma^\alpha 3\sigma^\alpha 1\pi^\alpha_{\beta\beta}$	(18)	$-\frac{1}{\sqrt{6}}\cdot(16)-\frac{1}{\sqrt{6}}\cdot(17)+\sqrt{\frac{2}{3}}\cdot(18)$
	$2\sigma 4\sigma 1\pi^3$	$2\sigma^\alpha 4\sigma_\beta 1\pi^{\alpha\alpha}_\beta$	(19)	$\frac{1}{\sqrt{2}}\cdot(19)-\frac{1}{\sqrt{2}}\cdot(20)$
		$2\sigma_\beta 4\sigma^\alpha 1\pi^{\alpha\alpha}_\beta$	(20)	
		$2\sigma^\alpha 4\sigma^\alpha 1\pi^\alpha_{\beta\beta}$	(21)	$-\frac{1}{\sqrt{6}}\cdot(19)-\frac{1}{\sqrt{6}}\cdot(20)+\sqrt{\frac{2}{3}}\cdot(21)$
	$3\sigma 4\sigma 1\pi^3$	$3\sigma^\alpha 4\sigma_\beta 1\pi^{\alpha\alpha}_\beta$	(22)	$\frac{1}{\sqrt{2}}\cdot(22)-\frac{1}{\sqrt{2}}\cdot(23)$
		$3\sigma_\beta 4\sigma^\alpha 1\pi^{\alpha\alpha}_\beta$	(23)	
		$3\sigma^\alpha 4\sigma^\alpha 1\pi^\alpha_{\beta\beta}$	(24)	$-\frac{1}{\sqrt{6}}\cdot(22)-\frac{1}{\sqrt{6}}\cdot(23)+\sqrt{\frac{2}{3}}\cdot(24)$

Table 3.10: Comparison of QMC energies obtained for CH using basis A and basis B. SCF denotes the single reference wavefunction using the SCF MOs; MCSCF(3e) and MCSCF(5e) refer to the wavefunctions described by the multi-reference expansions with 3 and 5 active electrons.

Wavefunction	Basis A		Basis B	
	Variational	QMC	Variational	QMC
SCF	-38.278094	-38.45926(209)	-38.278878	-38.46199(193)
MCSCF(3e)	-38.299271	-38.42748(469)	-38.300050	-38.41669(413)
MCSCF(5e)	-38.313511	-38.39825(698)	-38.314224	-38.41686(503)

Table 3.11: Determinant coefficients for each basis set for CH($^2\Pi$) with 3 active electrons (5 actual CSFs and 6 determinants)

Determinant	Basis A	Basis B
$3\sigma_\beta^\alpha 1\pi^\alpha$	0.986354	-0.986363
$4\sigma_\beta^\alpha 1\pi^\alpha$	-0.035836	0.036053
$3\sigma^\alpha 4\sigma_\beta 1\pi^\alpha$	0.023440	0.024106
$3\sigma_\beta 4\sigma^\alpha 1\pi^\alpha$	0.023440	0.024106
$3\sigma^\alpha 4\sigma^\alpha 1\pi_\beta$	-0.047277	-0.048619
$1\pi_\beta^{\alpha\alpha}$	0.149896	-0.149137

Table 3.12: Determinant coefficients for each basis set for CH($^2\Pi$) with 5 active electrons (18 actual CSFs and 24 determinants)

Determinant	Basis A	Basis B
$2\sigma_\beta^\alpha 3\sigma_\beta^\alpha 1\pi^\alpha$	-0.980840	0.980808
$2\sigma_\beta^\alpha 4\sigma_\beta^\alpha 1\pi^\alpha$	0.024132	-0.024035
$3\sigma_\beta^\alpha 4\sigma_\beta^\alpha 1\pi^\alpha$	0.093732	-0.094534
$2\sigma_\beta^\alpha 3\sigma_\beta 4\sigma^\alpha 1\pi^\alpha$	-0.007446	-0.007224
$2\sigma_\beta^\alpha 3\sigma^\alpha 4\sigma_\beta 1\pi^\alpha$	-0.007381	-0.007166
$2\sigma_\beta^\alpha 3\sigma^\alpha 4\sigma^\alpha 1\pi_\beta$	0.014952	0.014512
$3\sigma_\beta^\alpha 2\sigma_\beta 4\sigma^\alpha 1\pi^\alpha$	0.015645	0.015844
$3\sigma_\beta^\alpha 2\sigma^\alpha 4\sigma_\beta 1\pi^\alpha$	0.016172	0.016328
$3\sigma_\beta^\alpha 2\sigma^\alpha 4\sigma^\alpha 1\pi_\beta$	-0.032086	-0.032443
$4\sigma_\beta^\alpha 2\sigma_\beta 3\sigma^\alpha 1\pi^\alpha$	0.025450	-0.025427
$4\sigma_\beta^\alpha 2\sigma^\alpha 3\sigma_\beta 1\pi^\alpha$	0.027177	-0.027144
$4\sigma_\beta^\alpha 2\sigma^\alpha 3\sigma^\alpha 1\pi_\beta$	0.001741	-0.001731
$2\sigma_\beta^\alpha 1\pi_\beta^{\alpha\alpha}$	-0.153648	0.153175
$3\sigma_\beta^\alpha 1\pi_\beta^{\alpha\alpha}$	-0.029636	0.030320
$4\sigma_\beta^\alpha 1\pi_\beta^{\alpha\alpha}$	0.016937	0.017033
$2\sigma^\alpha 3\sigma_\beta 1\pi_\beta^{\alpha\alpha}$	-0.017591	0.017670
$2\sigma_\beta 3\sigma^\alpha 1\pi_\beta^{\alpha\alpha}$	0.012387	-0.012509
$2\sigma^\alpha 3\sigma^\alpha 1\pi_{\beta\beta}^\alpha$	0.005248	-0.005204
$2\sigma^\alpha 4\sigma_\beta 1\pi_\beta^{\alpha\alpha}$	0.000709	0.000858
$2\sigma_\beta 4\sigma^\alpha 1\pi_\beta^{\alpha\alpha}$	0.004293	0.004182
$2\sigma^\alpha 4\sigma^\alpha 1\pi_{\beta\beta}^\alpha$	-0.005044	-0.005083
$3\sigma^\alpha 4\sigma_\beta 1\pi_\beta^{\alpha\alpha}$	0.001658	0.001663
$3\sigma_\beta 4\sigma^\alpha 1\pi_\beta^{\alpha\alpha}$	-0.002235	-0.002221
$3\sigma^\alpha 4\sigma^\alpha 1\pi_{\beta\beta}^\alpha$	0.000582	0.000562

Figure 3.3: Time step extrapolations for CH using wave functions based on basis A and B, respectively.

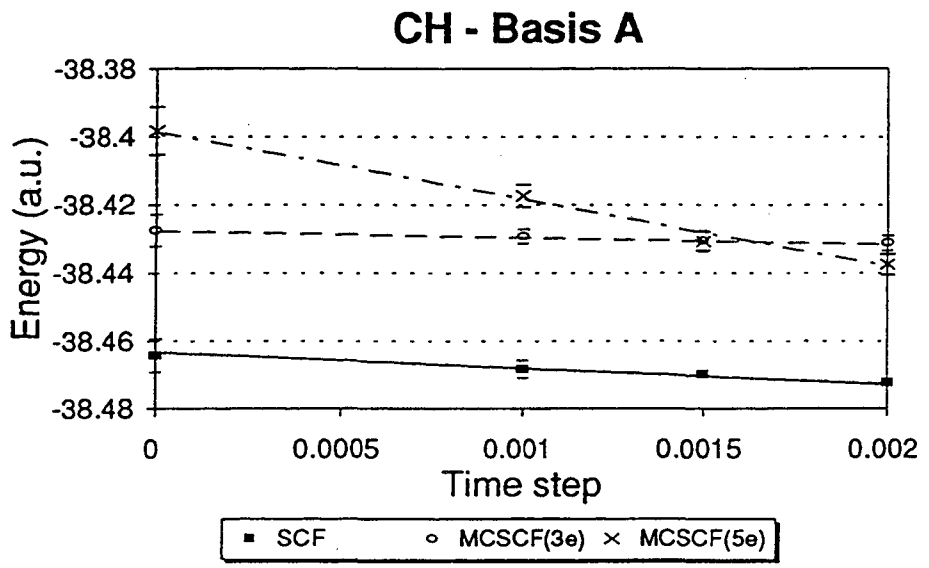

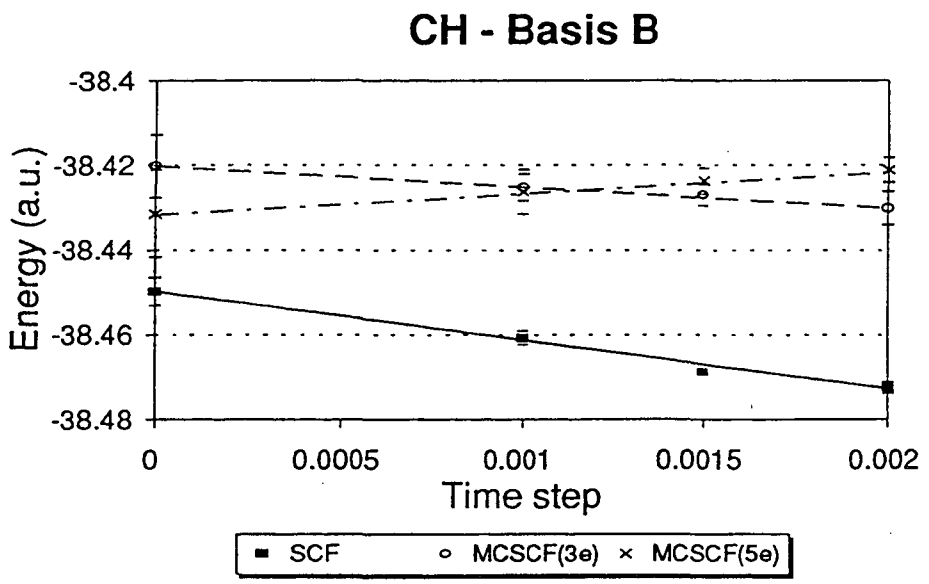

Figure 3.4: Variational and QMC results for three different types of wavefunction at Cade and Huo's equilibrium geometry, $R_e = 2.124a_0$. (a) Selected QMC results, (b) QMC and variational results.

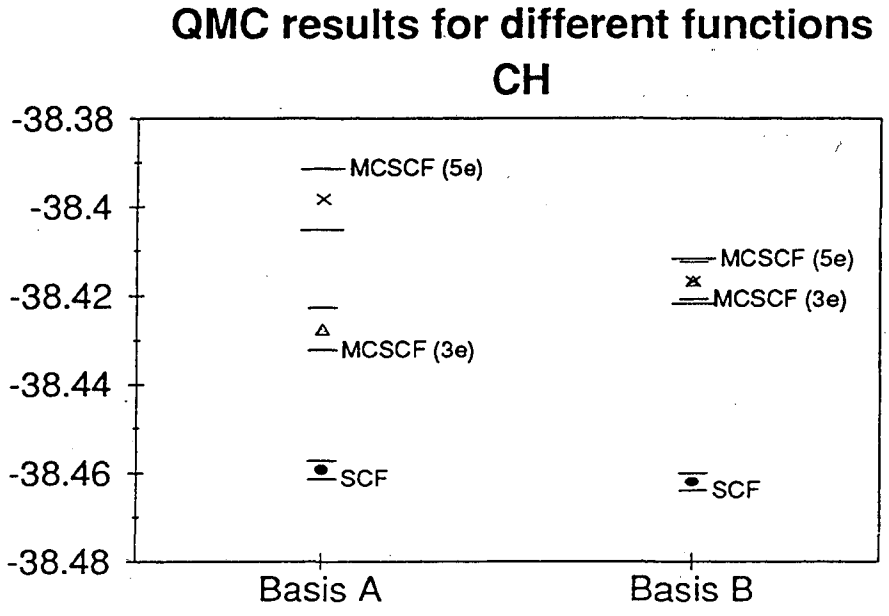

(a)

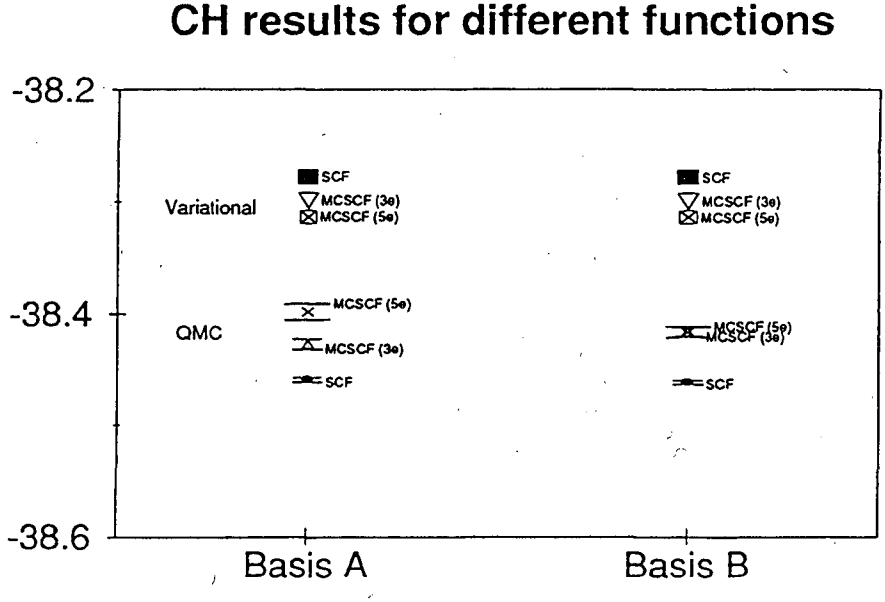

(b)

Figure 3.5: CH geometry optimization. (a) SCF comparison with basis B and C. (b) SCF vs different levels of CASSCF with basis B. (c) Effect of f-functions on the equilibrium geometry using basis C.

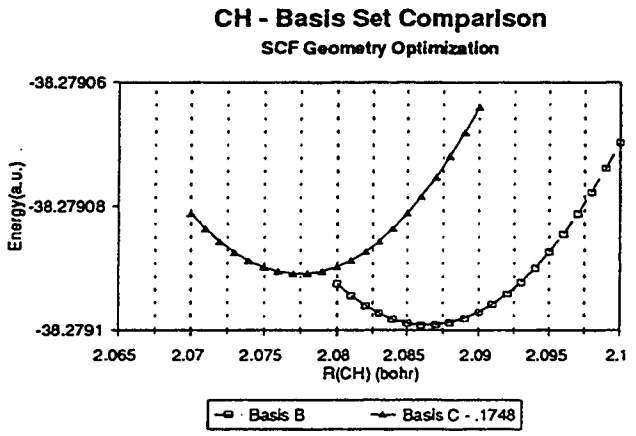

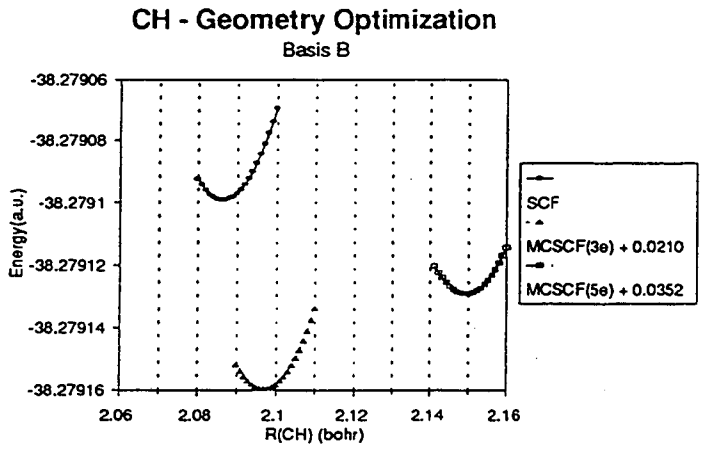

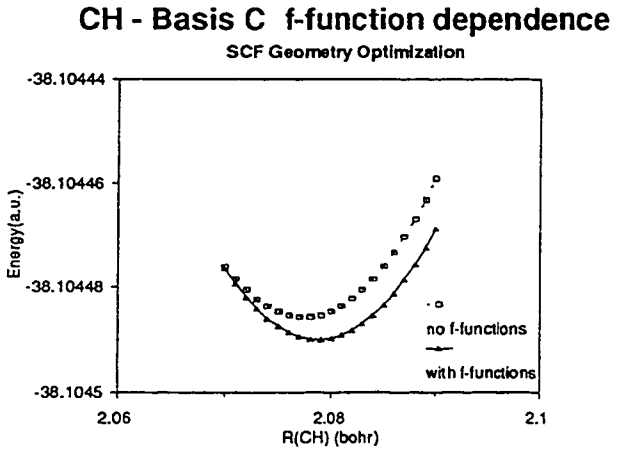

3.2.2.4 Binding energy

Binding energies for the CH radical were computed using HF Basis B wavefunctions for C. For this purpose, the QMC energy of C was evaluated using Basis B, and as it can be seen from Table 3.13, the improvement observed in the correlation energy recovered for the C-atom was excellent. Since we do not have a calculation done for carbon atom with comparable (multi-reference) wave functions, binding energies for MCSCF wavefunctions are not very meaningful.

Binding energies were also computed using Basis C for CH (Table 3.5) and the Clementi Basis (See Table 3.2). Even though the "quality"[12] of the one-particle part of the wave functions is different, the percent correlation obtained in each basis is comparable. All results were summarized in Table 3.4. Comparing our QMC values for D_e, we observe that the best result is 3.61(4) obtained from the Cade and Huo basis using the J_{een} correlation function, since the experimental value for the D_e of CH is around 3.64.[13]

Table 3.13: CH($^2\Pi$) binding energies using basis B.

System	Wavefunction	E_{QMC} (a.u.)	% correlation	D_e (eV)
C(^{3}P)	SCF	-37.83529(335)	94.8%	
H(^{2}S)		-0.50	100%	
CH($^2\Pi$)	SCF	-38.46199(193)	92.4%	3.45(10)
	MCSCF(3e)	-38.41669(413)	69.5%	2.21(14)
	MCSCF(5e)	-38.41686(503)	69.6%	2.22(16)

[12] It is necessary to make clear there is a distinction between the quality of Ψ_T in variational calculations and in QMC calculations, especially since there is no direct correlation in the results presented here.

[13] cf. Ref. [62].

3.2.3 Ethynyl Radical - C_2H

3.2.3.1 Introduction

Ethynyl radical(C_2H) is an abundant interstellar molecule, with lowest states

$$\begin{array}{ll} X^2\Sigma^+ & 1\sigma^2 2\sigma^2 3\sigma^2 4\sigma^2 1\pi^4 5\sigma \\ A^2\Pi & 1\sigma^2 2\sigma^2 3\sigma^2 4\sigma^2 1\pi^3 5\sigma^2 \\ B^2\Sigma^+ & 1\sigma^2 2\sigma^2 3\sigma^2 4\sigma 1\pi^4 5\sigma^2 \ . \end{array}$$

C_2H is a reaction intermediate in various combustion systems, as well as in the photolysis of acetylene, and it is abundant in the atmospheres of certain carbon-rich stars. The C_2H surface has a stable minimum at a linear CCH geometry.

Tucker[100] *et al.* were the first to identify C_2H in interstellar space as well as the first to show that it had a linear geometry in the ground state, $^2\Sigma^+$. The first significant *ab initio* calculations on ethynyl radical were presented by So and Richards[101] using an STO basis and the ALCHEMY programs. For the $\tilde{X}^2\Sigma^+$ state, they found the C-C bond length to be 1.789 Å and the C-H bond length, 1.0576 Å.[14]

Hillier *et al.*[102], optimized the geometry by CI on the two lowest states: $^2\Sigma^+$ and $^2\Pi$. The calculations were done at two different levels of basis sets; they used both STOs (DZ from Clementi[103]) and GTOs (contracted basis from Clementi[102]). They did two types of calculations: one consisted of an RHF calculation followed by a CI and the other consisted of an antisymmetrized product of strongly orthogonal geminals (APSG) calculation. Their final (equilibrium) geometry, reported from the RHF+CI method was $r_{CC} = 1.209$Å $= 2.285a_0$ and $r_{CH} = 1.065$ Å $= 2.012a_0$.

Likewise, Shih, *et al.*, [104] presented a theoretical study on the ethynyl radical: SCF and CI curves using DZP basis sets on the two lowest states, $\tilde{X}^2\Sigma^+$ and $\tilde{A}^2\Pi$. The curves in this study showed different minima for the SCF and CI curves. Their theoretical geometries for C_2H, which many later studies cite were: $r_{CH} = 2.008a_0$ and $r_{CC} = 2.266a_0$) for the SCF curve,[15] and $r_{CC} = 2.348a_0$ for the CI curve. In a later paper[106] they did more on the calculations of the potential curves, studied the behavior of C_2H with CC stretching and CCH bending vibrations. Results were compared and found in agreement with the emission spectrum.

Jacox[107] did matrix isolation studies to study the vibrational spectrum of C_2H. The stretching and stretching-interaction force constants of C_2H were determined, which were used to estimate the bond lengths. "The carbon-hydrogen bond was found to be exceptionally strong,

[14] It was unusual to optimize both bond lengths; most other studies contemporary to [101] only optimized one bond length.

[15] The optimize for r_{CC}, but they take r_{CH} from the astrophysical measurement of Barsuhn[105]. In this paper, they give $r_{CH} = 2.008a_0$ and $r_{CC} = 2.2274a_0$.

and the carbon-carbon bond is intermediate between that characteristic of ground-state C_2 and C_2H_2.[107]" It was shown by Andrews and Pimentel that a plot of the C-H stretching force constant against the C-C bond length is linear over a rather wide range of C-H bond lengths. Using this finding and making a couple other corrections (addition of stretching force constants and bond length of neutral CH) they deduced the bond-length for the C-C and C-H bonds. They also made an estimate of the rotational spacing for C_2H assuming a carbon-carbon bond length of 1.224Å (the mean bond lengths for ground state C_2 and C_2H_2) and a C-H bond length of 1.014Å. The resulting value agrees well with the value observed from the interstellar medium data. Years later, Jacox and Olson[108] carried another experiment in an argon matrix where a different region of the spectrum was studied. They presented "the first spectral survey of the near infrared absorption band system of C_2H" using Fourier transform absorption spectra.

Carrick, *et al.*[109, 110] deduced r_{CC} using IR spectroscopy to be 1.226Å ($2.317a_0$), assuming r_{CH} = 1.014 Å. The experiment was done using a color center laser spectrometer in which acetylene was radiated to form C_2H. They claimed to have problems in detection due to lots of polyacetylene being formed and blocking the mirrors, since C_2H is highly reactive with acetylene. Hence, argon was flowed in with the mixture in an attempt to prevent large deposits of polyacetylene on the mirrors.

Harding *et al.*[111] did an *ab initio* determination of the rate constant for

$$H_2 + C_2H \rightarrow H + C_2H_2,$$

and found the equilibrium geometry for C_2H in the process of plotting the PES for the above mentioned reaction. Using spin-optimized generalized valence bond (SOGVB) theory they got $r_{CC} = 2.31a_0$ and $r_{CH} = 2.03a_0$, using SOGVB-CI they found $r_{CC} = 2.32a_0$ and $r_{CH} = 2.04a_0$; and using polarization configuration interaction (POL-CI) they found $r_{CC} = 2.33a_0$ and $r_{CH} = 2.04a_0$. All calculations were done using a DZP basis set.

Fogarasi *et al.*[112] presented an *ab initio* calculation using the 6-311G** basis set and SDCI. They found an equilibrium geometry of r_{CH} = 1.067Å and r_{CC} = 1.209Å (1.205 and 1.063 if corrected for residual errors), which was in accordance with the experimental rotational constant. The single rotational constant available at the time was not enough to determine an experimental geometry, but they did a preliminary check to show that the ground state was linear. They were inspired by Carrick *et al.*[109, 110], and their reported estimate for the CC bond of 1.30Å, to do the calculation. They argue that "*all previous SCF calculations have shown that the Hartree-Fock approximation already gives a reasonable description of the electronic structure.... In all of our calculations on the bent molecule, the CI coefficient of the reference configuration remained above 0.95.*" [16] Previous results are compared with theirs, but the only results they

[16]This agrees with our previous experience with the CH radical.

consider of similar quality are those of Hillier *et. al.*[102], and So and Richards [101]. They also provided an excellent survey of work to date, both theoretical and experimental.

White and Schatz[113] developed analytical PESs for the lowest electronic states of ethynyl (C_2H), and acetylene (C_2H_2) based on fits to accurate *ab initio* calculations (a large-scale polarization configuration interaction, POL-CI, from Ref. [114]) for the respective molecular force fields, and using energies of formation from experiment. The zero point energy of C_2H was found to be 9 kcal/mol[111]. The bond lengths used as LEPS parameters for the fitting were $r_{CC} = 2.34799a_0$ and $r_{CH} = 2.1163a_0$ The bond lengths obtained from the fitted C_2H surface were $r_{CC} = 2.3379a_0$ and $r_{CH} = 2.0284a_0$.

Reimers *et al.*[115], used CASSCF to determine the full PES for C_2H using Huzinaga's basis sets, and 7 active electrons. The CASSCF wave functions for each state were computed with different basis sets. Since common methods to produce the C_2H radical include photolysis of C_2H_2 and electric discharges either in C_2H_2 or over polyacetylene[110], the lowest transition is poorly resolved.

Kraemer *et al.*[116], determined the molecular potential of the CCH ground state, $^2\Sigma^+$, at 75 internuclear geometries using CASSCF. Their equilibrium geometry was found to be $r_{CC} = 1.215226(114)\text{Å} = 2.296a_0$ and $r_{CH} = 1.070533(374)\text{Å} = 2.023a_0$. They are the first theoretical work to give an error associated to their estimate of this particular equilibrium geometry. Yan *et al.*[117] presented another spectroscopic study to examine the excited levels of C_2H and give further information on studying the vibronic coupling between the $\tilde{X}$ and $\tilde{A}$ states.

Table 3.14 summarizes work mentioned in this section which offer an equilibrium geometry for the ethynyl radical, as well as work of others who have computed C_2H properties in the process of estimating D_0 for acetylene.

Table 3.14: Equilibrium distances r_{CH} and r_{CC}, and total energies obtained for ethynyl radical, $C_2\dot{H}$ ($\tilde{X}^2\Sigma^+$).

Name	Year	R_{C-H} (a_0)	R_{C-C} (a_0)	Energy (a.u.)	Method and ZPE (kcal/mole)	Ref.
So and Richards	1975	1.998	2.228	-76.162256	ALCHEMY	[101]
Hillier *et. al.*	1975	2.012	2.285	-76.29797	RHF + CI (STOs and GTOs)	[102]
Shih, *et. al.*	1977	2.008	2.274	-76.12988	quoted from [105]	[104, 106]
		2.008	2.266		SCF/DZP	
		2.008	2.348	-76.3235	CI	
Harding *et. al.*	1982	2.03	2.31		SOGVB/DZP	[111]
		2.04	2.32		SOGVB-CI/DZP	
		2.04	2.33		POL-CI/DZP	
Fogarasi *et. al.*	1983	2.009	2.277	-76.4008	SDCI/6-31G** (corrected for residual errors)	[112]
White and Schatz	1984	2.0284	2.3379	-	Fitted to PES ZPE = 9	[113]
Kraemer *et. al.*	1986	2.023	2.296	-	CASSCF	[116]
Perić *et. al.*	1987	2.041	2.320	-	MRD-CI PES	[118, 119]
Osamura *et. al.*	1989	2.035	2.334	-76.22411	MCSCF/DZ	[120]
		2.041	2.307	-76.24730	MCSCF/DZP	
Curtiss and Pople	1989	2.012	2.230	-76.35347	MP2(full)/6-31G*	[121, 122]
Langhoff *et. al.*	1990	2.016	2.308	-76.976115	CPF	[37]
Montgomery and Petersson	1990	2.024	2.297	-76.59102	QCI + CBS ZPE = 8.4	[123]
Habibollahzadeh, *et. al.*	1992	2.009	2.296	-76.41542	MP2/6-311G**	[124]
		2.042	2.308		MCSCF/DZP	
		2.042	2.292	-75.92179	DMol/DNP	
		2.051	2.272	-75.92831	DMol/DN	
Jacox	1975	1.916	2.313	-	Expt. (matrix) + *ab initio*	[107]
Curl *et. al.*	1983	1.916	2.317	-	Expt. (IR) + *ab initio*	[109, 110]
this work	1993	1.991	2.227	-76.56938(500)	FNDMC - Basis B	-

3.2.3.2 QMC study of C_2H

Since in our experience with carbon atom and the CH radical Basis B gave the best results, we decided to use it for the rest of our calculations. Most of the earlier work claimed that the geometries obtained at the SCF level were good enough, but recent work on the species claims the opposite.[17] Given the uncertainty in obtaining derivatives by QMC methods, we would not be able to perform a geometry optimization for the species, so in order to do a QMC calculation one depends on experimental values and *ab initio* results. The ALCHEMY program does not provide the option to automatically optimize geometries at any level. Since we had also access to the GAMESS program[126], we carried out a geometry optimization at the SCF level with an STO-6G basis mimicking the Basis B given in Table 3.7. The assumption was that even if the Gaussian-based basis would not be the same as the STO basis obtained from ALCHEMY, the resulting curves from each program would be parallel to each other. We tested this assumption by doing a curve varying the R_{C-H} bond in each GAMESS and ALCHEMY, near the minimum found by GAMESS. The resulting curves are shown in Fig. 3.6. We can see from this figure that the curves are not parallel as assumed. An STO-NG basis set is expected to closely resemble the STO it emulates, therefore giving curves that should be, if not overlapping, at least parallel. However, we found that it wasn't that difficult to obtain a minimum with an STO basis, using ALCHEMY.[18] The section of the PES calculated using ALCHEMY closest to the minimum ($r_{CC} = 2.227a_0$ and $r_{CH} = 1.991a_0$) is shown in Fig. 3.7.

Figures 3.6 and 3.7 show that the R(C-H) distance is relatively constant, while greater variations occur on the R(C-C) coordinate. This and the equilibrium geometry obtained in the next section for C_2H_2, suggest that at the SCF level, the breaking of the C-H bond does not affect much the length of the second C-H bond. Or maybe just the fragment does not care for the existence of any other bonds on the second carbon.[19] However we should keep in mind that this was done as the SCF level, which does not treat dissociation correctly on its own, i.e., we might not want to extrapolate any conclusions to QMC.

The QMC energy obtained was -76.56938(500)a.u. The time step extrapolation to this calculation is shown in Fig. 3.8.

[17] Bauschlicher *et al.*[37, 125] will be presented in Sec. 3.2.4.1 since their work on C_2H was done as part of determining D_0's for C_2H_2 and C_2H.

[18] Actually in terms of wall clock time it proved more efficient to directly do a tight grid of energies using ALCHEMY than waiting for GAMESS and/or HONDO to produce their geometry optimization. Both optimizations done on the same IBM RISC workstation. This was the case for the C_2H_2 optimization as well.

[19] Here it would have been useful to have results from McLean's localized orbitals[127].

Figure 3.6: SCF energies obtained using STO vs. STO-6G basis sets. Energies from the GAMESS program have been shifted for convenience in plotting. R(C-C) is held constant at 2.276 a_0, ($r_{CH} = 1.991a_0$ and $r_{CC} = 2.276a_0$ was the minimum found by GAMESS).

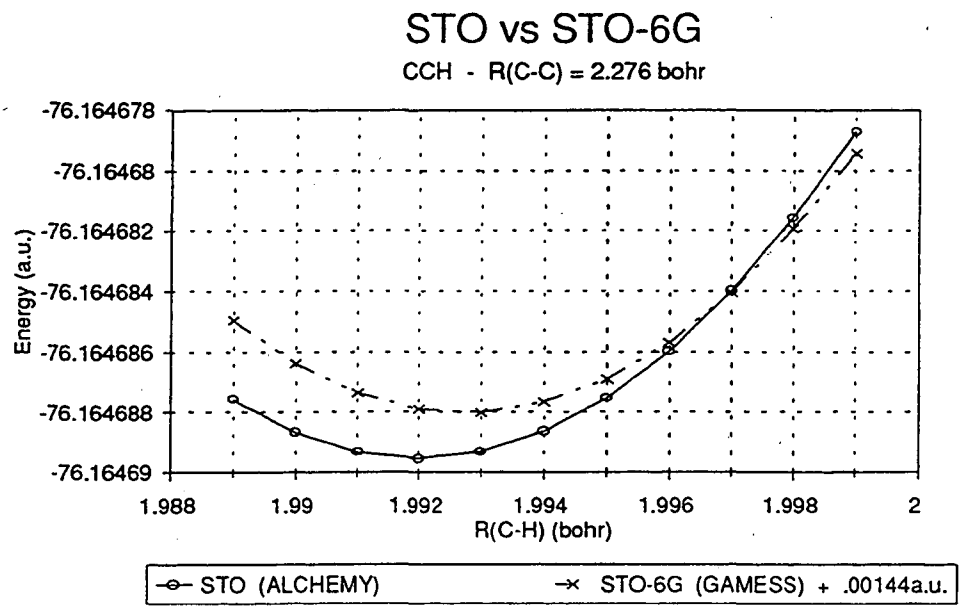

Figure 3.7: SCF PES of ethynyl radical using basis B.

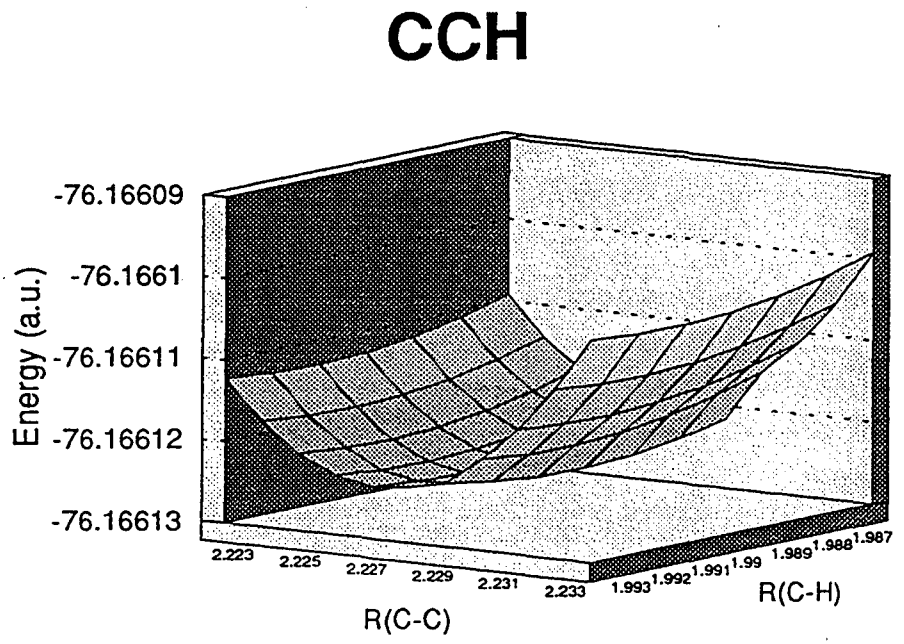

Figure 3.8: Time step extrapolation for C_2H with Basis B SCF.

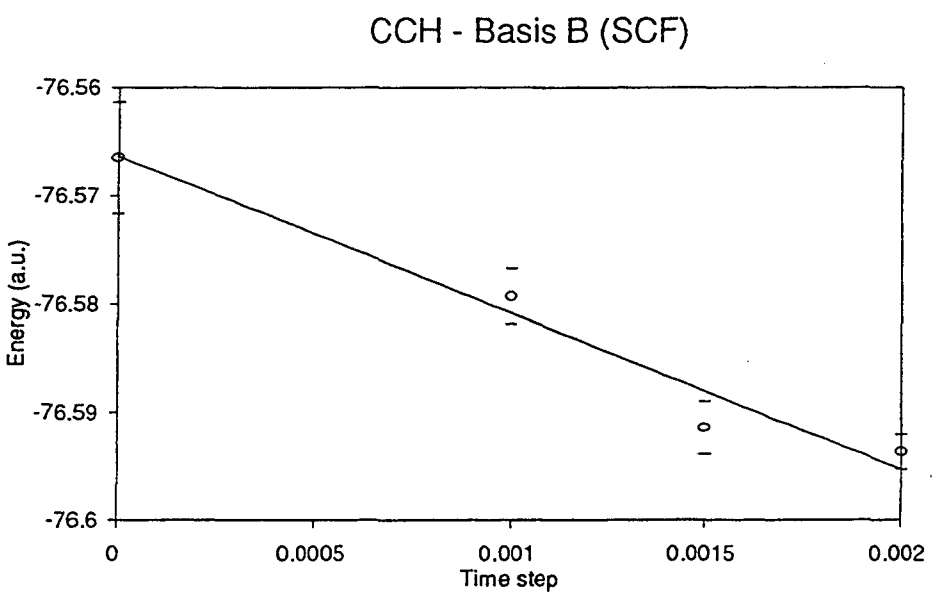

3.2.4 Acetylene - C_2H_2

3.2.4.1 Introduction

Lafferty and Thibault[128] provides some of the earliest experimental data for C_2H_2. They were the first ever to do high resolution IR (HRIR) on acetylene with different isotopes of carbon and determined the equilibrium bond distances to be r_e(C-H) = 1.060 Å($2.005a_0$) and r_e(C-C) = 1.203 Å($2.273a_0$).

Carter *et al.* presented in Ref. [129] a PES for ground-state acetylene, discussing in detail its dissociation and isomerization. The dissociation channels for acetylene are

$$C_2H_2(\tilde{X}\,^1\Sigma_g^+) \rightarrow \left[\begin{array}{l} H(^2S) + C_2H(\tilde{X}\,^2\Sigma^+) \\ \left\{\begin{array}{l} C(^3P) + CH_2(\tilde{X}\,^3B_1) \\ C(^1D) + CH_2(\tilde{A}\,^1A_1) \end{array}\right. \\ 2CH(\tilde{X}\,^2\Pi) \\ H_2(\tilde{X}\,^1\Sigma_g^+) + C_2(\tilde{X}^1\Sigma_g^+)\,. \end{array}\right. \tag{3.2}$$

A diagram with the relative energies of acetylene and its dissociation products according to Carter *et al.*, is shown in Fig. 3.9. A year later, Siegbahn presented thorough MCSCF and MC-CI studies of the fourth reaction of Eq. 3.2 in Ref. [93]. This work was already discussed in Sec. 3.2.2.1 when introducing his results for CH.

Recall also the analytical PES developed by White and Schatz[113] for the lowest electronic states of ethynyl (C_2H), and acetylene (C_2H_2). "Ground-state C_2H_2 is characterized by a stable minimum in the linear acetylene HCCH geometry and a higher minimum in the vinylidene (CCH2) configuration.[113]" ΔE from dissociation of C_2H_2 into C_2H + H was found to be 131.5 kcal/mole. The bond lengths obtained from the fitted C_2H_2 surface were $r_{CC} = 2.32a_0$ ($2.273a_0$, exptl [128]); $r_{CH} = 2.0385a_0$ ($2.005a_0$, exptl [128]).

Wodtke and Lee [130] found the C-H bond dissociation energy (BDE) in acetylene to be D_0(C_2H-H) = 132 ± 2 kcal/mol by studying the photodissociation of acetylene at 193.3nm with detection by the molecular time-of-flight method. Since C_2H was produced in the collission-free environment of a molecular beam, they assumed that the C_2H radical observed corresponds to the ground-state fragment. Shiromaru *et al.*[131] determined the bond dissociation energy of acetylene to be 5.75 ± 0.05 eV. This determination deduced the C-H bond dissociation energy from

$$D_0(\mathrm{R-H}) = E_{th}(\mathrm{H}^+) - I(\mathrm{H})\ , \tag{3.3}$$

where I(H) is the ionization potential of H, by measuring the threshold energy of H^+ in the process

$$\mathrm{RH} + h\nu \rightarrow R + H^+ + e^-\ . \tag{3.4}$$

Figure 3.9: Carter presented the first figure in Ref. [129]. They represent all possible dissociation channels for C_2H_2. The second figure compares the last column in the first figure to our QMC results.

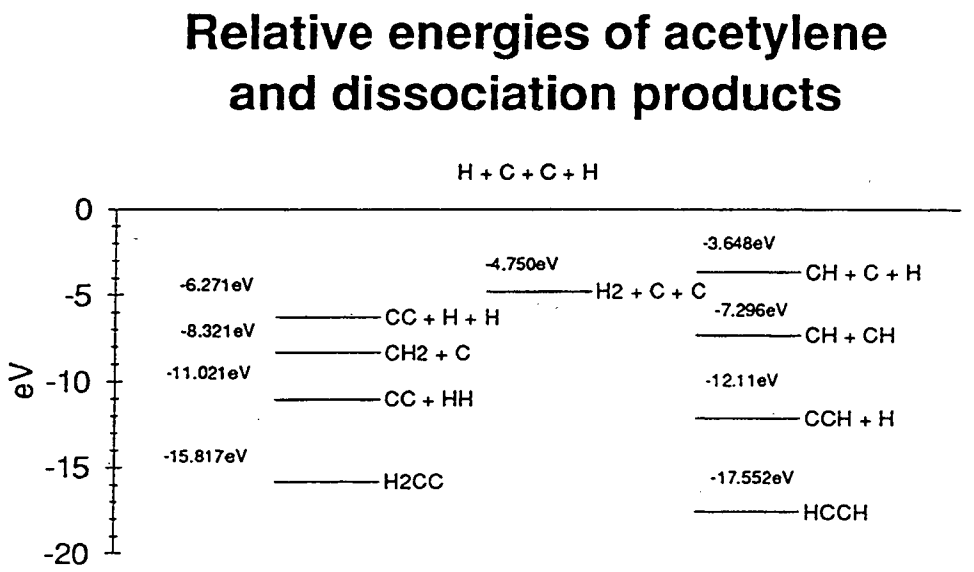

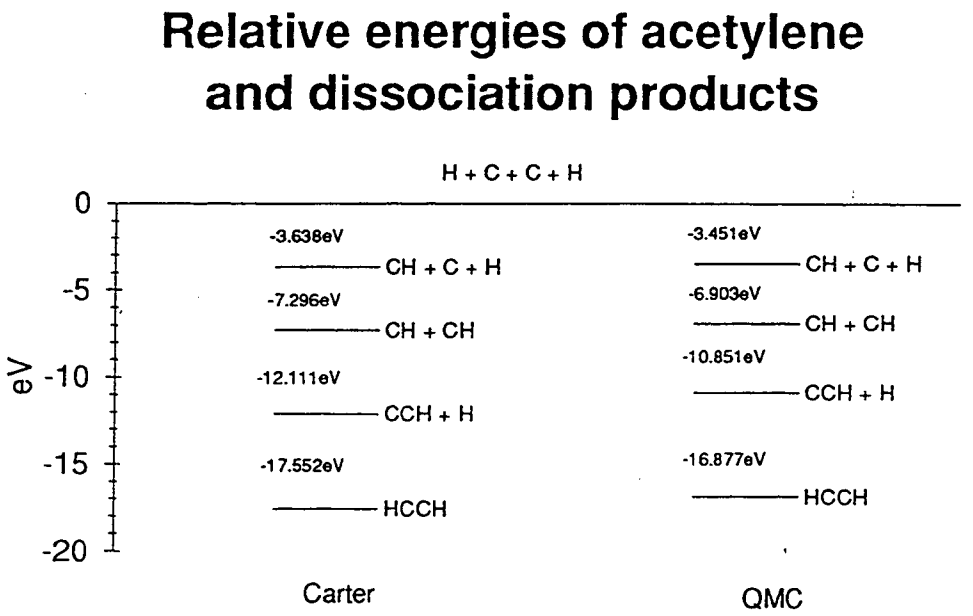

Perić *et al.*[132] recalculated the C-H curves at a C-C bond length of $2.55a_0$ and at H-C-C angles of 180°, 140° and 120°. The C-H distance was varied between 1.7 and $2.4a_0$ in intervals of $0.1a_0$. The potential curves for the C-C stretching vibrations were also calculated at the same value of the bond angle with the C-H distance held fixed at $2.0a_0$. The C-C distance was varied in the region 2.25-$2.95a_0$ at intervals of $0.1a_0$. Their result for the equilibrium geometry for the $\tilde{(X)}^1\Sigma_g^+$ state is $r_{CH} = 1.080$Å $= 2.041a_0$ and $r_{CC} = 1.228$Å $= 2.320a_0$.

In Ref. [121] Curtiss and Pople introduced the G-1 method[20] and found bond dissociation energies for ethylene,[21] acetylene and vinyl. For C_2H_2 ($r_{CC} = 1.216$Å and $r_{CH} = 1.066$Å) they got an energy of −77.07614a.u.(MP2(full)/6-31G*), and −77.13994a.u.(MP4/6-311G**), which were corrected to -77.18610a.u. In a second paper [122] they concluded that the dissociation energy is 5.79 eV(133.5 kcal/mole).

Another often cited work on acetylene is that of Fujii *et al.*[133, 134]. They studied decreases in the fluorescence quantum yield, Φ_f, of acetylene[22] to determine a dissociation energy of D_0(C_2H-H) = 132±2 kcal/mole.

Segall *et al.*[135] got 127(1.5) kcal/mol for the dissociation energy of acetylene by measuring the kinetic energy (KE) of the hydrogen atom fragment using Doppler multiphoton ionization spectroscopy. This result is in agreement with the unpublished work of Benson[136].

In Ref. [85] Green, Kinsey and Field launched the controversy which caused the re-re-evaluation of the dissociation energy of acetylene.[23] Using Stark anti-crossing (SAC) experiments they determined an upper-bound for the dissociation energy of acetylene of 529.89(1) kJ/mol = 126.647(2) kcal/mol, much lower than the consensus value.

Osamura *et al.*[120] made an interesting attack on Wodtke and Lee's[130] conclusions about evidence of pre-dissociation in C_2H_2. The argument is as follows: the electronic excitation of acetylene caused by UV light starts the process (presumably one obtains a $\pi \rightarrow \pi^*$ transition), the lowest excited singlet state is $\tilde{A}^1A_u$,(trans-bent structure) which has been identified both theoretically and experimentally. By assuming a potential energy curve similar to HCN, Wodtke and Lee suggested that the excited state $\tilde{A}^1A_u$ predissociates to the ground state of $C_2H(X^2\Sigma^+)$ and H. They used the GAMESS program to perform an *ab initio* study at the MCSCF level, doing all possible electron configurations among two bonding and two antibonding C-H orbitals and four π orbitals were taken into account. DZ and DZP basis sets were used, and the zero point vibrational energy[24] (ZPE) corrections were done using the DZ basis set. For $C_2H_2(X^1\Sigma_g^+)$ with DZ basis at $r_{CC} = 1.226$Å $= 2.317a_0$ and $r_{CH} = 1.075$ Å $= 2.031a_0$ they obtained a

[20] See Sec. 1.2.4 and Ref. [14].

[21] This bond dissociation energy disagrees with Shiromaru, Achiba and Lee in [131].

[22] "A sudden decrease in Φ_f suggests dissociative state crossing or coupling to a dissociation continuum."

[23] Ref. [137] is a previous study of this group on the acetylene system using Zeeman Anticrossing-Spectroscopy.

[24] Their results for C_2H are presented in Table 3.14.

total MCSCF energy of −76.91617a.u. With a DZP basis at r_{CC} = 1.215 AA = $2.296a_0$ and r_{CH} = 1.079Å = $2.039a_0$ they obtained an MCSCF energy of -76.94180a.u. These results are summarized in Table 3.15.[25] In conclusion, they show that the lowest excited state of acetylene smoothly connects to the corresponding states of C_2H without any surface crossing between the bound state and the dissociative states. The S_1 state of acetylene produces the first excited state of C_2H directly. The dissociation energy of 132±2 kcal/mole obtained by Wodtke and Lee is the energy required to form the excited state of $C_2H(^2\Pi)$ and the H atom.

Ervin *et al.*[140] used thermodynamic measurements to deduce the bond dissociation of acetylene and half a dozen other compounds. They got 131.3±7 kcal/mol by using the techniques of negative ion photoelectron spectroscopy and gas-phase proton transfer kinetics. Perić *et al.* present another *ab initio* study in Refs. [118, 119]. Wu and Carter [141] used *ab initio* generalized valence bond (GVB) and correlation-consistent configuration interaction (CCCI) theory within a DZP basis set and presented their result for acetylene to be 129.7 kcal/mol. They claimed this method is accurate within 1-5 kcal/mole in giving dissociation energies for single and double bonds.

Montgomery and Petersson [123] did an *ab initio* calculation to estimate the bond dissociation of acetylene, and got D_0 = 131.54 kcal/mole. They also estimated the error associated with their calculations. Their method consists of extrapolating to the complete basis set limit (CBS), and using previous results to claim that the associated error is less than 1 kcal/mole. They used CBS-QCI, the final value includes CBS extrapolations to the SCF, core, valence second order and valence higher-order contributions. Vibrational ZPEs are calculated from SCF/6−31G* harmonic frequencies scaled by a factor of 0.8929. Their results for the SCF, QCI and CBS extrapolations of both are given in Tables 3.14 and 3.15 for C_2H and C_2H_2, respectively. They also agreed very well with the electron affinity of CCH as found experimentally by Ervin *et. al.*[140].

Baushlicher *et al.*[37] obtained a value of 130.1±1.0 kcal/mol using the CASSCF method. They used MRCI and averaged coupled-pair functional method (ACPF) treatments based on CASSCF wavefunctions. Vibrational ZPE contributions were computed using coupled-pair functional (CPF) wavefunctions for C_2H and C_2H_2. Their calculation also involved extending the basis sets used to the HF limit. The geometries used for the energy calculations of C_2H and C_2H_2 were as follows: for the molecule, $r_{CC} = 2.292a_0$ and $r_{CH} = 2.010a_0$, and for the fragment, $r_{CC} = 2.308a_0$ and $r_{CH} = 2.016a_0$. Their results are summarized in table 3.15 with others.

In a later study[125] this same group determined the bond dissociation energy of C_2H. Once more they emphasized that a single-reference-based wave function is sufficient description for a closed-shell system, but for radicals such as C_2 and C_2H, a MRCI approach is more sensible. Anyway, since this time the main study was on the bond dissociation of ethynyl rather than

[25] They also give another reference[138, 139] to an experimental measurement for the geometries of acetylene: r_{CC} = 1.203Å = 2.273 a_0 and r_{CH} = 1.061Å = $2.005a_0$.

acetylene, i.e. they studied the breaking of C_2H into C_2 + H, the argument for a multi-reference approach was even stronger, even though they used an experimental geometry for C_2. It seems as if not even the CASSCF approach will give them the right optimized structure for the C_2 radical. From their conclusion[125]:

> "The experimental value is reduced and in better agreement with theory if the thermochemical D_0 value for C_2 is used in place of the spectroscopic value. The present calculations rule out the previous theoretical results of Wu and Carter thereby suggesting that the errors in their "correlation-consistent CI" method can be considerably larger when the fragments are not well described by a single reference configuration."
>
> "The C-H bond dissociation energy of C_2H is determined using the experimental geometry for C_2 and out previously optimized geometry for C_2H. The reference comprises 86.0% of the final MCPF wave function for C_2H because the $^1\Sigma_g^+$ state of C_2 is poorly described by a single-reference approach. This is different from C_2H_2 where the reference percentages were very similar for the equilibrium and dissociated geometries. Since single-reference-based approaches are expected to be less accurate for the C-H bond energy in C_2H we have also employed the CASSCF/MRCI approach."

(Nevertheless, one must keep in mind that as long as we do not know how these "improvements" on the trial function affect the location of its nodes, no benefit can be guaranted from using these techniques (MCSCF, CI, CASSCF) to obtain trial functions for QMC.)

Balko *et al.*[142] tackled the C_2H_2 problem once more by molecular beam. Their resulting bond dissociation is 131.4±0.5 using mass spectroscopy to analyze their product. They basically confirmed work done by Wodtke and Lee in [130], this time by examining the H atom velocity after dissociation instead of the C_2H fragment.

Habibollahzadeh *et al.*[124] used a large range of methods and basis sets to compare with their density functional theory (DFT) results using a local density approach (LDA). Some of their results are shown in Table 3.15. They claimed that their DFT-LDA results for D_0 show little dependence upon the computational procedure level used to obtain geometries. In other words they do their calculations with different geometries, optimized at different levels of theory, and they found that most results are consistent with each other as expected, i.e., their D_0 value was comparable for all calculations, while for the individual *ab initio* energies of the molecule and the fragment, the results come out very different.

Table 3.15 summarizes results reported in this section.

Table 3.15: Equilibrium distances r_{CH} and r_{CC}, total and dissociation energies for acetylene, C_2H_2 ($\tilde{X}^1\Sigma_g^+$).

Name	Year	R_{C-H} (a_0)	R_{C-C} (a_0)	Energy (a.u.)	D_0 (kcal/mole)	Method[a] and ZPE (kcal/mole)
Lafferty *et al.*	1964	2.005	2.273	-	-	Expt. (HRIR)
Herzberg		2.003	2.273	-	-	Expt.
Siegbahn	1981	1.997	2.294	-	-	MCSCF
		2.005	2.283	-	-	MC-CI
Watson *et al.*	1982	2.005	2.273	-	-	Expt
White and Schatz	1984	2.0385	2.32	-	131.5	POL-CI; ZPE = 16.4
Wodtke and Lee	1985	-	-	-	132(2)	molecular beam
Shiromaru *et al.*	1987	-	-	-	132.6(1)	Synchroton radiation
Perić *et al.*	1987	2.041	2.32	-	-	MRD-CI PES
Fujii *et al.*	1988	-	-	-	< 132.9(1.2)	fluorescence yield cutoff
Chen *et al.*	1988	-	-	-	≤ 132.3	ZAC
Curtiss and Pople	1988	2.015	2.299	-77.18610	133.5	G-1
Green *et al.*	1989	-	-	-	≤ 126.647(2)	SAC
Osamura *et al.*	1989	2.031	2.317	-76.91617	122	MCSCF/DZ
		2.039	2.296	-76.94180		MCSCF/DZP
Segall *et al.*	1989	-	-	-	≤ 127(1.5)	HCCH + $h\nu$ → C_2H + H(K.E.)
Benson *et al.*	?	-	-	-	≤ 126(1)	thermo
Ervin *et al.*	1990	-	-	-	131.3(7)	Neg. Ion. Photospec.
Wu and Carter	1990	-	-	-	129.7	GVB + CCCI/DZP
Montgomery and Petersson	1990	2.004	2.274	-77.30059	131.54	QCI + CBS ZPE = 16.5
Baushlicher *et al.*	1990	2.010	2.292	-77.197034	130.1(1.0)	MRCI on CASSCF ZPE = 16.68
Ruscic *et al.*	1990	-	-	-	131.6(1.0)	C_2H^- + H^+ threshold
Baldwin *et al.*	1990	-	-	-	131(1)	H (REMPI) velocity after dissociation
Balko *et al.*	1991	-	-	-	131.4(5)	(TOF) Photodiss.
Nicolaides *et al.*	1991	-	-	-77.0766382	-	CI-SD (6-31G**) ZPE = 18.4
Habibollahzadeh, *et al.*	1992	2.009	2.296	-77.14839	140.7	MP2/6-311G**
		2.042	2.308	-	-	MCSCF/DZP
		2.042	2.292	-76.63777	129.9	DMol/DNP
		2.051	2.272	-76.64453	130.0	DMol/DN
this work	1993	1.991	2.230	-77.29084(376)	130.74(3.92)	FNDMC (ΔZPE=8.23 from [37])

[a] See Appendix A.12 for glossary of abbreviations for methods.

3.2.4.2 QMC study of C_2H_2

We found an equilibrium geometry by doing a similar calculation on C_2H_2 as that done for C_2H using the ALCHEMY program at the SCF level. The corresponding PES is shown in Fig. 3.11. Contrary to our experience with C_2H, the minimum found by GAMESS and the one found by ALCHEMY II (STO) coincide,[26] and has $r_{CH} = 1.991a_0$ and $r_{CC} = 2.230a_0$. This was to be expected since the molecule is much better defined by a single reference wave function than the fragment. Figure 3.10 shows how for the C_2H_2 system the two programs find the same minimum, even if the curves are not perfectly parallel by about 10^{-4}a.u.

The QMC energy at this minimum geometry is -77.29084(376)a.u. In combination with the QMC energy at the SCF minimum of C_2H and using the estimated ZPE correction from Ref. [37] of 8.23 kcal/mole, we get D_0 = 130.74(3.92) kcal/mole. Time step extrapolations for this geometry and another geometry from the literature[97] are given in Fig. 3.12. Figure 3.13 shows histograms of the QMC energy data at the minimum geometry for each time step in the calculation.

Figure 3.10: Comparison of SCF energies obtained using STO and STO-6G basis sets for C_2H_2.

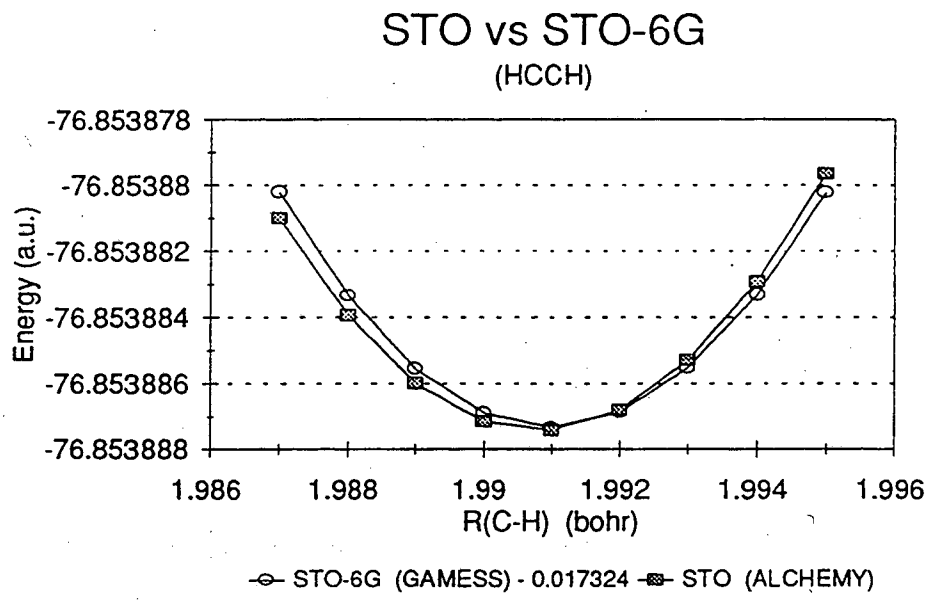

[26] As with the C_2H calculation, the GAMESS (STO-6G) curve has been shifted (in this case by 0.017324 a.u.) in order to make the comparison between the two curves easier.

Figure 3.11: Two views of the SCF PES computed for acetylene using ALCHEMY II.

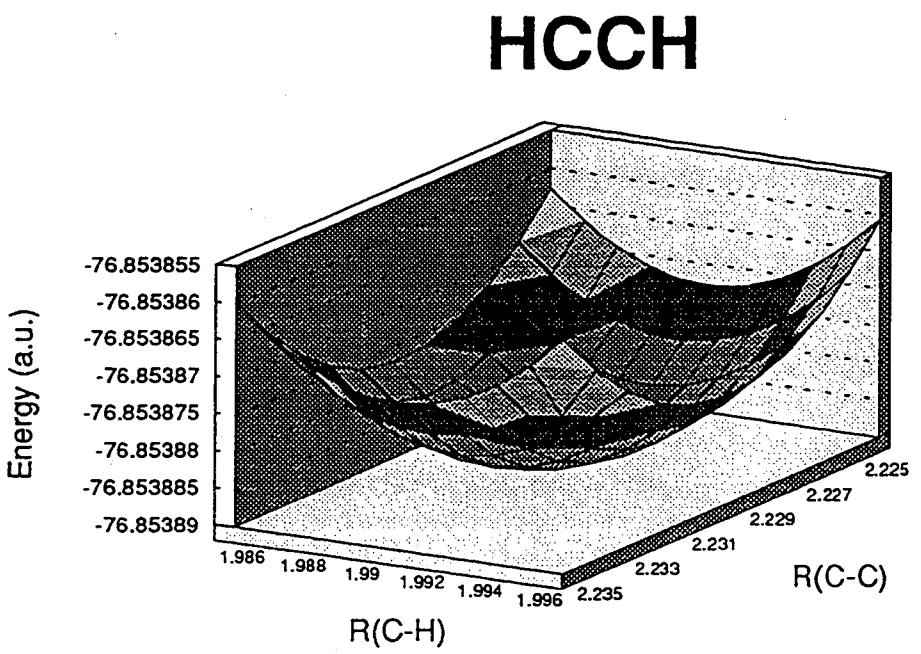

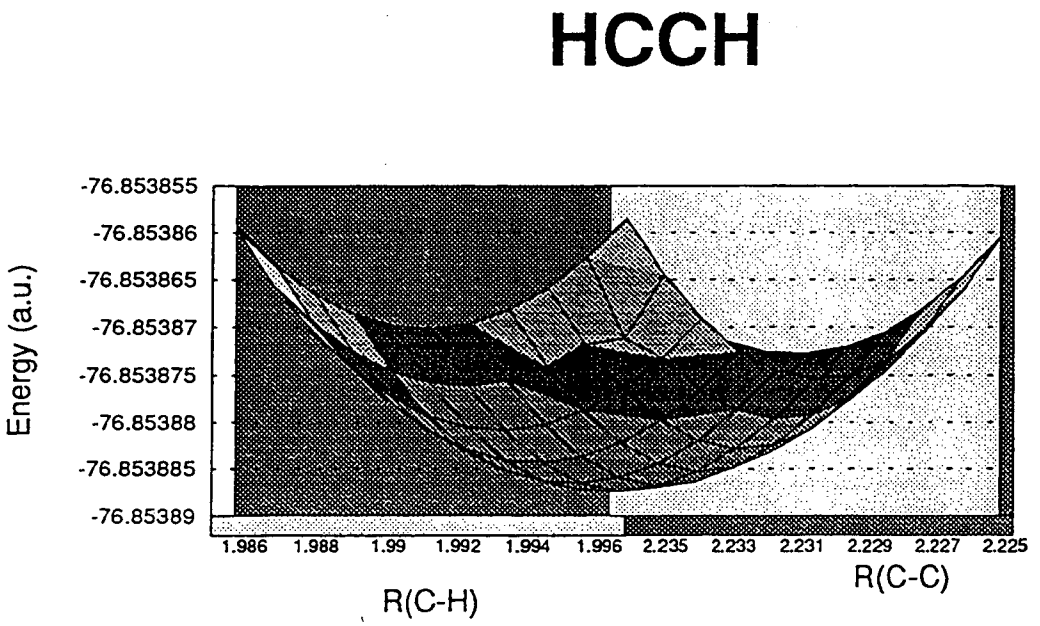

Figure 3.12: Time step extrapolation for C_2H_2 using basis B (SCF).

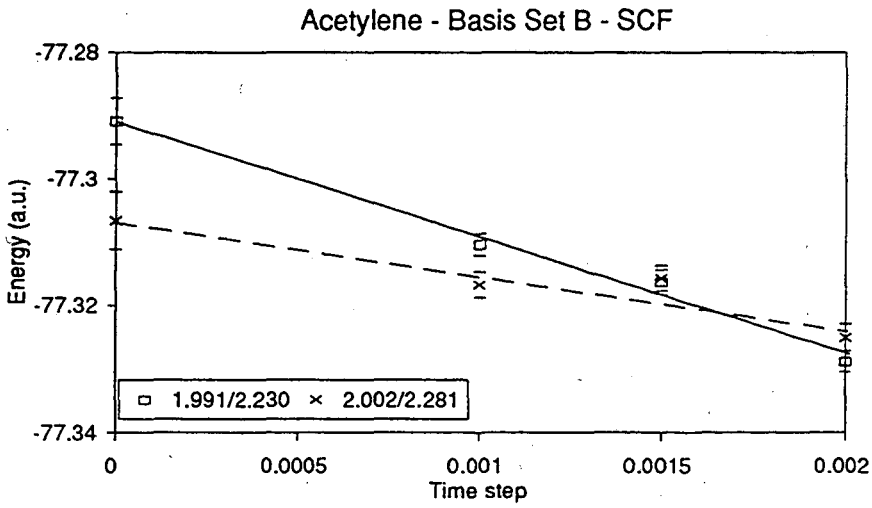

Figure 3.13: Histogram of energy data for C_2H_2 per time step.

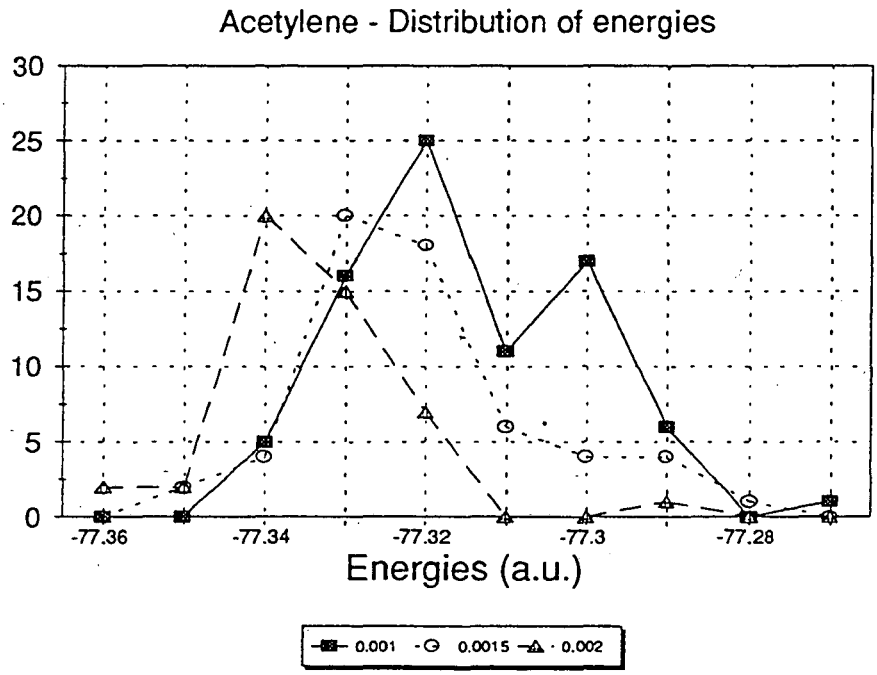

3.3 Discussion

The first aspect of our calculations we wish to discuss here is the choice of the equilibrium geometry. In [124] Habibollahzadeh *et al.* used a large range of methods and basis sets which are compared with density functional theory results. They argued that their DFT-LDA results showed little dependence upon the computational procedure level used to obtain geometries. In other words, they did their D_0 calculations at different geometries, each optimized at a different level of theory to be used in that particular calculation. They found that the D_0 results were consistent with others estimated at a different level of theory, although the individual values for the total energy were very different in each method. We are well aware, however, that findings from *ab initio* methods might not necessarily hold true for QMC. For instance, Fig. 3.12 shows a result for C_2H_2 at a geometry ($r_{CH} = 2.002a_0$, $r_{CC} = 2.281a_0$) taken from [97] and very close to the experimental geometry[143].

The C_2H radical presents a challenge in the determination of equilibrium geometries. The very nature of the open-shell radical suggests that contrary to $C_2H_2(^1\Sigma_g^+)$, whose ground-state can be reasonably described by a single reference, the ground state of $C_2H(^2\Sigma^+)$ cannot be properly described by a single-reference wave function. After the poor performance of CASSCF wave functions in the QMC calculations of the CH radical, we thought twice before investing into a CASSCF function for C_2H, and preferred to limit the present work to SCF trial functions. The logical next step is to find CASSCF wave functions for both C_2H and C_2H_2, examine the weight of the reference configuration in the expansion. Only if the leading coefficients are less than 0.85 would we recommend to try such wave functions in further QMC calculations. This suggestion is based on our experience with the CH radical as well as on results presented in Subramaniam *et al.*[62]. If the coefficients of the reference determinants remain high, a possible course of action would be to perform a MRCI calculation using the CASSCF wave function as the reference. This type of approach would introduce new problems, since the expansion keeps growing beyond QMC computational capabilities to the point that a truncation including only the predominant configurations would be required.[27] This type of truncation may be an additional source of error. A viable alternative would be a MCSCF limited to the configurations with the highest coefficients in the CASSCF.

Another point to emphasize is that the time step bias always exists. One cannot assume that a large enough basis and/or correlation function will "remove" it. All functions for all basis have shown that the bias is there and that in spite of its linearity and apparent flatness, to use the smallest time step as an accurate measure of the energy at $\tau = 0$, would have underestimated both the QMC energy and its variance. Inclusion of correlation functions, for

[27]The use of parallel systems might help in speeding up this type of computation, but it yet needs to be determined how large the expansion can be.

reduction of variance and time step bias, was explored for C and CH, but not for C_2H and C_2H_2.

The error bar of the bond dissociation energy calculation of C_2H_2 is very large, suggesting that further computations are necessary. However, we noticed that after a certain number of blocks the energies obtained did not contribute to the lowering of the variance, but oscillated around the already found average energy. It is not clear that further computations would reduce the statistical error without addition of correlation functions.

A small test was performed on the data to verify the validity of the reported error bar. Histograms done on the acetylene data were shown in Fig. 3.13. Since they closely resemble gaussian distributions, one normally reports an error given by

$$\sigma(\bar{x}) = \sqrt{\frac{1}{N(N-1)}\sum_{j=1}^{N}(x_j - \bar{x})^2}\,. \tag{3.5}$$

The jackknife is used to obtain unbiased estimates from a given distribution. A brief introduction of the jackknife statistic as discussed in [144] is given in Appendix A.11. To apply the jackknife method to our C_2H and C_2H_2 data we follow the steps presented in [145]:

(1) Generate N subsets that contain $N-1$ observations from the original N observations, i.e., $\{x_1, \ldots, x_{i-1}, x_{i+1}, \ldots, x_N\}, \{x_1, \ldots, x_{i-1}, x_i, x_{i+2}, \ldots, x_N\}$, etc.

(2) Calculate the average $\bar{x}_i$ for each subset.

(3) The jackknife estimate, $\sigma_{JK}(x_1, \ldots, x_N)$, of $\sigma(\bar{x})$ is

$$\sigma_{JK}(x_1, \ldots, x_N) = N \cdot \sigma(\bar{x}) - \frac{N-1}{N}\sum_{i=1}^{N}\sigma(\bar{x}_i) \tag{3.6}$$

The resulting variances of such a calculation are shown in Table 3.16 at each time step, and the values extrapolated from these are compared with our previous results in Table 3.17. The difference in the standard deviations is in all cases ~ 0.00002 a.u., and the difference in the D_0 is merely a 0.01 kcal/mole, while its variance increases by 0.05 kcal/mole. Clearly the bias in the standard deviation due to the non-gaussian nature of the energy distributions is negligible.

Table 3.16: Jackknife method applied to σ of each time step in QMC data to remove bias.

System	τ	# blocks	steps/block	Energy	$\sigma(\bar{x})$	$\sigma_{JK}(x_1, \ldots, x_N)$
	0.001	48	5000	-76.58054	0.00249	0.00251
C_2H	0.0015	40	3333	-76.59308	0.00212	0.00214
	0.002	72	2500	-76.59366	0.00161	0.00162
	0.001	81	5000	-77.31037	0.00173	0.00174
C_2H_2	0.0015	59	3333	-77.31630	0.00188	0.00189
	0.002	47	2500	-77.32879	0.00163	0.00167

Table 3.17: Extrapolated energies using QMC data and jackknife estimation of data.

	Extrapolated Energies (a.u.)		D_0
	C_2H	C_2H_2	(kcal/mole)
QMC data	-76.56938(500)	-77.29084(376)	130.74(3.92)
jackknife	-76.56938(506)	-77.29086(380)	130.75(3.97)

3.4 Conclusion and future directions

We found that the quality of the basis set is consistent on all fragments. That is, using the same atomic basis set on C and H produced similar results (% correlation energy recovered) for C, CH, C_2H and C_2H_2. However, our study suggests that a more complicated wavefunction does not imply a better recovery of the correlation energy. Since we acknowledge that our method is not variational (i.e. more is better), this does not come as a complete surprise to us. Long configuration expansions do not imply a better recovery of the energy, even if this were the case in the strict variational/*ab initio* sense. Another thing to point out is that the single reference runs for acetylene were much faster than the multi-reference runs for CH! This was expected given the difference in number of operations being carried out. This issue of trial function complexity extends to the correlation function as well. We found that prohibitively large correlation functions were not necessary in order to obtain good results (See Table 3.6).

In finding total energies, QMC provided results of similar quality to state-of-the-art methods for CH and C_2H, and improved on most other C_2H_2 results available. However, energy differences are the significant quantity chemically, since total energies are not available from experiment. Two such differences were computed using QMC: D_e for CH and D_0 for the C-H bond in C_2H_2. The binding energy of CH given by QMC is also competitive with previous results in the literature (See Table 3.4). The bond dissociation energy obtained for C_2H_2, on the other hand, was a bit of a disapointment. The value of $D_0 = 130.74(3.92)$kcal/mole, although agreeing with the currently accepted experimental value, does not contribute to the resolution of the now old controversy, given its large error bar. A jackknife estimation of the error showed that little bias is present in our result.

Much work remains to be done in order to reach any useful conclusions on doing QMC on polyatomic systems. Some of the main issues to be resolved are (1) the determination of equilibrium geometries; and (2) the reduction of the statistical variance. A direct (and not very efficient) way to solve the equilibrium geometry dilemma in QMC would be to create PES with given trial functions, similar to the PESs presented in this chapter using ALCHEMY. This would be computationally expensive when striving for meaningful accuracies. In reality, this problem could be addressed only by the successful implementation of energy gradient computations within

the QMC framework. Unfortunately this is not a trivial task, and pursuits along these lines have met limited success[72].

The second problem might prove to be the easier one to tackle, with the availability of massively parallel machines. In Chapter 2 we have already mentioned some efforts taking advantage of these new technologies[50, 51] in exact QMC methods. It remains to be seen if it is worthwhile to continue the pursuit of the FNDMC method with importance sampling, as done in this work, on these new systems. For example, in implementing QMC, it will prove advantageous the use of weights rather than branching in order to minimize the amount of communication required among processors. Also, larger numbers of walkers and electrons will become much easier to handle as the number of processors increases.

Chapter 4

Accelerated Variational Monte Carlo

Cójili púlgilu, ábrili ójilis, échili pólvili, púlgili mortili.

Popular

Here we will study the large-Z problem from the VMC standpoint. As mentioned in Chapter 2, computational approaches in QMC tend to introduce a separation of core and valence as Z gets large. This separation is justified by the fact that different step sizes are needed in order to efficiently sample all regions. Ideally one would want a method which would automatically differentiate core and valence without introducing any approximations, or biasing the process. Here we implement an acceleration method proposed by Batrouni and Reynolds [146] to modify the simulation without biasing it. In this chapter we shall review the theory of VMC, introduce an acceleration matrix to adjust for the different "velocities", and discuss the results of such an implementation.

4.1 Introduction

In 1953, Metropolis *et al.*[147] introduced an algorithm for performing simulations which has been extensively used in classical statistical mechanics and in QMC applications. The premise is very simple: Take a particle at position $\vec{R}$ in an ensemble and move it to a new position to generate a trial particle at position $\vec{R}'$, $\vec{R}' = \vec{R} + \vec{\xi}$, where $\vec{\xi}$ can be drawn from a known distribution.[1] The new $\vec{R}'$ will be accepted with probability

$$P(\vec{R} \rightarrow \vec{R}') = \min\left(1, \frac{f(\vec{R}')}{f(\vec{R})}\frac{T(\vec{R}' \rightarrow \vec{R})}{T(\vec{R} \rightarrow \vec{R}')}\right) \tag{4.1}$$

[1] For instance, $\vec{\xi}$ can be a Gaussian random variable, like χ in Eq. 2.37.

where $f(\vec{R})$ is the equilibrium distribution of the ensemble, and the T's are the transition probabilities of moving in either direction,[2] which are arbitrarily chosen. In the original Metropolis algorithm, T was a constant. The better the choice of T, the larger the acceptance probability P in Eq. 4.1 will be. Ceperley[19] pointed out that the acceptance ratio can be made close to one by choosing a value of $T(\vec{R} \rightarrow \vec{R}')$ which approximates $f(\vec{R}')/f(\vec{R})$ (where $f(\vec{R}) = \Psi_T^2(\vec{R})$). Based on this suggestion, many "improved algorithms" have been suggested.[3]

Among those improved methods, we mention Umrigar's recent accelerated Metropolis approach[150]. Umrigar suggested using spherical polar coordinates instead of cartesian coordinates for the Metropolis step, and then to vary the step size along radial and angular components such that core electrons have smaller radial and larger angular moves. Indeed, in spherical polar coordinates, the transition probability can be factored into a radial factor T_R and an angular part T_Ω, i.e., $T = T_R \cdot T_{\Omega|R}$. Since the radial factor is the one that hinders core electron movement, one may reduce the step size in the radial direction (thereby resulting in an enhanced radial transition probability T_R) to achieve a move with a reasonable probability of acceptance. However, this procedure can slow down equilibration in the radial direction even while significantly accelerating equilibration in the angular direction, if the step size for the radial component is chosen too small.

A method by Batrouni and Reynolds[146] introduces an acceleration matrix to modify the way the VMC simulation is performed without altering the final steady-state solution. Their approach borrows from the Fourier Acceleration method used to treat critical slowing down[4] [151, 152, 153] in choosing an acceleration matrix such that all coordinates move at comparable speeds.

4.1.1 Equilibration problem in variational Monte Carlo

We saw in Sec. 2.1.5 that VMC provides an exact method of computing the expectation values of any operator for a given wave function. For example, Eq. 2.40 shows how VMC can be used to evaluate the energy expectation value of a trial function, which is especially convenient when the trial function includes explicit interparticle correlation in its functional form. Our group has used VMC in the calculation of derivatives[47], the optimization of trial wavefunctions[41, 40, 35] and the equilibration of ensembles to be used in FNQMC, but others use VMC to compute energies as well as properties[5] using increasingly sophisticated wavefunction forms.[6]

[2] We can immediately(?) recognize that our Green's function in QMC (Eq. 2.38) corresponds to the transition probability in Eq. 4.1.

[3] For example, force bias[148, 149], accelerated Metropolis[150], etc.

[4] In the VMC case the critical point occurs as the nuclear charge $Z \rightarrow \infty$.

[5] Recall that since VMC does not involve a mixed distribution, one obtains "pure" $\langle \Psi_T | \hat{A} | \Psi_T \rangle$ elements[34].

[6] For example, Moskowitz and Schmidt work on optimizing very complicated correlated wave functions in [86, 87]; Umrigar, *et al.* had done likewise in [42]. Other studies involving uses of VMC are in [45, 154].

The Schrödinger equation we simulate in VMC,

$$\frac{df}{dt} = D\nabla^2 f + D\nabla\cdot(\vec{F}_Q f) , \tag{4.2}$$

is a Fokker-Planck equation which leads to the equation used in the propagation of the trajectories of the distribution $f(\vec{R}) = |\Psi_T|^2$:

$$\vec{R}' = \vec{R} + D\tau\vec{F}_Q + \sqrt{2D\tau}\vec{\eta} , \tag{4.3}$$

where $D = \frac{1}{2}$ is the diffusion constant, τ is the time step, $\vec{F}_Q = 2\nabla\Psi_T/\Psi_T$ is the quantum force, and η is a Gaussian random variable.[7] Equation 4.3 is a discretized Langevin equation. The Fokker-Planck equation is the differential equation for diffusion in velocity space, and the Langevin equation is the stochastic (i.e., one of the terms is a random function) equation for Brownian motion[155]. The Fokker-Planck equation refers to a distribution while the Langevin equation refers to the coordinates of the distribution. That is, the Langevin process describes individual trajectories, while the Fokker-Planck equation describes an ensemble of trajectories.

The transition probability corresponding to Eq. 4.3 is

$$T(\vec{R}\rightarrow\vec{R}') = (4\pi D\tau)^{-3N/2} \times e^{-[(\vec{R}'-\vec{R})-D\tau\vec{F}_q(\vec{R})]^2/4D\tau} , \tag{4.4}$$

and we readily recognize that $T(\vec{R}\rightarrow\vec{R}') = G_D(\vec{R}\rightarrow\vec{R}',\tau)$, where G_D is the diffusion Green's function (see Appendix A.10.1) after addition of importance sampling. A simple overview of the VMC algorithm is shown in flowchart form in Fig. 4.1.

Table 4.1 shows some features for a typical VMC walk of Ne where the electrons are moved one at a time. The main thing to point out in this example is that the acceptance ratio for the core electrons is under 10% although the overall acceptance ratio is 83%. Now we would like to turn our attention for a moment to the attempted $\langle\Delta R\rangle$ value which is what acceleration methods (like the one to be presented here) attempt to adjust. It is not surprising that core electrons would have larger attempted moves, since they experience larger repulsion from the nucleus. However, it is that larger move which causes them to be rejected more often than valence electrons. Figure 4.2 shows explicitly how the acceptance ratio goes down as the move for the innermost electrons goes up. The population and relative density columns also indicate that the moves by the innermost electrons constitute a sizeable portion of the simulation, even though they are the ones moving the least.

Since the VMC algorithm does not discriminate between core and valence electrons, reasonable moves for core electrons will result in inefficient sampling of the valence region, and vice versa. Generally for VMC, a time step is chosen such that about 50% of the proposed moves are accepted. There is no *a priori* principle which justifies this preference, but it is intuitively

[7] In FNQMC we have used χ to denote the Gaussian random variable. Here we follow the following notation: $\langle\chi^2\rangle = 2D\tau$, and $\langle\eta^2\rangle = 1$.

acceptable for a Metropolis walk where there are no different time scales. For our problem, this choice of time step results in core moves being rejected more frequently, therefore never achieving a "true" equilibration of the ensemble.[8] This situation only worsens as Z increases.

[8]Some work[29, 80] has been done which suggests that the overall acceptance should be $\geq$85% before all electrons move.

Figure 4.1: VMC algorithm

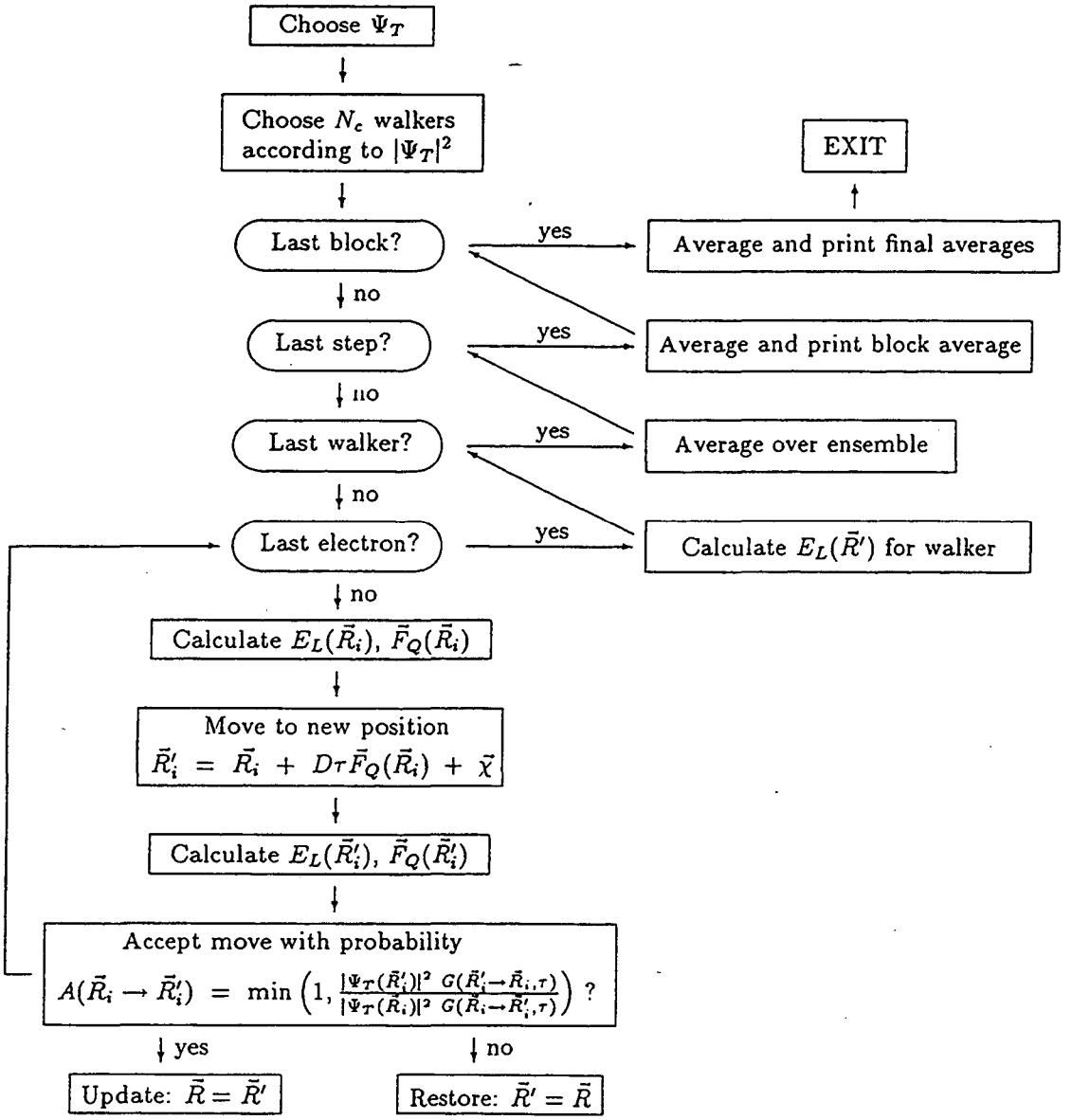

Table 4.1: Electron movement data of Ne using a guided Metropolis algorithm at $\tau = 0.03$ and 3000 MC steps. $[a, b)$ is defined as $a \leq R < b$. All quantities are in a.u. $\langle \Delta R \rangle = 0.23241 a_0$. Average acceptance ratio = 0.83.

R interval	Acceptance Ratio	Attempted $\langle \Delta R \rangle$	Accepted $\langle \Delta R \rangle$	Population[a]	Accepted $\langle \Delta \angle \rangle$	Relative Density
[0.0, 0.1)	0.09547	0.3981	0.02005	1919	5.5	0.74953
[0.1, 0.2)	0.31099	0.3853	0.07923	2806	17.5	0.15657
[0.2, 0.3)	0.64854	0.3642	0.19445	1655	32.1	0.03402
[0.3, 0.4)	0.82179	0.3117	0.23766	1401	30.9	0.01479
[0.4, 0.5)	0.88491	0.2906	0.24793	1669	25.7	0.01069
[0.5, 0.6)	0.92871	0.2861	0.25883	2068	22.2	0.00888
[0.6, 0.7)	0.95955	0.2820	0.26676	2221	19.6	0.00683
[0.7, 0.8)	0.97488	0.2840	0.27423	2177	17.7	0.00503
[0.8, 0.9)	0.98318	0.2823	0.27575	2094	15.2	0.00377
[0.9, 1.0)	0.98809	0.2829	0.27831	1889	13.8	0.00272
[1.0, 1.1)	0.98999	0.2802	0.27653	1658	12.3	0.00196
[1.1, 1.2)	0.99161	0.2856	0.28226	1415	11.5	0.00139
[1.2, 1.3)	0.99303	0.2848	0.28227	1268	10.7	0.00106
[1.3, 1.4)	0.99637	0.2798	0.27853	1035	9.5	0.00074
[1.4, 1.5)	0.99349	0.2837	0.28061	831	9.0	0.00051
[1.5, 1.6)	0.99636	0.2840	0.28271	746	8.4	0.00040
[1.6, 1.7)	0.99539	0.2754	0.27377	637	7.7	0.00030
[1.7, 1.8)	0.99823	0.2739	0.27328	535	7.2	0.00023
[1.8, 1.9)	0.99790	0.2797	0.27901	418	7.1	0.00016
[1.9, 2.0)	0.99876	0.2800	0.27954	339	6.6	0.00012

[a] This population is defined as the count of occurrences of an electron falling within each radial interval.

Figure 4.2: Acceptance ratio behavior in different radial intervals, for given attempted $\langle \Delta R \rangle$.

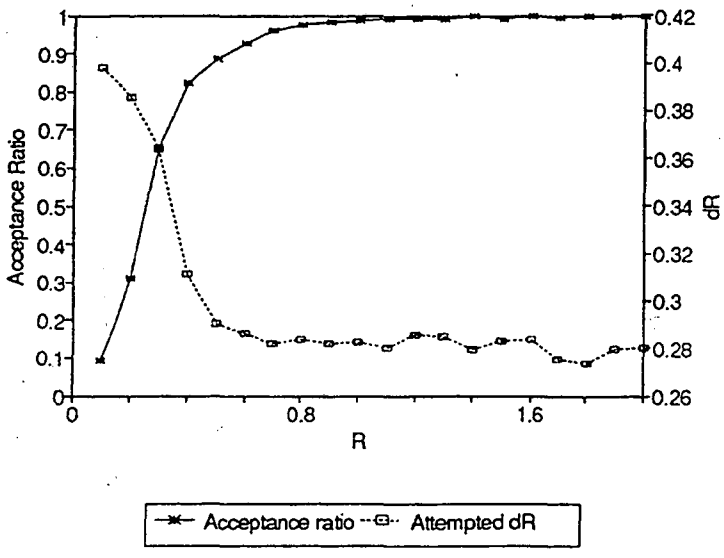

4.1.2 Acceleration methods

Fourier acceleration[151, 152, 153] has been used as a mechanism to overcome slowing down in Langevin-based simulations of critical phenomena and lattice-field theories, where multiple length scales are present. It leaves the steady-state distribution unaltered but the sampling is done more quickly, since the slower coordinates will move faster towards equilibrium. The following treatment comes from the description in [153, 156] of how it has been successfully applied to scalar field theories. We will attempt to point out the analogy with our case as the similarities arise.

In a simulation using Langevin updating on a lattice (the usual situation), the lattice is updated simultaneously. Each configuration is updated by a discrete Langevin equation,

$$\phi^{(n+1)}(x) \;=\; \phi^{(n)} \;-\; \epsilon\frac{\delta S}{\delta\phi^{(n)}(x)} \;+\; \sqrt{\epsilon}\eta^{(n)}(x)\;, \tag{4.5}$$

which is analogous to Eq. 4.3. In Eq. 4.5, ϕ is the scalar field evolving, ϵ is the Langevin time step and η is the Gaussian noise, drawn from a distribution

$$\langle\eta^{(n)}(x)\eta^{(m)}(y)\rangle_\eta \;=\; 2\delta_{nm}\delta(x-y)\;. \tag{4.6}$$

Equation 4.5 can also be written in momentum space as

$$\tilde{\phi}^{(n+1)}(p) \;=\; \tilde{\phi}^{(n)}(p) \;-\; \epsilon(p^2+m^2)\tilde{\phi}^{(n)}(p) \;+\; \sqrt{\epsilon}\tilde{\eta}^{(n)}(p) \tag{4.7}$$

where the modes with small momentum eigenvalues will require a small time step, slowing down the algorithm.

Fourier acceleration allows slow modes at low momentum to take large steps. A time step which depends on momentum can be introduced by somehow choosing this time step to be inversely proportional to momentum. All modes would now evolve at the same rate and (the?) critical slowing down is undone. The new updating algorithm would be

$$\phi^{(n+1)}(x) \;=\; \phi^{(n)}(n) \;-\; \hat{F}^{-1}\left[\epsilon(p)\hat{F}\frac{\delta S}{\delta\phi^{(n)}(x)} \;-\; \sqrt{\epsilon(p)}\hat{F}\eta^{(n)}(x)\right]\;, \tag{4.8}$$

where $\hat{F}$ is a Fourier transform and

$$\epsilon(p) \;=\; \frac{\epsilon({p^2}_m ax + m^2a^2)}{p^2a^2+m^2a^2}\;. \tag{4.9}$$

The accelerated algorithm is equivalent to introducing a time step which is nonlocal in position space:

$$\epsilon_{xy} \;=\; \sum_p e^{ip(x-y)}\epsilon(p)\;. \tag{4.10}$$

An equivalent description can be obtained from the Fokker-Planck equation

$$\frac{\partial\phi(x,\tau)}{\partial\tau} \;=\; -\frac{\delta S[\phi]}{\delta\phi(x,\tau)} \;+\; \eta(x,\tau)\;, \tag{4.11}$$

which, similarly to our Schrödinger equation in Eq. 4.2, will describe the equilibration of a distribution $P(\{\phi\},\tau)$,

$$P(\{\phi\},\tau) \propto P_0(\{\phi\}) + \sum_i C_i P_i(\{\phi\}) e^{-\varepsilon_i \tau} , \tag{4.12}$$

not unlike our wavefunction expansion in Eq. 2.17. The eigenvalues ε_i determine both the rate of approach to equilibrium and the autocorrelation times of the points along the simulation. Near a critical point, the lowest ε_i approaches zero and causes critical slowing down, just like when the electrons in the core approach each other or the nucleus (node). There is an infinite number of paths which will lead to the same stationary distribution. In other words, Eq. 4.11 can also be reasoned as

$$\frac{\partial \phi(x,\tau)}{\partial \tau} = \int dy \left(-Q_{xy} \frac{\delta S[\phi]}{\delta \phi(x,\tau)} + Q_{xy}^{1/2} \eta(x,\tau) \right) , \tag{4.13}$$

where Q_{xy} represents a positive definite matrix. Fourier acceleration consists of setting $Q_{xy} \propto \Delta(x-y)$, where Δ is the propagator corresponding to the lowest-mass particle. The kernel Q is local in momentum space, so the convolutions in Eq. 4.13 are evaluated using Fourier transforms as we have previously seen.

4.1.3 Accelerated variational Monte Carlo

In the VMC case, the critical point occurs at $Z \to \infty$. Since the asymptotic distribution of the walk described by Eq. 4.2 is a steady-state, we can solve for any asymptotic distribution such that

$$\frac{df}{dt} = D\nabla \cdot (\nabla + \vec{F}) f = 0 . \tag{4.14}$$

At this point we wish to introduce an acceleration matrix to speed things up. This is readily accomplished by multiplying Eq. 4.14 by a matrix M, i.e.,

$$\mathrm{M}\frac{df}{dt} = D\nabla \cdot \mathrm{M}(\nabla + \vec{F}) f = 0 . \tag{4.15}$$

Notice that in order for the steady state to remain unchanged regardless of the choice of acceleration matrix, M has to be real-symmetric, positive-definite, and independent of the coordinates, $\vec{R}$.[9] Taking notice that $\mathrm{M} \propto \tau$ when we integrate Eq. 4.15, we readily see that in our new Langevin equation $\mathrm{M} \propto \tau$ as well:

$$\vec{R}' = \vec{R} + D\tau \mathrm{M} \vec{F}_Q + \sqrt{2D\tau \mathrm{M}}\vec{\eta} . \tag{4.16}$$

Equation 4.16 will dictate the new trajectories for our configurations. Now the drift velocity $\vec{F}_Q$ is replaced by $\mathrm{M}\vec{F}_Q$, and all electron coordinates contribute to the drift of a single electron for

[9] In this regard, an analogous implementation of acceleration for FNQMC would be impeded by the branching term which is a function of the coordinates, $\vec{R}$.

a non-diagonal M. The new Green's function will be given by

$$G_{\mathrm{M}}(\vec{R} \rightarrow \vec{R}';\tau) \;=\; \frac{1}{(4\pi D\tau)^{3N/2}} e^{-(\vec{R}'-\vec{R}-D\tau \mathrm{M}\vec{F}_Q(\vec{R}))^2/4D\tau \mathrm{M}} \;. \tag{4.17}$$

And, therefore, the new acceptance probability will be given by

$$A_{\mathrm{M}}(\vec{R} \rightarrow \vec{R}';\tau) = \min\left(1, \frac{|\Psi_T(\vec{R}')|^2\; G_{\mathrm{M}}(\vec{R}' \rightarrow \vec{R};\tau)}{|\Psi_T(\vec{R})|^2\; G_{\mathrm{M}}(\vec{R} \rightarrow \vec{R}';\tau)}\right) \;, \tag{4.18}$$

which can be expanded and simplified as

$$A_{\mathrm{M}}(\vec{R} \rightarrow \vec{R}';\tau)$$
$$= \min\left(1, \frac{|\Psi_T(\vec{R}')|^2}{|\Psi_T(\vec{R})|^2}\; e^{[\frac{D\tau}{4}(\vec{F}_Q(\vec{R})\mathrm{M}\vec{F}_Q(\vec{R}) \,-\, \vec{F}_Q(\vec{R}')\mathrm{M}\vec{F}_Q(\vec{R}')) \,+\, \frac{1}{2}(\vec{F}_Q(\vec{R}) \,+\, \vec{F}_Q(\vec{R}'))(\vec{R}-\vec{R}')]}\right) \;. \tag{4.19}$$

We know that, in general, our quantum force can be written as $F_\alpha = \nabla U_{pp}$ where U is the "potential" $U_{pp} = -2\ln|\Psi_T|$. Assuming that this potential U is in fact harmonic near the minimum, we have

$$U \;=\; \frac{1}{2} a_{ij} q_i q_j \;. \tag{4.20}$$

In practice one uses a trial function constructed from a Gaussian basis set because one wishes a potential, U, that is smooth and harmonic; the cusp of the typical Slater type basis functions, which are commonly used in VMC, would violate this premise. One can immediately notice that there will be different potentials for the coordinates of different electrons. These differences in potentials are reflected in the quantum force, as given by Hooke's law, $\vec{F}_Q \;=\; \mathrm{a}\vec{q}$, in the force constants a_{ij}. Now all we need to do is choose M such that it cancels out the differences in $\vec{F}_Q$.

If we choose our matrix $\mathrm{M} \;=\; \mathrm{H}^{-1}$, where H is the Hessian of U, $\partial^2 U/\partial q_i \partial q_j$, it would cancel the a's responsible for the time scales,

$$\mathrm{M}\vec{F}_Q \;=\; \mathrm{a}^{-1}\mathrm{a}\vec{q} \;=\; \vec{q} \tag{4.21}$$

and when inserted in the new Langevin equation, the result is all modes relaxing at the same time on only one time scale. This is equivalent to expressing the quantum force in a coordinate system in which M is diagonal. The eigenvectors of M will be the basis for the new coordinate system.

In order to implement the choice of M discussed in this section, it is first necessary to find a minimum of the potential U for a given Gaussian trial function and then compute and invert the Hessian matrix of U. Here the minimization was done by the downhill simplex method[17] and the Hessian was computed by finite differences. Before incorporating the acceleration matrix into the random walk it was necessary to modify the walk slightly. The quantum force, $\vec{F}_Q$, and the Gaussian random variable $\vec{\eta}$ are treated as vectors since the new move updates normal coordinates and not individual electron coordinates. It is required to move all the electrons at once such that their modes could be mixed as required in the acceleration prescription.

4.2 Applications

The Batrouni-Reynolds accelerated VMC method was tested on the C, N, O and Ne atoms. To implement the method an acceleration matrix is introduced as described in the previous section, and for comparison purposes, the choice of $\mathbf{M} = \mathbf{1}$ (unit matrix) is used as the non-accelerated case. Section 4.2.1 presents results of this implementation at the microscopic level,[10], and Sec. 4.2.2 contains autocorrelation results.

4.2.1 Effect on simulation features

A direct observation and tabulation of the electron movements and their acceptance is the best way of determining if and when equilibration is achieved. As mentioned before, the comparisons in this section are done between the choices of $\mathbf{M} = \mathbf{1}$ (unit matrix), which is the equivalent to moving all electrons together, with the same old Green's function G (i.e., transition probability T), and $\mathbf{M} = \mathbf{H}^{-1}$ (Batrouni-Reynolds' choice for acceleration matrix). Ceperley *et al.*[19] showed that doing a MC computation where electrons are moved individually is much more efficient than if all electrons are moved at once, since the Slater determinant can be inverted[11] twice as fast when a single column (corresponding to the new electron position) has been updated. Also, when all electrons are moved together, the acceptance ratios are expected to be lower than when electrons move separately due to: (1) any individual electron's low acceptance probability (i.e., $G(\vec{R}_i \rightarrow \vec{R}'_i, \tau)$ small) may cause the entire update to be rejected; or (2) even when the individual acceptance ratios are reasonably large, the entire update has a lower acceptance ratio (and, therefore, a larger chance of being rejected) than if the electrons were moving singly since all n electrons contribute collectively to it (e.g., the expression $P_{all} \approx \prod_i^n P(R_i)^{n_i(R_i)}$, where $P(R_i)$ is the acceptance ratio for the i-th R and $n_i = n\times$(population in R_i)/(total population) gives a rough estimate of the acceptance ratio for moving all electrons together if the individual acceptance ratios for each electron are known.). Given the small acceptance ratios of core electrons, one would expect that very small time steps would be required to achieve an overall 50-85% acceptance ratio.

As expected, when moving all electrons together, large time steps could not be used without dramatically lowering the acceptance ratio. Take for instance the examples for Ne shown on Tables 4.1 and 4.2. On Table 4.1 an acceptance of 83% was obtained for $\tau = 0.03$, whereas moving the electrons together (Table 4.2) requires at least $\tau = 0.003$ to attain an acceptance above 75%. Similarly, there was a dissapointing lowering of acceptance when the acceleration matrix was introduced. This lowering changes from system to system. For example, in carbon the acceptance ratio decreased by about 4% at each time step, while in neon the decrease was

[10] More detailed description of this type of study can be found in [80].

[11] Recall that one needs to compute the quantity $E_L = \hat{\mathcal{H}}\Psi_T/\Psi_T$, and the Ψ_T used here is a Slater determinant.

around 1-2%. On the other hand, acceptance probabilities in N and O showed very little change with addition of acceleration.

When the Batrouni-Reynolds acceleration matrix was implemented, we noticed very few changes from the behavior for the unit matrix moving all electrons together, so we cannot say for certain if the resulting change is an improvement, or simply a statistical deviation from the regular walk. Figure 4.3 shows a comparison of both non-accelerated and accelerated runs for Ne atom at $\tau = .01$ for the average movement in each radial region, as well as the contribution to the global acceptance from each individual electron. We can see a slight improvement for the accelerated case, although the overall acceptance ratio and variance always favors the non-accelerated runs. Also, we can see in Fig. 4.3b that although the average move in most regions is enlarged by acceleration, in the core region, i.e. those closest to the nucleus,[12] the move is barely more (e.g., in the example in Fig. 4.3 this is about 10^{-2}) than that for the non-accelerated case. One would have hoped the improvement in the core to be much higher.

It has been claimed in [146] that there is a compromise in choosing a time step such that both the core or the valence are sampled efficiently. This means that small time steps, which produce reasonable moves for core electrons, result in inefficient sampling of the valence region. Similarly, large time steps which would correct this problem, produce large moves which are rejected in the core region, as we have already shown in Table 4.1 and Fig. 4.2. Since one of the goals of the acceleration matrix is to make all coordinates propagate at the same "speed" (given their distance R from the nucleus), it is therefore intuitive to desire to make moves ΔR which would be proportional to R, regardless of the chosen time step. The quantity $\Delta R/R$ gives the move relative to the electron's distance from the nucleus, and gives, therefore, a measure of who "wins" in the compromise described above. A comparison of this measurement is shown in Fig. 4.5 for Ne at $\tau = 0.005$ comparing the acceleration matrix with the case where no acceleration (i.e., the unit matrix is used) is applied. We observe that the displacement relative to the position of the electron (i.e., $\Delta R/R$) only improves for those electrons closest to the nucleus, which might be more a consequence of the choice of small τ than of acceleration. Since the objective of the acceleration was to improve the sampling of both core and valence, we would have hoped to see an improvement in all regions, possibly making the ratio $\Delta R/R$ constant for all values of R. More explicitly, the goal of the acceleration was to choose a $\Delta R \propto R$. If this were so, Fig. 4.5 would be constant/flat for all values of R. Instead we see a $1/R$ behavior which clearly indicates that ΔR is constant for all R, not necessarily an improvement from the old situation.

Reynolds suggested to study $\langle \Delta R/R \rangle$ in the core region at the initial stages of the walk[157]. The rationale behind this study was that we had optimized a configuration (which

[12] Although we feel reticent about using the term "core" to mark specific electrons since exchange happens so frequently (see Fig. 4.6), we will continue to refer to the electrons closest to the nucleus ($R < 0.1a_0$) as "core" electrons.

minimized $U = -\ln|\Psi_T|^2$ as discussed in Sec. 4.1.3) for which we created our acceleration matrix. Since we did our averages using that walker as the starting point,[13] we should look closely at the effect of the acceleration matrix in getting that walker out the low Ψ_T region.[14] Presumably, the configuration would move towards regions of larger Ψ_T in the first few steps of the walk, we observed the effect of M on the electrons closest to the nucleus ($R \leq 0.1$) during the first ten steps of this type of walk. These results are shown in Table 4.2. A highest $\langle \Delta R/R \rangle$ does not clearly result from either method, although for the smallest values of R, it is mostly dominated by the acceleration method. Figures 4.4 and 4.5 suggest that the apparent improvement of the acceleration matrix is really an effect of statistics rather than physics.

An important thing to point out is that except for carbon, in all instances the accelerated case does as well or significantly better than the non-accelerated one in moving the inner electrons. This can be inferred from the $\{\langle \Delta R/R \rangle : R \in [0, 0.1)\}$ as well as the overall average move, $\langle \overline{\Delta R} \rangle$, which is larger for the accelerated cases; even in the case of carbon $\langle \overline{\Delta R} \rangle$ is improved in these first few steps. The bad news is that the effect gets lost almost immediately after the first few steps...

Another problem is that the acceptance ratio seems to go down in the accelerated cases, except in the case of carbon in which the acceptance ratio is significantly improved with acceleration. As the walk progresses the average move as well as the acceptance ratio quickly increase as the first problematic configurations are moved out of unfavorable positions. As the walk progresses, the initial advantage the acceleration has, seems to vanish completely to the point that even the $\{\langle \Delta R/R \rangle : R \in [0, 0.1)\}$ goes below that of a non-accelerated walk.

Figure 4.4 shows the radial move among the different radial regions for more substantial runs. In these figures we can clearly see that, at least for the smaller time steps, the average radial move is constant among both core and valence. It is clear from this data and the individual electron data (Table 4.3) that exchange among core and valence is to blame for this.

In Table 4.3 we show $\langle R \rangle$ and $\langle \Delta R \rangle$ for the individual electrons in several atoms. All numbers collected in this table were obtained by allowing a single walker at the minimum configuration obtained for the creation of the acceleration matrix to take 50000 VMC steps. The important thing this table shows is that there is no distinction between core and valence electrons, or rather that these exchange frequently during the walk, as Batrouni and Reynolds stated in [146]. For example, Fig. 4.6 shows the high frequency of electron exchange occurring in a 50-step walk by a Ne walker (10 electrons).

[13] This was to avoid any problems which might come about from node crossing[31].

[14] This should not be confused with the "trapped" electron situation discussed in [158].

Table 4.2: Effects of acceleration on electron movement (ΔR) and acceptance ratios (AR) at beginning of a sample VMC simulation. Observations were done on the first 10 steps of the Monte Carlo walk from the minimum configuration for which M was computed.

Z	τ	Method[a]	$\{\langle\Delta R\rangle : R \in [0, 0.1)\}$	$\langle\overline{\Delta R}\rangle^b$	$\{\langle\Delta R/R\rangle : R \in [0, 0.1)\}$	$\{\langle AR\rangle : R \in [0, 0.1)\}$	$\langle\overline{AR}\rangle^c$
Carbon	0.003	No Acc.	0.04434	0.072054	9379748.87	0.89503	0.89503
		Acc.	0.01421	0.172002	722406.05	0.93471	0.93471
	0.005	No Acc.	0.05245	0.088024	11250141.24	0.85162	0.85162
		Acc.	0.01933	0.221034	1313055.14	0.98007	0.98007
	0.007	No Acc.	0.05810	0.099053	12563156.59	0.81087	0.81087
		Acc.	0.02192	0.257242	1560816.18	0.94732	0.94732
	0.01	No Acc.	0.05281	0.110335	18712724.29	0.69891	0.75269
		Acc.	0.01788	0.237804	1876494.60	0.71412	0.71412
Nitrogen	0.001	No Acc.	0.04172	0.047761	166.60	0.89134	0.90991
		Acc.	0.04259	0.047857	171.37	0.88587	0.90549
	0.002	No Acc.	0.04967	0.069110	282.29	0.83285	0.88293
		Acc.	0.05090	0.069486	290.46	0.83013	0.88120
	0.003	No Acc.	0.05548	0.083551	388.31	0.78739	0.86513
		Acc.	0.05671	0.083960	399.78	0.78394	0.86282
	0.004	No Acc.	0.06407	0.097902	434.59	0.83117	0.87406
		Acc.	0.06540	0.098204	444.24	0.82667	0.87063
Oxygen	0.001	No Acc.	0.03815	0.044137	140.22	0.78563	0.86491
		Acc.	0.03815	0.044149	140.22	0.78561	0.86489
	0.002	No Acc.	0.05067	0.060117	234.55	0.69886	0.82096
		Acc.	0.05067	0.060134	234.54	0.69882	0.82091
	0.003	No Acc.	0.07221	0.078213	148.67	0.79089	0.82693
		Acc.	0.07221	0.078236	148.67	0.79088	0.82692
Neon	0.003	No Acc.	0.05954	0.076191	47.49	0.64796	0.77601
		Acc.	0.06291	0.076498	50.74	0.63944	0.76935
	0.005	No Acc.	0.04795	0.087176	92.72	0.39139	0.66728
		Acc.	0.04818	0.089801	200.20	0.50090	0.70174
	0.007	No Acc.	0.01754	0.060442	450.38	0.11067	0.40915
		Acc.	0.01486	0.059095	477.88	0.08902	0.39405
	0.01	No Acc.	0.01654	0.015057	547.30	0.08763	0.08763
		Acc.	0.01302	0.011373	582.33	0.06539	0.06539

[a] $\mathbf{M} = \mathbf{H}^{-1}$ was used for the accelerated case and $\mathbf{M} = \mathbf{1}$ was used in the non-accelerated case.

[b] $\langle\overline{\Delta R}\rangle$ is the average ΔR of all electrons.

[c] $\langle\overline{AR}\rangle$ is the average acceptance ratio of all electrons.

Table 4.3: Average movement data for individual electrons in several atoms taking 50000 steps at given values of τ.

			No Acceleration		Acceleration	
	τ	i	$\langle R_i \rangle^a$	$\langle \Delta R_i \rangle^b$	$\langle R_i \rangle^a$	$\langle \Delta R_i \rangle^b$
N	0.02	1	0.620617	0.062723	0.766009	0.064051
		2	0.689745	0.062930	0.650934	0.063830
		3	0.701081	0.062828	0.692252	0.062425
		4	0.675181	0.062895	0.706517	0.062248
		5	0.723410	0.063575	0.699570	0.062637
		6	0.156155	0.053393	0.614143	0.062320
		7	0.782154	0.065510	0.337134	0.062320
O	0.015	1	0.588490	0.055341	0.577765	0.054620
		2	0.627224	0.055836	0.619178	0.055141
		3	0.581724	0.055094	0.598784	0.055222
		4	0.596178	0.055533	0.622888	0.055543
		5	0.545331	0.054828	0.616961	0.054910
		6	0.545960	0.054760	0.504539	0.054086
		7	0.515449	0.054136	0.485420	0.052864
		8	0.465596	0.053134	0.545825	0.054626
Ne	0.005	1	0.417705	0.041372	0.384710	0.042089
		2	0.473877	0.042182	0.408923	0.040374
		3	0.422525	0.041579	0.459692	0.040901
		4	0.404492	0.041088	0.456944	0.041036
		5	0.465128	0.042103	0.415626	0.040550
		6	0.412031	0.041504	0.408321	0.040824
		7	0.396812	0.041088	0.386719	0.040354
		8	0.422935	0.041659	0.437765	0.042427
		9	0.488359	0.042155	0.456371	0.040762
		10	0.395563	0.041080	0.425235	0.040458

[a] $\langle R_i \rangle$ is the average distance from the nucleus at which electron i remained during the walk.

[b] $\langle \Delta R_i \rangle$ is the average ΔR electron i moved during the walk.

Figure 4.3: Comparison of acceptance ratios and accepted $\langle \Delta R \rangle$'s for Ne at $\tau = .01$ when a unit matrix or M is used in the different radial regions.

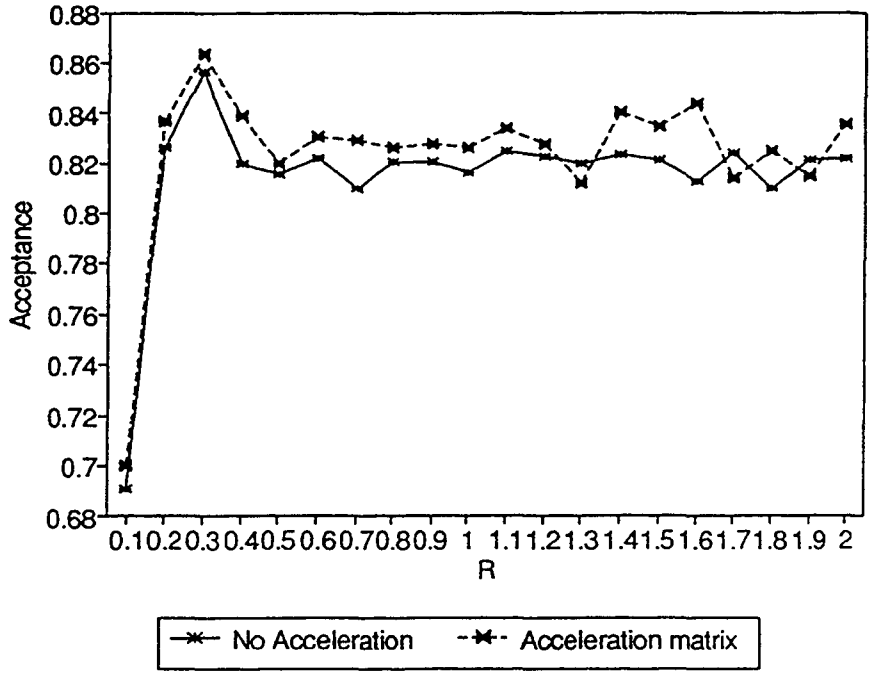

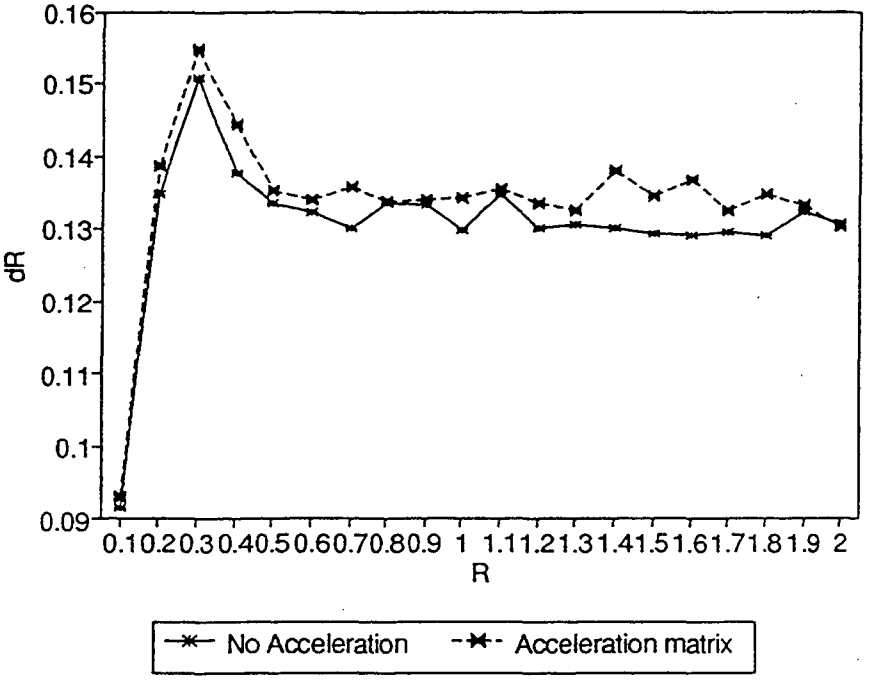

Figure 4.4: Average radial moves for non-accelerated as well as accelerated walks.

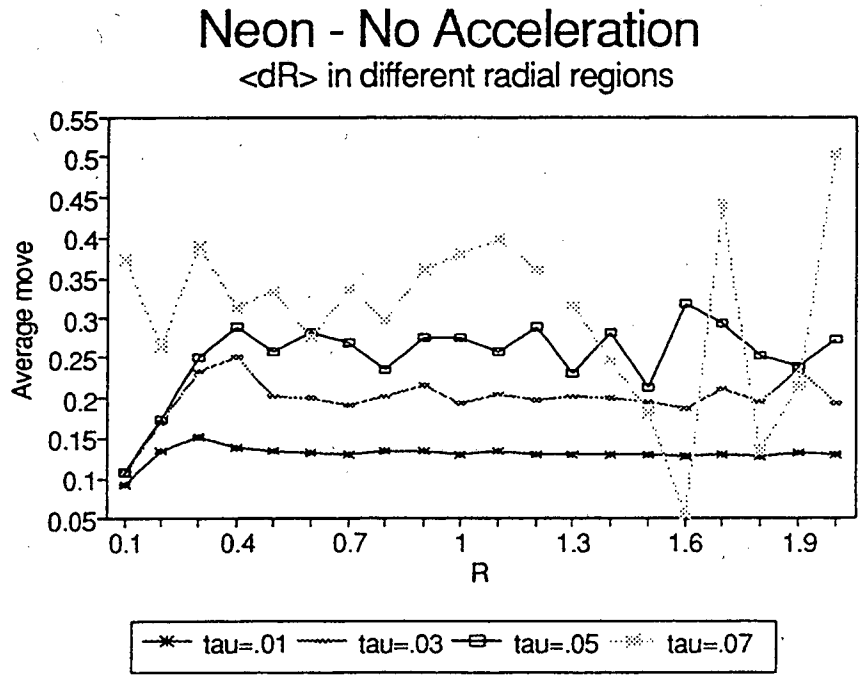

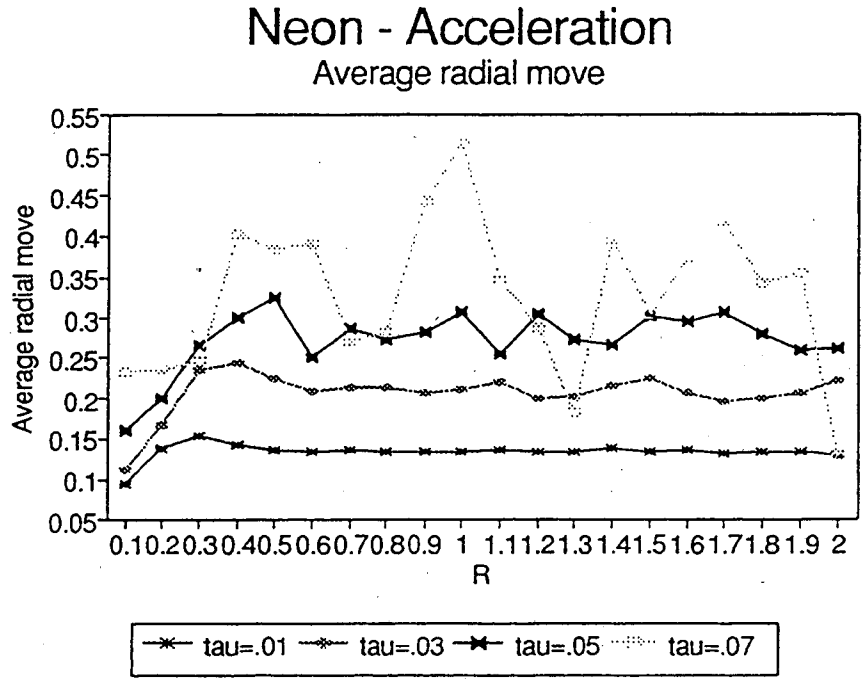

Figure 4.5: $\langle \Delta R/R \rangle$ vs R for both accelerated and non accelerated walks.

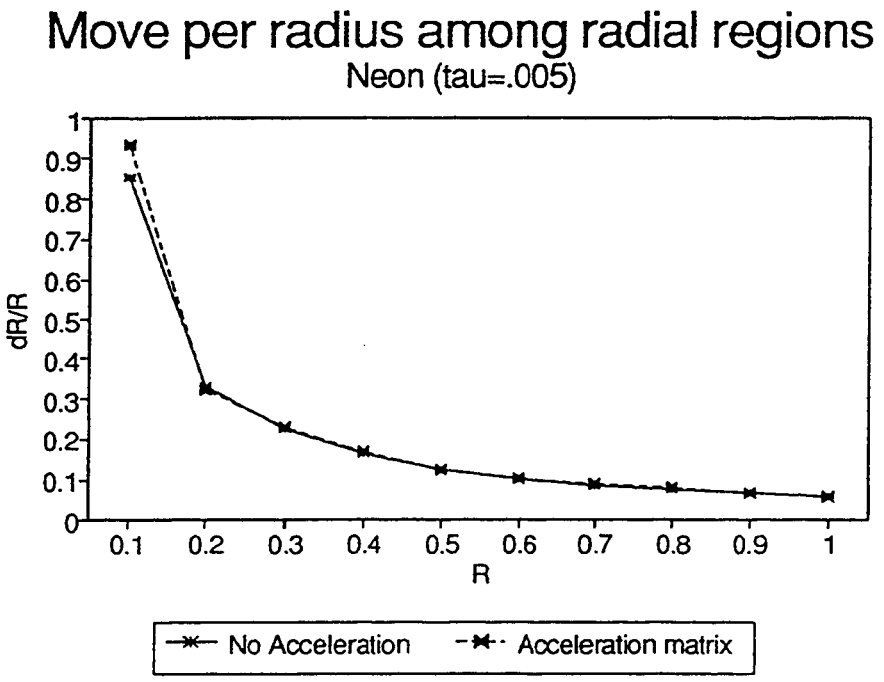

Figure 4.6: Electron exchange of a Ne walker in 50-step walk.

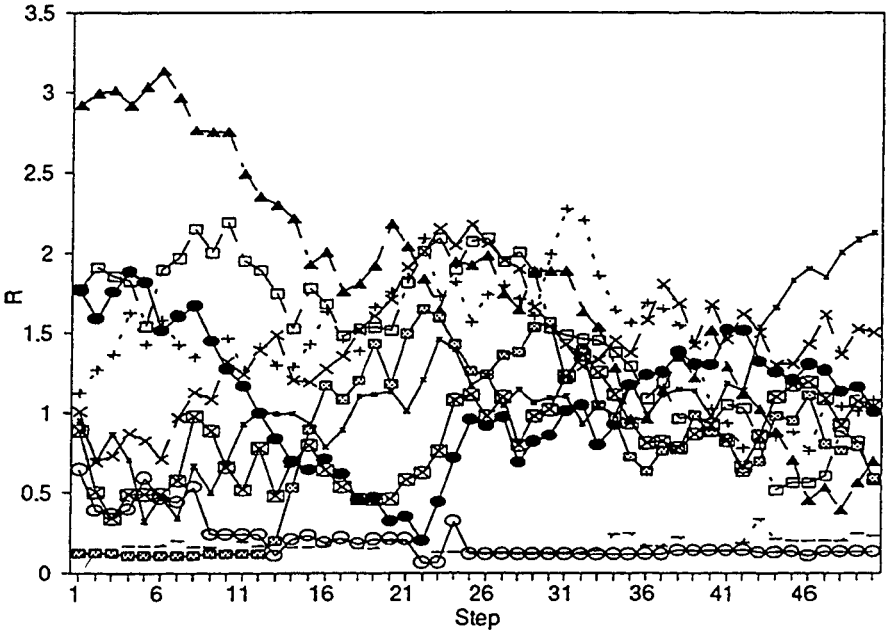

4.2.2 Effect on autocorrelation time

As mentioned in Sec. 2.1.4.1, we normally divide the steps in our walk into "blocks," and expect the subaverages of the local energy to be randomly distributed, i.e., uncorrelated. The value of the mean (block energy) for each block is

$$\bar{E}_b = \left(\frac{1}{N_s}\right)\sum_{s=1}^{N_s} E_s \tag{4.22}$$

and the total mean of block energies is

$$\bar{E} = \left(\frac{1}{N_b}\right)\sum_{b=1}^{N_b} \bar{E}_b \ . \tag{4.23}$$

The length of each of these blocks must be larger than the correlation time to guarantee no correlation among them. In our case, we can determine an appropriate number of steps per block, N_s by computing the autocorrelation among steps in the ensemble and using a block length at least 10 times the value of the autocorrelation length.

The autocorrelation time that Umrigar[150] used to give a measure of statistical inefficiency[159], is defined as

$$T_{corr} = \lim_{N_s \to \infty} N_s \left(\frac{\sigma_b^2}{\sigma^2}\right) \tag{4.24}$$

where

$$\sigma^2 = \frac{1}{N}\sum_{i=1}^{N}(E_i - \langle E \rangle) \tag{4.25}$$

and

$$\sigma_b^2 = \frac{1}{N_b}\sum_{i=1}^{N_b}(E_b - \langle E \rangle) \ . \tag{4.26}$$

For N measures, we will have only N/T_{corr} independent measures, so we try using N_b blocks of N_s steps each, where $N_s = 10T_{corr}$.[15] Since we are using a value of $N_s = 10T_{corr}$, we will assume that all $\bar{E}_b = E_i$ are independent and that, therefore, the limit in Eq. 4.24 becomes N_s[150]. The error bars we report are given by

$$\sigma_e = \sqrt{\frac{1}{N(N-1)}\sum_{j=1}^{N}(x_j - \bar{x})^2} \ , \tag{4.27}$$

as for QMC in previous chapters. There is no clear relation between T_{corr} and the error, but one would hope that a less correlated walk would converge faster since fewer steps are required to gather results and achieve equilibration.

The autocorrelation time as defined above should be a constant. However, since we are not computing it from a "truly infinite" walk (nor an infinite ensemble), we find that there is an

[15] Even though using $N_s = T_{corr}$ presumably has eliminated all correlation, it is usually preferred to play it safe and extend the block size beyond the auto-correlation time. Umrigar[150] suggests to use $N_s = 100T_{corr}$.

Table 4.4: Autocorrelation times (T_{corr}), energies (E_{HF}, E_{local}) and acceptance ratios (AR) for C,N,O and Ne atoms, for different ensemble sizes (N_k) and walk parameters (time step, τ, number of blocks, N_b, and number of steps per block, N_s).

	E_{HF} (a.u.)	Method	N_k	τ	$N_b \times N_s$	E_{local} (a.u.)	AR	CPU time[a]	T_{corr}
		No Acc.	200	0.03	20x1000	-37.64131(427)	.5539	3327.57	11.36
C	-37.6884	Acc.	200	0.006	20x1000	-37.65972(511)	.4625	3327.53	16.27
		No Acc.	400	0.03	50x1000	-37.68533(58)	.5680	11549.81	12.59
		Acc.	400	0.005	50x1000	-37.68683(58)	.5563	11587.81	35.40
N	-54.4009	No Acc.	400	.02	50x1000	-54.40254(214)	.5902	21735.02	9.30
		Acc.	400	.02	50x1000	-54.40128(221)	.5835	21791.11	10.21
O	-74.8094	No Acc.	400	.015	50x1000	-74.80309(328)	.5667	26665.34	14.30
		Acc.	400	.015	50x1000	-74.79583(577)	.5862	26721.11	46.06
		No Acc.	200	.01	20x1000	-128.54106(1114)	.5474	8476.60	12.86
		Acc.	200	.001	20x1000	-128.52363(1537)	.4258	8470.75	33.61
Ne	-128.54701	No Acc.	400	.01	50x1000	-128.54416(442)	.5474	32583.34	14.25
		Acc.	400	.001	50x1000	-128.54642(712)	.4283	32266.96	37.58
		No Acc.	500	.01	50x1000	-128.54582(354)	.5472	49817.69	12.01
		Acc.	500	.001	50x1000	-128.54180(575)	.4214	49707.08	31.69

[a] CPU times given in seconds

error associated with its estimation. The results shown in Table 4.4 corresponds to data from a walk with the specified parameters and therefore no error bars are shown on the acceptance ratio (AR) and T_{corr}.

The first set of runs (N = 20000) for carbon shows that the acceleration does poorly for both improving the variance as well as in decreasing correlation among steps. The autocorrelation function plotted in Fig. 4.7 for carbon (non-accelerated and accelerated), clearly shows this,[16] and the autocorrelation time confirms it numerically. For the second set of runs, on the other hand, we find that we can achieve equivalent variances in similar CPU time even though the autocorrelation gets worse. This should be obvious after our short discussion on the compromise when choosing τ. In order to increase acceptance, one has to bargain with the correlation as well, i.e., when the acceptance is too high, one increases the time step obtaining therefore a lower acceptance, lower variance and a shorter correlation. However when the acceptance is too low, one must reduce the time step and increase the variance as well as the correlation among steps. Since carbon requires a $\tau_{NoAcc} \propto 20\tau_{Acc}$, we expect much more correlated results for such a walk.

[16] The autocorrelation function is defined as 1 beginning at 0 steps and reaches 0 when the autocorrelation among steps disappears entirely.

For nitrogen the results are a bit more promising than for carbon. As a matter of fact, both accelerated and nonaccelerated results were equally correlated. However, although of all four systems studied nitrogen looks the best in terms of both variance and T_{corr}, it still indicates that the acceleration is not performing as expected.

The results for oxygen were far more dramatic. The correlation in oxygen is very strong for the accelerated walk (the autocorrelation extended up to 3500 steps), and it is not entirely clear why this extreme correlation is caused by the introduction of the acceleration matrix. It seems that as the number of electrons increases this increase in correlation will be inevitable (except when more sophisticated wave functions are accordingly used), which worsens the sampling efficiency as Z gets large. In the case of neon, once more the time steps needed to achieve comparable acceptance ratios were $\tau_{NoAcc} \propto 10\tau_{Acc}$.

The only consistent result in all cases is that both the correlation and the variance worsen with our choice of $\mathbf{M} = \mathbf{H}^{-1}$. Something to point out is that even in the cases of high T_{corr}, plotting the block energies indicates that they are random enough to be used in computing the E_{VMC}, as can be seen in Fig. 4.8 for oxygen, our most correlated case. It was also suggested that perhaps the poor variance might be a sign of a non-gaussian distribution of the resulting energies. However, as shown in Fig. 4.9, they clearly represent normal distributions of the sampled energies, and therefore, the assigned error bars should unbiasedly match those from standard deviation calculations.

Now we wish to make some comments on the merit of using the autocorrelation time for the evaluation of performance, as well as to compare our results with those recently published by Umrigar[150]. Umrigar claimed in his accelerated Metropolis paper that the "drawback of the Metropolis method is that the points sampled are sequentially correlated, resulting in a loss of computational efficiency," and therefore, autocorrelation is a good measure of efficiency. Accordingly he proposes that the autocorrelation time can be reduced by increasing $\langle \Delta R \rangle$ or by increasing acceptance. However, we claim here that this might not necessarily mean that the method is more efficient since another important consideration is how much of configuration space is being sampled, which a small autocorrelation does not guarantee.

From Umrigar's paper[150], we can see that the autocorrelation times in his Table I fall into two categories: (1) all electrons are moved together; or (2) one electron is moved at a time. The results regarding (1) are the ones that can be directly compared with ours, at least for Ne. Our accelerated T_{corr} result (T_{corr}= 34.29(1.73)) for that system compares with his algorithm 1 (simple Metropolis) for the "good" wave function (T_{corr} = 37(3.7)), while does much better than for his "simple" wave function (T_{corr} = 84(8.4)), and a little worse than algorithm 2 (Cartesian directed Metropolis) with a simple wavefunction (T_{corr} = 28(2.8)). The interesting thing to notice is that our M = 1 (non-accelerated) case, which is another Cartesian directed method, should match with his results for algorithm 2, but does much better (T_{corr} = 13.04(.65)) than his

simple ($T_{corr} = 28(2.8)$), and about the same as his good ($T_{corr} = 11(1.1)$) wavefunction case. His "simple" wavefunction consists of a single determinant multiplied by a simple electron-electron Jastrow factor, while in the "good" wavefunction the determinant is multiplied by Jastrow factors containing both electron-electron and electron-nuclear factors. The wavefunction we use for Ψ_T is not as sophisticated as his "simple" wavefunction, since we do not use any correlation factor. (We also obtain a much larger average acceptance as well as a lower σ value than algorithm 1 in both instances, but this might be due to the differences in the walk parameters.)

Something different caught our attention regarding category (2). Claiming that it takes twice as much computer time for the update of individual electrons, he multiplies his values of T_{corr} by a factor of 2. Although the argument about the factor in the computation time is correct[19], it is not clear how the autocorrelation time can be dependent on an external circumstance, such as computer time. One thing to note, however, is that without this "adjustment," his value of T_{corr} for his good Ne wavefunction is under 1, which seems unreasonable. A value of $T_{corr} < 1$ implies that a walker takes less than one step to become decorrelated!

We did similar estimations of autocorrelation times, using the old non-accelerated VMC method which moves and updates electrons individually, and found some surprises. In order to compare with the T_{corr} values published by Umrigar, we studied the Ne and Ar systems, and discovered that the autocorrelation length was always invariably small (i.e., $T_{corr} \leq 1$). For Argon, just like Umrigar's value for the "good" Ne wave function, our value of T_{corr} was repeatedly under 1. We cannot speak for Umrigar's data,[17] but we can explain what caused our low T_{corr}. To understand how this is possible one needs to look again at Eq. 4.24 where T_{corr} is defined. We found in the data used to compute T_{corr} that ocassionally there were huge fluctuations (or spikes) present among the normal random noise (see Fig. 4.10). These spikes in the sampled energies contribute little to the individual block rms (σ_b) for large blocks (i.e., large N_s), but are significant in determining the overall rms (σ) and, therefore, lead to inappropriately small values of T_{corr}. This phenomenon is related to the quality of the wavefunction and the magnitude of the energy. The quality of the wavefunction in VMC determines how much the energy will oscillate as one samples space (See Appendix A.8). Note that for the exact wave function, one would obtain an infinite correlation time, since all the local energies would equal the exact energy. The second important factor to take into account is that as the total energies become larger with system, more accurate wavefunctions are needed in order to reduce these oscillations and get more meaningful results. For instance, in the case of carbon the largest oscillation present was of the order of .5 a.u., while for argon there were oscillations of several hundred a.u. present. To illustrate this, Fig. 4.10b shows also a similar plot of the accelerated VMC implementation.

[17] Umrigar's values were computed by following a single walker for a million steps.

Figure 4.7: Typical autocorrelation functions for non-accelerated and accelerated runs of carbon atom.

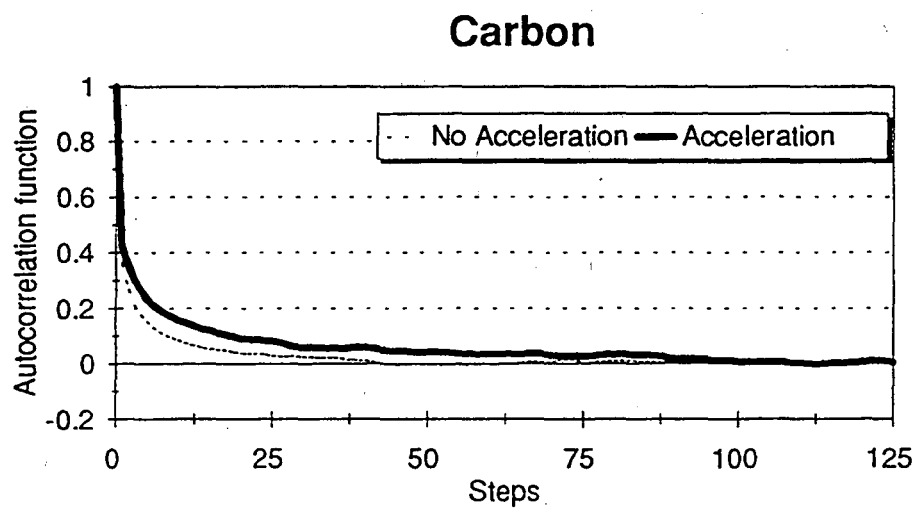

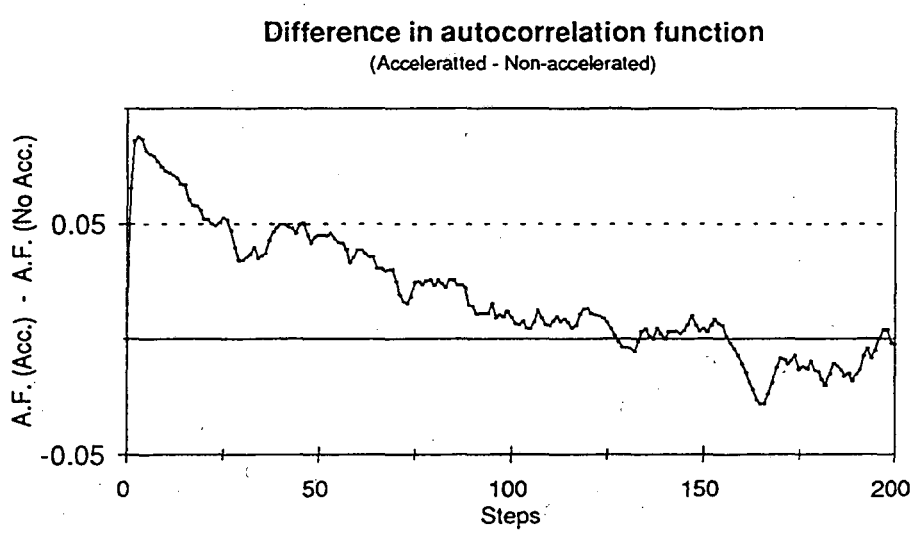

Figure 4.8: Block energies for non-accelerated and accelerated oxygen calculations.

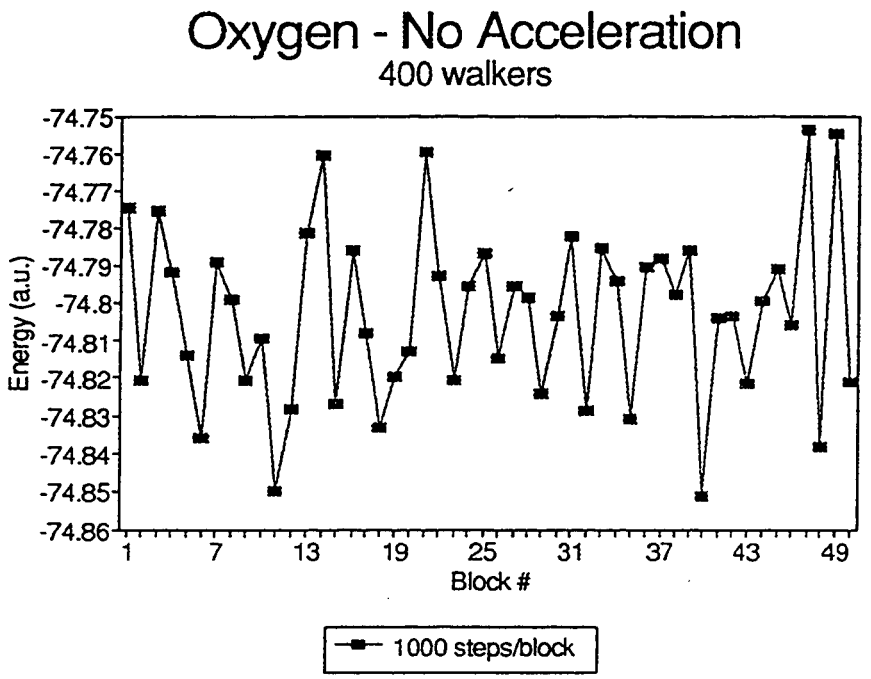

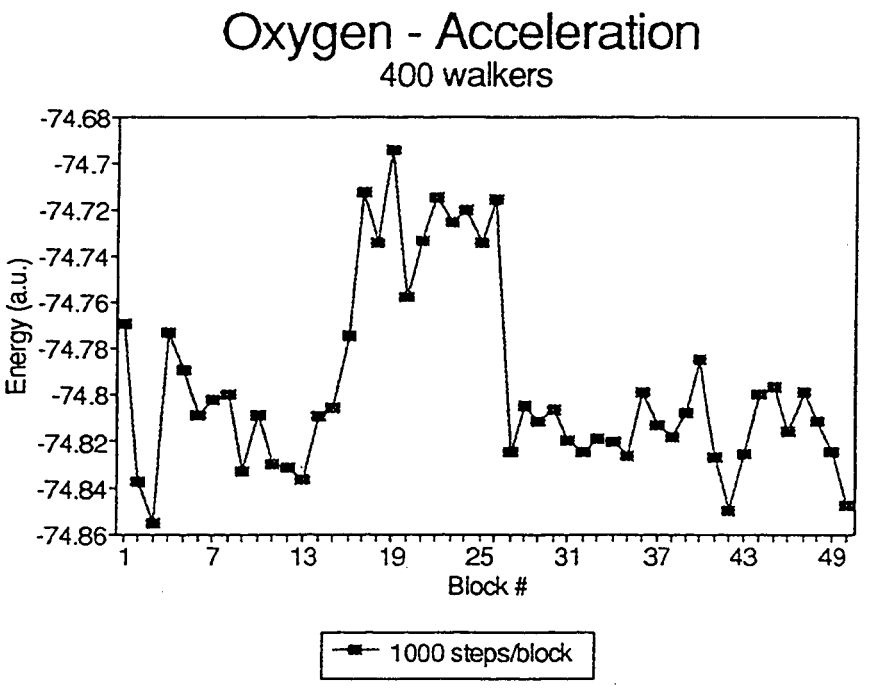

Figure 4.9: Energy distribution of non-accelerated and accelerated runs for oxygen. 400 walkers, 50000 steps.

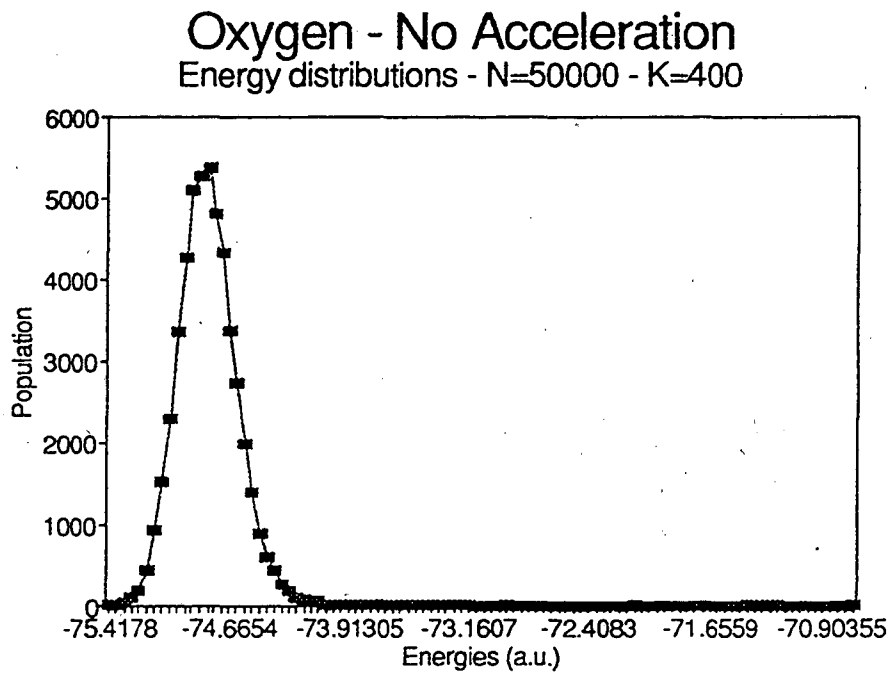

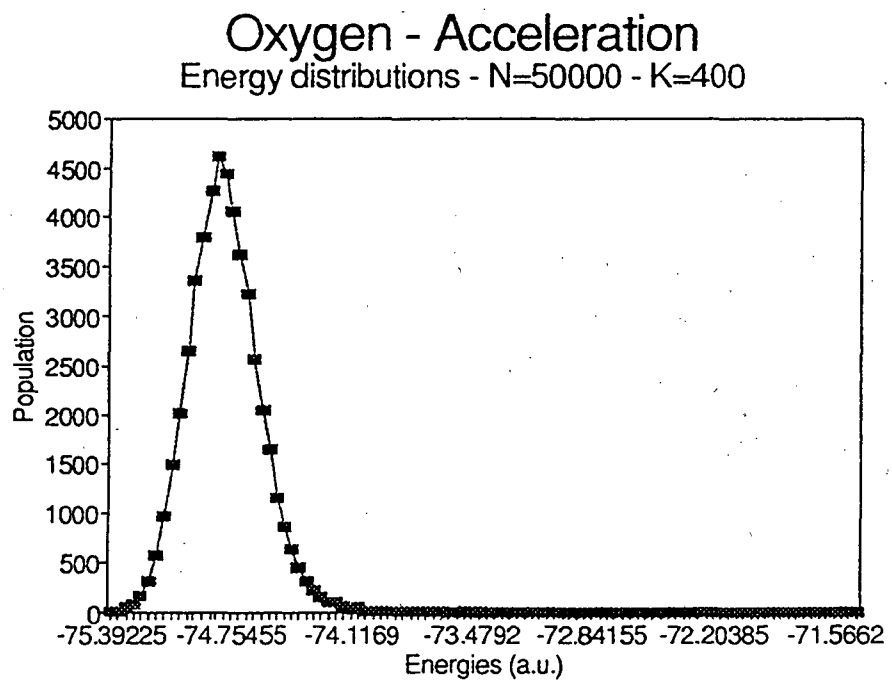

Figure 4.10: Energies along sample VMC walks.

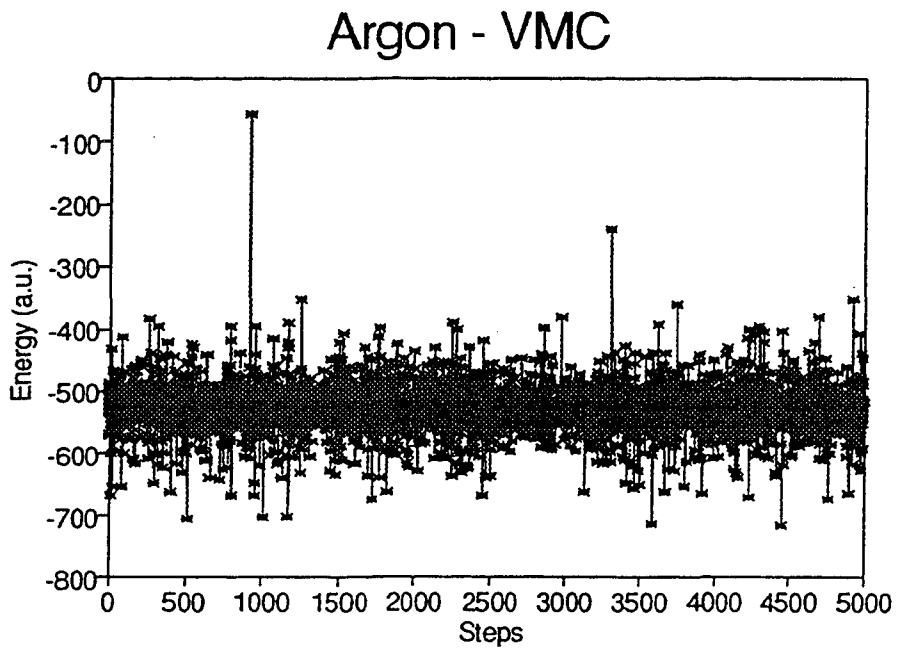

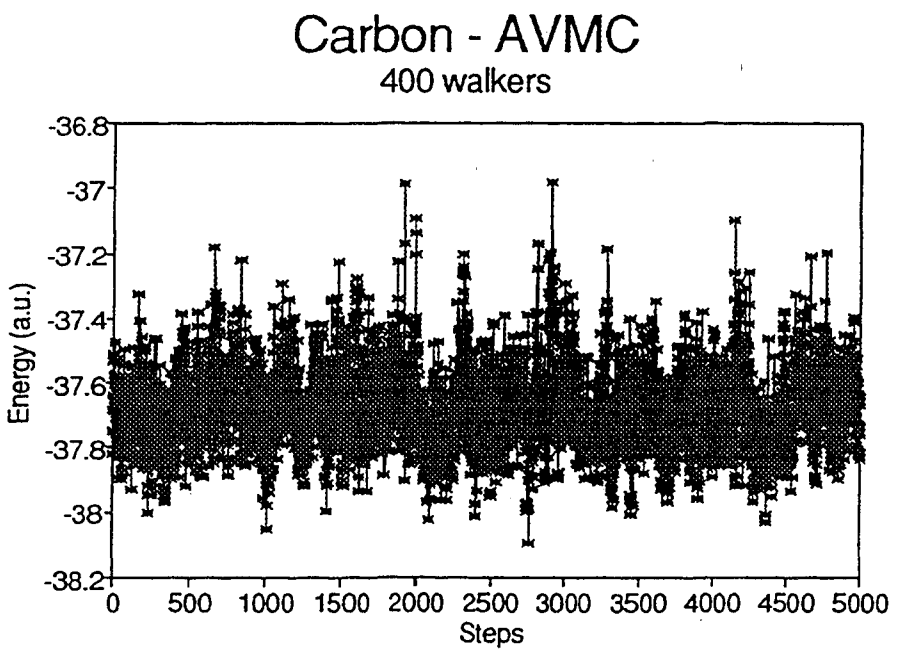

4.3 Conclusion and future directions

We have implemented the Batrouni-Reynolds acceleration method based on an acceleration matrix and found dissapointing results. The core electrons, which are responsible for the bottleneck in the equilibration of the ensemble are not being consistently moved, as hoped. The acceleration matrix failed to move the electrons by an amount proportional to their distance from the nucleus, while the autocorrelation of the walk was greatly increased. These results suggest one must rethink the choice of matrix used.

A different approach by Sun *et al.*[160] delivers better results in differentiating between core and valence, by taking second derivatives of the pseudopotential $\mathcal{P} = -ln|\Psi_T|^2$ into acount in addition to the commonly used first derivatives (or quantum force). Preliminary results suggest that this might be a simpler and unbiased alternative to acceleration. With this method, acceptance in the core has been increased for Ne, Ar and KCl by a factor of five by adding only diagonal elements.

Epilogue

Persons attempting to find a motive in this narrative will be prosecuted; persons attempting to find a moral in it will be banished; persons attempting to find a plot in it will be shot.

Mark Twain - "The adventures of Huckleberry Finn"

In spite of the limited success of the work presented here, I believe QMC still has a very promising future. It is clear that knowledge about the nodes of the wavefunction, which is the only truly meaningful information to be known, is very limited by our current means. Perhaps in the future it will be possible to indirectly examine the location of these infamous nodes, but until then, the efforts on "optimizing" wavefunctions should be redirected towards more productive efforts in speeding up the algorithm.

Parallelization of Monte Carlo codes promises to speed up somewhat the process of obtaining the results. However, the claims of the speed up factor might be more luscious than the actual results. Only after parallel machines are made widely available as well as more standard compilers which will make codes portable among machines and operating systems without excessive effort (i.e., extensive rewrite of algorithms), we will know if the parallel architecture is really as exceptional as promised.

Appendix A

Definitions

Quidquid latine dictum sit, altum viditur

Source unknown

The purpose of this section is to provide essential definitions which are fundamental in the preceding work. Rigorous proof of the arguments hereby presented is beyond the scope of the present work, and references to their source will be given in each section.

A.1 Atomic units

In molecular calculations, quantum chemists generally work in a system of units known as atomic units (a.u.). The electronic Hamiltonian for a molecular system with N electrons and M atomic centers is written explicitly as

$$\hat{\mathcal{H}} = -\sum_{i=1}^{N} \frac{\hbar}{2m_i}\nabla_i^2 - \sum_{i=1}^{N}\sum_{A=1}^{M} \frac{Z_A e^2}{4\pi\varepsilon_0 r_{iA}} + \sum_{i=1}^{N}\sum_{j>i}^{N} \frac{e^2}{4\pi\varepsilon_0 r_{ij}} , \tag{A.1}$$

where Z_A is atomic number of nucleus A, r_{ij} is the distance between electrons i and j, and r_{iA} is the distance between electron i and nucleus A. Introducing a set of units such that $\hbar = 1$, $m = 1$, $e = 1$, and $\kappa_0 = 4\pi\varepsilon_0 = 1$, Eq. A.1 becomes

$$\hat{\mathcal{H}} = -\sum_{i=1}^{N} \frac{1}{2}\nabla_i^2 - \sum_{i=1}^{N}\sum_{A=1}^{M} \frac{Z_A}{r_{iA}} + \sum_{i=1}^{N}\sum_{j>i}^{N} \frac{1}{r_{ij}} . \tag{A.2}$$

Many other physical quantities such as distance, energy and time may be expressed using the four basic defined units above. The Bohr radius a_0 defines the atomic unit of length, known as the *bohr* and is given by

$$a_0 = \frac{4\pi\varepsilon_0\hbar^2}{me^2} = 1 . \tag{A.3}$$

Similarly, energy is defined in terms of the *hartree* as

$$E = \frac{me^4}{\kappa_0^2 \hbar^2} = 1 \; hartree \; . \tag{A.4}$$

The ground state of the hydrogen atom is -$\frac{1}{2}$ hartree. A list of atomic units and their significance is given in Table A.1. Table A.2 gives some common energy unit conversions.

A.2 Born-Oppenheimer Approximation

The Hamiltonian of a molecular system is given as follows:

$$\hat{\mathcal{H}} \;=\; \hat{T}_r + \hat{T}_R + \hat{V}(\vec{r}_i, \vec{R}_A) \tag{A.5}$$

where

$$\hat{T}_r \;=\; \sum_{i=1}^{N_e} \frac{(\hat{p}_i)^2}{2m_i} \;=\; \sum_{i=1}^{N_e} -\frac{\hbar^2}{2m_i}\nabla_i^2 \tag{A.6}$$

is the kinetic energy of the electrons ($\hat{p}_i$ and m_i are the momentum operator and mass for electron i),

$$\hat{T}_R \;=\; \sum_{A=1}^{N_{nuc}} \frac{(\hat{p}_A)^2}{2M_A} \;=\; \sum_{A=1}^{N_{nuc}} -\frac{\hbar^2}{2M_A}\nabla_A^2 \tag{A.7}$$

is the kinetic energy of the nuclei, and

$$\hat{V}(\vec{r}_i, \vec{R}_A) \;=\; \hat{V}_{ee} \;+\; \hat{V}_{nn} \;+\; \hat{V}_{ne} \tag{A.8}$$

is the potential energy which has electron-electron, nuclear-nuclear, and electron-nuclear contributions, given by

$$\hat{V}_{ee} \;=\; \frac{1}{2}\sum_{i=1}^{N_e}\sum_{j>i}^{N_e} \frac{e^2}{|\vec{r}_i - \vec{r}_j|} \; , \tag{A.9}$$

$$\hat{V}_{nn} \;=\; \frac{1}{2}\sum_{A=1}^{N_{nuc}}\sum_{B>A}^{N_{nuc}} \frac{e^2 Z_A Z_B}{|\vec{R}_A - \vec{R}_B|} \; , \tag{A.10}$$

and

$$\hat{V}_{ne} \;=\; -\sum_{i=1}^{N_e}\sum_{A=1}^{N_{nuc}} \frac{e^2 Z_A}{|\vec{R}_A - \vec{r}_i|} \; , \tag{A.11}$$

respectively. Using Eq. A.5, the Schrödinger equation becomes

$$\hat{T}_r\Psi(\vec{r}_i, \vec{R}_A) \;+\; \hat{T}_R\Psi(\vec{r}_i, \vec{R}_A) \;+\; \hat{V}\Psi(\vec{r}_i, \vec{R}_A) \;=\; E\Psi(\vec{r}_i, \vec{R}_A) \tag{A.12}$$

Assume that the eigenfunctions $\Psi(\vec{r}_i, \vec{R}_A)$ of the Hamiltonian $\mathcal{H}$ are separable in the following form (called a *Born-Oppenheimer product*):[1]

$$\Psi(\vec{r}, \vec{R}) \;=\; \phi(\vec{R})\psi(\vec{r}, \vec{R}) \; . \tag{A.13}$$

[1] It may seem that this is what we ultimately want to prove. However, this is a common practice when a separation of variables is desired.

Table A.1: Atomic Units[a]

Quantity	Natural Unit	SI equivalent
Mass	$m = 1$ (electron mass)	9.1091×10^{-31} kg
Charge	$\lvert e \rvert = 1$ (electronic charge)	1.6021×10^{-19} C
Angular momentum	$\hbar = 1$	1.0545×10^{-34} J· s
Permittivity	$\kappa_0 = 4\pi\varepsilon_0 = 1$	1.1126×10^{-10} $C^2 \cdot J^{-1} \cdot m^{-1}$
Length	$\kappa_0\hbar^2/me^2 = a_0 = 1$ (bohr) (Bohr radius)	5.29167×10^{-11} m
Energy	$\mathcal{E}_a = me^4/\kappa_0^2\hbar^2 = e^2/\kappa_0 a_0 = 1$ (hartree) (twice the ionization energy of atomic hydrogen)	435944×10^{-18} J
Time	$\kappa_0^2\hbar^3/me^4 = 1$ (period of an electron in the first Bohr orbit)	2.41889×10^{-17} s
Speed	$e^2/\kappa_0\hbar = 1$ (speed of an electron in the first Bohr orbit)	2.18764×10^6 m · s^{-1}
Electric potential	$me^3/\kappa_0^2\hbar^2 = e/\kappa_0 a_0 = 1$ (potential energy of an electron in the first Bohr orbit)	27.211 V
Magnetic dipole moment	$e\hbar/m = 1$ (twice a Bohr magneton)	1.85464×10^{-23} $J \cdot T^{-1}$
Electric dipole moment	$ea_0 = 1$	8.4784×10^{-30} C · m
Electric polarizability	$e^2 a_0^2 \mathcal{E}_a^{-1}$	1.6488×10^{-41} $C^2 m^2 J^{-1}$
Electric field	$\mathcal{E}_a e^{-1} a_0^{-1}$	5.1423×10^{11} V · m^{-1}
Wave function	$a_0^{-3/2}$	2.5978×10^{15} $m^{-3/2}$

[a]Taken from Refs. [1] and [11].

Table A.2: Conversion factors for energy units used throughout this work.

	eV	hartree (au)	cm^{-1}	kcal mol^{-1}
1 eV =	1	3.675×10^{-2}	8065	96.48
1 hartree (au) =	27.21	1	$2.195 \times 10^{+5}$	627.51
1 cm^{-1} =	1.2399×10^{-4}	4.556×10^{-6}	1	2.859×10^{-3}
1 kcal mol^{-1} =	4.337×10^{-2}	1.5936×10^{-3}	349.8	1

Now substituting Eq. A.13 into Eq. A.12 we get

$$\phi(\vec{R})\hat{T}_r\psi(\vec{r},\vec{R}) + \hat{T}_R\phi(\vec{R})\psi(\vec{r},\vec{R}) + \hat{V}(\vec{r},\vec{R})\phi(\vec{R})\psi(\vec{r},\vec{R}) = E\phi(\vec{R})\psi(\vec{r},\vec{R}) . \tag{A.14}$$

Since

$$\hat{T}_R\phi(\vec{R})\psi(\vec{r},\vec{R}) = \phi(\vec{R})\hat{T}_R\psi(\vec{r},\vec{R}) + \psi(\vec{r},\vec{R})\hat{T}_R\phi(\vec{R}) - \sum_A \frac{\hbar^2}{M_A}\vec{\nabla}_A\phi(\vec{R})\cdot\vec{\nabla}_A\psi(\vec{r},\vec{R}) , \tag{A.15}$$

Eq. A.14 becomes

$$\left\{-\sum_A \frac{\hbar^2}{M_A}\vec{\nabla}_A\phi(\vec{R})\cdot\vec{\nabla}_A\psi(\vec{r},\vec{R}) + \phi(\vec{R})\hat{T}_R\psi(\vec{r},\vec{R})\right\}$$
$$+ \psi(\vec{r},\vec{R})\hat{T}_R\phi(\vec{R}) + \phi(\vec{R})\hat{T}_r\psi(\vec{r},\vec{R}) + \hat{V}(\vec{r},\vec{R})\phi(\vec{R})\psi(\vec{r},\vec{R}) = E\phi(\vec{R})\psi(\vec{r},\vec{R}) . \tag{A.16}$$

Neglecting the terms in brackets corresponds to the *adiabatic* approximation, i.e. the electrons change positions many times before the nuclei shift their positions by any considerable amount:

$$\left|-\sum_A \frac{\hbar^2}{M_A}\left[\vec{\nabla}_A\phi\cdot\vec{\nabla}_A\psi\right] + \phi\hat{T}_R\psi\right| \ll |\psi\hat{T}_R\phi| \tag{A.17}$$

which holds when $|\vec{\nabla}_A\psi(\vec{r}_i,\vec{R}_A)| \ll |\vec{\nabla}_A\phi(\vec{R}_A)|$.[2] Equation A.16 becomes

$$\frac{\psi}{\phi}\hat{T}_R\phi + \left[\hat{T}_r + \hat{V}\right]\psi = E\psi . \tag{A.18}$$

Terms in brackets constitute the Hamiltonian for fixed-nuclei (i.e., $\hat{T}_R = 0$), which is also known as the *electronic Hamiltonian*, $\hat{\mathcal{H}}_{el} = \hat{T}_r + \hat{V}(\vec{r},\vec{R})$. The functions, $\psi(\vec{r},\vec{R})$ are chosen to be eigenfunctions of $\hat{\mathcal{H}}_{el}$,

$$\hat{T}_r\psi(\vec{r},\vec{R}) + \hat{V}(\vec{r},\vec{R})\psi(\vec{r},\vec{R}) = \varepsilon(\vec{R})\psi(\vec{r},\vec{R}) , \tag{A.19}$$

and the energy eigenvalues, $\varepsilon(\vec{R})$ depend parametrically on $\vec{R}$. Using Eq. A.19, Eq. A.18 becomes

$$\hat{T}_R\phi(\vec{R}) + \varepsilon(\vec{R})\phi(\vec{R}) = E\phi(\vec{R}) . \tag{A.20}$$

[2] This is so since changes in electronic coordinates are much larger than changes in nuclear coordinates.

Assuming that the adiabatic approximation holds, the problem reduces to the following system of equations:

$$\hat{T}_r\psi_k(\vec{r},\vec{R}) + \hat{V}(\vec{r},\vec{R})\psi_k(\vec{r},\vec{R}) = \varepsilon_k(\vec{R})\psi_k(\vec{r},\vec{R}) \tag{A.21}$$

$$\hat{T}_R\phi_{kl}(\vec{R}) + \varepsilon_k\phi_{kl}(\vec{R}) = E_{kl}\phi_{kl}(\vec{R}) \ . \tag{A.22}$$

A stationary state of the system is given by

$$\Psi_n(\vec{r},\vec{R}) = \psi_k(\vec{r},\vec{R})\phi_{kl}(\vec{R}) \ , \tag{A.23}$$

where ψ_k are the eigenfunctions of the "electronic" Hamiltonian,

$$\hat{\mathcal{H}}_{el} = \hat{T}_r + \hat{V}(\vec{r},\vec{R}) \ , \tag{A.24}$$

and ϕ_{kl} are the eigenfunctions of the "nuclear" Hamiltonian,

$$\hat{\mathcal{H}}_{nuc} = \hat{T}_R + \varepsilon_k(\vec{R}) \ . \tag{A.25}$$

The nuclear Schrödinger equation, $\hat{\mathcal{H}}_{nuc}\Psi_n = E\Psi_n$, is solved to describe the vibration, rotation and translation of the molecular system.

A.3 Slater-type and Gaussian-type orbitals (STOs and GTOs)

In Sec. 1.1 we mentioned the basis functions which are used to describe the AOs in the LCAO approximation in a very vague fashion. It is clear that many types of functions could be used, from simple exponentials to the complex Hylleras expansions[161]. However the two types of basis functions which are most used in molecular electronic structure calculations are the Slater-type orbitals (STOs) and the Gaussian-type orbitals (GTOs). The general form of the Slater-type function (STF) is,

$$\chi_S = x^a y^b z^c r^l e^{-\zeta r} \quad \text{or} \quad \chi_S = Y_l^m(\theta,\phi) r^l e^{-\zeta r} \ , \tag{A.26}$$

in Cartesian and spherical polar coordinates, respectively. Table A.3 shows a transformation between the spherical polar and the Cartesian orbitals. This table is particularly useful to those who use quantum chemistry codes based on Gaussian orbitals to obtain wave functions.[3] These programs output 6-$d(x^2,\ y^2,\ z^2,\ xy,\ xz,\ yz)$ functions instead of the 5 physical ones($3r^2 - r^2,\ xz,\ yz,\ xy,\ x^2 - y^2$), and likewise there will be 10-f functions instead of 7, and so on. The Cartesian Gaussian-type functions (GTFs) are, similarly, given by

$$\chi_G = x^a y^b z^c r^l e^{-\zeta_g r^2} \tag{A.27}$$

[3]Such as GAMESS and HONDO which we use in QMC to obtain the trial function.

Even though STFs provide a more accurate description of the cusp behavior in the orbitals, they are much more difficult to integrate. This is why most computations are performed with linear combinations of Gaussian functions[4] which are fit to resemble the correct cusp behavior.

A.3.1 Nomenclature

At this point it is useful to say a few words about the nomenclature used in the literature to label these basis sets. Clementi provides a good source of atomic STO basis sets in Ref. [103]. Similarly, Huzinaga[94], Dunning[95, 162] and Pople have provided atomic GTO basis sets. Pople's nomenclature corresponds to linear combinations of contracted Gaussians. The first type of basis sets are the Slater-type orbitals expanded in K Gaussians, or STO-KG, where K is the expansion number[5]. Larger exponents ζ will produce tighter orbitals, while smaller ζ's bring about orbitals which are diffuse. These properties are used in the linear combination to approximate the cusp of the STO's they try to emulate. As K increases, the better the approximation becomes. Huzinaga introduced the terms double-zeta (DZ), triple zeta (TZ), etc., where the number of zeta refers to the number of basis functions added for each AO[6].

Since increasing the number of functions also increases the number of integrals to be computed, it is wise to limit the expansions, or at least to choose the functions involved carefully. This gives rise to the so-called split valence basis sets. The idea here is to get rid of the extra-functions in the core region, since they are not that important in bonding anyway. The notation for these "split valence" basis sets is given by a K-LMNG symbol where K is the number of functions in the core; LMN describe the number of primitives used to expand the valence functions; and G simply means that all basis functions are expanded in terms of Gaussians.

The next level of expansion is the inclusion of *polarization* functions[163]. These polarization functions are functions beyond the AOs which are needed in the ground state atomic configuration, e.g., p-functions for H atom, d-functions for C atom, etc. In the Huzinaga nomenclature the inclusion of polarization functions is added to the DZ, TZ, QZ terms to become DZP, TZP, etc. to imply double-zeta+polarization, etc. The Pople nomenclature becomes K-LMNG* to indicate polarization on "heavy atoms," i.e., $Z > 1$; and K-LMNG** when there is polarization on everything including H-atom.

In general, to indicate the level of the calculation, the convention of "(level of theory)/(basis set)" is used. For example, HF/STO-3G means a Hartree-Fock calculation done at the minimal STO basis set level, and MP2/6-31G means that the Møller-Plesset method to second order with a 6-31G basis has been used. When a geometry optimization has been performed, it is

[4] These functions are usually said to be formed by "contracted primitive" Gaussians.

[5] Although $K \geq 2$, the standard minimal STO basis set is the STO-3G, and the largest used is STO-6G.

[6] "Zeta" comes from the greek letter ζ used to denote the exponent in the radial part of the wave function.

Table A.3: Slater Type Orbitals in Cartesian coordinates and in spherical polar coordinates, according to the type of molecular bond to which they contribute.

Orbital	n	l	m	$Y_l^m(\theta,\phi)r^l e^{-\zeta r}$	$x^a y^b z^c r^l e^{-\zeta r}$	Bond Type
1s	1	0	0	$e^{-\zeta r}$		σ
2s	2	0	0	$re^{-\zeta r}$		σ
$2p_z$		1	0	$r\cos\theta e^{-\zeta r}$	$ze^{-\zeta r}$	σ
$2p_x$			1	$r\sin\theta e^{i\phi}e^{-\zeta r}$	$xe^{-\zeta r}$	π
$2p_y$			-1	$r\sin\theta e^{-i\phi}e^{-\zeta r}$	$ye^{-\zeta r}$	π
3s	3	0	0	$r^2e^{-\zeta r}$		σ
$3p_z$		1	0	$r^2\cos\theta e^{-\zeta r}$	$rze^{-\zeta r}$	σ
$3p_x$			1	$r^2\sin\theta e^{i\phi}e^{-\zeta r}$	$rxe^{-\zeta r}$	π
$3p_y$			-1	$r^2\sin\theta e^{-i\phi}e^{-\zeta r}$	$rye^{-\zeta r}$	π
$3d_{3z^2-r^2}$		2	0	$r^2(3\cos^2\theta-1)e^{-\zeta r}$	$(3z^2-r^2)e^{-\zeta r}$ $(2z^2-x^2-y^2)e^{-\zeta r}$	σ
$3d_{xz}$			1	$r^2\sin\theta\cos\theta e^{i\phi}e^{-\zeta r}$	$xze^{-\zeta r}$	π
$3d_{yz}$			-1	$r^2\sin\theta\cos\theta e^{-i\phi}e^{-\zeta r}$	$yze^{-\zeta r}$	π
$3d_{x^2-y^2}$			2	$r^2\sin^2\theta e^{2i\phi}e^{-\zeta r}$	$(x^2-y^2)e^{-\zeta r}$	δ
$3d_{xy}$			-2	$r^2\sin^2\theta e^{-2i\phi}e^{-\zeta r}$	$xye^{-\zeta r}$	δ
$\vdots$						$\vdots$
4f		3	0	$r^3(\frac{5}{3}\cos^3\theta-\cos\theta)e^{-\zeta r}$	$r^3(\frac{5}{3}z^3-zr^2)e^{-\zeta r}$ $(\frac{2}{3}z^3-x^2z-y^2Z)e^{-\zeta r}$	σ
			1	$r^3(5\cos^2\theta-1)\sin\theta e^{i\phi}e^{-\zeta r}$	$(5z^2x-xr^2)e^{-\zeta r}$ $(4z^2x-x^3-xy^2)e^{-\zeta r}$	π
			-1	$r^3(5\cos^2\theta-1)\sin\theta e^{-i\phi}e^{-\zeta r}$	$(5z^2y-yr^2)e^{-\zeta r}$ $(4yz^2-yx^2-y^3)e^{-\zeta r}$	π
			2	$r^3 cos\theta\sin^2\theta e^{2i\phi}e^{-\zeta r}$	$(zx^2x-zy^2)e^{-\zeta r}$	δ
			-2	$r^3\cos\theta\sin^2\theta e^{-2i\phi}e^{-\zeta r}$	$2xyze^{-\zeta r}$	δ
			3	$r^3\sin^3\theta e^{3i\phi}e^{-\zeta r}$	$(x^3-3xy^2)e^{-\zeta r}$	ϕ
			-3	$r^3\sin^3\theta e^{-3i\phi}e^{-\zeta r}$	$(3x^2y-y^3)e^{-\zeta r}$	ϕ

common to see the // symbol between two such descriptions. For instance, MP4/6-31G*//STO-6G means that an MP4 calculation was carried out with a 6-31G* basis set, on a geometry found using HF/STO-6G.[7]

A.4 The variational principle

The variational principle, given by

$$E = \frac{\int \Psi^* \hat{\mathcal{H}} \Psi d\tau}{\int \Psi^* \Psi d\tau} \geq E_0 \ , \tag{A.28}$$

allows us to compute upper bounds to the ground-state energy, E_0, for any given trial function. A consequence of the variational principle is that by minimizing the variational energy with respect to the (variational) parameters in the trial function, one will get closer to the exact ground-state energy. However, one might find poor trial functions, that is poor in describing the system, which still give very good variational energies.

A.5 Configuration State Functions

In electronic structure theory, the electrons are assigned to orbitals to specify a given configuration. This configuration may be characterized by a a set of occupation numbers describing the assignment and number of electrons in each orbital. An orthonormal set of configuration state functions (CSF's) [92, 164] is associated with each configuration. These CSF's are eigenfunctions of $\hat{S}^2$ and $\hat{S}_z$, and may be a linear combination of Slater determinants. The n-particle basis of a CI calculation is built by CSF's formed from different configurations of same symmetry and spin eigenvalues. A better description of how CSF's are defined and generated is given in [92].

A.6 Density matrices and natural orbitals

One can write the expectation value of a physical quantity[165] as

$$\Omega_{op} = \Omega_0 + \sum_{i=1}^{N} \Omega_i + \frac{1}{2!} \sum_{i>j=1}^{N} \Omega_{ij} + \frac{1}{3!} \sum_{i>j>k=1}^{N} \Omega_{ijk} + \cdots \tag{A.29}$$

and evaluate this expression in terms of density matrices[165],

$$\langle \Omega_{op} \rangle = \langle \Psi | \Omega_{op} | \Psi \rangle \quad = \quad \int dx \ \Psi^* \Omega_{op} \Psi$$

[7] Notice that an HF/STO-6G calculation can be abbreviated to simply STO-6G.

$$= \Omega_0 + \int dx_1 \Omega_1 \gamma(x_1'|x_1) + \int dx_1 dx_2 \; \Gamma(x_1' x_2'|x_1 x_2)$$
$$+ \int dx_1 dx_2 dx_3 \; \Omega_{123} \Gamma(x_1' x_2' x_3'|x_1 x_2 x_3) \; + \cdots \qquad \text{(A.30)}$$

where

$$\gamma(x_1'|x_1) = N \int dx_2 dx_3 \cdots dx_N \; \Psi^*(x_1', x_2, \cdots, x_N) \Psi^*(x_1, x_2, \cdots, x_N) \; , \qquad \text{(A.31)}$$

and $\gamma(x_1'|x_1)dv_1$ is the probability of finding *any* of the electrons within the volume dv_1 around point r_1 having spin σ_1 where all the other particles have arbitrary positions and spin; and

$$\Gamma(x_1' x_2'|x_1 x_2) = \begin{pmatrix} N \\ 2 \end{pmatrix} \int dx_3 dx_4 \cdots dx_N \; \Psi^*(x_1', x_2', x_3, \cdots, x_N) \Psi^*(x_1, x_2, x_3, \cdots, x_N) \; , \qquad \text{(A.32)}$$

and $\Gamma(x_1' x_2'|x_1 x_2)dv_1$ is the probability of finding any of the electrons within the volume dv_1 around point r_1 having spin σ_1 and another electron within volume dv_2 around point r_2 having spin σ_2, when all others have arbitrary positions and spins. $\gamma(x_1'|x_1)$ is known as the first-order reduced density matrix and $\Gamma(x_1' x_2'|x_1 x_2)$ is the second order reduced density matrix. The general expressions for the density matrix is

$$\Gamma(x_1' x_2' \cdots x_p'|x_1 x_2 \cdots x_p)$$
$$= \begin{pmatrix} N \\ p \end{pmatrix} \int dx_{p+1} \cdots dx_N \; \Psi^*(x_1' x_2' \cdots x_p' x_{p+1} \cdots x_N) \Psi(x_1 x_2 \cdots x_p x_{p+1} \cdots x_N) \qquad \text{(A.33)}$$

$$\Gamma(x_1' x_2' \cdots x_p'|x_1 x_2 \cdots x_p) = \Psi^*(x_1' x_2' \cdots x_p') \Psi(x_1 x_2 \cdots x_p) \qquad \text{(A.34)}$$

All their diagonal elements are positive definite, and have normalization,

$$\int dv_1 \; \gamma(x_1|x_1) = N \qquad \text{(A.35)}$$

$$\int dv_1 dv_2 \; \Gamma(x_1 x_2|x_1 x_2) = \begin{pmatrix} N \\ 2 \end{pmatrix} \; . \qquad \text{(A.36)}$$

γ may not be diagonal, but one can always find a linear transformation to diagonalize it. The elements of γ in diagonal form are the *natural spin orbitals*. Natural orbitals (NOs) give the most rapidly convergent CI wavefunctions.

A.7 Dissociation energies

A.7.1 Zero Point Energy

The "correct" way of estimating the zero point energy (ZPE) is by computing exactly by how much the first vibrational level differs from the bottom of the electronic well. Therefore,

to estimate the zero point energy, one is required to know the vibrational frequencies of the system in question (*all modes included*), which is not always the case. One approximation very commonly used is

$$D_0 = D_e - (\omega_e/2 - \omega_e x_e/4) \tag{A.37}$$

where ω_e are the harmonic frequencies and x_e are the anharmonicity constants, both hopefully[8] obtained spectroscopically.

The result with some systems is that anharmonicities are either not easily available for all species involved, or the experimental data available does not necessarily agree, as is the case for C_2H. In the case of the bond dissociation of C_2H_2, theoreticians have used the accepted experimental frequencies for C_2H_2 and compute (when their computational method allows it, which is NOT the case for QMC) the frequencies for C_2H. The difference of their respective ZPEs gives the offset from D_e.

A.7.2 Isodesmic and isogyric reactions

In an isodesmic reaction the reactants and the products contain the same types of bonds, so they allow us to get bond energies without ever breaking the bond. Because of this, one gets cancellation of errors due to incomplete basis sets and deficient correlation. For example, Zhao and Francisco[166] calculated the ΔH_r^0 for the reaction FO + HOH $\rightarrow$ HO + FOH (which retains its total of one OF and two OH bonds throughout the reaction) at different basis sets and levels of theory, and found little difference among the results.

In isgyric reactions the number of electron pairs (and therefore, the number of unpaired electrons) is conserved. These reactions allow to compare bond dissociation energies (BDEs) computed by very accurate *ab initio* methods(e.g. G-1, GFMC) with heats of formation established from calorimetry. For instance, Pople *et al.* used this concept in Ref. [167] to determine atomization energies of molecules of the form AH_n. They reduce the basis functions usually assigned the hydrogen to determine the breaking of the A-H bond by determining each bond energy relative to H_2, and then convert it to atomization energies by using the exact energy of the hydrogen molecule. For this purpose, the isogyric reaction AH + H $\rightarrow$ A + H_2 is considered.

A.8 Local energy

The quantity

$$E_L(\vec{R}) = \frac{\hat{\mathcal{H}}\Psi(\vec{R})}{\Psi(\vec{R})}, \tag{A.38}$$

[8] For some systems, such as C_2H for instance, one has trouble finding agreement for such data.

known as the *local energy*, is a constant for the exact wavefunction at all points in space. However for an approximate wavefunction the local energy is not a constant, and it will not converge during a stochastic MC simulation. Nevertheless, the variance, which depends on the quality of the wave function, will converge to a specified value which decreases as the approximate wave function approaches the exact.

A.8.1 Cusp condition

If Ψ is an approximate wave function, the local energy has, in general, infinite singularities for $r_{ij} = 0$ and $r_{i\alpha} = 0$ in the potential $V(\vec{R})$ of Eqn. 2.14. These singularities can be cancelled by the kinetic energy by imposing the cusp conditions[168, 169], which describe the correct discontinuity in the derivative of the wave function. These conditions can be summarized as in the limit of two particles (electron or nucleus) of masses m_i and m_j with charges q_i and q_j respectively, approach other,[9]

$$\left[\frac{1}{\Psi}\frac{\partial\langle\Psi\rangle}{\partial r_{ij}}\right]_{r_{ij}=0} = \mu_{ij} q_i q_j \tag{A.39}$$

where $\mu_{ij} = m_i m_j/(m_i + m_j)$ is the reduced mass and $\langle\Psi\rangle$ is the average of Ψ around an infinitesimal sphere around $r_{ij} = 0$. For a Ψ of form $\Psi = A \cdot C$ where only C is a function of interparticle distances, this translates into the conditions,

$$\frac{1}{\Psi}\frac{\partial\Psi}{\partial r_{ij}}\bigg|_{r_{ij}=0} = \begin{cases} \frac{e^2}{8D} = \frac{1}{4} & \text{for } ij \text{ of equal spins} \\ \frac{e^2}{4D} = \frac{1}{2} & \text{for } ij \text{ of opposite spins} \end{cases} \tag{A.40}$$

when the particles are two electrons and

$$\frac{1}{\Psi}\frac{\partial\Psi}{\partial r_{i\alpha}}\bigg|_{r_{i\alpha}=0} = -Z_\alpha\frac{e^2}{2D} = -Z_\alpha \tag{A.41}$$

for an electron and a nucleus. For instance, Eqs. A.40 and A.41 translate to a wave function $\Psi \propto e^{e^2 r_{ij}/4D}$ (for opposite spin electrons), which can be satisfied in practice by choosing the leading term in a correlation function of the form e^U to be $a = \frac{1}{2}$. Similar arguments are used to choose the electron-nuclear correlation.

A.9 Growth estimator

In practice, the average of the local energy, $\langle E_L\rangle$, does not give a good estimator for E_T. If we consider the initial populations $f_0 = \phi_0$ and $f_1 = e^{-(E_0-E_T)\tau}\phi_0$, and take their ratio,

[9] This is known as Kato's cusp condition.

f_1/f_0,

$$\begin{aligned} \frac{f_1}{f_0} &= e^{-(E_0-E_T)\tau} \\ \ln\left(\frac{f_1}{f_0}\right) &= -(E_0-E_T)\tau = (E_T-E_0)\tau \\ E_0 &= E_T - \frac{1}{\tau}\ln\left(\frac{f_1}{f_0}\right) \end{aligned} \tag{A.42}$$

we can notice that the population ratios should determine the value for the new reference energy. This constitutes the growth estimator and it is the only estimator for some systems, such as the particle-in-a-box.

A.10 Green's functions

The differential equation which we are interested in solving is of the general form

$$\mathrm{L}u = -f \tag{A.43}$$

where L is a differential operator[170]. In our specific case, L will be associated with the Hamiltonian in Sec. 2.1.4.1. In order to solve Eq. A.43 it will be convenient to associate an inverse operator L^{-1} to the operator L such that

$$\mathrm{L}\mathrm{L}^{-1} = \mathrm{L}^{-1}\mathrm{L} = I \tag{A.44}$$

where I is the identity operator. If this is possible, it becomes obvious that a solution to Eq. A.43 will be

$$u = -\mathrm{L}^{-1}f\,. \tag{A.45}$$

It is known that the inverse of a differential operator is an integral operator. If we introduce the integral operator G defined over the domain $0 \leq x \leq l$ by

$$Gf = \int_0^l f(x)G(x,y)dx \tag{A.46}$$

we see that $-G$ may be interpreted as the inverse operator L^{-1}. The Green's function $G(x,y)$ associated with the differential operator L is called the kernel of operator G. It is also true that the Green's function should satisfy all homogenous boundary conditions, i.e.

$$\mathrm{L}G(x,\xi) = 0 \quad \text{for } x \neq \xi\,. \tag{A.47}$$

A.10.1 Free Particle Green's function

Let us start with the Schrödinger equation for the free particle($V = 0$):

$$-\frac{\hbar^2}{2m}\nabla^2\Psi = i\hbar\frac{d\Psi}{dt} \tag{A.48}$$

and rewrite it as a diffusion equation of form $\nabla^2 u = \frac{1}{D}\frac{\partial u}{\partial t}$,

$$\nabla^2 \Psi = \frac{2m}{i\hbar}\frac{\partial \Psi}{\partial t} \tag{A.49}$$

where $D = \frac{i\hbar}{2m}$, is the imaginary diffusion coefficient. We know the solution for such a particle to be

$$\Psi_{1d} = \frac{1}{\sqrt{2\pi\hbar}} e^{\frac{i}{\hbar} p\, x} \quad \text{and} \quad \Psi_{3d} = \frac{1}{(2\pi\hbar)^{3/2}} e^{\frac{i}{\hbar}\vec{p}\cdot\vec{x}} \tag{A.50}$$

in one-dimension and three-dimensions, respectively. In addition, we know the Fourier transforms between coordinate and momentum space in one dimension to be,

$$\psi(x) = \frac{1}{(2\pi\hbar)^{1/2}} \int_{-\infty}^{\infty} e^{ipx/\hbar} \phi(p)\, dp \tag{A.51}$$

$$\phi(p) = \frac{1}{(2\pi\hbar)^{1/2}} \int_{-\infty}^{\infty} e^{-ipx/\hbar} \psi(x)\, dx\ . \tag{A.52}$$

It is also well known how the wavepacket $|\Psi(0)\rangle$ evolves with time. By inserting unity it can be writen in momentum representation we get

$$\begin{aligned} |\Psi(0)\rangle &= \int dp\ \ |p\rangle\langle p|\Psi(0)\rangle \\ &= \int dp\ \ |p\rangle \phi(p,0)\ . \end{aligned} \tag{A.53}$$

And by then applying the time evolution operator,

$$\mathcal{U}(t,0) = e^{-i\hat{H}t/\hbar} = e^{i\hat{p}^2 t/2m\hbar} \text{ (for the free particle, } \hat{H} = \tfrac{\hat{p}^2}{2m}) \tag{A.54}$$

to Eq. A.53 and get $|\Psi(t)\rangle$,

$$\begin{aligned} |\Psi(t)\rangle &= \mathcal{U}(t,0)|\Psi(0)\rangle \\ &= \int \mathcal{U}(t,0)|p\rangle\ \phi(p,0)\ dp \\ &= \int e^{i\hat{p}^2 t/2m\hbar}|p\rangle\ \phi(p,0)\ dp \\ |\Psi(t)\rangle &= \int e^{ip^2 t/2m\hbar}|p\rangle\ \phi(p,0)\ dp\ , \end{aligned} \tag{A.55}$$

which can then be transformed to coordinate representation by projection with $\langle x|$,

$$\begin{aligned} \langle x|\Psi(t)\rangle = \Psi(x,t) &= \int e^{-ip^2 t/2m\hbar}\langle x|p\rangle \phi(p,0)\ dp \\ &= \frac{1}{(2\pi\hbar)^{1/2}} \int_{-\infty}^{\infty} e^{ipx/\hbar} e^{-ip^2 t/2m\hbar} \phi(p,0)\ dp\ . \end{aligned} \tag{A.56}$$

Now we are ready to use the Fourier transforms in Eqs. A.51-A.52 to get

$$\Psi(x,t) = \frac{1}{2\pi\hbar}\int_{-\infty}^{\infty} dx' \int_{-\infty}^{\infty} dp\ e^{-ip^2 t/2m\hbar} e^{ip(x-x')/\hbar}\ \Psi(x',0)\ . \tag{A.57}$$

We can write this expression using a Green's function,

$$\Psi(x,t) \;=\; \int_{-\infty}^{\infty} dx'\; G_0(x,x';t,0)\,\Psi(x',0)\;, \tag{A.58}$$

where we introduce $G_0(x,x';t,0)$ as the *Free Particle Green's function*:

$$G_0(x,x';t,0) \;=\; \frac{1}{2\pi\hbar}\int_{-\infty}^{\infty} dp\; e^{-ip^2t/2m\hbar}e^{ip(x-x')/\hbar}\;. \tag{A.59}$$

We can evaluate this expression by completing the square in the exponential. To accomplish this, rearrange the exponent as follows

$$\begin{aligned} -\frac{i}{\hbar}\left[\frac{p^2}{2m}t \;-\; p(x-x')\right] &= -\frac{i}{\hbar}\{a[p-\theta]^2 - a\theta^2\} \\ &= -\frac{i}{\hbar}\{ap^2 \;-\; 2ap\theta\} \end{aligned} \tag{A.60}$$

where $a = t/2m$ and $\theta = m(x-x')/2t$. The integral then can be solved as a simple Gaussian integral (Can use $\int_{-\infty}^{\infty} e^{-ibp^2}\,dp \;=\; \sqrt{\frac{\pi}{ib}}$ from the friendly neighborhood table of integrals):

$$\begin{aligned} G_0 &= \frac{1}{2\pi\hbar}\int_{-\infty}^{\infty} e^{-\frac{it}{2m\hbar}[p-m(x-x')/t]^2}e^{im(x-x')^2/2\hbar t}\,dp \\ &= \frac{1}{2\pi\hbar}e^{im(x-x')^2/2\hbar t}\int_{-\infty}^{\infty} e^{-\frac{it}{2m\hbar}[p-m(x-x')/t]^2}\,dp \\ &= \frac{1}{2\pi\hbar}\sqrt{\frac{2m\pi\hbar}{it}}e^{im(x-x')^2/2\hbar t} \\ G_0 &= \sqrt{\frac{m}{2\pi\hbar it}}e^{im(x-x')^2/2\hbar t} \end{aligned} \tag{A.61}$$

Now we should be able to get the *diffusion Green's function* by using the diffusion coefficient defined above (Using the definition for D, $D \;=\; i\hbar/2m$, one can solve for $\hbar$: $\hbar \;=\; -2imD$.):

$$G_D \;=\; \sqrt{\frac{1}{4\pi Dt}}e^{-(x-x')^2/4Dt} \tag{A.62}$$

The free particle Green's function represents the spreading of the wave packet.

A.10.2 Integral equations

In *integral equations*,[10] the unknown appears under the integral sign. In *Fredholm equations*, the range of integration is fixed, and likewise, in *Volterra equations* the range is not fixed. A *Fredholm equation of the first kind* with kernel $\hat{\mathcal{K}}(x,z)$ is defined as

$$f(x) \;=\; \int_a^b \hat{\mathcal{K}}(x,z)y(z)\,dz\;, \tag{A.63}$$

[10]This section comes from [170] with some help from [171].

and those corresponding to a *Fredholm equation of the second kind* have the unknown function y outside the integral as well, i.e.,

$$f(x) = y(x) + \int_a^b \hat{\mathcal{K}}(x,z)y(z)\,dz\ , \tag{A.64}$$

Equation A.64 is also known as a non-homogeneous Fredholm equation of the second kind with kernel $\hat{\mathcal{K}}(x,z)$. For our purposes, Eqs. A.63 and A.64 can be written in a more general form as

$$\hat{\mathcal{K}}y - \lambda y = f\ , \tag{A.65}$$

where $\lambda = 0$ refers to the Fredholm equation of the first kind, and $\lambda = 1$ to the Fredholm equation of the second kind. When $f(x) = 0$, Eq. A.65 is an eigenvalue problem where λ are the eigenvalues and $y(x)$ are the eigenfunctions of linear operator $\hat{\mathcal{K}}$.[11]

Second kind integral equations (like Eq. A.64) are easier to handle and can be solved by a method of successive approximations.[12] That is, $y(x)$ can be found by expansion in approximate $y_i(x)$ as follows. Let us modify Eq. A.64 using the general notation from Eq. A.65 and write

$$f(x) = y(x) - \lambda \int \hat{\mathcal{K}}(x,z)y(z)\,dz \tag{A.66}$$

as

$$f = y - \lambda\hat{\mathcal{K}}y\ . \tag{A.67}$$

Equation A.67 can be rewritten as $y = f + \lambda\hat{\mathcal{K}}y$. Taking the zeroth-order approximation to be $y_0(x) = f(x)$ one can get the first-order approximation to be

$$y_1 = f + \lambda\hat{\mathcal{K}}f \tag{A.68}$$

Equation A.68 can be used to obtain the second-order approximation, and so on. Similarly, the nth-order approximation can be found from the recurrence relation

$$y_n = f + \lambda\hat{\mathcal{K}}y_{n-1}\ . \tag{A.69}$$

When these approximations tend to a limit as $n \to \infty$, this limit provides a solution to Eq. A.67.

A.11 The jackknife statistic

If $\hat{\theta}_1$ and $\hat{\theta}_2$ are estimators for any statistical quantity θ, then for any real $R \neq 1$, one can define the *generalized jackknife*[144],

$$G(\hat{\theta}_1, \hat{\theta}_2) = \frac{\hat{\theta}_1 - R\hat{\theta}_2}{1 - R}\ . \tag{A.70}$$

[11] In Sec. 2.1.6, we can associate $y(x)$ with the trial wave function and/or STA Green's function, $\hat{\mathcal{K}}$ with the Hamiltonian, and $f(x)$ with the exact GF.

[12] This method is used in Sec. 2.1.6 to obtain the exact Green's function when only an approximate Green's function is known.

A useful theorem says that if the bias of $\hat{\theta}_k$ is given by

$$E[\hat{\theta}_k] = \theta + b_k(n,\theta) \ , \qquad k = 1,2 \tag{A.71}$$

where $b_2(n,\theta) \neq 0$ and $R = \frac{b_1(n,\theta)}{b_2(n,\theta)}$, then $E[G(\hat{\theta}_1,\hat{\theta}_2)] = 0$. This implies that $G(\hat{\theta}_1,\hat{\theta}_2)$ is an unbiased estimator for θ, if R is known and given as above. In many cases although $G(\hat{\theta}_1,\hat{\theta}_2)$ is not unbiased, it contains less bias than either $\hat{\theta}_1$ or $\hat{\theta}_2$.

In the method of Quenouille, $\hat{\theta}_1$ and $\hat{\theta}_2$ are chosen as follows. Suppose $\hat{\theta}$ is an estimator defined on the random sample $\{x_1, x_2, \ldots, x_n\}$, and then partition this sample into N subsets of size M, i.e., $NM = n$. A new random sample can be formed by deleting *one* subset from the original sample. We now define an estimator $\hat{\theta}^i$ to be the estimator $\hat{\theta}$ defined on the new sample, and the estimators $J_i(\hat{\theta})$ and $J(\hat{\theta})$ be defined as

$$J_i(\hat{\theta}) = N\hat{\theta} - (N-1)\hat{\theta}^i \ , \tag{A.72}$$

and

$$\begin{aligned} J(\hat{\theta}) &= \frac{1}{N}\sum_{i=1} J_i(\hat{\theta}) \\ &= N\hat{\theta} - (N-1)\overline{\hat{\theta}^i} \ , \end{aligned} \tag{A.73}$$

where $i = 1, \ldots, N$. $J(\hat{\theta})$ is known as the *jackknife* and $J_i(\hat{\theta})$ are known as the *pseudo-values of the jackknife*. $J(\hat{\theta})$ and $J_i(\hat{\theta})$ are special cases of $G(\hat{\theta}_1,\hat{\theta}_2)$ where $R(N) = \frac{(N-1)}{N}$, $\hat{\theta}_1 = \hat{\theta}$ and $\hat{\theta}_2 = \frac{1}{N}\sum_{i=1}^{N}\hat{\theta}^i = \overline{\hat{\theta}^i}$, and the bias of $J(\hat{\theta})$ is lower than the bias of $\hat{\theta}$.

A.12 Glossary

		Reference
ACPF	averaged coupled-pair functional method	[37]
APSG	antisymmetrized product of strongly orthogonal geminals	[102]
CASSCF	complete active space self-consistent field	1.2.2
CBS	complete basis set	1.1
CCCI	correlation-consistent CI	[141]
CI	configuration interaction	1.2.1
CSF	configuration state function	[92]
DFT-LDA	density functional theory - local density approximation	e.g., [124]
DMC	diffusion Monte Carlo	2.1.2
DZ	double zeta	A.3.1, A.3
DZP	double zeta + polarization	A.3.1
FCI	full configuration interaction	c.f. 1.2.1
FNA	fixed-node approximation	2.1.4.2
FNDMC	fixed-node diffusion Monte Carlo	2.1.2
FNDQMC	fixed-node diffusion quantum Monte Carlo	2.1.2
G-1	Gaussian-1	1.2.4, [14]
G-2	Gaussian-2	1.2.4, [15]
GFMC	Green's function Monte Carlo	2.1.6
GFMC + RN	Green's function Monte Carlo with Release-Node	2.1.6
GTO / GTF	Gaussian-type orbital/function	A.3
GVB	generalized valence bond (theory)	[172]
HF	Hartree-Fock	1.1
HRIR	high resolution infrared (spectroscopy)	[128]
LEPS	London-Eyring-Polanyi-Sato semiempirical potential surface	Ref. [173]
MBPT	many-body perturbation theory	1.2.3,[10]
MC	Monte Carlo/multi-configuration	1.2.1, 2.1.1
MCSCF	multi-configuration self-consistent field	1.2.1
MP2, MP4	Møller-Plesset perturbation theory to 2nd and 4th order	1.2.3, [10]
MRCI	multi-reference CI	1.2.1, e.g., [37]
PES	potential energy surface	1.1
POL-CI	polarization configuration interaction	[113]
QCI	quadratic CI	[6]
QMC	quantum Monte Carlo	2.1.2
RHF	restricted Hartree-Fock	e.g.[1]
SAC	Stark anti-crossing	[85]
SCF	self-consistent field	1.1
SDCI	singles and doubles CI	1.2.1
SOGVB	spin-optimized generalized valence bond	[172]
STA	short-time approximation	2.1.4.1
STO / STF	Slater-type orbital/function	A.3
TOF	time-of-flight (spectroscopy)	e.g., [130, 142]
UHF	unrestricted Hartree-Fock	[1]
VMC	variational Monte Carlo	2.1.5,4.1.1
ZAC	Zeeman anti-crossing	[137]
ZPE	zero point energy	A.7.1

Appendix B

Other results

Due to budget cuts, the light at the end of the tunnel has been turned off.
Source unknown

B.1 Fluorine

The work on F atom was done by Terray[38] as part of the spline study, but I finished collecting the data and computing the results. Unfortunately, aside from this short summary, there is no other written record of this work.

Two QMC energies were computed for F atom using large basis sets, taking advantage of the spline capabilities. The single-determinant calculation gives $E_{QMC} = -99.70631(154)$a.u. for a linear fit of the data and $E_{QMC} = -99.71239(137)$a.u. for a quadratic fit. The multi-determinant calculation gives $E_{QMC} = -99.70085(185)$a.u. using all time steps (shown in Fig. B.1a), and $E_{QMC} = -99.715085(3045)$a.u. if using only values of $\tau = 0.001$-0.003 (shown in Fig. B.1b).

The single determinant calculation was done using a QZ basis set from Clementi[103] multiplied by a correlation function of the J_{een} form, with parameters optimized by Moskowitz and Schmidt in [86]. The multi-determinant was done using a trial function with 11 determinants from a Gaussian-based CI calculation, obtained from the NASA-Ames group, multiplied by J_{ee} and J_{en} factors. The expansion was truncated to all determinants with expansion coefficients ≥ 0.03. The energy calculation of the F^- species was not completed. The energies at $\tau = 0.005, 0.008$ were computed using Clementi's DZ basis set, and correlation factors of J_{ee} and J_{en} form.

Table B.1: QMC energies at different time steps for F using single- and multi-determinant trial functions

	F		F^-
τ	SD	MD	
0.001	-99.722875(652)	-99.735473(2137)	
0.002	-99.730701(470)	-99.7574(16)	
0.003	-99.742894(4927)	-99.777107(1404)	
0.005	-99.769198(640)	-99.838676(7501)	-99.895092(1374)
0.008	-99.811701(681)	-99.929457(3548)	-99.935111(1621)

Table B.2: Basis set used for F ($1s^2 2s^2 2p^5$) single-determinant calculation

1s	2s	2p	Type	ζ
0.94710	-0.22694	0.0	1s	8.5576
0.03718	-0.00530	0.0	1s	14.9766
0.00013	0.23918	0.0	2s	1.8214
0.00093	0.68592	0.0	2s	2.6730
0.00068	0.31489	0.0	2s	4.9007
0.02602	-0.21822	0.0	2s	6.5736
0.0	0.0	0.17830	2p	1.2657
0.0	0.0	0.56185	2p	2.0580
0.0	0.0	0.33658	2p	3.9285
0.0	0.0	0.01903	2p	8.2041

Table B.3: Gaussian basis set used for F multi-determinant calculation

ζ	Contraction coefficients			
1s				
103109.5	0.000063	-0.000014	-0.000018	-0.000732
15281.01	0.000503	-0.000116	-0.000133	0.000608
3441.539	0.002669	-0.000614	-0.000737	0.000293
967.0948	0.011196	-0.002582	-0.003011	0.005563
314.0353	0.039106	-0.009197	-0.011067	0.010287
113.4423	0.112250	-0.027425	-0.031769	0.046675
44.64473	0.247226	-0.066403	-0.084499	0.127204
18.94287	0.367951	-0.121494	-0.142888	0.152680
8.532743	0.290898	-0.147909	-0.252759	0.594124
3.919401	0.078119	-0.010708	0.148094	-1.301773
1.568157	0.003627	0.370578	1.140773	-0.961524
0.623290	0.000828	0.513164	-0.064733	2.992322
0.240861	0.000153	0.258116	-1.048755	-1.853800
2p				
245.3303	0.000950	-0.001054	-0.001310	
56.91901	0.007954	-0.008808	-0.012466	
17.60457	0.039133	-0.043291	-0.056793	
6.274995	0.129617	-0.154371	-0.246869	
2.447030	0.268628	-0.377441	-0.552836	
0.995060	0.341639	-0.250014	0.344794	
0.403973	0.309840	0.267864	0.815206	
0.154810	0.169633	0.491699	-0.330665	
0.059326	0.043328	0.290617	-0.595629	

Table B.4: Trial function used for F^- ($1s^2\ 2s^2\ 2p^6$) calculation

1s	2s	2p	Type	ζ
0.89308	-0.20022	0.0	1s	8.93690
0.03498	-0.00852	0.0	1s	14.84990
0.00446	0.62675	0.0	2s	3.27783
0.08884	-0.09809	0.0	2s	8.10301
-0.00055	0.48432	0.0	2s	1.85159
0.0	0.0	0.47039	2p	2.07537
0.0	0.0	0.30842	2p	3.93342
0.0	0.0	0.09885	2p	1.46603
0.0	0.0	0.24705	2p	0.95683
0.0	0.0	0.01686	2p	8.32950

Figure B.1: Energy vs time step for F using single- and multi-determinant trial functions.

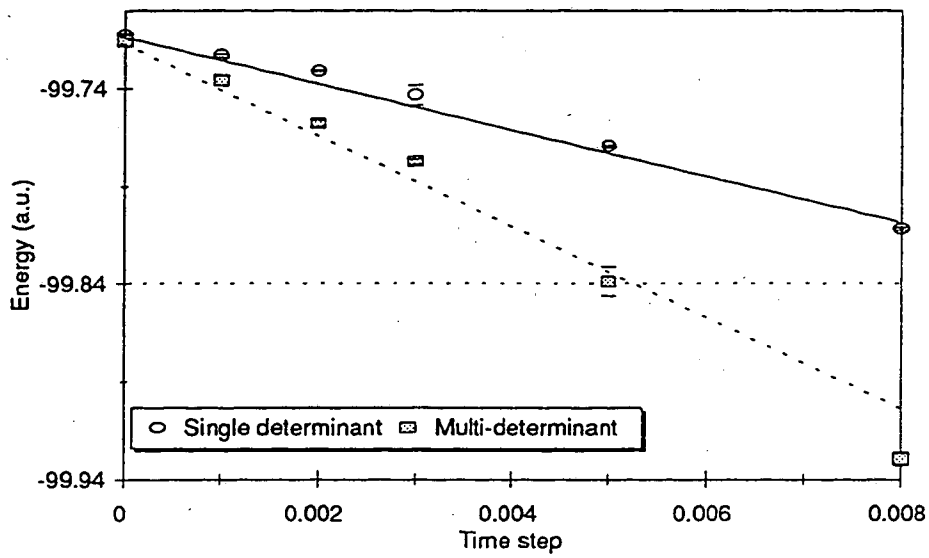

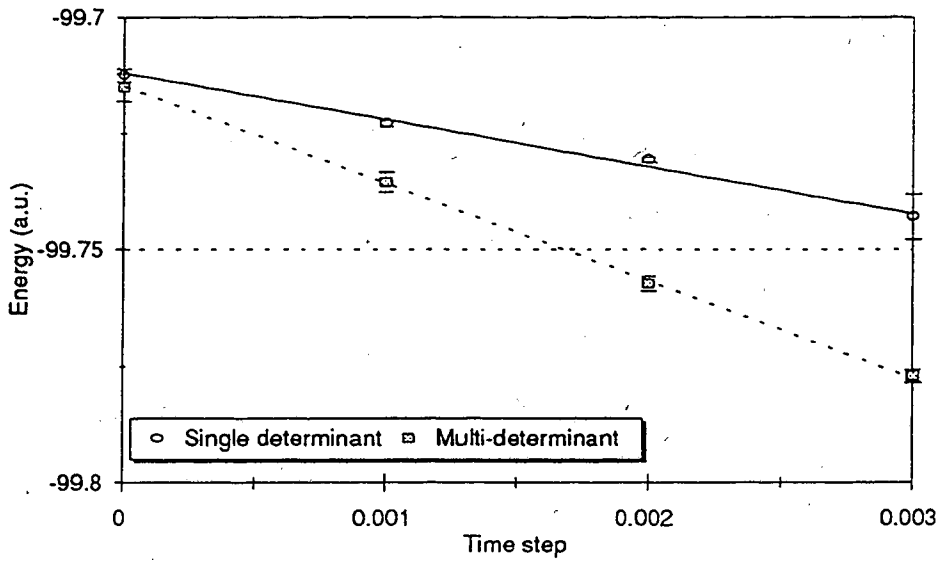

Appendix C

Programs

If builders built buildings the way programmers write programs, then the first woodpecker that came along would destroy civilization.
Weinberg's Second Law

This appendix presents the *ab initio* and QMC programs used in this work. The latest version of the QMC program, QMagiC 7.53, is throughly documented. The *ab initio* programs are documented elsewhere.

C.1 Monte Carlo Programs

C.1.1 QMagiC

This section contains a short description of the different versions available, how they differentiate from each other, and what they each do. Historically, there have been several versions of QMagiC, as well as other QMC codes running in our group,[1] for both single and multi-determinant wave functions. To make life easier for any newcomer who might need to choose a code to get started, here I will go over some of the ones that are still around in Sec. C.1.1.1. Section C.1.1.3 will contain the input specifications for the most current multi-determinant version of QMagiC, used for the calculations in Chapter 3. Section C.1.1.2 will give an overview of how to perform a QMC run.

C.1.1.1 A bit of history

After version 7.2, well documented in Dr. Hammond's thesis[72] for both single- and multi-determinant Ψ_T's, the single-determinant code diverged from the multi-determinant code. In an effort to make the codes more modular (i.e., easier to add and modify outside modules, such

[1] e.g., Barnett's QMC code and Owen's QMagic 9.0 programs.

as ECPCTL, DRVCTL, OPTCTL) independently of the main QMC procedure, version 7.4 moves the link to these options to a higher level, i.e., before the QMC walk is setup. With this upgrade, also came an upgrade in the input. To make it more HONDO-like, the QMCFLG flag in the $CNTRL namelist became a RUNFLG flag to indicate which of the outside modules (available in the specific version) to run (see NAMELIST &CNTRL in the next section). Likewise, the old RUNFLG in the $WALK namelist became QMCFLG to indicate which type of QMC walk was to be performed.

There exist versions of QMagiC 7.5 which run on UNICOS, CTSS, and VMS, all currently stored in CFS. This version was the one modified to include the acceleration method and the C and F atom calculations in Chapter 4 and Appendix B.1. Version 7.53 made available by Dr. B.L. Hammond was used for the rest of the calculations in Chapter 4, given its multi-determinant capabilities. Version 7.5 and 7.53 have several differences, due to the single- and multi- determinant nature of their algorithms, as well as difference in options for correlation functions (See Table C.1).

Conversion between machines can be accomplished by substituting the subroutines at the end of the program, by the equivalent system calls in the new system. Adjustments may be necessary to comply with the precision of the new machine. Table C.1 shows the different versions of the program which I have knowledge of and that can be found stored at NERSC in CFS (ID# 030334).

Some important changes in the latest upgrade (version 7.5 to 7.53) to make conversion easier to those who are familiar with version 7.5 and/or find input decks for the 7.4-7.5 versions (most input decks found in CFS correspond to v7.5) are:

(1) Namelists and data sets begin now with "&" instead of "$".

(2) BLOCK DATA DEFAULT in 7.5 and previous versions became SUBROUTINE SETDEFS in version 7.53. This is where the default values for the input variables are stored.

(3) Inclusion of IPUNFMT variable in the &CNTRL namelist to control the format of the XX files (inxx and outxx).

(4) Unit 1 should be called "inxx," and it must exist in the working directory even if the ensemble is to be generated randomly.

C.1.1.2 How to perform a QMC calculation

In order to do any MC (VMC or FNDQMC) run using QMagiC, one needs two separate input files:

(1) unit 5 - input deck describing the trial function Ψ_T and the parameters for the walk(s); and

(2) unit 1 - (fort.1 for v7.5, inxx for v7.53) XX file containing an initial ensemble and guesses for trial energy, E_T, and initial random number.

Table C.1: Versions of QMagiC currently available (and stored in CFS)

Version	SD	MD	S_{ee}	J_{een}	Spline	UNICOS	CTSS	VMS
7.0	x		x					x
7.1		x	x			x		x
7.2[a]	x		x			x		x
7.2[b]		x	x	x	x	x	x	
7.3-7.31	x		x					x
7.4-7.42	x		x			x	x	x
7.5[c]	x			x	x	x	x	x
7.53[d,e]		x	x		x	x		
7.6[f]	x		x	x	x		x	

[a] used for H_3 work (Sec. 2.2.2)
[b] used for multi-determinant work on F atom (Appendix B.1)
[c] used for work on C atom (Sec. 3.2.1)
[d] used for work on CH, C_2H and C_2H_2 in Chapter 3
[e] Documented here (Appendix C.1.1.3)
[f] Version 7.5 was modified to include acceleration and become version 7.6

Regardless of the version of QMagiC being used, the following steps are recommended to perform a QMC calculation:

(0) Choose the trial function: use, if necessary, the codes mentioned in Sec. C.2 to obtain the appropriate MO vectors, and include in DATA &VEC using correct format (See Sec. C.1.1.3).

(1) Prepare input file for chosen trial function as described in Sec. C.1.1.3, preferably not from scratch.

(2) Do a VMC calculation (RUNFLG=0) to verify the input and to generate an ensemble (start with IGUESS=-1).

(3) Do a short fixed-node calculation with a large time step (one to give about 75% acceptance ratio) followed by a VMC run to discard the least favorable configurations and reequilibrate the ensemble.

(4) It is recommended to do a fixed-node calculation to estimate the serial correlation among steps and therefore determine the size of the blocks and the time step one might want to use for the extrapolation. This can be done by performing a fixed-node calculation with 50000 steps and using that data compute where the auto-correlation function becomes 0. The block size for that time step should be multiplied by at least 10 to give blocks which will be uncorrelated.

(5) Now you are ready to do the first time step.

C.1.1.3 QMagiC 7.53 Input

Data sets are defined to resemble NAMELIST format (i.e., starting with a &name and ending with &END.

DATA **&BANNER** – one line (80 characters) title for run

DATA **&BASIS**

Let us start with Example 1. The numbers to the left indicate line numbers to be used for input description to follow.

Example 1 - CH($^2\Pi$) basis set shown in Table 3.7 without f-functions

```
 0    &BASIS
 1    ********* Methylidyne - MD fn - 3 active B.S.1 *********
 2    C1     6.     0.     0.     0.     0.0000     0.10     0.     0.
 3        1S     9.055
 4        1S     5.025
 5        3S     6.081
 6        2S     2.141
 7        2S     1.354
 8        2P     6.510
 9        2P     2.6005
10        2P     1.4436
11        2P     0.9023
12        3D     3.6407
13        3D     2.0211
14        3D     1.373
15
16    H1     1.     0.     0.     2.124     0.0000     0.10     0.     0.
17        1S     1.600
18        1S     1.000
19        1S     0.625
20        2P     2.000
21        2P     1.40
22        3D     2.33
23
24    &END
```

Line number	Input	Description
2	title	80-character line with description of basis set
3	SYMB, Z, x, y, z, λ, ν	description of atom #1 in free format
	SYMB	atomic symbol (up to 3 characters)
	Z	atomic number
	x, y, z	cartesian coordinates
	λ, ν	J_{en} parameters
4 - 14	TYPE, ζ	basis set for atom #1 in free format
	TYPE	orbital type, i.e., Slaters: 1S, 2S, etc.; Gaussians: G1S, G2S, etc. will allocate number of functions in shell, i.e., 1 for s-shell, 3 for p-shell, and 6 for d-shell.
	ζ	orbital exponent ζ assign to all functions in each shell.
15	blank line indicating that we are done with an atom	
16 - 23	new atom, repeat as for atom #1 in lines 2-15	
24	&END	indicates basis input is done

NAMELIST &PSIT

EECFLG = 0 use Jastrow function for electron-electron correlation (J_{ee} in Table 3.1)
= 1 use double exponential form for electron-electron function (S_{ee} in Table 3.1)

EECF contains parameters for electron-electron correlation function
EECF(1) a (DEFAULT = 0E+00)
EECF(2) b (DEFAULT = 1.E+00)
EECF(3) intended for a_2 in quadratic Jastrow (DEFAULT = 0E+00)
EECF(4) intended for b_2 in quadratic Jastrow (DEFAULT = 0E+00)

Example 2

```
&PSIT
  EECF=0.5,1.0,0.0,0.0,
  EECFLG=0,
&END
```

DATA **&WFN** Describes the electronic configuration in each determinant. The configuration given by WFN should match with the number of AOs in each MO given by &VEC. A line contains the input for each determinant as follows:

DETCO(i), (SPIN(i,j), j = 1,NMO), for i = 1, # determinants

DETCO	coefficient of Slater determinant	
SPIN	UOC	empty MO
	ALP	MO occupied by α electron
	BET	MO occupied by β electron
	DOC	full (doubly occupied) MO

Example 3 - C(^{3}P) atom

```
&WFN
   1.0   DOC DOC ALP ALP
&END
```

Example 4 - CH($^2\Pi$) with the data from Table 3.11

```
&WFN
  -0.986363   DOC DOC DOC UOC ALP UOC
   0.036053   DOC DOC UOC DOC ALP UOC
   0.024106   DOC DOC ALP BET ALP UOC
   0.024106   DOC DOC BET ALP ALP UOC
  -0.048619   DOC DOC ALP ALP BET UOC
  -0.149137   DOC DOC UOC UOC DOC ALP
&END
```

DATA &VEC The MO coefficients are input in this data set using standard HONDO format. As mentioned before, there will be 3 p orbitals ordered p_x, p_y, p_z for each p-function listed in &BASIS, and 6 d orbitals ordered d_{xx}, d_{yy}, d_{zz}, d_{xy}, d_{xz}, d_{yz} for each d-functions listed in &BASIS.

WARNING Basis sets based on 5 spherical polar functions require transformation to 6 cartesian d-functions using Table A.3 according to which type of bond they contribute before being entered to QMagiC.

Format : For each MO include 5 coefficients per line preceeded by the MO#, and the line# of the MO.

Example 5 See here Ψ_T put together using NAMELIST &PSIT and DATA sets &BASIS, &WFN and &VEC

```
&BASIS
  H3 -- double-zeta
  H1      1.        0.        0.        0.
  1S      0.925
  1S      1.275
  2P      1.700

  H2      1.        1.757     0.        0.
  1S      0.925
  1S      1.275
  2P      1.700

  H3      1.        3.514 0.        0.
  1S      0.925
  1S      1.275
  2P      1.700

&END
&PSIT   EECFLG=0, EECF=0.5,1.0,   &END
&WFN
  1.0 DOC ALP
&END
  ----- ORBITALS FROM -UHFOP- -----
&VEC
  1 1-0.20954905E+00-0.27364559E+00-0.24217891E-01 0.00000000E+00 0.00000000E+00
  1 2 0.15493964E+00-0.47114330E+00 0.00000000E+00 0.00000000E+00 0.00000000E+00
  1 3-0.20954905E+00-0.27364559E+00 0.24217891E-01 0.00000000E+00 0.00000000E+00
  2 1-0.74489537E+00-0.65921496E-01-0.37165521E-02 0.00000000E+00 0.00000000E+00
  2 2 0.00000000E+00 0.00000000E+00 0.46624546E-01 0.00000000E+00 0.00000000E+00
  2 3 0.74489537E+00 0.65921496E-01-0.37165521E-02 0.00000000E+00 0.00000000E+00
&END
```

NAMELIST &CNTRL

RUNFLG	= 0	MC walk (run QMCCTL) (DEFAULT)
	= 1	optimization of trial function parameters (run OPTCTL)
NOPRP	= 0	do not compute properties (DEFAULT)
	= 1	compute properties
IPRINT	= 0	normal printing (DEFAULT)
	= 1	print averages after every block
	= 2	print debug information
IPUNFMT	determines format of punch files inxx and outxx	
IPUNFMT(1)	= 0	inxx file is a sequential unformatted file (do not use on Cray)
	= 1	inxx file is a sequential formatted file
IPUNFMT(2)	= 0	outxx file is a sequential unformatted file (do not use on Cray)
	= 1	outxx file is a sequential formatted file
IPUNCH	= −1	do not create new file
	= 0	write MO vectors to outxx file (only) at end of run (outxx file is overwritten)
	= +1	add MO vectors to the end of the outxx file after every block
ISTART	(Not sure it works on Cray.)	
	= 0	read only XX vectors and MO spline
	= 1	read all data but execute new walk
	= 2	continue old walk
STATOL	smallest AO coefficient to be included in an MO (DEFAULT = 1.E-06)	
REETOL	smallest r_{ee} allowed if IGUESS = −1 or ICHECK = +1 in &GUESS (DEFAULT = 1.E-01)	
RENTOL	smallest r_{en} allowed if IGUESS = −1 or ICHECK = +1 in &GUESS (DEFAULT = 1.E-01)	
PSITOL	smallest $\|\Psi_T\|$ allowed if IGUESS = −1 or ICHECK = +1 in &GUESS (DEFAULT = 0.E+00)	
DETOL	determinant zero value used to avoid dividing by zero when computing $1/\Psi_T$ near a node (DEFAULT = 1.E-25)	
FQTOL	cutoff on quantum force (DEFAULT = 1.E+25)	
ACCINV	(DEFAULT = 1.E-03)	
TINY	(DEFAULT = 1.E-37)	

Example 6 `&CNTRL RUNFLG=0, IPRINT=1, IPUNFMT=1,1, &END`

NAMELIST &WALK Program is capable of doing up to 10 consecutive MC walks. Parameters for each run are given in this namelist; i.e., i-th run is described by QMCFLG(i), NUMBLK(i), BLKTIM(i) and TSTEP(i) as follows:

QMCFLG(10) = 0 do VMC walk
= 1 do fixed-node walk

NUMBLK(10) number of blocks of each one of the walks requested using QMCFLG

BLKTIM(10) time in (1/hartree's) for each block such that
BLKTIM/TSTEP = number of steps per block in each walk

TSTEP(10) time step to be used in each walk

KONORM number of walkers in the ensemble
(DEFAULT = 100)

KONMAX maximum size of ensemble; if a fixed-node walk has been requested in QMCFLG, program will make sure that KONMAX $\geq$ 2×KONORM if ensemble overflows (i.e., branches beyond maximum number of walkers allowed in the ensemble, KONMAX), it will be renormalized to KONORM
(DEFAULT = KONORM for VMC walk)
(DEFAULT = 2×KONORM for FN walk)

KONMIN minimum size of ensemble
(DEFAULT = KONORM/4)

RAN initial random number (between 0 and 1)
= 0 create initial RAN from time and date it IGUESS = −1
read in from inxx file if IGUESS = +1
> 0 RAN is used

ETRIAL trial energy to be used in QMC walks for branching

ETW factor by which trial energy is updated using the average local energy from the previous block (i.e., ETRIAL = ELOCAL×ETW)
(DEFAULT = 0.5E+00)

Example 7 Sample walk used for CH($^2\Pi$) with 400 walkers

```
&WALK
  RUNFLG= 0, 1,
  NUMBLK= 25, 50,
  BLKTIM= 5.0, 10.0,
  TSTEP= 0.050, 0.003,
  KONORM=400, KONMAX=800, ETRIAL=0.0,
  ETW=0.5,
&END
```

NAMELIST &GUESS

IGUESS	$= -1$	generate initial configurations at random (DEFAULT)
	$= +1$	read initial configurations from inxx
IFILL	$= 1$	fill ensemble by making copies of configurations available in inxx (DEFAULT)
	$= 0$	do not fill ensemble - if not enough configurations in the inxx file, program stops and an error message is printed
ICHECK	$= 0$	do not check configurations (DEFAULT)
	$= 1$	check for "bad" configurations using tolerances in &CNTRL, i.e., electrons too close to each other, or to a nucleus. arranges configurations in order of descending Ψ_T and keeps upper half

Example 8

```
&GUESS
  IGUESS=+1,ICHECK=0,IFILL=1,EGUESS=0.0,
&END
```

NAMELIST &SPLINE

ISPLINE	= 0	do not use spline for MOs (DEFAULT)
	= 1	use spline to approximate radial part of MOs
NSPLIN	number of knots to be used when generating the cubic spline (DEFAULT = 500)	
SSCALE	SSTEP×NSPLIN (DEFAULT = 1.E+00)	
SSTEP	SSCALE/NSPLIN (DEFAULT = 2.0E-03)	
IPRNT	= 0	(DEFAULT)
	= 1	print TELL-A-GRAF input of spline to unit
	= 2	print some information from fitting
	= 3	print debug information
ITENS	used for adjustment of the tension in the spline	
	= 1	cubic spline (DEFAULT)
LSPMAX(20)		
LSPMMAX	m number of maximum shell included, e.g., 0 for s, 1 for p_x, 2 for p_y, 3 for p_z and so on. (DEFAULT = 4)	
NPARM	Number of parameters (DEFAULT = 5)	
NGRID	Number of data points to be printed out in TELL-A-GRAF input file when IPRNT=1; we recommend to make NGRID = NSPLIN	

Example 9

```
&SPLINE
  ISPLINE=1, NSPLIN=500, LSPMAX=4, LSPMMAX=4, SSTEP=0.002,
  SSCALE=1.0, IPRNT=0, ITENS=1, NPARM=4, NGRID=0,
&END
```

NAMELIST &FIX Option to be used to fix the Gaussian behavior around the origin by replacing knots of the spline in the region near 0. New knots need to be provided by user from file unit 8. The connecting points of the two functions may not be smooth and any discontinuity in the derivatives of the curve will create problems. To verify the derivatives match everywhere, one can print out the first and second derivatives of the spline as well with a simple modification of the subroutine SMOOTH: add FP and FPP to the write statement which prints out the grid points to the TELL-A-GRAPH file.

IFXFLG(MO #, angular momentum)	= 0	do not change knots
	= 1	change knots for IFIX file (unit 8)
NFXKNOT(MO)	number of knots changed for each 1 appearing in IFXFLG	
NSUM	number of lines in fort.8 = $\sum$ NFXKNOT	
YFXF1(MO)	First derivative of the new MO	
YFXS1(MO)	Second derivative of the new MO	

C.1.2 Acceleration routines

As mentioned in Sec. C.1.1.1, the acceleration modules (min.f and hss.f) link to a modified 7.5SD version of QMagiC (qmc76.f), and use '$' notation (instead of &) for NAMELIST and DATA groups.

C.1.2.1 Input specifications for QMC76

NAMELIST $ACC

ACCFLG	= 0	No acceleration is used, i.e., M and $M^{1/2}$ are set equal to unit matrix
	= 1	Acceleration matrix is read from input file (unit 5) Matrix is input in HONDO format (see DATA $AMAT1 and $AMAT2)
EIGMAX		maximum eigenvalue of acceleration matrix

DATA $AMAT1 includes the M matrix in HONDO format, as output from HESSIAN module

DATA $AMAT2 includes the $M^{1/2}$ matrix in HONDO format, as output from HESSIAN module

NAMELIST &HSS

DELTA	Δ value used in computing the Hessian of the wave function by finite differences (DEFAULT = 0.00002×max ($\|\bar{R}\|$, 0.001))
CUTOFF	minimum eigenvalue of acceleration matrix (needed to invert M and compute $M^{1/2}$)

C.1.2.2 How to perform an accelerated VMC calculation

In order to perform an accelerated run on a given system, the following steps must be taken:

[1] Compile and link "qmc76.f" "min.f" and "hss.f".

[2] Obtain M and $M^{1/2}$ as follows:

(a) Choose good Gaussian-based Ψ_T (using HONDO or GAMESS) for the system of interest.

(b) Run qmc76 with option RUNFLG=3 to obtain minimum of potential U (See Sec. 4.1.3). Minimum configuration is stored in units 4 and 6.

(c) Copy minimum configuration to XX file and run qmc76 again with options RUNFLG=2 and QMCFLG=2. Output is in the form of two data sets $AMAT1 and $AMAT2 printed to units 6 and 8.

[3] Data sets $AMAT1 and $AMAT2 should be copied to unit 5.

[4] We are finally ready to do an AVMC calculation: run qmc76 using ACCFLG=1. Any Ψ_T may be used for the acceleration walk.

Table C.2: *Ab initio* programs used in this work, and contact person (e-mail address) to obtain code and documentation.

Program	Contact
ALCHEMY	adm2464@ibm.com
GAMESS	mike@si.fi.ameslab.gov
HONDO	michel@kgnvma.vnet.ibm.com

C.2 *Ab initio* programs

C.2.1 ALCHEMY II, HONDO and GAMESS

QMC with importance sampling requires us to have previously chosen a trial function by standard methods. As mentioned in Sec. C.1.1.3, the MO vectors needed for &VEC can be obtained from a canned *ab initio* program. The programs used in this work were ALCHEMY II[99], HONDO[174, 175], and GAMESS[126]. HONDO was used to obtain wavefunctions for the H_3 work (Sec. 2.2.2) and the acceleration runs (Chapter 4). ALCHEMY and GAMESS were used for work in Chapter 3. HONDO amd GAMESS are based on Gaussian orbitals. The ALCHEMY program provides the capability of computing Slater-type wvae functions for linear molecules, which suited our needs for the C_2H_2 system and its fragments. Table C.2 shows where to find documentation for these programs.

Bibliography

[1] A. Szabo and N.S. Ostlund. *Modern Quantum Chemistry. Introduction to Advanced Electronic Structure Theory.* McGraw-Hill Publishing Company, second edition, 1989.

[2] W.J. Hehre, L. Radom, P.v.R. Schleyer, and J.A. Pople. Ab initio *Molecular Orbital Theory.* Wiley, New York, first edition, 1986.

[3] J.A. Pople and D.L. Beveridge. *Approximate Molecular Orbital Theory.* McGraw-Hill, New York, first edition, 1970.

[4] W.G. Richards and J.A. Horsley. Ab Initio *Molecular Orbital Calculations for Chemists.* Clarendon Press, Oxford, first edition, 1970.

[5] C.C.J. Roothan. New Developments in Molecular Orbital Theory. *Rev. Mod. Phys.*, 23:69, 1951.

[6] J.A. Pople, M. Head-Gordon, and K. Raghavachari. Quadratic configuration interaction. A general technique for determining electron correlation energies. *J. Chem. Phys.*, 87:5968, 1987.

[7] S.R. Langhoff and E.R. Davidson. Configuration Interaction Calculations on the Nitrogen Molecule. *Int. J. Quantum Chem.*, 7:61–72, 1974.

[8] D.R. Hartree, W. Hartree, and B. Swirles. . *Phil. Trans, R. Soc. London. Ser.*, A238:299, 1939.

[9] B.O. Roos, P.R. Taylor, and P.E.M. Siegbahn. A complete active space SCF method (CASSCF) using a density matrix formulated super-CI approach. *Chem. Phys.*, 48:157–73, 1980.

[10] C. Møller and M.S. Plesset. Note on an Approximation Treatment for Many-Electron Systems. *Phys. Rev.*, 46:618–22, 1934.

[11] D.A. McQuarrie. *Quantum Chemistry.* University Science Books, first edition, 1983.

[12] I.N. Levine. *Quantum Chemistry.* Allyn and Bacon, Inc., Boston, third edition, 1983.

[13] J.A. Pople, R. Seeger, and R. Krishnan. Variational Configuration Interaction Methods and Comparison with Pertubation Theory. *Int. J. Quantum Chem. Symp.*, 11:149–63, 1977.

[14] J.A. Pople, M. Head-Gordon, D.J. Fox, K. Raghavachari, and L.A. Curtiss. Gaussian-1 theory: A general procedure for prediction of molecular energies. *J. Chem. Phys.*, 90:5622, 1989.

[15] L.A. Curtiss, K. Raghavachari, G.W. Trucks, and J.A. Pople. Gaussian-2 theory for molecular energies of first- and second-row compounds. *J. Chem. Phys.*, 94:7221–30, 1991.

[16] S.E. Koonin. *Computational Physics.* Addison-Wesley, N.Y., 1986.

[17] W.H. Press, B.P. Flannery, S.A. Teukolsky, and W.T. Vetterling. *Numerical Recipes.* Cambridge University Press, 1986. Fortran edition.

[18] J.B. Anderson. A random-walk simulation of the Schrödinger equation: H_3^+. *J. Chem. Phys.*, 63:1499–1503, 1975.

[19] D. Ceperley, G.V. Chester, and M.H. Kalos. Monte Carlo simulation of a many-fermion study. *Phys. Rev. B*, 16:3081, 1977.

[20] P.J. Reynolds, D.M. Ceperley, B.J. Alder, and W.A. Lester, Jr. Fixed-node quantum Monte Carlo for molecules. *J. Chem. Phys.*, 77:5593, 1982.

[21] J.B. Anderson. Quantum chemistry by random walk. H ^{2}P , H_3^+ D_{3h} $^1A_1$, H_2 $^3\Sigma_u^+$, Be ^1S. *J. Chem. Phys.*, 65:4121, 1976.

[22] C.A. Traynor, J.B. Anderson, and B.M. Boghosian. A quantum Monte Carlo calculation of the ground state energy of the hydrogen molecule. *J. Chem. Phys.*, 94:3657–64, 1991.

[23] J.B. Anderson. Quantum chemistry by random walk: A faster algorithm. *J. Chem. Phys.*, 82:2662–63, 1985.

[24] J.W. Moskowitz and K.E. Schmidt. The domain Green's function method. *J. Chem. Phys.*, 85:2868, 1986.

[25] P.J. Reynolds, R.K. Owen, and W.A. Lester, Jr. Is there a zeroth order time-step error in diffusion quantum Monte Carlo? *J. Chem. Phys.*, 87:1905–6, 1987.

[26] J.B. Anderson and D.R. Garmer. Validity of random walk methods in the limit of small time steps. *J. Chem. Phys.*, 87:1903–4, 1987.

[27] S.M. Rothstein and J. Vrbik. A Green's function used in diffusion Monte Carlo. *J. Chem. Phys.*, 87:1902–3, 1987.

[28] J.W. Moskowitz and K.E. Schmidt. Erratum: the domain Green's function method[J. Chem. Phys. 85, 2868 (1986)]. *J. Chem. Phys.*, 87:1906, 1987.

[29] R.K. Owen. *Quantum Monte Carlo Methods and Lithium Cluster Properties.* PhD thesis, U.C. Berzerkeley, December 1990.

[30] P.J. Reynolds, M. Dupuis, and W.A. Lester, Jr. Quantum Monte Carlo calculation of the singlet-triplet splitting in methylene. *J. Chem. Phys.*, 82:1983–90, 1985.

[31] W.A. Glauser, W. A. Brown, W.A. Lester, Jr., D. Bressanini, B.L. Hammond, and M.L. Koszykowski. Random-walk approach to mapping nodal regions of n-body wave functions: Ground-state Hartree-Fock wave functions for Li-C. *J. Chem. Phys.*, 97:9200–15, 1992.

[32] B.H. Wells. *Methods in Computational Chemistry*, volume 1, pages 311–350. Plenum, N.Y., 1987.

[33] R.N. Barnett, P.J. Reynolds, and W.A. Lester, Jr. H + H_2 reaction barrier: A fixed-node quantum Monte carlo study. *J. Chem. Phys.*, 82:2700–7, 1985.

[34] R.N. Barnett. *Quantum Monte Carlo for Atoms and Molecules.* PhD thesis, U.C., Berkeley, November 1989.

[35] Z. Sun, R.N. Barnett, and W.A. Lester, Jr. Optimization of a multideterminant wave function for quantum Monte Carlo: $Li_2(X\ ^1\Sigma_g{}^+)$. *J. Chem. Phys.*, 96:2422, 1992.

[36] David R. Garmer. *Accurate Quantum Chemical Calculations for Small Molecules Via the Random Walk Method.* PhD thesis, Pennsylvania State University, August 1987.

[37] C.W. Bauschlicher, Jr., S.R. Langhoff, and P.R. Taylor. Theoretical study of the C-H bond dissociation energy of acetylene. *Chem. Phys. Lett.*, 171:42–8, 1990.

[38] L. Terray, 1990. Private communication.

[39] D.R. Garmer and J.B. Anderson. Potential energies for the reaction $F + H_2 \rightarrow HF + H$ by the random walk method. *J. Chem. Phys.*, 89:3050–6, 1988.

[40] S. Huang, Z. Sun, and W.A. Lester, Jr. Optimized trial functions for quantum Monte Carlo. *J. Chem. Phys.*, 92:597–602, 1990.

[41] Z. Sun, S.-Y. Huang, R.N. Barnett, and W.A. Lester, Jr. Wave function optimization with a fixed sample in quantum Monte Carlo. *J. Chem. Phys.*, 93:3326, 1990.

[42] C.J. Umrigar, K.G. Wilson, and J.W. Wikins. Optimized Trial Wave Functions for Quantum Monte Carlo Calculations. *Phys. Rev. Lett.*, 60:1719, 1988.

[43] C.J. Umrigar, K.G. Wilson, and J.W. Wilkins. *A Method for Determining Many Body Wavefunctions*, volume 33 of *Computer Simulation Studies in Condensed Matter Physics*, pages 185–94. Springer-Verlag, Berlin Heidelberg, 1988.

[44] W.L. McMillan. Ground State of Liquid He^4. *Phys. Rev.*, 138:442, 1965.

[45] S.A. Alexander, R.L. Coldwell, G. Aissing, and A.J. Thakkar. Calculating Atomic and Molecular Properties Using Variational Monte Carlo Methods. *Int. J. Quantum Chem. Symp.*, 26:213–27, 1992.

[46] R.L. Coldwell and R.E. Lowther. Monte Carlo Calculation of the Born-Oppenheimer Potential between Two Helium Atoms using Hylleras-Type Electronic Wave Functions. *Int. J. Quantum Chem., Symp.*, 12:329–41, 1978.

[47] Z. Sun, W.A. Lester, Jr., and B.L. Hammond. Correlated sampling of Monte Carlo derivatives with iterative-fixed sampling. *J. Chem. Phys.*, 97:7585–9, 1992.

[48] S. Zhang and M.H. Kalos. Exact Monte Carlo Calculation for Few-Electron Systems. *Phys. Rev. Lett.*, 67:3074, 1991.

[49] D.M. Ceperley and B.J. Alder. Quantum Monte Carlo for molecules: Green's function and nodal release. *J. Chem. Phys.*, 81:5833–44, 1984.

[50] J.B. Anderson, C.A. Traynor, and B.M. Boghosian. Quantum chemistry by random walk - Exact treatment of many-electron systems. *J. Chem. Phys.*, 95:7418–25, 1991.

[51] J.B. Anderson, C.A. Traynor, and B.M. Boghosian. An exact quantum Monte Carlo calculation of the Helium Helium intermolecular potential. *J. Chem. Phys.*, 99:345–51, 1993.

[52] M.H. Kalos. Exact Monte Carlo for Few-Fermion Systems. *J. Stat. Phys.*, 63:1269–81, 1991.

[53] D. Ceperley. The Simulation of Quantum Systems with Random Walks: A New Algorithm for Charged Systems. *J. Comp. Phys.*, 51:404–22, 1983.

[54] M.H. Kalos. Monte Carlo Calculations of the Ground State of Three- and Four- Body Nuclei. *Phys. Rev.*, 128:1791–5, 1962.

[55] R.C. Grimm and R.G. Storer. Monte-Carlo Solution of Schrödinger's Equation. *J. Comp. Phys.*, 7:134–56, 1971.

[56] D.M. Arnow, M.H. Kalos, M.A. Lee, and K.E. Schmidt. Green's function Monte Carlo for few fermion problems. *J. Chem. Phys.*, 77:5562–72, 1982.

[57] D.L. Diedrich and J.B. Anderson. An Accurate Quantum Monte Carlo Calculation of the Barrier Height for the Reaction $H + H_2 \rightarrow H_2 + H$. *Science*, 258:786, 1992.

[58] C.A. Traynor and J.B. Anderson. Parallel Monte Carlo calculations to determine energy differences among similar molecular structures. *Chem. Phys. Lett.*, 147:389–94, 1988.

[59] R.J. Harrison and N.C. Handy. Quantum Monte Carlo calculations on Be and LiH. *Chem. Phys. Lett.*, 113:257, 1985.

[60] D.R. Garmer and J.B. Anderson. Quantum chemistry by random walk: Methane. *J. Chem. Phys.*, 86:4025–9, 1987.

[61] P.J. Reynolds, R.N. Barnett, B.L. Hammond, and W.A. Lester, Jr. Molecular Physics and Chemistry Applications of Quantum Monte Carlo. *J. Stat. Phys.*, 43:1017–26, 1986.

[62] R.P. Subramaniam, M.A. Lee, K.E. Schmidt, and J.W. Moskowitz. Quantum simulation of the electronic structure of diatomic molecules. *J. Chem. Phys.*, 97:2600–8, 1992.

[63] D.R. Garmer and J.B. Anderson. Quantum chemistry by random walk: Application to the Potential Energy Surface for $F + H_2 \rightarrow HF + H$. *J. Chem. Phys.*, 86:7237–9, 1987.

[64] J.Z.H. Zhang and W.H. Miller. Quantum reactive acattering via the S-matrix version of the Kohn variational principle: Integral cross sections for $\mathrm{H} + \mathrm{H}_2(v_1 = j_1 = 0) \rightarrow \mathrm{H}_2(v_2 = 1, j_2 = 1, 3) + \mathrm{H}$ in the energy range $E_{\mathrm{total}} = 0.9 - 1.4$ eV. *Chem. Phys. Lett.*, 153:465, 1988.

[65] J.C. Nieh and J.J. Valentini. Experimental Observation of Dynamical Resonances in $\mathrm{H} + \mathrm{H}_2$ Reaction. *Phys. Rev. Lett.*, 80:519, 1988.

[66] D.G. Truhlar and C.J. Horowitz. Functional representation of Liu and Siegbahn's accurate *ab initio* potential energy calculations for $\mathrm{H} + \mathrm{H}_2$. *J. Chem. Phys.*, 68:2466, 1978.

[67] B. Liu. *Ab initio* potential energy surface for linear H_3. *J. Chem. Phys.*, 58:1925, 1973.

[68] P. Siegbahn and B. Liu. An accurate three-dimensional potential energy surface for H_3. *J. Chem. Phys.*, 68:2457, 1978.

[69] B. Liu. Classical Barrier Height for $\mathrm{H} + \mathrm{H}_2 \rightarrow \mathrm{H}_2 + \mathrm{H}$. *J. Chem. Phys.*, 80:581, 1984.

[70] P.J. Reynolds, R.N. Barnett, and W.A. Lester, Jr. Quantum Monte Carlo Study of the Classical Barrier Height for the $H + H_2$ Exchange Reaction: Restricted versus Unrestricted Trial Functions. *Int. J. of Quantum Chem. Symp.*, 18:709–17, 1984.

[71] W. Kolos and L. Wolniewicz. Potential-Energy Curves for the X $^1\Sigma_g^+$, b $^3\Sigma_u^+$, and c $^1\Pi_u$ States of the Hydrogen Molecule. *J. Chem. Phys.*, 43:2429, 1965.

[72] B.L. Hammond. *Monte Carlo for the Electronic Structure of Molecules.* PhD thesis, U.C. Berkeley, November 1988.

[73] P.J. Reynolds. Overcoming the Large-Z problem in Quantum Monte Carlo. *Int. J. Quantum Chem. Symp.*, 24:679–80, 1990.

[74] B.L. Hammond, P.J. Reynolds, and W.A. Lester, Jr. Valence quantum Monte Carlo with *ab initio* effective core potentials. *J. Chem. Phys.*, 87:1130–6, 1987.

[75] V. Bonifacic and S. Huzinaga. Atomic and molecular calculations with the model potential method. I. *J. Chem. Phys.*, 60:2779–86, 1974.

[76] S. Huzinaga, L. Seijo, Z. Barandiaran, and M. Klobukowski. The *ab initio* model potential method. Main group elements. *J. Chem. Phys.*, 86:2132–45, 1987.

[77] G.B. Bachelet, D.M. Ceperley, and M.G.B. Chiocchetti. Novel Pseudo-Hamiltonian for Quantum Monte Carlo Simulations. *Phys. Rev. Lett.*, 62:2088, 1989.

[78] B.L. Hammond, P.J. Reynolds, and W.A. Lester, Jr. Damped-Core Quantum Monte Carlo Method: Effective Treatment for Large-Z Systems. *Phys. Rev. Lett.*, 61:2312–15, 1988.

[79] J. Carlson, J.W. Moskowitz, and K. Schmidt. Model Hamiltonians for atomic and molecular systems. *J. Chem. Phys.*, 90:1003, 1989.

[80] Z. Sun, M.M. Soto, and W.A. Lester, Jr. Characteristics of Electron Movement in Variational Monte Carlo Simulations. *J. Chem. Phys.*, 100:1278–89, 1994.

[81] D.M. Ceperley and B.J. Alder. Ground state of solid hydrogen at high pressures. *Phys. Rev. B*, 36:2092–2106, 1987.

[82] D.R. Garmer and J.B. Anderson. Quantum chemistry by random walk: Application to the potential energy surface for $F + H_2 \rightarrow HF + H$. *J. Chem. Phys.*, 86:7237–9, 1987.

[83] P.A. Christiansen. Effective potentials and multiconfiguration wave functions in quantum Monte Carlo calculations. *J. Chem. Phys.*, 88:4867–70, 1988.

[84] P.A. Christiansen and L.A. Lajohn. Local potential error in quantum Monte Carlo calculations of the Mg ionization potential. *Chem. Phys. Lett.*, 146:162–4, 1988.

[85] P.G. Green, J.L. Kinsey, and R.W. Field. A new determination of the dissociation energy of acetylene. *J. Chem. Phys.*, 91:5160–3, 1989.

[86] K.E. Schmidt and J.W. Moskowitz. Correlated Monte Carlo wave function for atoms He through Ne. *J. Chem. Phys.*, 93:4172, 1990.

[87] J.W. Moskowitz and K.E. Schmidt. Correlated Monte Carlo wave functions for some cations and anions of the first row atoms. *J. Chem. Phys.*, 97:3382–5, 1992.

[88] Paul E. Cade and Winifred M. Huo. Electronic Structure of Diatomic Molecules. VI.A. Hartree-Fock Wavefunctions and Energy Quantities for the Ground States of the First-Row Hydrides, AH. *J. Chem. Phys.*, 47:614, 1967.

[89] H.P.D. Liu and G. Verhaegen. Electronic States of CH and NH. *J. Chem. Phys.*, 53:735–45, 1970.

[90] G.C. Lie and E. Clementi. Study of the electronic structure of molecules. XXI. Correlation energy corrections as a functional of the Hartree-Fock density and its application to the hydrides of the second row atoms. *J. Chem. Phys.*, 60:1275, 1974.

[91] G.C. Lie, J. Hinze, and B. Liu. Valence excited states of CH. I. Potential curves. *J. Chem. Phys.*, 59:1872–86, 1973.

[92] A.D. McLean and B. Liu. Classification of configurations and the determination of interacting and noninteracting spaces in configuration interaction. *J. Chem. Phys.*, 58:1066, 1973.

[93] Per E.M. Siegbahn. Large scale contracted MC-CI calculations on acetylene and its dissociation into two $CH(^2\Pi)$ radicals. *J. Chem. Phys.*, 75:2314, 1981.

[94] S. Huzinaga. Gaussian-Type Functions for Polyatomic Systems. I. *J. Chem. Phys.*, 42:1293, 1964.

[95] T.H. Dunning, Jr. Gaussian Basis Functions for Use in Molecular Calculations. III. Contraction of $(10s6p)$ Atomic Basis Sets for the First-Row Atoms. *J. Chem. Phys.*, 55:716–23, 1971.

[96] C.W. Bauschlicher, Jr. and S.R. Langhoff. Theoretical D_0 for NH(X $^3\Sigma^-$). *Chem. Phys. Lett.*, 135:67–72, 1987.

[97] A.D. McLean and M. Yoshimine. *Tables of Linear Molecule Wave Functions.* IBM, 1967. A supplement to paper *Computation of Molecular Properties and Structure* which appeared in IBM Journal of Research and Development in November, 1967.

[98] Z. Sun, 1992. Private communication.

[99] A.D. McLean, M. Yoshimine, B.H. Lensfield, P.S. Bagus, and B. Liu. ALCHEMY II from MOTECC90, 1990. available from IBM Research Division, Almaden research Center, 650 Harry Road, San Jose, CA 95120-6099.

[100] K.D. Tucker, M.L. Kutner, and W. Weltner, Jr. . *Astrophys. J. Lett.*, 103:L115, 1974.

[101] S.P. So and W.G. Richards. Low-Lying Electronic States of the Ethynyl Free Radical. *J. Chem. Soc. Faraday II*, 71:660–3, 1975.

[102] I.H. Hillier, J. Kendrick, and M.F. Guest. A theoretical study, including correlation, of the low-lying states of the ethynyl radical. *Mol. Phys.*, 30:1133–1138, 1975.

[103] E. Clementi and C. Roetti. Neutral and Ionized Atoms $Z \leq 54$. *Atomic Data and Nuclear Data Tables*, 14(3-4):177, 1974.

[104] S. Shih, S.D. Peyerimhoff, and R.J. Buenker. Theoretical Prediction of the Vertical Electronic Spectrum of the C_2H Radical. *J. Mol. Spec.*, 64:167–79, 1977.

[105] J. Barsuhn. Molecular Calculations Concerning a New Candidate for the Unidentified Emission Line at 89.190 GHz. *Astrophys. Lett.*, 12:169, 1972.

[106] S.K. Shih, S.D. Peyerimhoff, and R.J. Buenker. Calculated Potential for the Description of the Emission Spectrum of the C_2H Radical. *J. Molec. Spect.*, 74:124–35, 1979.

[107] M.E. Jacox. Matrix Isolation Study of the Vibrational Spectrum and Structure of HC_2. *Chem. Phys.*, 7:424–32, 1975.

[108] M.E. Jacox and W.B. Olson. The $\tilde{A}\,^2\Pi - \tilde{X}\,^2\Sigma^+$ transition of HC_2 isolated in solid argon. *J. Chem. Phys.*, 86:3134–42, 1987.

[109] P.G. Carrick, J. Pfeiffer, Jr. R.F. Curl, E. Koester, F.K. Tittel, and J.V.V. Kasper. Infrared absorption spectrum of C_2H radical with color center laser. *J. Chem. Phys.*, 76:3336, 1982.

[110] P.G. Carrick, A.J. Merer, and Jr. R.F. Curl. $\tilde{A}\,^2\Pi \leftarrow \tilde{X}\,^2\Sigma^+$ infrared electronic transition of C_2H. *J. Chem. Phys.*, 78:3652–8, 1983.

[111] L.B. Harding, G.C. Schatz, and R.A. Chiles. An *ab initio* determination of the rate constant for $H_2 + C_2H \rightarrow H + C_2H_2$. *J. Chem. Phys.*, 76:5172–3, 1982.

[112] G. Fogarasi, J.E. Boggs, and P. Pulay. Theoretical equilibrium geometrey, vibrational frequencies and the first electronic transition energy of HCC. *Mol. Phys.*, 50:139–51, 1983.

[113] K.A. White and G.C. Schatz. Analytical Potential Energy Surfaces for Ethynyl, Acetylene, and Vinyl. *J. Chem. Phys.*, 88:2049–57, 1984.

[114] L.B. Harding, A.F. Wagner, J.M. Bowman, G.C. Schatz, and K.J. Christoffel. Ab Initio Calculation of the Transition-State Properties and Addition Rate Constants for $H + C_2H_2$ and Selected Isotopic Analogues. *J. Phys. Chem.*, 86:4312, 1982.

[115] J.R. Reimers, K.R. Wilson, E.J. Heller, and S.R. Langhoff. CASSCF-wave packet *ab initio* prediction of electronic and vibrational spectra: Application to the $A(^2\Pi) \leftarrow X(^2\Sigma^+)$ absorption of C_2H at 3000K. *J. Chem. Phys.*, 82:5064–77, 1985.

[116] W.P. Kraemer, B.O. Roos, P.R. Buenker, and Per Jensen. An Ab Initio Calculation of the Rotation-Vibration Energies of the $\tilde{X}^2\Sigma^+$ State of CCH Using the Nonrigid Bender Hamiltonian. *J. Molec. Spec.*, 120:236–8, 1986.

[117] W.B. Yan, J.L. Hall, J.W. Stephens, M.L. Richnow, and R.F. Curl. Color Center laser spectroscopy of vibrationally excited C_2H. *J. Chem. Phys.*, 86:1657–61, 1987.

[118] Perić, R.J. Buenker, and S.D. Peyerimhoff. *Ab initio* investigation of the vibronic structure of the C_2H spectrum II. Calculation of diabatic potential surfaces for the three lowest-lying electronic states in C_2H. *Mol. Phys.*, 71:673–91, 1990.

[119] Perić, S.D. Peyerimhoff, and R.J. Buenker. *Ab initio* investigation of the vibronic structure of the C_2H spectrum III. Calculation of vibronic energies and transition probabilities in the $X^2\Sigma^+$, $A^2\Pi$ system. *Mol. Phys.*, 71:693–719, 1990.

[120] Y. Osamura, F. Mitsuhashi, and S. Iwata. A theoretical study of the photodissociation of acetylene in its lowest excited singlet state. *Chem. Phys. Lett.*, 164:205–9, 1989.

[121] L.A. Curtiss and J.A. Pople. Theoretical study of structures and energies of acetylene, ethylene and vinyl radical and cation. *J. Chem. Phys.*, 88:7405–9, 1988.

[122] L.A. Curtiss and J.A. Pople. Theoretical study of the C-H bond dissociation energy of acetylene. *J. Chem. Phys.*, 91:2420–3, 1989.

[123] J.A. Montgomery, Jr. and G.A. Petersson. On the C-H Bond Dissociation Energy of Acetylene. *Chem. Phys. Lett.*, 168:75–8, 1990.

[124] D. Habibollahzadeh, J.S. Murray, M. Grodzicki, J.M. Seminario, and P. Politzer. C-H Bond Dissociation of Acetylene: Local Density Functional Calculations. *Int. J. of Quantum Chem.*, 42:267–72, 1992.

[125] C.W. Bauschlicher and S.R. Langhoff. Theoretical study of the C-H bond dissociation energy of C_2H. *Chem. Phys. Lett.*, 173:367–70, 1990.

[126] M.W. Schmidt, K.K. Baldridge, J.A. Boatz, J.H. Jensen, S. Koseki, M.S. Gordon, K.A. Nguyen, T.L. Windus, and S.T. Elbert. GAMESS. *QCPE Bulletin*, 10:52–54, 1990.

[127] A.D. McLean, 1992. Private communication.

[128] W.J. Lafferty and R.J. Thibault. High Resolution Infrared Spectra of $C_2^{12}H_2$, $C^{12}C^{13}H_2$, and $C_2^{13}H_2$. *J. Mol. Spec.*, 14:79–96, 1964.

[129] S. Carter, I.M. Mills, and J.N. Murrell. A potential energy surface for the ground state of acetylene, $H_2C_2(\tilde{X}\ ^1\Sigma_g^+)$. *Mol. Phys.*, 41:191–203, 1980.

[130] A.M. Wodtke and Y.T. Lee. Photodissociation of Acetylene at 193.3 nm. *J. Phys. Chem.*, 89:4744–51, 1985.

[131] H.Shiromaru, Y. Achiba, K. Kimura, and Y.T. Lee. Determination of the C-H Bond Dissociation Energies of Ethylene and Acetylene by Observation of the Threshold Energies of H^+ Formation by Synchrotron Radiation. *J. Phys. Chem.*, 91:17–9, 1987.

[132] M. Perić, S.D. Peyerimhoff, and R.J. Buenker. Theoretical study of the U.V. spectrum of acetylene. III. *Ab initio* investigation of the valence-type singlet electronic states. *Mol. Phys.*, 62:1339–56, 1987.

[133] M. Fujii, A. Haijima, and M. Ito. Predissociation of Acetylene in $\tilde{A}\,^1A_u$ State. *Chem. Phys. Lett.*, 150:380, 1988.

[134] A. Haijima, M. Fujii, and M. Ito. Predissociation of the acetylene $\tilde{A}\,^1A_u$ state and its mechanism. *J. Chem. Phys.*, 92:959–68, 1990.

[135] J. Segall, R. Lavi, Y. Wen, and C. Wittig. Acetylene C-H Bond Dissociation Energy Using 193.3nm Photolysis and Sub-Doppler resolution H-Atom Spectroscopy: 127 $\pm$ 1.5 kcal mol^{-1}. *J. Phys. Chem.*, 93:7287, 1989.

[136] S. Benson, 1989. Private communication cited in *J. Phys. Chem.* 93:7287, 1989.

[137] Y. Chen, D. Jonas, C. Hamilton, P.G. Green, J.L. Kinsey, and R.W. Field. Acetylene: Isomerization and Dissociation. *Ber. Bunsenges. Phys. Chem.*, 92:329–36, 1988.

[138] J.K.G. Watson, M. Herman, J.C. van Craen, and R. Colin. The $\tilde{A} - \tilde{X}$ Band System of Acetylene. *J. Mol. Spec.*, 95:101–32, 1982.

[139] J.C. van Craen, M. Herman, R. Colin, and J.K.G. Watson. The $\tilde{A} - \tilde{X}$ Band System of Acetylene: Analysis of Medium-Wavelength Bands, and Vibration-Rotation Constants for the Levels $n\nu_3'(n = 4 - 6)$, $\nu_2' + n\nu_3'(n = 3 - 5)$, and $\nu_1' + n\nu_3'(n = 2, 3)$. *J. Mol. Spec.*, 111:185–97, 1986.

[140] K.M. Ervin, S. Gronert, S.E. Barlow, M.K. Gilles, A.G. Harrison, V.M. Bierbaum, C.H. DePuy, W.C. Lineberger, and G.B. Ellison. Bond strengths of Ethylene and Acetylene. *J. Am. Chem. Soc.*, 112:5750–9, 1990.

[141] C.J. Wu and E.A. Carter. Ab Initio Bond Strengths in Ethylene and Acetylene. *J. Am. Chem. Soc.*, 112:5893–5, 1990.

[142] B.A. Balko, J. Zhang, and Y.T. Lee. 193 nm photodissociation of acetylene. *J. Chem. Phys.*, 94:7958–66, 1991.

[143] K.P. Huber and G. Herzberg. *Molecular Spectra and Molecular Structure.* Van Nostrand Rheinhold, New York, 1979.

[144] H.L. Gray and W.R. Schucany. *The generalized jackknife statistic*, volume 1 of *Statistics: textbooks and monographs.* M. Dekker, New York, 1972.

[145] G.T. Barkema. *Monte Carlo Methods on Distributed Systems.* PhD thesis, Rijksuniversiteit te Utrecht, October 29 1992.

[146] G.G. Batrouni and P.J. Reynolds. Accelerated Green's function Monte Carlo: Avoiding Critical Slowing Down in Simulations Containing Large-Z Atoms. *unpublished.*

[147] N. Metropolis, A.W. Rosenbluth, M.N. Rosenbluth, A.H. Teller, and E. Teller. Equation of State Calculations by Fast Computing Machines. *J. Chem. Phys.*, 21:1087–92, 1953.

[148] M. Rao and B.J. Berne. On the force bias Monte Carlo simulation of simple liquids. *J. Chem. Phys.*, 71:129, 1979.

[149] M. Rao, C. Pangali, and B.J. Berne. On the force bias Monte Carlo simulation of water: methodology, optimization and comparison with molecular dynamics. *Mol. Phys.*, 37:1773–1798, 1979.

[150] C.J. Umrigar. Accelerated Metropolis Method. *Phys. Rev. Lett.*, 71:408, 1993.

[151] G.G. Batrouni, G.R. Katz, A.S. Kronfeld, G.P. Lepage, B. Svetitsky, and K.G. Wilson. Langevin simulations of lattice field theories. *Phys. Rev. D*, 32:2736, 1985.

[152] G.G. Batrouni and B. Svetitsky. Accelerated dynamics in simulations of first-order phase transitions. *Phys. Rev. B*, 36:5647, 1987.

[153] C.T.H. Davies, G.G. Batrouni, G.R. Katz, A.S. Kronfeld, G.P. Lepage, P. Rossi, B. Svetitsky, and K.G. Wilson. Fourier acceleration in lattice gauge theories. III. updating field configurations. *Phys. Rev. D*, 41:1953, 1990.

[154] J.W. Moskowitz and M.H. Kalos. A New Look at Correlations in Atomic and Molecular Systems. I. Application of Fermion Monte Carlo Variational Method. *Int. J. Quantum Chem.*, 20:1107–19, 1981.

[155] S. Chandraskhar. Stochastic Problems in Physics and Astronomy. *Rev. Mod. Phys.*, 15:1, 1943.

[156] G. Parisi. *Progress in Gauge Field Theory*, volume 115, page 351. Plenum, New York, 1984.

[157] P.J. Reynolds, 1991. Private communication.

[158] R.N. Barnett, P.J. Reynolds, and W.A. Lester, Jr. Monte Carlo Determination of the Oscillator Strength and Excited State Lifetime for the Li $2^2S \rightarrow 2^2P$ Transition. *Int. J. Quantum Chem.*, 42:837–47, 1992.

[159] J.J. Morales, M.J. Nuevo, and L.F. Rull. Statistical error methods in computer simulations. *J. Comp. Phys.*, 89:432, 1990.

[160] Z. Sun, M.M. Soto, R.N. Barnett, and W.A. Lester, Jr. An Approach for Improved Variational Monte Carlo. *To be published.*

[161] E.A. Hylleraas. Über den Grundzustand des Heliumatoms. *Zeitschrift für Physik*, 48:469, 1928.

[162] T.H. Dunning, Jr. Gaussian Basis Functions for Use in Molecular Calculations. I. Contraction of (9*s*5*p*) Atomic Basis Sets for the First-Row Atoms. *J. Chem. Phys.*, 53:2823–33, 1970.

[163] T.H. Dunning, Jr. Gaussian Basis Functions for Use in Molecular Calculations. IV. The Representation of Polarization Functions for the First-Row Atoms and Hydrogen. *J. Chem. Phys.*, 55:3958–66, 1971.

[164] B. Liu and M. Yoshimine. The alchemy configuration interaction method. I. The symbolic matrix method for determining elements of matrix operators. *J. Chem. Phys.*, 74:612–6, 1981.

[165] Per-Olov Løwdin. *Correlation problem in many-electron quantum mechanics I. Review of different approaches and discussion of some current ideas*, volume Advances in Chemical Physics, Vol. II, pages 207–412. Interscience Publishers, Inc., New York, 1959.

[166] Y. Zhao and J.S. Francisco. *Ab initio* studies of the structure and thermochemistry of FO radicals. *Chem. Phys. Lett.*, 167:285–90, 1990.

[167] J.A. Pople, B.T. Luke, M.J. Frisch, and J.S. Binkley. Theoretical Thermochemistry. 1. Heats of Formation of Neutral AH_n Molecules (A = Li to Cl). *J. Phys. Chem.*, 89:2198–2203, 1985.

[168] W. Kolos and C.C.J. Roothaan. Correlated Orbitals for the Ground State of the Hydrogen Molecule. *Rev. Mod. Phys.*, 32:205, 1960.

[169] C. R. Myers, C.J. Umrigar, J.P. Sethna, and J.D. Morgan III. Fock's expansion, Kato's cusp conditions, and the exponential ansatz. *Phys. Rev. A*, 44:5537–46, 1991.

[170] G.F. Roach. *Green's functions.* Cambridge University Press, second edition, 1982.

[171] I. Stakgold. *Green's functions and boundary value problems.* John Wiley & Sons, Inc., first edition, 1979.

[172] W.A. Goddard III and R.C. Ladner. A Generalized Orbital Description of the Reactions of Small Molecules. *J. Am. Chem. Soc.*, 93:6750–6, 1971.

[173] R.D. Levine and R.B. Bernstein. *Molecular Reaction Dynamics and Chemical Reactivity.* Oxford University Press, First edition, 1987.

[174] M. Dupuis, J.D. Watts, H.O. Villar, and G.J.B. Hurst. HONDO version 7.0, 1987. available from IBM Corporation, Scientific and Engineering Computations, Dept. 48B/MS 428, Neighborhood Road, Kingston, N.Y. 12401.

[175] M. Dupuis and A. Marquez. HONDO version 8.3. available from IBM Corporation, Dept. MLM/MS 428, Neighborhood Road, Kingston, N.Y. 12401.

LAWRENCE BERKELEY NATIONAL LABORATORY
UNIVERSITY OF CALIFORNIA
TECHNICAL & ELECTRONIC INFORMATION DEPARTMENT
BERKELEY, CALIFORNIA 94720